Spring 2016

Synthesis and Mechanistic Investigations of Transition Metal Complexes and Ligands for Chemotherapeutic Applications

Jimmie Lee Bullock Jr.
Old Dominion University, jlbulloc09@gmail.com

SYNTHESIS AND MECHANISTIC INVESTIGATIONS OF LIGANDS AND TRANSITION METAL COMPLEXES FOR CHEMOTHERAPEUTIC APPLICATIONS

by

Jimmie Lee Bullock Jr.

B.S. Chemistry, May 2013, Longwood University
B.S. Biology, May 2013, Longwood University

A Thesis Submitted to the Faculty of
Old Dominion University in Partial Fulfillment of the
Requirements for the Degree of

MASTER OF SCIENCE

CHEMISTRY

OLD DOMINION UNIVERSITY
May 2016

Approved by:

Alvin A. Holder	(Director)
Stephen J. Beebe	(Member)
John B. Cooper	(Member)
Lesley H. Greene	(Member)
Guijun Wang	(Member)

ABSTRACT

SYNTHESIS AND MECHANISTIC INVESTIGATIONS OF TRANSITION METAL COMPLEXES AND LIGANDS FOR CHEMOTHERAPEUTIC APPLICATIONS

Jimmie Lee Bullock Jr.
Old Dominion University, 2016
Director: Dr. Alvin A. Holder

Transition metal complexes have played a critical role in antitumor therapy with many complexes incorporating platinum, ruthenium, and lanthanum having been investigated in preclinical and clinical trials. The best known transition metal therapeutic is cisplatin, which is utilized in nearly 50% of all cancer therapies, despite its significant toxic side effects. The toxic side effects of current FDA approved platinum-based chemotherapeutics are often overlooked due to the "special status" granted to these drugs due to their ability to fight, what is often considered an incurable disease with life expectancies often measured in months. Oncology drug development has therefore now focused on developing new complexes with less toxicity and which inhibit cancer cell growth by different mechanisms of action when compared with platinum-based therapeutics.

Understanding exactly how a biological agent elicits its observed activity is perhaps the most critical step in drug discovery and is a question left unanswered by many. Take for instance NAMI-A and KP1019, both Ru(II)-based chemotherapeutics currently in clinical trials, despite their unsolved mechanisms of action. Detailed mechanistic investigations have the potential to inform the design of next generation chemotherapeutics. Therefore, in the first half of this thesis, we investigated the mechanisms of actions of some transition metal complexes incorporating Co(III), Ru(II), and/or V(IV) metal centers. Utilizing spectroscopic, biophysical, and molecular biological techniques such as UV-visible and fluorescence binding assays, isothermal titration

calorimetry, and flow cytometry, we investigated the ability of these unique transition metal complexes to interact with CT DNA, inhibit cellular proliferation in mammary breast cancer cells, and modify cell signaling pathways. This information provides valuable insight into the potential mechanism of action of these compounds, which is expected to be different for each unique molecular structure. Additionally, a novel localized ablation technique involving a transition metal therapeutic and nanosecond pulsed electric field technology was developed and investigated. In the second half of this thesis, we focused attention on the development of new ligands and complexes which can be screened for their potential chemotherapeutic activity. Using simple, clean, and efficient organic and inorganic reactions small libraries of molecules were synthesized and characterized using a variety of spectroscopic techniques including: ^{1}H, ^{13}C, and ^{19}F NMR spectroscopy, high resolution mass spectroscopy, and X-ray crystallography, where appropriate. From this work a new potential lead molecule(s) may be identified which may show enhanced chemotherapeutic activity. Additionally, structurally similar ligands and complexes will lead to structure-activity relationship studies which are also an integral part of drug discovery in lead optimization.

This thesis is dedicated to my family and friends, who have continually and unrelentingly pushed me to be the best man I could possibly be.

ACKNOWLEDGEMENTS

There are several people that I would like to acknowledge and thank for their encouragement and support during my tenure at Old Dominion. I would like to thank my research advisor, Dr. Alvin Holder, for allowing me to conduct my work in his laboratory. I must also express my extreme gratitude to Dr. Stephen J. Beebe, my "bioelectrics godfather", who has served as a second research advisor, committee member, and great mentor. He has graciously provided me with training, resources, and insight into all aspects of my molecular biological projects and a variety of other non-work related topics. Together they have allowed me to thrive as an independent scientist, while pursuing my research goals during my tenure in their respective labs.

Secondly, I would like thank all of the members of my thesis committee: Drs. John B. Cooper, Lesley H. Greene, and Guijun Wang. Despite their busy schedules each has taken the time to get to know me as a student and a scientist. Together, they have provided invaluable insight and perspective during my time at Old Dominion, ultimately making me a better scientist. Also, I want to thank my undergraduate research advisors: Drs. Amorette R. Barber, Chris G. Gulgas, and R. Adam Franssen for giving me a strong foundation in research, pushing me to apply to graduate school, and for their continued constant words of wisdom and thoughtful advice during my graduate career.

A big thank you goes out to all of the faculty, staff, and students of the Department of Chemistry and Biochemistry and the Frank Reidy Research Center for Bioelectrics who, have provided support and friendship throughout my time in the program. I would especially like to recognize core lab manager Dr. Yu "Ellen" Jing for her help, knowledge, and training on instrumentation within the Center and Katherine "Tye" Harlow for her assistance with nsPEFs and cell culture at the beginning of my work. I would also like to thank all the current and former

members of the Holder and Beebe groups for their many, varied contributions to my work and life during this process. I consider myself fortunate to have had the chance to spend time with a group of people that worked well not only as colleagues, but as friends. The unique nature of our little groups has brought me into contact with people of various background and cultures and I will not soon forget our entertaining, educational, and enlightening conversations.

During my years at Old Dominion, I was fortunate to be surrounded by a number of friends and colleagues that enriched my graduate experience. Richard Jones proved a great partner for discussion on all topics in the lab or the local pubs. I am sure we are likely the only two graduate students who have bonded over a mutual interest in tattoo TV shows and the realization that a "MONSTER" Del Vecchio's pizza is simply too much food for two people! Drs. Jason Collins and Wassim Obeid introduced me to the city of Norfolk outside of the lab and I cannot thank them enough for all they have done for me. They have been the greatest confidantes and bowling mates I have ever had the pleasure of rolling with! Without Jason and Wassim pushing me when I needed it – both verbally and by example – this thesis wouldn't have been possible. Thank you gentlemen for our conversations, both scientific and often non-scientific, they always made the days more enjoyable, and I thank you for your continued friendship.

Finally, I would like to thank my family as they are the foundation for my strength, self-confidence, and drive. Thanks especially to my mother, Ms. Arlene Seelie-Bullock, and little brother, Victor, for always believing in me, even when I didn't believe in myself. I couldn't imagine having a better support group than you two. Lastly, thank you to my amazing fiancé, Danielle. Thank you for being my inspiration, for always standing by my side, for putting up with my non-stop chemistry/biochemistry talk, for accepting my crazy work hours, and for always

(maybe not willingly) editing my papers and this thesis for grammatical errors. Thank you for supporting me without question and for providing my life with balance.

This thesis research was supported by the NSF is the form of an NSF CAREER Award (awarded to Dr. A.A. Holder CHE-1431172), The Frank Reidy Center for Bioelectrics, Electroblate Incorporated, and Old Dominion University in the form of the Old Dominion University - University Fellowship awarded to Jimmie Lee Bullock Jr. from the new faculty startup package for Dr. A.A. Holder.

NOMENCLATURE

$\Delta\Psi_m$	mitochondrial membrane potential
Ac-DEVD-AMC	N-Acetyl-Asp-Glu-Val-Asp-7-amido-4-methylcoumarin
$CHCl_3$	chloroform
CT DNA	calf thymus DNA
DMEM	Dulbecco's modified eagle's medium
DMF	dimethylformamide
DMSO	dimethyl sulfoxide
DNA	deoxyribonucleic acid
EB	ethidium bromide
ECT	electrochemotherapy
EDTA	ethylenediamine tetracetic acid
EF_{50}	half maximal inhibitory electric field
EtOH	ethanol
ESI MS	electrospray ionization mass spectroscopy
FBS	fetal bovine serum
FT IR	Fourier transform infrared resonance spectroscopy
H2AX	histone 2.AX
HCl	hydrochloric acid
IC_{50}	half maximal inhibitory concentration
ITC	isothermal titration calorimetry
IRE	irreversible electroporation
K_{app}	binding constant
kV	kilovolts

K_q	quenching constant
MeATSC	9-anthracenethiosemicarbazone
MeCN	acetonitrile
MeOH	methanol
MHz	megahertz
NMR	nuclear magnetic resonance
ns	nanosecond
nsPEF	nanosecond pulse electric field
PBS	phosphate buffered saline
PCA	pyridine-2-thiocarboxamide
PDT	photodynamic therapy
phen	1,10-phenanthroline
oda	2,2'-oxydiacetate
RBF	round bottom flask
RCD	regulated cell death
RNA	ribonucleic acid
sal-*L*-tryp	*N*-salicylidene-*L*-tryptophanate
TLC	thin layer chromatography
TMRE	tetramethylrhodamine methyl ester
TSC	thiosemicarbazone
z-VAD-FMK	benzyloxycarbonyl-Val-Ala-Asp-(O-methyl)-fluoromehylketone

TABLE OF CONTENTS

Page

LIST OF FIGURES

Figure Page

Figure Page

LIST OF SCHEMES

LIST OF TABLES

CHAPTER 1

INTRODUCTION

BIOINORGANIC CHEMISTRY: METALS IN MEDICINE

Metal ions play pivotal roles in a plethora of biological processes, and the study of the roles of these metal ions in biological systems falls into the rapidly developing interdisciplinary field known as bioinorganic chemistry. When compared to other branches of natural sciences, bioinorganic chemistry seems to be a young discipline, however, there is a copious amount of information on the effects of metals on biological systems. For instance, the hazardous toxicities of metal ions such as mercury, lead and chromium on the environment have been well publicized.[1] While on the other hand, it is know that some metals such as iron, copper and zinc are absolutely required to support life as we know it.[2, 3] Scientists in this field are exploiting the unique properties of "toxic" metals such as arsenic, gadolinium, platinum, and technetium, to develop metal complexes that can be employed as therapeutic and diagnostic agents.[3, 4] The introduction of metal ions into a biological system for the treatment or diagnosis of diseases is just one of the many subdivisions within the field of bioinorganic chemistry.

While the field of bioinorganic chemistry is considered by many to be a relatively new field, this is contrary to historical fact, which has shown that metals were used in potions which trace back to the ancient civilizations of Mesopotamia, Egypt, India, and China.[5-8] Many of the inorganic compounds utilized in these times were used in an empirical way with little attempt to design the compounds, and with little to no understanding of the molecular basis of their mechanism of action. As science has evolved, so too have the uses of the metals and the methods

---

This thesis is formatted based on the *Journal of Inorganic Biochemistry*

experimentalists utilize to intentionally introduce these complexes into the human biological system. Figure 1 and table 1 present selected examples of successful therapeutic and diagnostic agents. Magnevist and Cardiolite, Gd^{III} and $^{99m}Tc^{I}$ complexes, respectively, have drastically increased our understanding and detection of diseases through imaging of living tissues using single photon emission computed tomography (SPECT) and magnetic resonance imaging (MRI) scans.[9] Thanks to these diagnostic methods, malignant growth, cardiologic diseases, and atherosclerosis in patients can be detected early; furthermore, such imaging agents enhance research as they, for example, enable researchers to visualize the activity of the brain *in vivo*.

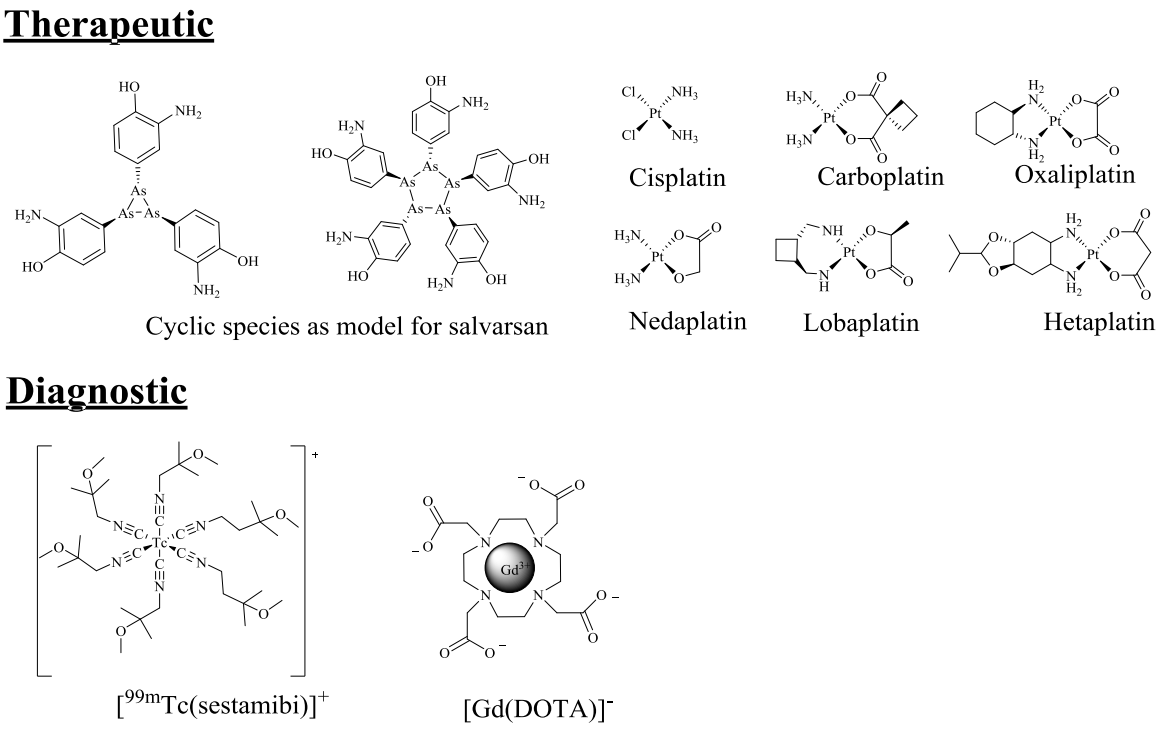

Figure 1. Examples of successful therapeutic and diagnostic metallodrugs.

The applications of various metal centers utilized as therapeutics reaches as far as the imagination of the scientist who envision them. One of the first reported metallodrugs, salvarsan (also known under its working name Ehrlich 606, as it was the 606th compound tested by Ehrlich and colleagues), was reported by German Nobel Laureate Paul Ehrlich in 1912.[10] The compound is an organoarsenic based antimicrobial agent used specifically for the treatment of syphilis (caused by spirochete *Treponema pallidum*). While the origins of the compound can be further traced to Pierre Bechamp in 1863 (famous for the Bechamp process for the production of aniline) the exact composition of the complex remains elusive. It is hypothesized that the compound exists as a mixture of 3-amino-4-hydroxyphenyl-arsenic(III) compounds, however, computational structural models have failed to determine the exact chemical composition.[11] Salvarsan in combination with mercury and bismuth was the standard treatment regime for syphilis until World War II, when it was finally replaced by penicillin. Salvarsan provided an effective demonstration for Ehrlich's belief that it is possible to fight infectious diseases through a systematic search for drugs that kill invading microorganisms without damaging the host, his idea of 'Magic Bullets'.

Table 1. Some metal compounds in clinical use

Compound Example (Brand name)	Function	Comment
Active Complexes		
cis-$[Pt^{II}Cl_2(NH_3)_2$ (cisplatin)	Anti-cancer	*Trans*-isomer inactive
$[Gd^{III}(DTPA)(H_2O)]^{2-}$ (Magnevist)	Extracellular contrast agent for MRI	Low toxicity
$[^{99m}Tc^{I}(CNCH_2C(CH_3)_2OCH_3)_6]^{+}$ (Cardiolite)	Myocardial imaging	Positively charge complex taken up by the heart
Vitamin B_{12}	Coenzyme	Deficiency causes pernicious anemia
Active metals		
Li_2CO_3	Prophylaxis for bipolar disorders	Li forms weak complexes, labile
$[Au^{I}$(thiomalate)] (myocrisin)	Antirheumatoid arthritic	Facile thiol exchange on Au^{I}
Ammonium potassium Bi^{III} citrate (De-Nol)	Antibacterial, antiulcer	Strong binding of Bi to thiols, facile exchange
$Na_2[Fe^{II}(CN)_5(NO)]\cdot 2H_2O$ (Nipride)	Hypotensive	Releases NO, vasodilator
(Bleomycin)	Anticancer	Requires Fe for DNA attack
p-xylyl-bicylam-8HCl (AMD3100)	Anti-HIV, stem cell mobilization	May bind to metals *in vivo*
$CaCO_3$, $Mg(OH)_2$	Antacid	Slow release of alkali
$La_2^{III}(CO_3)_3$ (Fosnol)	Chronic renal failure	Reduces phosphate absorption

CANCER AND CHEMOTHERAPEUTIC AGENTS

Cancer (or neoplasm), is a term used to describe over two hundred diseases which can affect various tissues, organs, and organ systems throughout the body. One hallmark of cancer is the uncontrolled autonomous growth of tissue beyond normal boundaries, which allows for the formation of tumors (neoplasms).[12, 13] There can be two major forms of neoplasms: encapsulated or nonencapsulated. Encapsulated benign tumors facilitate the invasion and destruction of adjacent tissue; whereas nonencapsulated malignant tumors grow rapidly, and spread to various regions of the body and metastasize. These metastases (or secondary growths) are the cause of over 90% of cancer related deaths.[14-16]

Cancer is an incredibly complex disease.[17-20] There is an inherent connection between genotype (characteristics arising from genetic coding) and phenotype (characteristics expressed by the organism) but the correlations are often weak. Genetic abnormalities occur on the way to tumorigenesis as there must be a successive accumulation in mutations in proto-oncogenes and suppressor genes which deregulate the cell cycle. Key events in this progression are single point mutations in the DNA, chromosomal aberrations such as translocations or deletions, and changes that affect chromatin structure such as methylation of DNA or acetylation of histone. The multitude of influential factors in cancer inception and progression make it very difficult to predict its occurrence. Additionally, the presence of highly controversial and highly resistant "cancer stem cells" further compounds the complexity of the disease.[17, 21, 22]

Despite extensive research and various treatment regimens cancer remains among the leading causes of death worldwide and is the 2nd leading cause of death in the U.S.A., with 14.1 million new cases and 8.2 million deaths in 2012 alone.[23-25] In the United States, one in three women and one in two men will develop cancer during their lifetime. Between the 1950s and 2006

the changes in death rates related to major disease in the U.S.A. have dropped considerably, except from those deaths related to cancer. The global burden of disease study commissioned in 1990 (as a collaborative effort between the World Health Organization, Harvard School of Public Health, the University of Auckland, the Institute for Health Metrics and Evaluation, and the World Bank) reported updates in 2004 and 2010 which projects the incidence of cancer death to increase to 12 million by 2030.[26-29]

Cancer Chemotherapy

Common cancer therapies include surgery, radiotherapy, and chemotherapy. Combinations of the three are commonly utilized and are based on the location of the cancer, potential for successful outcome, and various other risk factors.[30, 31] Chemotherapeutic (or neoplastic) drugs aim to selectively kill malignant tumor cells. Current therapies are divided into categories based on their mechanisms of actions and usually include categories such as: alkylating agents, antimetabolites, anthracyclines, plant alkaloids, and topoisomerase inhibitors. Common examples of antimetabolites: mercaptopurine and 5-fluorouracil are DNA base pair analogues which are utilized to enzymatically inhibit DNA replication in acute leukemia and colorectal/pancreatic cancer, respectively.

While there have been significant advances in the development of chemotherapeutic agents, serious problems lies within their narrow margin of safety (i.e., therapeutic index TD_{50}/LD_{50}). The positive effects of the agents are often hindered by nonspecific adverse effects. Nonselective biodistribution often means large doses are required in order to obtain high local concentrations within the tumor cells. The emergence of targeted therapies has drastically reduced these adverse effects. Prodrugs are often administered to improve the selectivity of cancer drugs.[20,

[32] This approach has been utilized extensively by exploiting some of the unique properties of tumor cells such as hypoxia, specific enzymatic profiles, and low pH values.

The emergence of targeted therapies has reduced non-selective effects from chemotherapeutic agents but drug resistance remains a major problem.[33] Even more prevalent today is the emergence of multidrug resistance (MDR), which occurs when cancer cells develop cross-resistance to structurally similar drugs. The pathways and mechanisms that lead to MDR often include drug modification or inactivation (as is the case with cisplatin by glutathione), decreases permeability or increases drug effects by MDR pumps.

The 1965, Rosenburg and coworkers serendipitously discovered the star of the anticancer chemotherapeutic world, cisplatin, (cis-diamine-dichloroplatinum(II), *cis*-$[PtCl_2(NH_3)_2]$) (Platinol), a square planar Pt^{2+} complex.[34] While the complex was first shown to inhibit cell growth in the bacterium *Escherichia coli*, today approximately 50% of all patients undergoing chemotherapy are treated with this alkylating agent. Cisplatin was the first metal based medicinal agent to enter into worldwide clinical trials and gained FDA approval 1978 for the treatment of genitourinary tumors and is generally combined with one or multiple organic anticancer drugs, such as 5-fluorouracil, cyclophosphamide, or gemcitabine.[35-38] After the initial surgical removal of malignant tissue, the patient undergoes cycles of intravenous injections of cisplatin. The mechanism of action has been intensively studied and is facilitated by the diffusion of cisplatin into cells in its chloride form (due to variance in intra- and extra-cellular $[Cl^-]$). The Pt^{2+} of the $[Pt(NH_3)_2(OH_2)Cl]^+$ (obtained following an intracellular aquation event) unit binds covalently to deoxyribonucleic acid (DNA), more specifically, to the N-7 of either guanine (G) or adenine (A) in the dinucleotide sequences GG and AG to form interstrand cross-links and 1,2- or 1,3-intrastrand cross-links.[39] Such cisplatin−DNA adducts, together with cellular pathways activated

in response to cisplatin, lead to expression of p53, replication arrest, transcription inhibition, cell-cycle arrests, DNA repair, and apoptosis.[40]

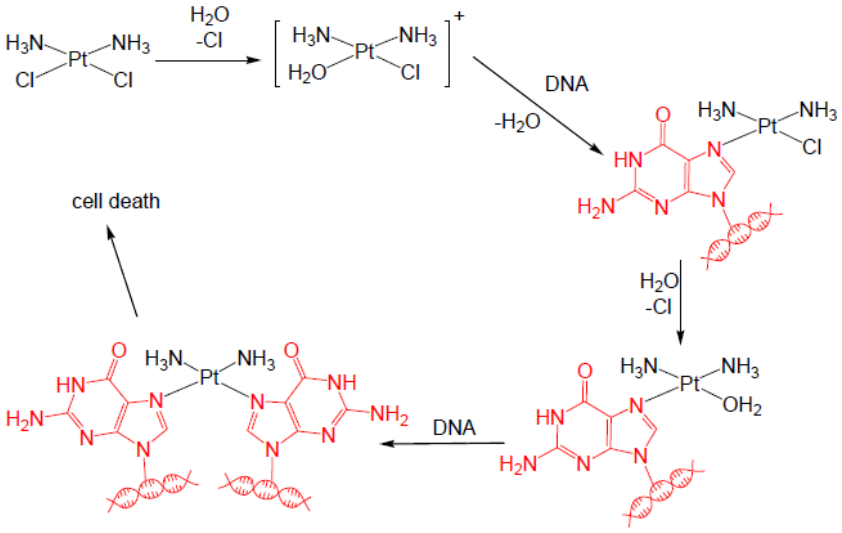

Figure 2. Mechanism of action of cisplatin.

While cisplatin remains one of the most widely prescribed anticancer drugs to date, side effects including nephrotoxicity (kidney poisoning), ototoxicity (loss of high frequency hearing), peripheral neuropathy and the emergence of cisplatin-resistant cancers decrease it effectiveness.[38, 41, 42] As previously stated, MDR resistance to cisplatin is often facilitated by its' inactivation due to glutathione or other sulfur rich proteins. The sulfur groups provide good ligands for coordination to the platinum metal center according to Person's hard/soft acid-base theory, thereby not allowing the complex to reach its intended molecular target. There have also been reports of enhanced levels of other sulfur rich detoxification agents such as metallothioneins in cells which are insensitive to cisplatin.[43, 44] Cisplatin derivatives such as oxaliplatin and carboplatin, work through a similar

DNA damage mechanism but were designed with the focus of lowering the levels of other unwarranted side effects caused by cisplatin.

Metal complexes as chemotherapeutic agents

While small organic molecules have and continue to dominate the pharmaceutical industry, the near number of infinite possible metal-ligand combinations and complexes makes metal-based therapeutic agents an interesting area of study with many potential benefits. Such organic molecules are limited in terms of geometry due to the hybridization of carbon to sp (linear), sp^2 (trigonal-planar) and sp^3 (tetrahedral). Besides these shapes, geometries of pyramidal, triagonal bipyramidal and octahedral can be obtained with metals (higher coordination numbers and geometries with even larger metal ions can also be achieved). Additionally, these higher coordination number and non-limitations to low hybridization options allows for a variety of substituents (ligands), to coordinate around the metal leading to various stereoisomers and stereochemical flexibility.[45] Furthermore, modifications can be made to the ligands to tailor them to a specific function or target.[46] Additionally, most metal-based complexes have been reported to mitigate the side effects of the organic parent molecule (a ligand) while increasing their biological activity.

Despite the earlier report of Ehrlich's chemotherapeutic agent, salvarsan, the discovery of cisplatin is often regarded as the birth of metal based chemotherapy; and ultimately sparked the rise to investigate metal based anticancer agents. Prior to this, it was thought that heavy metals could not be utilized due to their inherent toxicities. One notable exception is Fowler's solution (1% $KAsO_2$), which gave rise to popular arsenotherapies utilized until the late 1950s.[47, 48]

In the 1930s,[49] Collier and Krauss reported the first ever structure activity relationship study on metal complexes, introducing a rationale which stated that: "The effect of a heavy metal on experimental murine cancer is not only due to the metal alone but also to the structure of the compound and the type of compound." This is the single most important concept when it comes to the design of metal based anticancer agents! Take for instance cisplatin, it was first actually described in 1844 by Peyrone as Peyrone's chloride. Initial experiments in the 1960s by Rosenberg and coworkers failed to produce a compound with viable biological activity, until it was discovered that the compound exists in two isomeric forms, *cis* and *trans*. The latter, transplatin is more stable and is inactive. Biological studies conducted after this discovery lead to the confirmation that the active isomer, cisplatin, possessed potent anticancer activity in sarcoma-180 cells.[50, 51] Therefore, the structure of the compound plays a pivotal role on the observed biological activity, and by extension so do the ligands bound to the metal center.

After the booming success of cisplatin, many other metal complexes were quickly investigated for their anticancer potential due to their unique chemical reactivities.[52, 53] The d block metals (transition metals), in particular, have been extensively researched and many have been found to possess good cytotoxic potential. There are many examples of complexes which possess photochemical, anticancer, or both of these activities in a variety of cell lines. These metals offer a variety of coordination geometries which allows for the synthesis of compounds with various stereochemistries that are not obtainable via conventional organic molecules. There are a number of critical factors which can be modified using coordination complexes: geometry, stereochemistry, ligand binding affinity, ligand shapes, counter ions, etc. Given the volume of papers, books, and other records in recent years it is apparent that there has been much effort to

increase the number of therapeutic metal complexes, however, they still remain a minority of all therapeutics on the market to date.

Development of new metal based anticancer agents

Drug discovery is a long multi-stage process which includes: synthesis, characterization, proof of biological activity, as well as pre-clinical and clinical screening. Testing for the biological activity requires intense measurements of the effects *in vitro* (in multiple cancer cell lines) and *in vivo* (in animals). With the majority of successful pharmaceuticals originating in university settings, a large amount of ground work is done in research labs across the world. There are three main strategies to the development of new tumor-inhibiting complexes: (1) synthesis of classical and non-classical derivatives of cisplatin; (2) synthesis of non-platinum based complexes; or (3) synthesis of platinum complexes linked to a carrier system.

The first seems the least attractive as this will lead to drugs with a similar chemistry (and therefore side effects) to that of cisplatin. However, mitigation of some of these side effects can be accomplished as demonstrated by carboplatin and oxaliplatin, respectively. The second approach is perhaps the riskiest (but most attractive) as it seeks to utilize central metal atoms other that platinum. While there are a plethora of transition metals to try, each possesses its own wide range of activity, oxidation state, coordination geometries, and chemical properties which have to be considered. With so many possibilities producing a lead molecule from this group may be difficult but the window for breakthrough is greater. Lastly, linking platinum complexes to carrier molecules has long been known by the concept of drug targeting. Drugs produced from this strategy often have enhanced toxicity toward malignant cells. Even recently, groups continue to

work on this idea by specifically targeting mitochondrial DNA, by utilizing mitochondrial-penetrating sequences covalently bound to cisplatin.[54]

There are two main issues with anticancer drug development: time and variance. With many of the potential leads for pharmaceutical companies coming from individual research labs time is precious. It often take up to 6 years to take one target molecular from conceptualization to conclusion of preclinical trials.[55] Additionally another major problem is the leap between the preclinical *in vitro* and *in vivo* studies to clinical trials. It is at this step that major differences between the animal models utilized begin to differ significantly from the treatment of actual human patient tumors.[56]

NON-PLATINUM BASED CHEMOTHERAPEUTIC AGENTS

Despite the toxicity and side effects of cisplatin and its many derivatives they remained the gold standard in the treatment of many varieties of cancer since FDA approval dating back to 1978. Due to the inherent limits of cisplatin and other platinum based chemotherapeutics there has been extensive research on the use of other metals in medicine. As discussed in previous sections, several other metals including ruthenium, rhenium, and osmium have been investigated as possible chemotherapeutics.

Ruthenium

Ruthenium based compounds have arguably emerged as the best candidates for a viable alternative to platinum-based drugs in cancer therapy. There are three main properties that make ruthenium compounds well suited for medicinal applications: (i) rate of ligand exchange, (ii) the range of accessible oxidation states, and (iii) the ability of ruthenium to mimic iron in binding to

certain biological molecules.[57] Many ruthenium complexes have been evaluated for clinical applications, particularly in the treatment of cancer, due in part, to Ru(II) and Ru(III) complexes having similar ligand exchange kinetics to those of Pt(II) complexes and cellular division rates.[58] Ligand exchange is an important determinant of biological activity, as very few metal-based drugs reach the biological target without being modified.[59]

Ruthenium is unique amongst the platinum group metals in that each of its common oxidation states Ru(II), Ru(III) and Ru(IV) are all readily accessible under physiological conditions. In a biological environment glutathione, ascorbate and single electron transfer proteins can be used to reduce Ru(III) and Ru(IV), while molecular oxygen and cytochrome oxidase readily oxidize Ru(II).[59] In these oxidation states the ruthenium center is predominantly hexacoordinate with octahedral geometry, and Ru(II) complexes tend to be more biologically inert than related Ru(III) and Ru(IV) complexes. Coordinatively saturated and substitutionally inert polypyridyl Ru(II) compounds have cytotoxic effect which are partially attributed to noncovalent interactions with nucleic acids, particularly DNA.[60-62] Recently several studies have shown that other factors such as modification of cell membrane and cell adhesion properties, topoisomerase I and II inhibition,[63] or mitochondrial-mediated apoptosis,[61] could be responsible for cytotoxicity.

The low toxicity of ruthenium drugs is derived from the fact that ruthenium can mimic iron in biological systems. This fact allows it to bind to many biomolecules, including serum transferrin and albumin.[64] These two proteins are used by mammals to solubilize and transport iron; as such ruthenium possesses natural advantages over Pt-based drugs. Since rapidly dividing cells, for example cancer cells, have a greater requirement for iron, they increase the number of transferrin receptors located on their cell surfaces, thereby sequestering more of the circulating metal-loaded transferrin.[65]

Anticancer Ruthenium Agents

The potential anti-cancer activity of ruthenium compounds were first examined by Clarke and co-workers who studied chloro-ammino derivatives of the general formula $[Ru(NH_3)_{6-x}Cl_x]^{Y+}$.[66-68] The compounds were chosen due to similarities with cisplatin to allow for binding of the complexes with nucleic acids. $[Ru^{II}(NH_3)_5Cl]^+$ and its aqua analog $[Ru^{II}(NH_3)_5H_2O]^{2+}$ have been extensively studied and show rapid binding to DNA with an affinity constant of approximately 5000 M^{-1} (Figure 3 a). The hypothesized binding product of the complex with DNA involves substitution of the chloride/aqua ligand and coordination to N^7 nitrogen of guanine in the DNA major groove. Despite strong binding to N^7 of guanine, similar to cisplatin, penta-ammineruthenium complexes do not show efficient anti-cancer activity. In contrast, *cis*-$[Ru^{III}(NH_3)_4Cl_2]^+$ and *fac*-$[Ru^{III}(NH_3)_3Cl_3]$ shown in figure 3 B and C, respectively, have been tested against multiple tumor cells and show comparable *in vivo* activity to cisplatin.[69-71] Clarke and co-workers have rationalized that the *in vivo* tumor environment reduces the inactive Ru(III) complex to the corresponding active Ru(II) drug which is able to substitute its chlorido ligands much more rapidly and bind to DNA.[72] Unfortunately many of these complexes are far too insoluble for pharmaceutical use.[70]

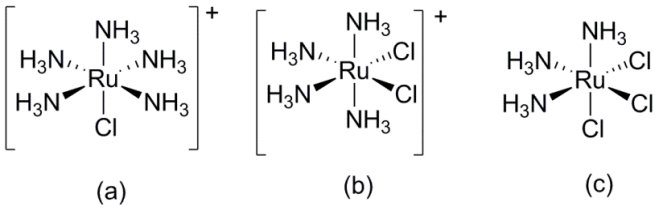

Figure 3. Some chloro-ammino ruthenium derivatives. (a) $[Ru^{II}(NH_3)_5Cl]^+$, (b) *cis*-$[Ru^{III}(NH_3)_4Cl_2]^+$, (c) *fac*-$[Ru^{III}(NH_3)_3Cl_3]$

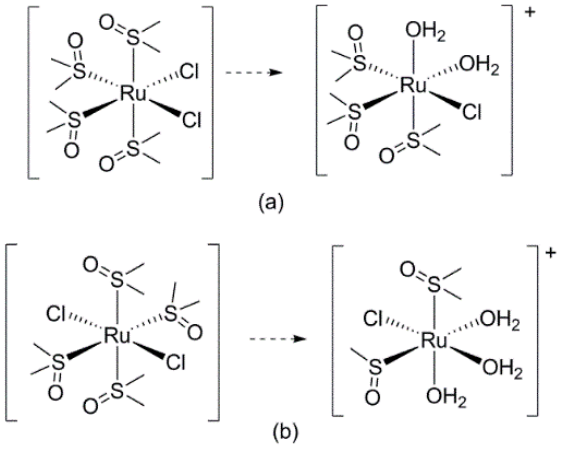

Figure 4. Dimethyl-sulfoxide containing ruthenium complexes. (a) *cis*-[$Ru^{II}(DMSO)_4Cl_2$] and the corresponding aqua species, (b) *trans*-[$Ru^{II}(DMSO)_4Cl_2$] and the corresponding aqua species.

The initial solubility issues can be highly improved by coordinating a DMSO molecule as opposed to the previously utilized NH_3 ligands as shown in figure 4. Mestroni, Alessio and co-workers conducted *in vitro* and *in vivo* studies on *cis*- and *trans*-[$Ru^{II}(DMSO)_4Cl_2$] complexes.[73] Monoadduct formation was observed for the *cis*-isomer, whereas the *trans*-complex, similar to cisplatin, showed the ability to form DNA biadducts leading to both intra- and inter-strand cross-links.[73] Both isomers coordinate the N^7 position of guanine residues in DNA, however the *trans* isomer has been shown bind more rapidly and is almost sixteen (16) times more active than the *cis* isomer in P388 leukemia cells.[74] The encouraging results obtained with *trans*-[$Ru^{II}(DMSO)_4Cl_2$] are at the epicenter of the search for other *trans*-DMSO ruthenium complexes as anti-cancer agents. Na[*trans*-[$Ru^{III}(DMSO)(Im)Cl_4$]] (where Im = imidazole) (NAMI) and its imidazolium salt NAMI-A represents the greatest achievements in this area as it was the first Ru compound to enter clinic trials in 2000, and has since entered phase II clinical trials.[75] NAMI-A is practically

noncytotoxic in common cancer cell lines but has turned out to be a specifically anti-metastatic drug. The mechanism by which NAMI-A exerts its anti-metastatic activity is not yet completely elucidated. As with many other ruthenium complexes it is thought that both of its chlorido ligands are lost though aquation before it binds with biomolecules such as DNA. NAMI inhibits the actions of DNA and RNA polymerases, but does not form significant DNA interstrand cross-linking.[76] Thus, it is hypothesized that the anti-metastatic activity of NAMI arises from a mechanism different than that of cisplatin, such as protein-DNA cross-links.[77]

Scheme 1. Structural representation of KP1019 and NAMI-A.

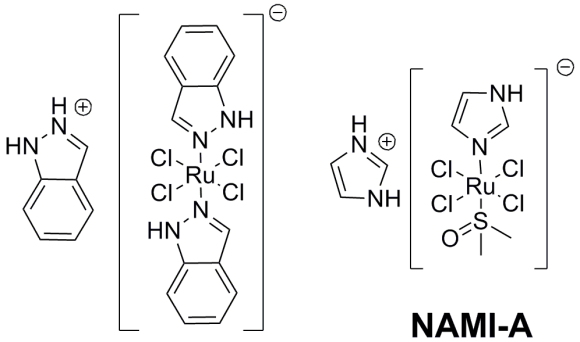

KP1019 (*trans*-[tetrachlorobis(1*H*-indazole)ruthenate(III) was the second Ru complex to enter clinical trials in 2003 and represents one of the most successful complexes in terms of anticancer ruthenium complexes as it reduces tumor sizes in rats and triggers apoptosis *in vitro*.[78] Despites KP1019s success, its mechanism of action remains up for debate. For example, KP1019 has been shown to bind transferrin, and transferrin receptor-mediated endocytosis has been implicated as a mechanism of drug internalization.[79, 80] However, drug uptake occurs in the absence of KP1019-loaded transferrin, suggesting other mode of internalization.[80] Furthermore, the

mechanism by which the drug exits the endosomes and gains access to intracellular targets remains unclear.

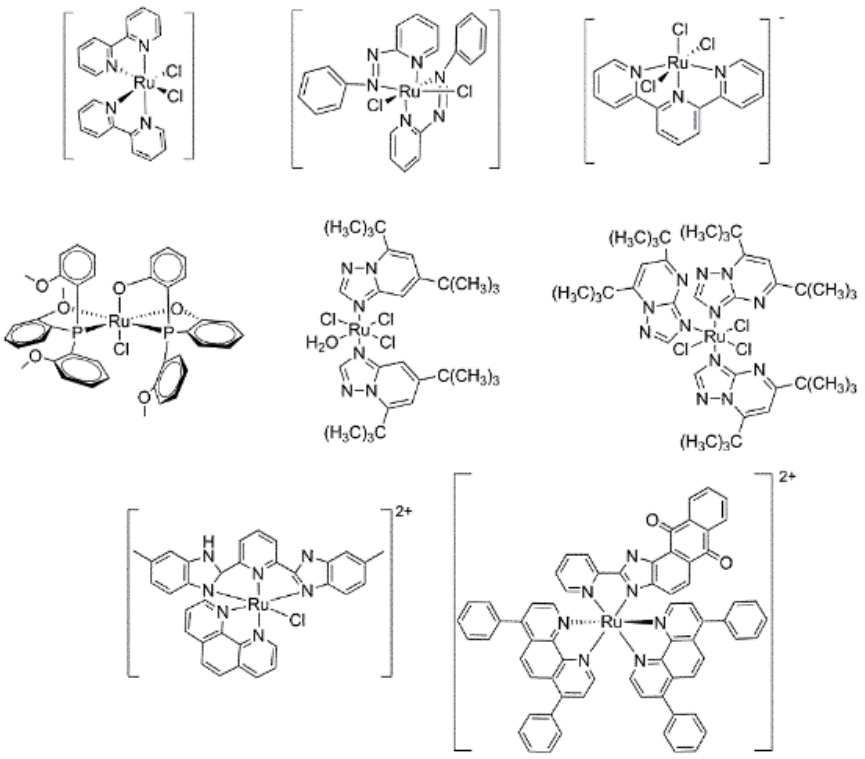

Figure 5. Ruthenium complexes with chloride and/or heterocyclic ligands.

While ruthenium complexes with coordinated chloride ligands served as a strong starting point, additional and extensive research has focused on the coordination of polypyridyl ligands to the ruthenium metal center. The first report by Dwyer and co-workers in the early 1950s,[81-83] showed a family of tris(polypyridyl) complexes had bacteriostatic and antiviral activities (in some instances, the growth of Gram-positive bacteria was inhibited at a concentration of 1 mM for $[Ru(phen)_3](ClO_4)_2$ (where phen = 1,10 phenanthroline).[81] Figure 5 shows a few examples of such Ru(II) complexes of the type *cis*-$[Ru^{II}(L)_2Cl_2]$ (where L = any bidentate heteroaromatic ligand)

that have been prepared and are being investigated for their anti-tumor properties. One of the first studied complexes *cis*-$[Ru^{II}(bpy)_2Cl_2]$ (where bpy = 2,2'-bipyridine) has been tested against many cell lines but is mostly inactive as an anti-tumor agent.[84] In contrast, Reedijk and co-workers have shown that one isomer of *cis*-$[Ru^{II}(azpy)_2Cl_2]$ (where azpy = 2-phenylazopyridine) exhibits high toxicity comparable to that of cisplatin against a series of cell lines.[84-86] Barbec and co-workers reported high cytotoxicity comparable to that of cisplatin and carboplatin with their complex *mer*-$[Ru^{II}(tpy)Cl_3]^-$ which contains a tridentate terpyridine ligand.[87] This complex similar to cisplatin was shown to form a high number of interstand cross-links.[87] Bouwan and co-workers have shown a novel complex $[Ru^{III}(PAn_3)P(An)(phenolate)_2Cl]$ shows toxicity similar to cisplatin, and enhanced toxicity in cisplatin-resistant cell lines.[88] Tan *et al*.[89] reported a series of ruthenium-norharman complexes which are highly cytotoxic to a variety of cancer cell lines with IC_{50} values well below those of cisplatin and NAMI-A. Lakomska *et al*.[90] have developed two Ru(III) complexes based on triazolopyrimidine ligands. The bulky substituents in the heterocyclic ligands significantly enhance the cytotoxicity of both complexes which is attributed to high lipophilicity which facilitates high cellular uptake. Both show much higher cytotoxicity than cisplatin against human lung carcinoma A-549 and T47D breast carcinoma cell lines with IC_{50} values in the range of 0.02-2.4 μM.[90]

Arenes are known to stabilize ruthenium(II) complexes and provides a hydrophobic face which may facilitate biomoelcular recognition and transportation of ruthenium through cell membranes; thus the potential uses of ruthenium-arene complexes are gaining much attention in literature.[91-95] The "half-sandwich" Ru(II) mono-arene complexes often possess good aqueous stability and the arene ligand is relatively inert towards displacement under physiological conditions. Following the entrance of an organometallic titanium(IV) complex (titanocene

dichloride $[Ti(Cp)_2Cl_2]$ Cp = η^5-C_5H_5) into clinical trials as an anticancer drug, Dyson and his co-workers have conducted much work on ruthenium-arene complexes specifically as it related to highly cytotoxic RAPTA (Ruthenium Arene PTA) complexes, $[(\eta^6\text{-arene})Ru(pta)(Cl)_2]$ (where pta = 1,3,5-triaza-7-phosphatricyclo[3.3.1.13.7]decane) (Figure 6).[96-98] Protonation of pta ligands influences the solubility properties of the complex and at physiological pH environments the predominant species carries no charge and can thus be easily transported across the lipid membrane and move freely into and within the cells.[96]

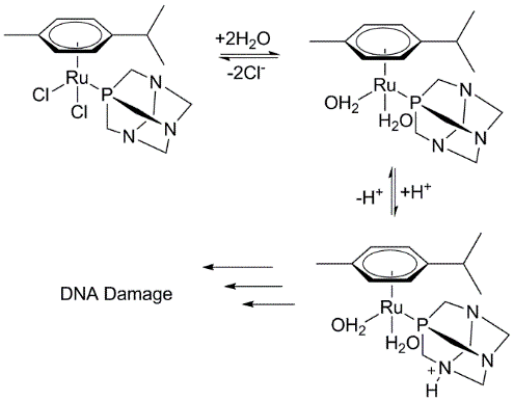

Figure 6. Aquation and protonation of RAPTA-C complex prior to DNA damage. Adapted from Scolaro *et al*.[98]

The RAPTA complexes have been extensively studied since their inception and interestingly in gel shift assays it selectively binds to DNA at pH values close to or lower than its pK_a value.[98] The attractiveness of this series of complexes is that they select target cells which possess metabolic activity, similar to those associated with increase or accelerated cell division. *In vivo* biological screening of a series of nine complexes of the generic formula $[(\eta^6\text{-arene})Ru(pta)(Cl)_2]$ (arene = *p*-cymene, toluene, benzene, benzo-15-crown-5, 1-ethylbenzene-2,3-

dimethylimidazolium tetrafluoroborate, ethyl benzene, hexamethylbezene) synthesized by Dyson *et al.*[98] failed to produce a complex with IC_{50} comparable to cisplatin, however [(η^6-arene)Ru(pta)$(Cl)_2$] did reduce the number and weight of metastasis cells similar to NAMI-A with a higher system clearance rate.[98] A related compound prepared by Maysinger and co-workers showed the synergistic effect which can be obtained from pairing a ruthenium(II)-arene complex with a known chemotherapeutic agent: letrozole. The ruthenium(II)-letrozole complex, shown in figure 7, was shown to exhibit significantly higher activity towards cancer cells line when compared with compounds analogous to RAPTA-C (a ruthenium drug presently in pre-clinical trials).[99]

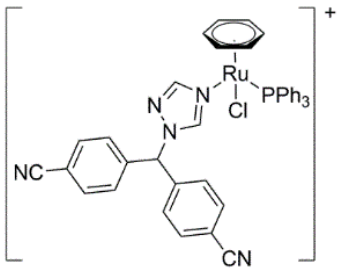

Figure 7. Ruthenium-letrozole complex as by Castonguay *et al.*[99]

Sadler and co-workers have also conducted extensive work on ruthenium-arene complexes for similar applications. Cytotoxicities obtained for a series of complexes with the generic formula [(η^6-arene)Ru(en)(Cl)]$^+$ indicated that the cytotoxic behavior increased as a function of the size of the coordinated arene (benzene < *p*-cymene < biphenyl < dihydroanthracene < tetrahydroanthracene), such that in wild and cisplatin resistant A2780 human ovarian cancer cells, the biphenyl complex showed similar toxicity to carboplatin and the tetrahydroanthracene complex showed similar toxicity to cisplatin.[100] Structure activity studies with these compounds indicated

that single ligand exchange (presence of bidentate ligand) facilitates high cytotoxicity. Binding studies indicate the formation of monoadducts with N^7 of guanine similar to results observed with other ruthenium complexes.[100, 101]

Beckford and co-workers are conducting work in the synthesis of ruthenium-arene complexes containing thiosemicarbazone (TSC) ligands.[102, 103] TSCs possess a broad range of medicinal application including antitumor, antibacterial, and antiviral properties all of which can be modified and enhanced by coordination to a metal ion. A series of complexes as shown in figure 9 of the general formula [(η^6-p-cymene)Ru(TSC)(Cl)]Cl were recently reported and their biological properties were studied.[102, 103] Studies indicate *in vitro* activity as anticancer agents against human colon cancer cell lines, with a moderate DNA interaction. Complexes showed comparable anticancer activity to cisplatin and other similar ruthenium-arene complexes currently under investigation; however, no complex provided activity similar to etoposide (an anticancer drug belonging to the topoisomerase inhibitor class). Two of the complexes ([(η^6-*p*-cymene)Ru(pEtTSC)Cl]Cl and [(η^6-*p*-cymene)Ru(pPhTSC)Cl]Cl showed a modest capability of inhibiting topoisomerase II enzymes at low concentrations which may still give these complexes applications in anticancer drug development.[103] This highlights the ability of Ru(II)-complexes to increase the bioactivity of parent ligands, while increasing bioavailability.

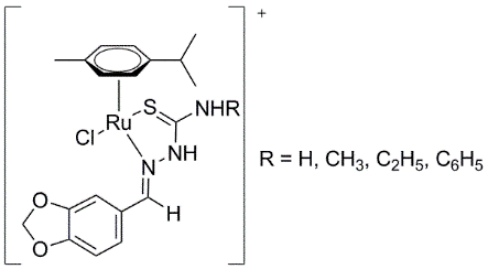

Figure 8. Structure of arene ruthenium(II)-TSC complexes.[103]

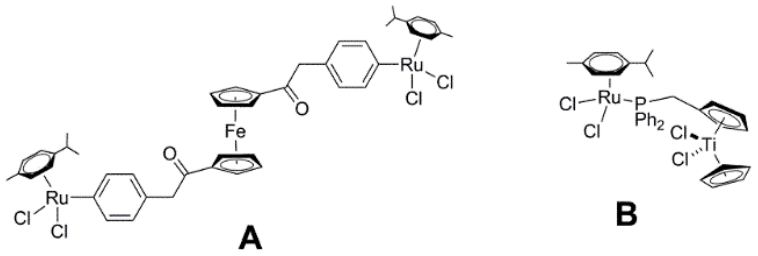

Figure 9. Heteronuclear arene ruthenium complexes containing a ferrocene (A) and titanocene (B) moiety.

Similar to binuclear and multinuclear ruthenium complexes, strategies have been employed in synthesizing multinuclear and heteronuclear ruthenium-arene complexes which modify the mode of action of the metal based drug. Two heteronuclear complexes containing ruthenium(II)-arenes with ferrocene and titanocene were recently prepared and are shown in in figure 10.[104, 105] *In vitro* studies demonstrate the cytotoxicities correlate with the lipophilicity and water solubility of the complexes similar to other ruthenium(II) complexes. Dinuclear, trinuclear, tetranuclear, hexanuclear, and octanuclear systems can all be found in literature, with each system showing a different level of activity and degree of selectivity towards certain cancer cell lines. Dinuclear complexes containing pyridone linkers have provided insight into the correlation present between the spacer length and cytotoxicity (Figure 10 A),[106, 107] while the thiophenolato-bridged *p*-cymene ruthenium complex $[(p^{i}PrC_6H_4Me)_2Ru_2(\mu_2SC_6H_5)_3]Cl$ shows activity against human ovarian cancer cell lines in the nanomolar range (Figure 10 B).[108] A dinuclear (η^6-arene)ruthenium(II) benzaldehyde TSC complex as shown in figure 10 C was shown to exhibit moderate *in vitro* activity (IC_{50} = 9 μM) against oesophageal cancer cells.[109]

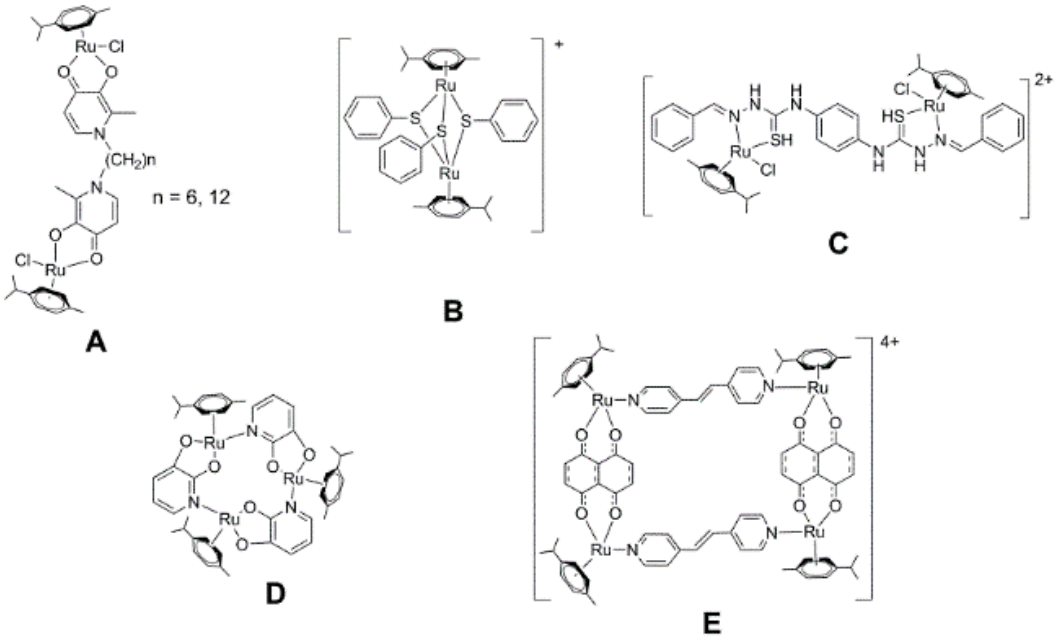

Figure 10. Selected example of multinuclear arene ruthenium complexes. Bridging ligands include: pyridone (A),[106, 107] thiophenolato (B),[108] thiosemicarbazone (C),[109] Trinuclear metalla-cycle (D),[110] tetranuclear arene ruthenium complex (E).[111]

More complex ruthenium containing metallocycles, such as those shown in figure 10 D, have also been investigated for their anticancer potential.[110] The tri-ruthenium metallocycle remains stable under neutral pH, however under the reduced pH environment within cancer cells the trimeric structure is converted to the activated monomeric species.[110] Rectangular shaped metalla-cycles of the general formula $[(arene)_4Ru_4(ox)_2(N\text{-}N)_2]^{4+}$ as shown in figure 10 E (arene = p-cymene, hexamethylbenzene; ox = oxalato, oxamido, 1,4-benzoquinonato-2,5-dilato, 3,6-dichloro-1,4-benzoquinonato; N-N = pyrazine, 4,4'-bipyridine, 1,2-bis(pyridyl)ethylene, 1,2-bis(4-pyridyl)ethane) have been tested against multiple cancer cell lines.[111] The activity of these metal-cycles against normal and cisplatin resistant ovarian cancer cell lines indicate moderate to

excellent activity, depending on the size of the linker utilized, in some cases IC_{50} values as low as 4 μM were obtained. Similarly, metalla-assemblies containing polypyridyl-porphyrin derivatives and dinuclear ruthenium complexes have been reported.[112]

Ruthenium photodynamic therapeutic agents

One of the other major themes in the evolving world of ruthenium chemotherapeutics is the utilization of polypyridyl ligand architectures for photodynamic therapy (PDT).[113, 114] Due to the attractive photophysical properties and site specific DNA binding, much research has focused on these complexes. As the rules that govern the cellular uptake and cellular localization of these systems are determined numerous applications ranging from cellular imaging to therapeutics are rising.[58, 115]

Polyazaaromatic ruthenium(II) complexes are generally well suited for use as photosensitizers and are an integral portion of PDT.[116] The properties of such complexes can be varied by varying the ligands chelated to the metal center as shown by their different photophysical and photochemical behaviors in the presence and absence of DNA.[116] Ruthenium(II) complexes are capable of interacting with DNA forming three distinct interaction geometries: (1) the complex be can externally associated in the electrostatic environment of the DNA double helix, (2) it can be absorbed into the DNA grooves, or (3) it can intercalate between two DNA bases pairs via one of its ligands. Barton *et al.*[117] have confirmed many of these binding modes showing $[Ru(bpy)_3]^{2+}$ shows a weak interaction with DNA either by intercalation or electrostatic interaction; while in contrast $[Ru(phen)_3]^{2+}$ and $[Ru(DIP)_3]^{2+}$ (where DIP = 4,7-diphenyl-1,10-phenanthroline) show strong affinity for DNA.

Hundreds of molecules have already been shown to photosensitize singlet oxygen production, many of which are polypyridyl Ru(II) complexes due to their large absorbance spectra and long excited-state lifetimes. Barton *et al.*[117] have shown excitation of $[Ru^{II}(bpy)_3]^{2+}$, $[Ru^{II}(phen)_3]^{2+}$, $[Ru^{II}(DIP)_3]^{2+}$ shown in figure 11, induces the production of singlet oxygen and DNA single strand breaks.[117] High quantum yields of singlet oxygen productions from (0.1 to 1.0 depending on the complex and solvent) have been determined for a variety of Ru(II) complexes.[118] Photoinduced ligand substitution is also possible whereby a metal complex would either release a biologically active molecule or bind to nucleic acids or protein active sites.

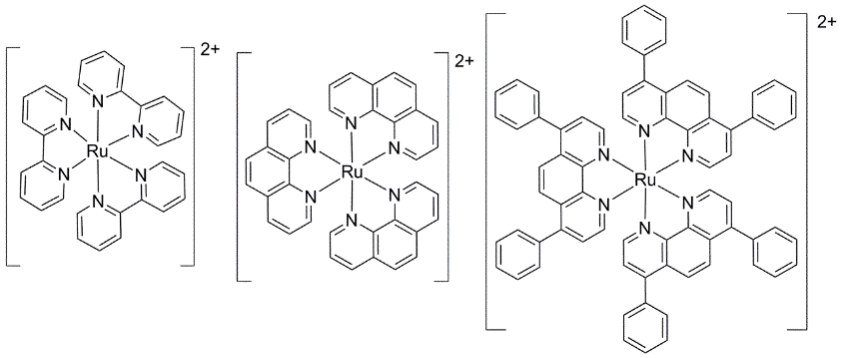

Figure 11. $[Ru^{II}(bpy)_3]^{2+}$, $[Ru^{II}(phen)_3]^{2+}$, and $[Ru^{II}(DIP)_3]^{2+}$

Improving the selectivity of anticancer drugs towards cancer cells is the main goal of drug optimization; thus a prodrug strategy offers significant promise. Light-triggered prodrugs provide an efficient approach for controlling the localization of cytotoxicity. One example of this concept of localized activation was reported by Gasser and co-workers using, $[Ru(dppz)_2(CppH)]^{2+}$ (where CppH=2-(2-pyridyl)pyrimidine-4-carboxylic acid). The complex localized with the mitochondria of cells and shows similar inhibitor activity to cisplatin,[119] and greater activity in cisplatin resistant

cells. A photolabile functionality, 3-(4,5-dimethoxy-2-nitrophenyl)-2-butyl ester (DMNPB), makes the active $[Ru(dppz)_2(CppH)]^{2+}$ (where dppz = dipyrido[3,2-a:2',3'-c]phenazine) moiety within $[Ru(dppz)_2(Cpp\text{-}ODMPNB)]^{2+}$ innocuous to both cancerous (HeLa and U2OS) and non-cancerous (MRC-5) cells (IC_{50} > 100 μM).[120] Irradiation at 350 nm releases the photolabile DMNPB ester forming the active complex $[Ru(dppz)_2(CppH)]^{2+}$ as shown in figure 12 below. IC_{50} values obtained before irradiation (> 100 μM) indicate nontoxic behavior of the complexes containing the DMNPB ester; while after irradiation values (17.5 and 17.2 μM) are comparable with those of cisplatin 12.0 and 32.6 μM in HeLa and U2OS, respectively.[120] Though still in the prototype stage, light triggered prodrugs hold potential for designing sophisticated properties well-suited for controllable cytotoxic action under physiological conditions.

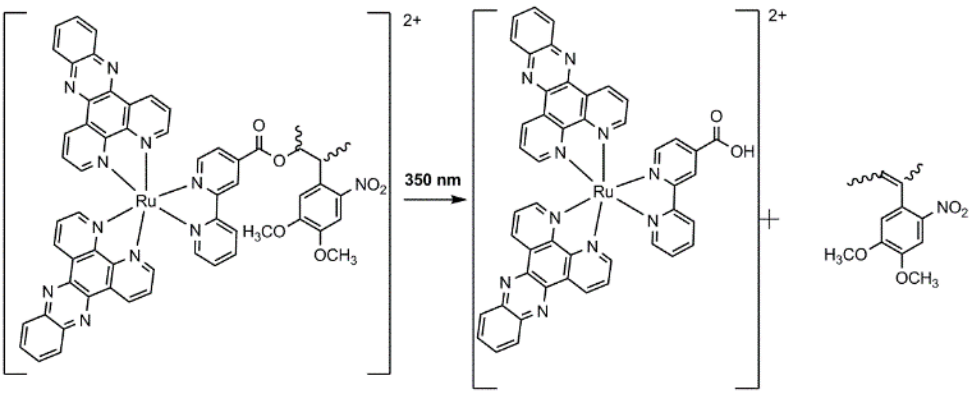

Figure 12. Photocleavage of DMNPB ester moiety to form active $[Ru(dppz)_2(CppH)]^{2+}$.[120]

As the search for adequate PDT agents continues to evolve the systems being utilized are also constantly evolving. The above discussion describes examples of systems containing mononuclear/multinuclear ruthenium complexes and some PDT-active complexes.[121-124] Dinuclear complexes certainly offer increased variation in shape and size and have the potential

to show greater specificity, however their applications as potential DNA-binding agents remains largely unexplored. Mixed metal dinuclear complexes offer even more advantages over ruthenium-ruthenium dinuclear complexes as the second metal utilized may possess its own biological application making for dual-application complexes or enhanced biological function. Sakai and co-workers have tethered a tris(bpy)ruthenium(II) derivative to a *cis*-$PtCl_2(amine)_2$ moiety to incorporate a known DNA intercalating unit with a known DNA binding unit.[125] The complex $[\{Ru(bpy)_2\mu\text{-}bpy(CONH(CH_2)_3NH_2)_2\}PtCl_2](PF_6)_2\cdot 3H_2O$ shows efficient cleavage of PBR322 DNA to nicked and linearized forms only following irradiation ($\lambda_{irr} = 470 \pm 10$ nm) at atmospheric conditions.[125] Liang *et al*.[126] reported biological application of $[(phen)_2Ru(bpibH_2)Co(phen)_2](ClO_4)_5\cdot 2H_2O$ (where $bpibH_2$ = 1,4-bis([1,10]phebanthroline-[5,6-d]imidazol-2-yl)-benzene) which includes Ru(II)-Co(III) metal centers. During this present study the system does not show cytotoxic behavior comparable to cisplatin, however, information from this study can enhance the understanding of the mechanism for the binding of metal polypyridyl complexes to nucleic acid.[126]

Holder *et al*.[127] reported the synthesis, characterization and biological properties of two ruthenium(II)-vanadium(IV) complexes: $[Ru(pbt)_2(tpphz)VO(sal\text{-}L\text{-}tryp)](PF_6)_2\cdot 6H_2O$ (where pbt = 2-(2'-pyridyl)benzothiazole), tpphz = tetrapyrido[3,2-a:2‘,3‘-c:3‘‘,2‘‘-h:2‘‘‘,3‘‘‘-j]phenazine , and sal-*L*-tryp = N-salicylidene-L-tryptophanate) and $[Ru(pbt)_2(phen_2DTT)VO(sal\text{-}L\text{-}tryp)](PF_6)_2\cdot 5H_2O$ (where phen2DTT = 1,4-bis(1,10-phenanthrolin-5-ylsulfanyl)butane-2,3-diol), the structures of which are shown in figure 13.[237] Biological screenings showed the monomer $[VO(sal\text{-}L\text{-}tryp)(phen)]\cdot H_2O$ and $[Ru(pbt)_2(tpphz)VO(sal\text{-}L\text{-}tryp)]Cl_2$ were the most active against A431 carcinoma cells with IC_{50} values comparable to those obtained for cisplatin as shown in table 2, while showing significantly less toxicity to non-cancerous HFF (human foreskin fibroblast).

This qualitative study gives indication that mixed-metal ruthenium(II)-vanadium(IV) complexes may be good PDT agents.

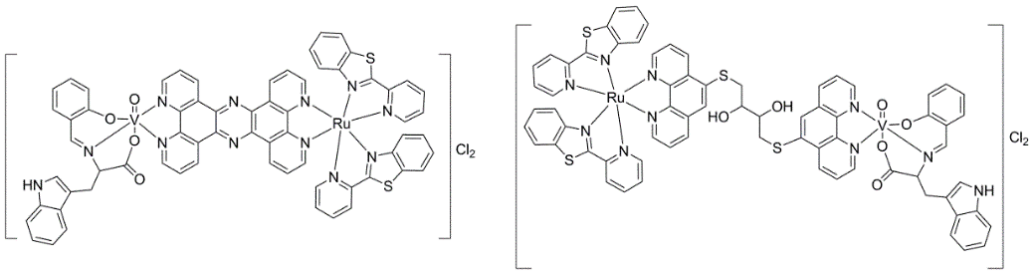

Figure 13. $[Ru(pbt)_2(tpphz)VO(sal\text{-}L\text{-}tryp)]Cl_2$ and $[Ru(pbt)_2(phen_2DTT)VO(sal\text{-}L\text{-}tryp)]Cl_2$.[127]

Table 2. Anti-proliferative data obtained from complexes by Holder *et al*. Data expresses as IC_{50} value in μM. (Reprinted with permission)[127]

	IC_{50} / [μM]	
Species	A431	HFF
$[Ru(pbt)_2(tpphz)VO(sal\text{-}L\text{-}tryp)]Cl_2$	41.3 ± 7.6	100.7 ± 17.7
$[Ru(pbt)_2(phen_2DTT)VO(sal\text{-}L\text{-}tryp)]Cl_2$	48.6 ± 13.1	41.3 ± 7.6
$[VO(sal\text{-}L\text{-}tryp)(phen)]\cdot H_2O$	41.3 ± 7.6	41.3 ± 7.6
Cisplatin	41.3 ± 7.6	41.3 ± 7.6

Arguably one of the greatest contributors to the field of mixed-metal Ru(II)-PDT agents, Karen Brewer, has reported multiple supramolecular complexes, which possess at least two Ru(II) metal centers and one Pt(II) binding site. In a landmark report, $[\{bpy)_2Ru(dpp)\}_2Ru(dpp)PtCl_2](PF_6)_6$ (shown below), was shown to cleave DNA in the absence

of molecular oxygen, thereby showing singlet oxygen generation to not be the only method of facilitating DNA damage. This discovery, along with subsequent investigations has lead the convention of both type I and type II PS.[128]

Scheme 2. $[\{bpy)_2Ru(dpp)\}_2Ru(dpp)PtCl_2]^{6+}$ as by Brewer and co-workers.[128]

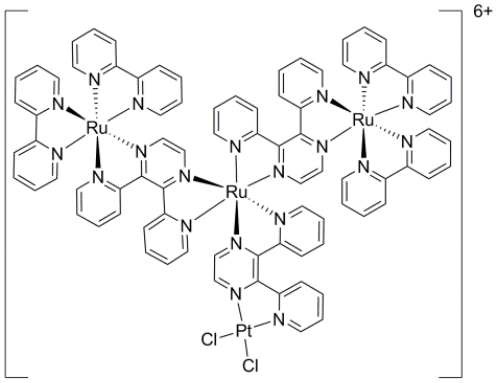

Utilizing known drug molecules, such as Ru(II) incorporating chloride ligands, is often a good starting point for the development of novel drugs. In a similar fashion much research in PDT-Ru(II) PS development has focused on mimicking Photofrin. Photofrin, a FDA approved porphyrin-based photosensitizer,[129, 130] has been shown to generate singlet oxygen through an energy transfer upon photoexcitation in the visible region causing cell death. While photoexcitation leads to cell death, Photofrin also suffers from dark toxicity and purification difficulties, thus it is imperative to find alternatives to eliminate negative attributes.[130] Masico first reported on the use of tetraruthenated porphyrins as potential photosensitizers for photodynamic therapy in the late 1990s.[131] Polypyridyl ruthenium(II) substituents covalently linked to porphyrins offer enhanced water solubility while maintaining the intercalation properties of the ruthenium metal center.[132, 133] Swavey and co-workers have combined the properties of fluorinated porphyins with those of ruthenium polypyridyl complexes to create highly active photosensitizers for use in

photodynamic therapy. An example structure is shown below of a ruthenium porphyrin complex [*cis*-H_2(DPDPFPP)Ru_2(bpy)$_4Cl_2(PF_6)_2$] (where DPDPFPP = 5,15-(4-pyridyl)-10,20-(pentafluorophenyl)porphyrin), exhibits the ability to bind and photocleave supercoiled DNA when irradiated with low-energy light.[134] Cell studies indicate a low dark toxicity of the complex towards both melanoma and normal cells, however, under visible light melanoma cells reveal extensive apoptosis.[134]

Scheme 3. Example ruthenium-porphyrin complex

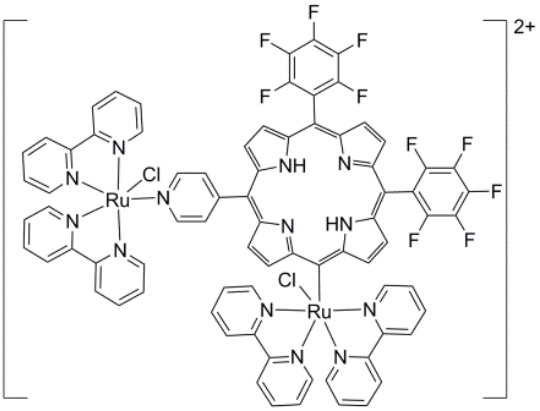

In another study a new porphyrin 5,15-(4-pyridyl)-10,20-(pentafluorophenyl)porphyrin (H_2DPDPFPP) and its diruthenium(II) analogue ([*trans*-H_2(DPDPFPP)Ru_2(bpy)$_4Cl_2(PF_6)_2$]) were examined for their interaction with linearized pUC18 plasmid (Figure 14).[135] Gel electrophoresis studies showed interactions between the metallated porphyrin and DNA which was confirmed by UV-visible spectroscopic titrations with CTDNA which resulted in a binding constant of 10^5 M^{-1}.[135] More recent studies by Swavey and co-workers have found that multi-nuclear porphyrin systems behavior similarly.

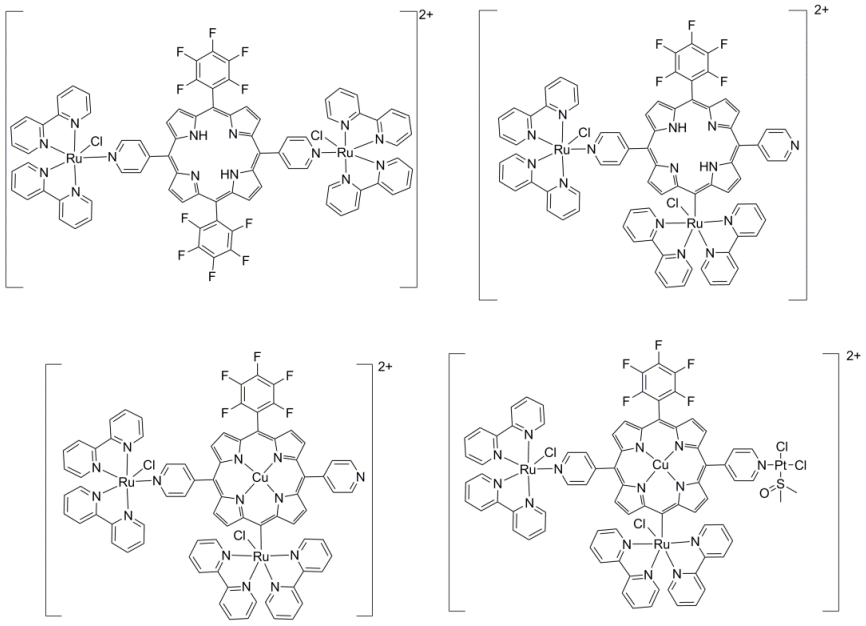

Figure 14. Structure of metallophorphyrin complexes as by Swavey and co-workers.[135, 136]

As with conventional ruthenium complexes, arenes stabilizing face caps have also found applications in porphyrin based Ru-PDT systems. Dyson and co-workers recently reported the first conjugation between a porphyrin and arene-ruthenium system and evaluated its biological applications in against human melanoma cells.[137] Five 5,10,15,20-tetra(4-pyridyl)porphyrin (TPP) areneruthenium(II) derivatives were prepared and characterized as potential photosensitizing chemotherapeutic agents as shown in figure 15. Cellular uptake and localization microscopy studies of $[Ru_4\text{-}(\eta^6\text{-}C_6H_5CH_3)_4(TPP)Cl_8]$ and $[Rh_4(\eta^5\text{-}C_5Me_5)_4(TPP)Cl_8]$ revealed that they accumulated in the melanoma cell cytoplasm in granular structures different from lysosomes. Thus, the porphyrin arene-ruthenium(II) derivatives represent a promising new class of organometallic photosensitizers able to combine chemotherapeutic activity with the photodynamic therapeutic treatment of cancer.[137]

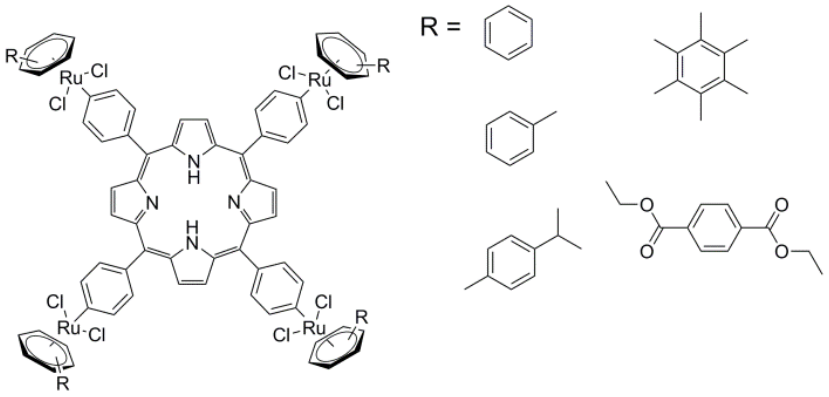

Figure 15. 5,10,15,20-tetra(4-pyridyl)porphyrin (TPP) arene-ruthenium(II) complex prepared by Dyson and coworkers.[137]

Cobalt

Cobalt is an essential trace element found in all animal species. It is one of the most important trace metals and in the form of vitamin B_{12} (cobalamin) the metal plays a number of critical roles in multiple biological functions including DNA synthesis, formations of red blood cells, maintenance of the nervous system, and in growth and development.[138] The metal also plays a role in a least eight cobalt dependent proteins. Within cobalamin, cobalt exists in the +1 oxidation state (although it can undergo oxidation to the +2 and +3 states) and adopts an octahedral geometry. The cobalt(I) ion is equatorially coordinated to four nitrogen atoms of a corrin ring, and axially to 5.6-dimethylbenzimidazoled and either cyanide, hydroxide, methyl, or 5'-deoxyadenosy groups.[139] The cobalamins themselves are utilized as pharmaceutical agents in the treatment of hypocobalaminemia.[140]

Despite their well-known versatility, cobalt derivatives have not been explored extensively as inorganic pharmaceuticals as compared with other metals, possibly due to their natural

genotoxic and mutagenic rates at high concentrations. In fact the most significant medical advancement in terms of cobalt compounds is the clinical development of Doxovir (CTC-96) for Herpes labialis (or herpes simplex virus 1).[141] The first reported bioactive complexes were reported in the 1950s,[142] and since then there has been significant interest in cobalt(III) complexes of bidentate mustards,[143, 144] which appear to act selectively on hypoxic tumor cells. Interestingly, these complexes show activity against leukemia and lymphoma cells as well as various bacterial strains. Cobalt complexes are also reported to possess various other activities including insulin-mimetic properties, antifungal, and antioxidant activity.[145, 146]

Cobalt Anticancer Agents

Given the prominent role of cobalt in biological processes, humans have evolved mechanisms to overcome cobalt overload. Due to this fact, cobalt is viewed as less toxic to humans than non-essential metals such as platinum. This fact has prompted many researchers to investigate cobalt-containing compounds as less toxic alternatives to platinum-based anticancer drugs. The first biological study of these complexes was conducted by Dwyer et al.[147] in the 1950s. The toxicity of tris-acetylacetane cobalt(III), tris-ethylenediamine cobalt(III) nitrate isomers, 1,8-bis(salicylideneamino)-3-,6-dithiaocatance cobalt(III) chloride, 1,10-bis(salicyclindeneamino)-4,7-dithiadecane cobalt(III) iodide, and tris-glycine cobalt(III) were investigated in mice after intraperitoneal injection (shown in figure 16). The doses required to induce death were reasonably high for all cobalt complexes tested (ranging from 75-165 mg kg^{-1}), highlighting the low systemic toxicity of cobalt. While the anticancer properties of these complexes were never investigated these studies did contribute to the realization that cobalt-containing complexes possess vast biological potential.[145, 146, 148]

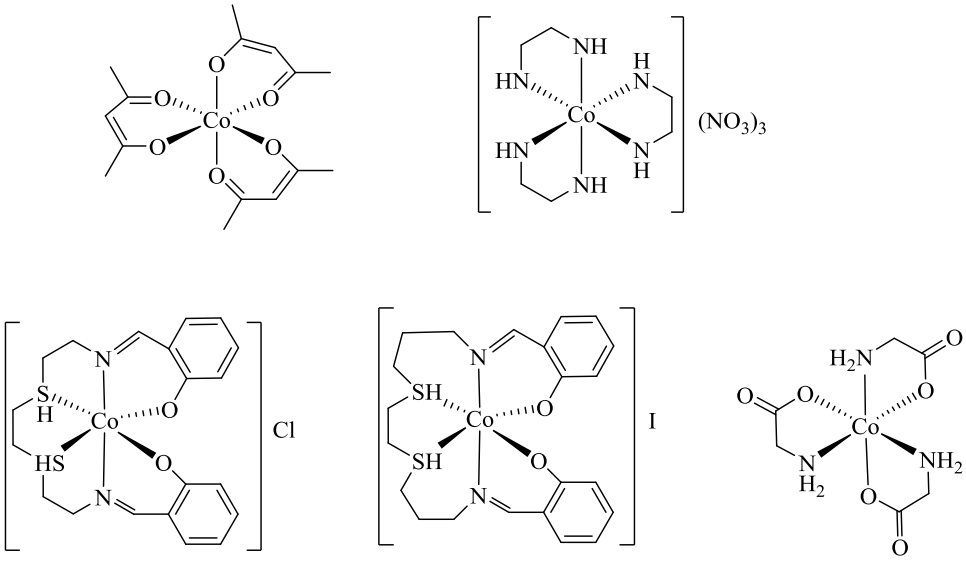

Figure 16. Chemical structures of cobalt(III) coordination complexes used in early biological studies.

Cobalamin bioconjugates for targeted delivery

One attractive exploit of cobalt based drugs is to utilize the fact that rapidly proliferative cells have higher requirement for cobalamin than non-transformed or normal cells. Therefore, this dependence can be exploited by preparing cobalamin-drug bioconjugates to exploit this dependence with selectivity for cancer cells (select examples shown in figure 17). In general, the bioconjugate consists of a cytotoxic drug tethered to a cobalamin via the β-axial position (through the Co-C bond). Grissom et al.[149] developed a cobalamin-chloroambucil bioconjugated which was capable of killing leukemia cells to the same extent of free chlorambucil. The bioconjugate was shown to be extracellularly inert, but once internalized via receptor mediated endocytosis, was activated via b-axial bond cleavage, thereby releasing the drug in its active form. Toxicity can be attenuated in the presence of excess cobalamin, proving the cobalamin moiety is responsible for the cellular uptake. Cyanocobalamin has been used to deliver antineoplastic agents such as

cisplatin to breast and ovarian cancer cells.[150, 151] The platinum compound was fused to cyanocobalamin through a Pt-cyanide bond, however, biological studies have shown this treatment to be less effective than free cisplatin.[150] One highlight of this class of compounds are nitrosylcobalamins, which possess a NO moiety in the β-axial position.[152] Mechanistic studies have shown that nitrosylcobalamins release NO upon cell entry leading to metabolism inhibition, DNA damage and apoptosis with selectivity for cancer cells over normal cells. *In vivo* studies conducted in dogs showed tumor reduction ranging from 43 – 77%, with one case showing complete remission following treatment for six months.[153] Given these encouraging resulting it is expected that this class of drugs will shortly enter into human trials.

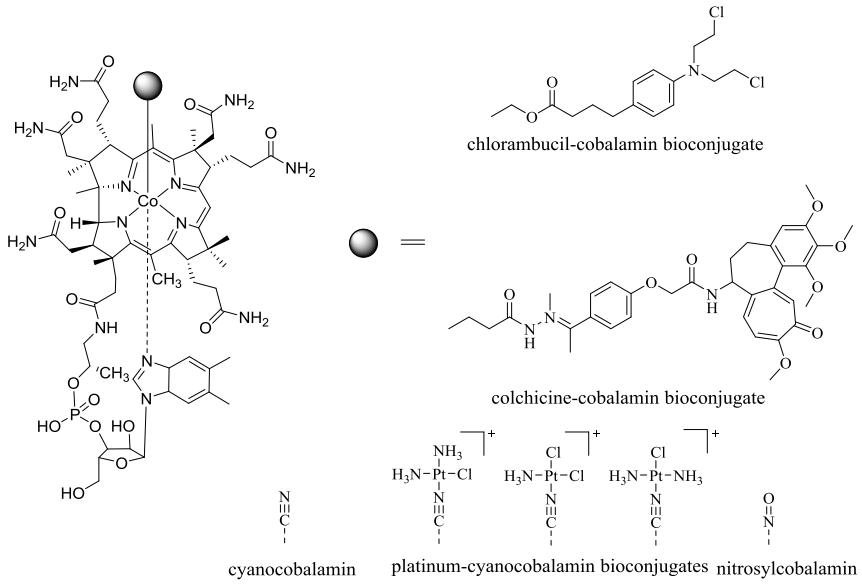

Figure 17. Chemical structures of cobalamin–drug bioconjugates.

Cobalt carbonyl-nonsteroidal anti-inflammatory drugs (NSAIDs) conjugates

Cobalt(III) complexes have also been proposed as alternatives to platinum based anticancer agents. The first report appeared in 1956,[142] where it was shown that cobalt(III) complexes could specifically target enzymes.[154] The complex contains an acetal ligand and was shown to inhibit

growth of murine leukemia cells. Some of the most famous Co(III) complex are those that fall into the category of cobalt-alkyne analogues such as those which incorporate dicobalt hexacarbonyl. Initially these complexes were utilized as labelling agents, for instance ethinylestradiol was tethered to $[Co_2(CO)_6]$ and were used to monitor the binding of steroids to estrogen receptors in breast cancer cells.[155] Jung[156] and then Ott and Gust et al.[157] investigated the anticancer properties of these $[Co_2(CO)_6]$-acetylene complexes and found the complexes had the ability to inhibit cancer cell proliferations and this was strongly dependent on the chemical nature of the acetylene moiety. The most active drug in the series showed that a Co-alkyne complexes bearing an acetylsalicylic acid derivative was the most potent (figure 18). This evolving class of compounds is labelled as cobalt-carbonyl-nonsteroidal anti-inflammatory drugs (NSAID) conjugates; they are highly active against breast cancer cell lines, owing to their increased intracellular levels due in part to their lipophilic characteristic when compared with their free ligands.[156, 157] Recent studies have indicated that the potent activity of this class of compound is multifactorial and may be due to COX inhibition, caspase-3 cleavage, and matrix metalloproteinase dysfunction.[154, 156, 158] Despite not knowing the exact mode of action of these compounds, they are often combined with other cytostatic agents such as imatinib, a tyrosine kinase inhibitor, which elicits an additive or syngergistic effect on the proliferation inhibition of acute and chronic myeloid leukemia cells (HL-60, LAMA-84), and CML-T1).

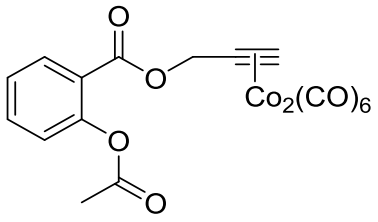

Figure 18. Co-alkyne complex incorporating acetylsalicylic acid

Given the success of cobalt-carbonyl complexes many small molecules and biomolecules containing dicobalt-carbonyl moieties have been prepared, however, overall these studies have proved somewhat disappointing. Fructopyranose derivatives coupled to $[Co_2(CO)_6]$ through an alkyne functionality, similar to auranofin (a gold-based NSAID) displayed modest activity (IC_{50} > 20 μM), against MCF-7 breast cancer cells.[159] Attachment of dicobalt octacarbonyl to deoxyuridines has improved antiproliferative activity (IC_{50} = 5 – 50 μM in MCF-7 and MDA-MB-231 cells.[160] In contrast the conjugation of $[Co_2(CO)_6]$ into the scaffold of a targeting peptide, leucine enkphalin (primary amino acid sequence Tyr-Gly-Gly-Phen-Leu), produced the first organometallic peptide bioconjugate to show significant toxicity against multiple tumor cell lines including HeLa and HepG2.[161] More recently, a number of cobalt(II) complexes attached to NSAIDs, such as mefenamic acid, naproxen, and tolfenamic acid have been prepared and shown to interacted with duplex DNA and HSA with high antioxidant activity (high scavenging efficacy against hydroxyl and superoxide radicals).[162, 163] Unfortunately, the anticancer potential for these complexes has yet to be explored.

Hypoxia activated cobalt(III) prodrugs

A popular strategy with cobalt drugs, similar to many other metal therapeutics, is to employ a cobalt(III) prodrug which is reduced *in vitro* to a more reactive Co(II) species in the harsh tumor microenvironment.[164] This selective localized reduction event often prompts Co(III) prodrugs to be identified as hypoxia selective antitumor agents. The aforementioned cobalt(III) nitrogen mustards are selective in this manner as shown below in figure 19. Another example in this strategy involves linking a neoplastic drug to the Co(III) metal center, which serves as a chaperone. One

report involved the linking of matrix metalloproteinase inhibitor (MMP), marimastat, with a Co(III)-tris(2-methylpyridyl)amine (TPA) chaperone to inhibit overexpressed metalloproteinases in tumor patients.[165] The Co(III)-TPA chaperone transports the drug and is reduced in the tumor environment to a Co(II) species resulting in the release of the inhibitor intracellularly. This prodrug strategy is often utilized, however, it was noted that in this case both the prodrug and the free inhibitor promote and potentiate metastasis.[165]

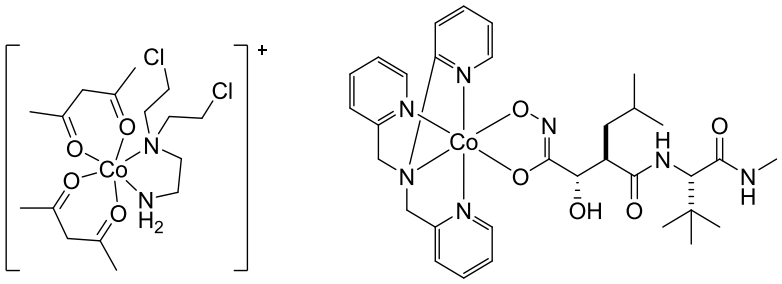

Figure 19. Examples of Co(III)-nitrogen and Co(III)-marimastat complexes

Apart from TPA, other tetradentate ligand systems have also been used as chaperones for Co(III) agents. Ware et al showed that Co(III)1,4,7,10-tetraazacyclododecane (cyclen) complex were effective chaperones for toxins such as 8-hydroxyquinoline (8-HQ) and azachloromethylbenindoline (azaCBI, a DNA minor groove binder).[166] These complexes showed 20-fold increase in selective potency toward colorectal and adenocarcinoma cells in hypoxic vs oxic conditions. Larger macrocyclic ligands such as 1,4,8,11-tetraazacyclotetradecane (cyclam), have also been utilized to chaperones for azaCBI. Among this series the most effective complex displayed 81 – 212-fold greater toxicity under hypoxia than 20% oxygen against a panel of human cancer cells.[167] Despite this fact, cytotoxicity could not be enhanced by overexpressing one-

electron reductase, NADPH or cytochrome P450 oxidoreductase which are known initiators of hypoxia activated prodrugs.[167]

While typically less utilized due to their enhanced reactivity (leading to more unwarranted side effects), Co(II) complex have also seen some applications as anticancer drugs.[148, 168-171] One such study reported on a series of salen complexes which stated that the associated anti-proliferation activity was dependent on both the type and position of the substituents on the aromatic rings (figure 20).[172] Additionally, there have been reports of 2-substituted benimidazoles possessing good antitumor activity against HeLa and HCT-115 cell lines.

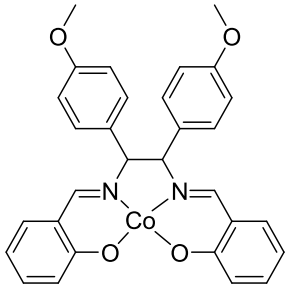

Figure 20. Example of a Co(II)-salen complex

FINDING THE TARGET

All of the above discussed examples represent the new era in drug discovery – gone are the days of serendipity and welcomed are the days of rational design. The rational design process of metallodrugs does not differ much from the process of designing a new organically based drug molecule. While rationally designed metallodrugs dominate current literature there is still a lack of studies working to elucidate the exact mechanism behind the observed bioactivity of these complexes. The critical first steps of this process involve the identification of the target associated with the disease and the elucidation of the molecular targets affected within the disease's etiology.

In the world of traditional medicinal chemistry, the identification of these targets is often facilitated through the use of genomics and proteomics. A medicinal inorganic chemist involved in similar research would be classified under the emerging field of "metallomics", which supports target validation. Metallomics is the full characterization of the metal or metalloid species present in a cell of tissue type, inclusive of their interaction with the genome, transcriptome, proteome, and metabolome.[173] Research in this field is broadly tasked with comprehensively and completely understanding the metal uptake, trafficking, biological function, and excretion of these compounds.[140]

Biological targets of metallodrugs have been comprehensively reviewed and critically evaluated quite recently,[174, 175] and often a logical starting point for many researchers is to use what is already present within the body, as these systems work with these existing building blocks. Seven of the 21 naturally occurring amino acids, the building blocks for proteins, possess donor atoms (N, O, or S) which may allow for coordination or affiliation with a metallodrug. More specifically, metal-binding sites exist at the N-terminus of many naturally occurring proteins, such as the N-terminus of the Cu(II) and Ni(II) binding ATCUN motif, which possess three site for interaction with a metal.[176, 177] Therefore, many metallodrugs possess a natural target in proteins as they may be able to alter the protein structure. Other proteins, such has metalloenzymes, require the presence of a metal center to be functional. If a chelating agent is administered that can strongly bind the metal ion, the target metalloenzyme may become inactivated.[178]

Another popular target for metallodrugs is DNA, whether it be nuclear or mitochondrial. All base pairs possess the necessary atoms (N, O) which can be bound by a metal ion. Of particular importance is the binding interaction which take place at the N^7 position of adenine and guanine within the major groove of helical DNA. With enough open binding sites, a metal ion can

covalently bind to form both intra- and inter-strand cross links. Additionally, the incorporation of planar hydrophobic groups which can insert between the base pairs in a process known as intercalation, facilitated by noncovalent forces can occur increasing binding strength. These, so-called dual mode DNA binding metallodrugs not only bind covalently to the DNA but additionally intercalate as well, while other metallodrugs selectively target a specific sequence.

Biophysical chemists are increasingly investigating the factors which promote metabolism of metals within the human body, as well as potential pharmacological effects. This has given rise to a number of bioanalytical chemists who are now studying the mode of action of metallodrugs by identifying their specific molecular targets.[179] These studies now aim to utilize a variety of analytical techniques such as mass spectrometry,[180, 181] capillary electrophoresis and a variety of other hyphenated techniques to probe the interactions of metal ions with proteins.[182,183]

In drug development, it is critical to gain as much detailed information about the target of the molecule as possible. This information can then be further utilized to rationally design next generation drug molecules, which have a better fit (binding affinity) for the target as opposed to other competitive binding sites, resulting in a decrease in side effects. On the other hand, a simplistic one molecule-one target approach can pigeonhole the application of a drug molecule, making it difficult to treat complex diseases such as Alzheimer's disease(AD) or Parkinson's, for which more radical multifaceted targeting molecules are needed.[184]

A 2005 study by the US National Cancer Institute (NCI) highlighted the diversity of metal complex being investigated in anticancer research, including approximately 1000 metal-containing compounds in a study.[185] The main aim was to establish correlations between observed cytotoxicity and the gene expression profiles of various cell lines. While the study confirmed that there are a wide array of potential mechanisms of action for metal-based compounds four

fundamental classes were identified: (i) binding to sulfydryl groups, (ii) chelation, (iii) generation of ROSs, and (iv) production of lipophilic ions.[185] These categories demonstrate the broad array of mechanisms and potential targets of metallodrugs. Similarly, while one metallodrug may act in different ways it may also be active against a variety of diseases. For instance, gold(I) compounds (i.e. auranofin) were traditionally employed to treat rheumatic arthritis but are slowly being integrating into anticancer clinic studies as well.

As opposed to high-throughput screening or brute force searching for potentially active complexes it is becoming more popular, with the assistance of computational methods,[186] to study the binding pocket of proteins and tailor molecules to nicely docks onto the protein. For example, PIM kinases are enzymes located on the proviral insertion site of the moloney murine leukemia virus that can be selectively inhibited by inert half-sandwich ruthenium-indolocarbazole complexes (i.e. NP309 and its derivatives) such as those developed by Meggers et al.[187] These organoruthenium complexes have demonstrated an extremely good fit in the ATP binding pockets of PIM1 and PIM2 inactivating these PIM kinases, which in return leads to restored apoptosis in former drug resistant cancer cells.[187, 188]

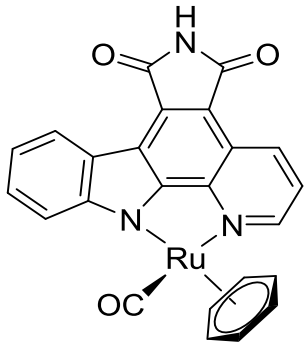

NP309

While the fit of a drug is fundamentally important, it cannot be overshadowed that the molecule must be able to reach its cellular target. Since many metallodrugs are injected into the blood steam or muscle, the molecule will contact many other biological substances which may alter its composition, for example cisplatin's reaction with sulfur rich cysteine residues. The most common substrate for metallodrugs is human serum albumin (HSA, 0.65 mM),[183] which may act as a reservoir or transport vehicles in the case of ruthenium drugs due to iron mimetic properties. This substrate can also be exploited as HSA has been shown to accumulate in tumor cells due to increased demand for iron.[189, 190] Another common protein which may interact with metal ions is apo-transferrin (Tf), which normally binds iron(III) but can also interact with main group,[191] transition metal,[192] and lanthanide metal ions.[193]

While metal centers have been the focus of many researchers the ligands bound to the metal center also play a critical role in the bio-activity of complexes. Ligands are most often, but not limited to, organic compounds that bind to metal ions, thus modifying the physical and chemical properties of the ion(s). Ligands can be introduced to the system to limit the adverse effects of metal ion overload, inhibit selected metalloenzymes, or facilitate metal ion re-distribution. Some

of the aforementioned effects include modifying reactivity and lipophilicity, stabilizing specific oxidation states, and contributing to substitution inertness; however purposeful design today can go way beyond these effects. Tailored, multifunctional ligands for metal-based medicinal agents offer many exciting possibilities, and can play an integral role in muting the potential toxicity of a metallodrug to have a positive impact in areas of diagnosis and therapy.

It is important to ask which parts of the active compound are essential for activity: the metal itself, the ligands, or the intact complex of metal plus, at least, some of the ligands? Many metallodrugs are "pro-drugs", and undergo ligand substitution and/or redox reactions before they reach the target site. Thus, a rational design of potential therapeutic/diagnostic agents is needed to achieve specific targeting features and to control toxicity (side-effects), by controlling thermodynamic and kinetic processes of metal complexes. Tailored, multifunctional ligands for metal-based medicinal drugs offer many exciting possibilities, including targeting specific tissues, membrane receptors, or endogenous molecules, and can play an integral role in modulating the potential toxicity of a metallodrug to achieve success in areas of diagnosis and therapy. Additionally, with the diverse and infinite number of mechanisms of these metallodrugs there is renewed hope that they can overcome developed resistance;[194] examples of overcome drug resistance from malaria research and cancer research suggest this hope may not be in vain.[195, 196]

RESEARCH GOALS

Although there are numerous known, effective metal complexes employed as agents against a variety of human diseases, there is still need to improve and search for potentially more effective drugs. The mechanisms of action of many current transition metal therapeutics also remains largely unexplored or misunderstood and in order to further rationally design transition

metal complexes and conduct structure activity relationship (SAR) studies, it is critical to fully elucidate these mechanisms of actions. Therefore, the aims of this thesis are twofold: (1) to conduct preliminary mechanistic studies on the bioactivity of transition metal complexes and (2) to design and synthesize novel ligands and complexes for future mechanistic and structure activity relationship studies. In part 1 (Chapters 2 and 3) a variety of cell-free and cell-based assays are utilized to investigate the mechanism of action of various transition metal complexes; while part 2 (Chapters 4 and 5) focuses on the development of small libraries of molecules for future SAR studies.

In chapter 2, a Co(III) complex, $[Co(phen)_2(MeATSC)](NO_3)_3 \cdot 2.5H_2O \cdot EtOH$, was tested for its chemotherapeutic potential against a model metastatic breast cancer system, as well as for its interaction with CT DNA in order to mimic cellular DNA. After revealing the complexes ability to induce apoptosis further studies believed to be critical to its ability to inhibit cancer cell growth are discussed. In addition, nanosecond pulse electric field (nsPEF) technology was combined with $[Co(phen)_2(MeATSC)](NO_3)_3 \cdot 2.5H_2O \cdot EtOH$ in hopes of developing a novel localized ablation therapy. Synergistic studies were conducted and the observed effects of this novel locoregional ablation treatment therapy are discussed.

In chapter 3, to further work previously conducted within our lab, a oxidovanadium(IV) complex was synthesized and characterized via conventional spectroscopic techniques and X-ray crystallography. In addition, a novel binuclear Ru(II)-V(IV) complex, $[Ru(pbt)_2(phen_2DTT)VO(oda)](PF_6)_2 \bullet 2.0H_2O \bullet 0.5C_2H_5OH$, was synthesized, characterization and studied for its binding interactions with CT DNA. In this chapter we discuss the utility of isothermal titration calorimetery (ITC) as a method for determining binding and thermodynamic parameters associated with transition metal/DNA interactions. This chapter discusses work

conducted in collaboration with Ms. Kathy Currie (Undergraduate Student, ODU) on the synthesis and binding interactions of the complexes presented. Comments on the antimetastatic potential of the complexes will also be made.

In chapter 4, the synthesis and characterization of a novel series of *N,S* coordinating ligands and subsequent complexes is discussed. Utilizing a one-pot synthetic scheme analytically pure pyridine-2-thiocarboamides (PCAs) were prepared in a single step reaction. The molecular structure was confirmed using a variety of spectroscopic techniques, to include in one case X-ray crystallography, confirming the utility of the modified Willgernot-Kindler reaction scheme utilized. Analytically pure ligands were complexed with either Co(III) or Ru(II) precursor molecules and the characterization of these coordination complexes is discussed as well. Finally, in chapter 5, the synthesis and characterization of a library of novel thiadiazol and triazolothiadiazol containing ligands will be discussed. The compounds prepared represent a proof of concept model for the synthetic procedure and will be further investigated for their biological activity.

CHAPTER 2

PRELIMINARY MECHANISTIC STUDIES OF A Co(III)-COMPLEX AND NSPEFs: A POTENTIAL LOCOREGIONAL ABLATION TECHNIQUE FOR TREATMENT OF METASTATIC BREAST CANCER

INTRODUCTION

Metastatic breast cancer is the most common malignant disease in western women, with approximately 1.7 million new breast cancer diagnoses in 2014.[15, 197] In many patients, it is not the primary tumor, but the metastases at distant sites that are the main cause of death. While rates of metastasis and mortality have slightly decreased over the last two decades, the disease is still considered incurable even with advances in early detection and systemic adjuvant therapies.[198] Chemotherapy only increases the 15 year survival rate of women under 50 by 10%; in elderly women this increase is only 3%.[199, 200] Currently, no technology exists for the accurate prediction of metastasis and therefore patients are subjected to the toxic side effects of classic chemotherapy which substantially affect the patients' quality of life.[201-203]

Advances in genomics and cell biology have increased the opportunity for rational design of targeted drugs and therapies to inhibit the function of specific molecules, including those contributing to the proliferation of cancer cells.[204-207] Although, targeted therapies may offer enhanced efficacy and improved selectivity (and therefore less nonspecific toxicity), most often their effects are not durable when they are used alone. Cellular pathways operate in vast interconnected webs as opposed to information superhighways, therefore with multiple redundancies, alternative pathways may be activated in response to inhibition of a specific pathway. This redundancy further promotes the emergence of resistant cells under the selective

pressure of the targeting agent, resulting in drug resistance.[33] For this reason, combination therapies are often needed to effectively treat many tumors and infectious diseases.[33, 208]

As discussed in chapter 1, following the widespread success of cisplatin, a variety of transition metal coordination compounds have been extensively studied for their biological properties.[209, 210] Specifically, polypyridyl coordination complexes have been extensively investigated due to their unusual binding properties and general photoactivity; these coordination compounds have been shown to be suitable candidates as DNA secondary structure probes, photocleavers, and antitumoral drugs.[211, 212] The effects of size, shape, hydrophobicity, and the charge on the binding of the complex to DNA have been studied by changing the type of heteroaromatic ligands or metal center.[213, 214] The vast majority of such studies have been focused on complexes of Ru(II),[215-217] but to a far lesser extent, on other metal complexes. For instance, Barton *et al*.[214] has reported that chiral phenanthroline–cobalt(III) complexes recognize different local structures of DNA.

To date, the only cobalt-based therapeutic that has reached clinical trials is Doxovir (CTC-96), a Co(III) Schiff base complex effective against drug-resistant herpes simplex virus 1 (HSV1).[141] The mechanism of action of Doxovir, however, is not fully understood. A substantial amount of literature on bioactive cobalt derivatives has been published in the last decade, demonstrating their rich potential in medicinal applications.[164, 218] However, the rationale behind the design and mechanisms of many of these agents has not been clearly elucidated. An understanding of how the unique properties of cobalt complexes interplay with biology to elicit therapeutic effects is clearly necessary for the development of cobalt-based drugs.

For many years, thiosemicarbazones and their metal complexes have been found to exhibit a wide range of applications that stretch from their use in analytical chemistry, through

pharmacology to nuclear medicine.[219-223] In 1994,[224] and more recently, cobalt(III) complexes with TSCs and methyl substituted phenanthroline ligands have been reported as anti-cancer agents as they inhibit cell growth of several cancer cell lines.[225-229 230] The present level of interest in metal complexes of TSCs stems from the fact that the inherent biological activity of the organic ligand is enhanced upon coordination to the metal center.[231]

While extensive research has been conducted on chemotherapeutic drugs, many effectively target specific molecular processes such as DNA replication which is not unique to cancerous cells leading to unwarranted side effects. Therefore, in attempts to mitigate harmful side effects low dose chemotherapeutic drugs are often combined with alternative treatments such as: targeted,[232] immuno-,[233] and radiation-therapies.[234] In particular, electrochemotherapy (ECT) which utilizes conventional electroporation with electric fields in the micro- to milli-second range has found widespread success.[235-238] ECT cause large pores or defects to form in the plasma membrane, thereby allowing for the entry of poorly permeable drugs such as bleomycin to ablated tumors.[239] Concepts from this conventional electroporation techniques have been further exploited and now extended to irreversible electroporation (IRE), which uses stronger electric fields to destroy plasma membranes entirely causing tumor necrosis without the utilization of drugs.[240] Although ECT and IRE are not generally utilized in the United States, both have found widespread application in Europe for the treatment of cancer.[241]

As opposed to these conventional electroporation techniques, nanosecond pulsed electric fields (nsPEFs) are an emerging alternative novel treatment for cancer.[242, 243] While nsPEFs can be regarded as an extension of conventional electroporation, generally, pulse duration of only 10 ns to several hundred ns, and electric field intensities of 10 kV/cm to several hundred kV/cm are utilized. This feat is accomplished by storing electrical energy in capacitors and then releasing it

in sub-microsecond bursts also known as "pulsed power".[244, 245] For comprehension of the "pulsed power" concept consider the release of one joule of energy in one second versus releasing the same energy over one nanosecond. If the stored energy was release over one second the peak power would be only 1 watt, not even enough energy to power a light bulb, however, if released over one nanosecond the peak power would be one gigawatt (10^9), a billion times greater. This energy could light an entire medium sized city for that nanosecond.

Due to these ultrashort pulse durations, nsPEFs have been shown to induce a specific series of unique biological effects such as apoptosis,[246-249] calcium fluctuation and phosphatidylserine translocation,[250-252] with little hyperthermal effects. Researchers in this area typically fall into a newly emerging field known as bioelectrics (coined by Dr. Karl Schoenbach – Frank Reidy Center for Bioelectrics) and are concerned with investigating the effects of short burst electrical stimuli on cells and tissue for various basic science and therapeutic applications. Despite the relatively new evolution of this field, there has been extensive modeling[253, 254] and experimental studies[249, 255-259] which detail effects on plasma membranes and intracellular membrane such as the endoplasmic reticulum,[250, 260-262] mitochondria,[251, 255, 263, 264] and the nucleus/DNA. Given the broad-based effects of nsPEFs on cellular structure and function it is unsurprising that there are also reports on the utility of this technique for cancer ablation.[259, 265, 266] Recently it was reported that µS- and ns-PEFs can be utilized as a locoregional minimally invasive treatment for hepatocellular carcinoma.[259, 265, 266] Additionally, nsPEF have been shown to induce apoptosis in a variety of cell types, including pancreatic cancer, melanoma and HeLa cells.[246, 267, 268] NsPEFs have also been proven effective to eliminate murine melanoma and murine basal cell carcinoma *in vivo*.[269-272]

Herein we present our efforts to study the mechanism by which, a non-platinum complex, $[Co(phen)_2(MeATSC)]\cdot 2.5H_2O\cdot C_2H_5OH$ (**1**),[273] inhibits breast cancer cell growth. In this study, a highly metastatic 4T1-luc mouse mammary cancer cell line was utilized to mimic tumor growth and metastasis in its human counterpart.[274-276] Due to these properties we have set out to test the efficacy of the complex in inhibiting their proliferation, as well as discern the mechanism of action in cell-free and cell-based assays. While utility of nsPEF has been proven *in vivo* as a drug free therapy for the treatment of breast cancer,[277] no such investigation has been conducted where a transition metal chemotherapeutic agent is combined with nsPEF technology. As such, a novel combination therapy involving treatment of cells with nsPEFs and a Co(III) transition metal agent will be explored.

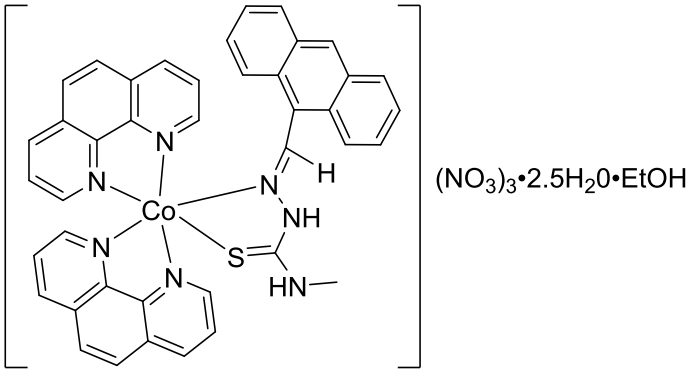

$[Co(phen)_2(MeATSC)](NO_3)_3\cdot 2.5H_2O\cdot C_2H_5OH$ **(1)**

EXPERIMENTAL

General

$[Co(phen)_2(MeATSC)](NO_3)_3\cdot 2.5H_2O\cdot C_2H_5OH$ (**1**) was provided by Dr. A.A. Holder and was prepared at The University of Southern Mississippi by Ms. Jessa Faye Arca.[273] The buffer

solutions were prepared with doubly-distilled water from a Milli-Q system. Fetal bovine serum (FBS) and DMEM were obtained from Mediatech, Inc. (Manassas, VA). CellTiter 96® AQ_{ueous} One Solution Cell Proliferation Assay (MTS), and Caspase-3/7 Glo kits were purchased from Promega Corporation (Madison, WI). CT DNA was purchased from Sigma (St. Louis, MO).

Stability of 1 in PBS buffer

The stability of **1** in PBS buffer was examined by UV-visible spectrometry using a Cary 5000 UV-2450 spectrophotometer. Spectra were collected from samples dissolved in a PBS solution containing: NaCl (137 mM), KCl (2.7 mM), Na_2HPO_4 anhydrous (10 mM), and KH_2PO_4 (2 mM), pH 7.4, with the solutions having 5 % DMSO added to aid in solubility. Spectra (240 nm - 1000 nm) were recorded every ten minutes over twenty-four hours. Data was fit utilizing Agilent UV-Vis ChemStation software.

DNA binding UV-visible titration studies

Electronic absorption titration experiments were conducted on a Agilent 453 diode array spectrophotometer at room temperature. Electronic absorption titration experiments were performed with a fixed concentration of **1** (10 μM) but variable nucleotide concentration ranging from 0 to 100 μM. 3 mL solutions of the blank PBS and the Co(III) complex were placed in two 1 cm pathlength curvettes. Then aliquots of buffered CT DNA solution were added to each to eliminate background absorbance from DNA itself. Before each spectra was recorded, the Co(III)-CT DNA solutions were allowed to equilibrate at room temperature for 5 min. Data was fit utilizing Agilent UV-Vis ChemStation software.

Competitive fluorescence binding studies

The relative binding of **1** to CT DNA was determined with ethidium bromide (EB)-bound CT DNA solution in Tris-HCl/NaCl buffer (pH = 7.2) on a Cary Eclipse Fluorescence

Spectrophotometer with a Peltier 4 position multi-cell holder and temperature probe accessories. In displacement experiments a solution containing 10 µM DNA and 0.33 µM EB (saturated binding conditions), was titrated with concentrated solution of **1** to generate solutions with various mole ratios of complex to CT DNA. The influence of the addition of complex to the EB-DNA complex was obtained by recording the variations in the fluorescence emission spectra with excitation at 525 nm and emission at 605 nm with slit widths of 5 nm at various temperatures.

Cell culture

4T1 cells (mouse mammary breast cancer) were obtained from American Type Culture Collection (ATCC). 4T1 cells were transformed with pGL4.50*luc2*/CMV/H_{ygro}. 4T1-*luc* cells were maintained in the logarithmic stage of growth in high glucose DMEM (Dulbecco's Modified Eagle's Medium) supplemented with 10% fetal bovine serum (FBS), 1% non-essential amino acids (NEAA) and 1% antibiotics (100 units/mL penicillin and 100 µg/mL streptomycin) at 37 °C in a humidified atmosphere containing 5% CO_2 and were used at passages 3 to 25. Except where indicated, analyses were performed on same passage cells within two weeks after thawing. Cell line used in these studies was tested and shown to be free of mycoplasma and viral contamination.

Preparation of stock solutions of complex 1

An 80 mM stock solution of complex **1** was prepared by dissolving 39.6 mg of complex in 500 µL of DMSO. All other stock solutions were diluted to the desired concentration using complete media along with the respective vehicle control (DMSO) ≥0.5%.

Cytotoxicity studies

Cell viability following exposure to complex **1** was assessed via the CellTiter 96® AQ_{ueous} One Solution Cell Proliferation (MTS) Assay (Promega, Madison, WI). Briefly, cells were seeded on a 96 well plate (2.5 x 10^4 cells/well) in 100 µL of medium and incubated for 4 hours.

Following incubation, fresh solutions containing complex **1** at various concentrations were prepared in complete medium. Seeding media was removed and cells were then treated with 100 µL of **1** in complete media at various concentrations (0 – 200 µM) and incubated for 24 hours at 37 °C in 5% CO_2. After 24 hours incubation, the cells were treated with 20 µL of the CellTiter 96® AQ_{ueous} One Solution Reagent containing [3-(4,5-dimethylthiazol-2-yl)-5-(3-carboxymethoxyphenyl)-2-(4-sulfophenyl)-2H-tetrazolium (MTS) and phenazine ethosulfate. Following one hour incubation, the absorbance was measured at 492 nm using either a µQuant™ Microplate spectrophotometer or VersaMax ELISA Microplate reader. To block autophagy, cells were preincubated at 37 °C for four hours with 600 nM necrostatin-1 (Sigma-Aldrich, St. Louis, MO) prior to the addition of complex **1**. To inhibit caspase activity, cells were preincubated with 10 mM benzyloxycarbonyl-Val-Ala-Asp-(O-methyl)-fluoromehylketone (z-VAD-FMK) for four hours prior to the addition of complex **1**. The compound as well as all positive and negative controls were tested in triplicate on cells at various passage numbers.

Caspase 3/7 Activity

Caspase 3/7 activity was determined by Caspase-Glo 3/7 kit using tripeptide substrate sequences Ac-DEVD-AMC (Promega, Madison, WI). According to manufacturer's instruction, for each analysis, cells were plated in triplicate on 96-well plates (2.5×10^4 cells per well) in the presence or absence of pan caspase inhibitor z-VAD-FMK for four hours. Seeding media was removed and cells were then treated with 100 µL of complex **1** in complete media at different concentrations and incubated for 24 hours at 37 °C in 5% CO_2. After twenty four hour incubation, plates were equilibrated to room temperature for 30 minutes and 100 µL of Caspase-Glo 3/7 reagent was added to each well and the contents were gently mixed using a plate shaker at 300 rpm for 30 seconds. Luminescence was read using a FLUOstar Omega luminometer (BMG

Labtech), after thirty-five minute incubation at room temperature, which measured linear catalytic rate for the substrate. Increase in activity was calculated based on activity of control (sham-treated) cells.

Analysis of autophagy by flow cytometry

Autophagy was detected using Cyto-ID® autophagy detection kit (Enzo Life Science, Farmingdale, NY) using Cyto-ID™ green autophagy detection reagent, which selectively labels green vacuoles associated with the autophagic pathway, with minimal background lysosomal staining. Briefly, cells were harvested from culture and plated on a 24 well plate (7.0×10^4 cells per well) for four hours in the presence or absence of 600 nM necrostatin-1. After incubation, the supernatant was discarded and cells were treated with 100 µL of complex **1** in complete media at different concentrations (0 – 80 µM) and incubated for various times (1 – 24 h) at 37 °C in 5% CO_2. After incubation, cells were washed with twice with PBS, centrifuged (1000 rpm for 5 minutes), and the supernatant was discarded. The cells were resuspended in 250 µL fresh indicator free DMEM containing 5% FBS. The staining solution was prepared by diluting 1 µL of Cyto-ID® green detection reagent to 1 mL with indicator free DMEM containing 5% FBS. Then 250 µL of the staining solution was added to the cell suspension and each vial was gently vortexed. The samples were then incubated for 30 minutes at 37 °C, centrifuged, washed with 1X assay buffer (500 µL) and resuspended in 1X assay buffer. The cell samples were then analyzed on a Becton Dickinson FACSAria flow cytometer in the FL-1 and FL-2 channels for 10,000 events. Autophagic activity was estimated measuring the mean fluorescence intensity (MFI) value. Positive controls for inducing autophagy included: Rapamycin (500 nM), Chloroquine (120 µM), and starvation (DMEM - FBS). Results shown are representative of multiple experiments performed in triplicate. Data was analyzed using FlowJo_V10 software.

Flow cytometric analysis of calcium flux and mitochondrial membrane potential (ΔΨm)

The levels of intracellular calcium were determined using Fluo-4 Direct (Molecular Probes, Eugene, OR) and depolarization of the ΔΨm was detected using tetramethylrhodamine ethyl ester (TMRE) (Immunochemistry Technologies LLC, Bloomington, MN). Briefly, cells were seeded on a 24 well plate ($7.0x10^4$ cells per well) for four hours. After four hour incubation, media was removed and cells were then treated with 500 µL of complex **1** in complete media at different concentrations for either 2, 4, or 6 hours at 37 °C in 5% CO_2. At the specified time points (2, 4, and 6 h) cells were then harvested using 150 µL trypsin-EDTA 1X (ThermoFisher Scientific, Waltham, MA), pelleted and the supernant was removed. Cells were then preincubated with 1x Fluo-4 Direct calcium reagent loading solution for 60 min at 37 °C. During the last 15 min of Fluo-4 incubation, 200 nM TMRE was added to the solution. At the end of incubation, cells were washed 2x with PBS and resuspended in culture media (500 µL) and analyzed on a Becton Dickinson FACSAria flow cytometer. The average red fluorescence intensity (10,000 cells) was analyzed on the FL-2 channel and green fluorescence was read on the FITC channel. The green emission of Fluo-4 increases when calcium increases and TMRE red emissions decreases when ΔΨm decreases. Data was analyzed using FlowJo_V10 software.

Flow cytometric analysis of histone 2.AX (H2AX) phosphorylation

Cells were harvested and plated on a 24 well plate (1.0×10^5 cells per well) for 3 hours. After three hours, media was removed and cells were treated with 500 µL of complex **1** in complete media at different concentrations and incubated for various 18 hours at 37 °C in 5% CO_2. After eighteen hour incubation cells were washed, harvested via trypsinization, and resuspended in fixation/permeabilization solution (BD Cytofix/Cytoperm™, BD Biosciences) for 20 min at 4°C. After washing twice in 1x BD Perm/Wash™ buffer, cells were incubated with monoclonal anti-

γH2AX (Ser139) (Cell Signaling Technology) for 1 hr at 37°C and followed by incubation with a secondary Alexa 488-conjugated goat anti-rabbit IgG for 45 min at room temperature (Molecular Probes, Invitrogen). After washing twice in BD Perm/Wash buffer, the fluorescence of 10,000 cells was analyzed using a Becton Dickinson FacsAria flow cytometer (488nm, FL-1). Positive control for inducing DNA damage included incubation of cells with 16.5 μM cisplatin for 2 hours prior to fixation.

Determination of cellular viability following exposure to nsPEFs

Cells were harvested from culture via trypsinization and resuspended in the fresh cell culture medium at a density of 3.2 $x10^5$ cells/ml. 130 μL of cell suspension was placed in a 0.1-cm gap-width cuvette (Biosmith, San Diego, CA) and exposed to nsPEFs. 4T1-luc cells were exposed one, five, or ten pulses with duration of 60 ns and electric field strength ranging from 0 to 60 kV/cm. Cells where then plated on a 96 well plate ($2.5x10^4$ cells per well). Cellular viability was assessed after 24 hours using the CellTiter 96® AQ_{ueous} One Solution Cell Proliferation (MTS) Assay as describe above.

The 60 ns pulses were produced by a Blumlein circuit switched by a pressurized spark gap.[278] The Blumlein circuit consisted of two 50 Ω coaxial cables, which gave a total impedance of 100 Ω. This value was chosen to match the impedance of the cable, Z, to the resistance of the cell suspension between the two electrodes, R. In this case, the energy stored in the cables is transferred into the load in the form of a rectangular power pulse, with the pulse duration determined by the length of the cable and the speed of electromagnetic waves in the dielectric of the cable.[279] For the cables used in this device, the dielectric constant is $\varepsilon_r = 2.25$, producing a wave velocity $v = c/(\varepsilon_r)^{1/2}$ of 2×108 m/s with c being the speed of light in a vacuum. The total pulse duration, T, for the Blumlein circuit is determined by the length of the two cables, l,

as T = l/v. The rise time of the pulse (e.g., the time to reach a steady state mode with a current of I = Vo/Z) is determined by the closing switch, where V_o is the value of the applied voltage. In this device, a spark gap with a closing time of less than 10 ns was used to produce 60 ns and 300 ns pulses with amplitude jitter of less than 5%. Since the amplitude of the voltage applied is below 1 kV for pulses with duration in excess of 1 μs, a pulse generator using MOS field effect transistors (BIMOSFET; IXBH 40N160, IXYS Corporation, Santa Clara, CA) could be used. The rise time of these pulses is ~50 ns, which is short compared to the pulse duration. The maximum voltage of the long pulse was 1.6 kV, limited by the maximum operating voltage of the BIMOSFET; the maximum voltage of the short pulses was 5 kV, limited by the hold-off voltage of the cable connectors.

Determination of cellular viability following exposure to both 1 and nsPEFs

Cell viability following exposure to both complex **1** and nsPEF was assessed via the CellTiter 96® AQ_{ueous} One Solution Cell Proliferation (MTS) Assay similar to above describe procedures. Briefly, cells were seeded on a 24 well plate (5.0 x 10^4 cells/well) in 500 μL of medium and incubated for 4 hours. Cells were then treated with 500 μL of complex **1** in complete media at different concentrations and incubated for 24 hours at 37 °C in 5% CO_2. After twenty four hour incubation, the cells were washed twice with PBS, harvested, pelleted and resuspended in culture medium. 130 μL of cell suspension (3.2 x 10^4 cells) was placed in a 0.1-cm gap-width cuvette (Biosmith, San Diego, CA) and exposed to ten pulses with duration of 60 ns and electric field strength ranging from 0 to 60 kV/cm. 100 μL of cell suspension (100 μL ≈ 2.4 x 10^4 cells) where then plated on a 96 well plate and cellular viability was assessed after 24 hours using the CellTiter 96® AQ_{ueous} One Solution Cell Proliferation (MTS) Assay as describe above.

RESULTS AND DISCUSSION

The electronic absorption spectra of complex **1** consists of three well-resolved bands in the range of 200–450 nm, specifically with $\varepsilon = 19 \times 10^3\ M^{-1}\ cm^{-1}$, $9.1 \times 10^3\ M^{-1}\ cm^{-1}$, and $9.6 \times 10^3\ M^{-1}\ cm^{-1}$ at 294, 378 (shoulder), and 392 nm, respectively.[273] The high energy absorption bands in the spectra of **1**, below 300 nm are assigned to $\pi \rightarrow \pi*$ intra-ligand charge transfer transitions and the band found around 400 nm is assigned to ligand-to-metal charge transfer (LMCT). Kinetic experiments were conducted monitoring any changes in the high energy absorption bands over twenty-four hours, in PBS to ensure inertness in buffered conditions. As shown in figure 21 there are only minimal changes (<0.005 absorbance units) in the electronic absorbance spectrum over the time period, confirming the complex is inert in the selected buffered solution, with the complex never reaching one half-life over the course of the experiment. Upon the addition of DNA, the above bands exhibited slight hypochromism accompanied with a slight blue shift. Hypochromisim and bathochromism in the UV absorption spectrum following addition of DNA, indicates the complex can interact with DNA, most likely through stacking interactions between an aromatic ring and the base pairs of DNA.[280] The extent of hypochromism exhibit is often an indicator of the strength of intercalation, as shown in figure 22, only slight hypochromism exist indicating the weakness of this interaction.

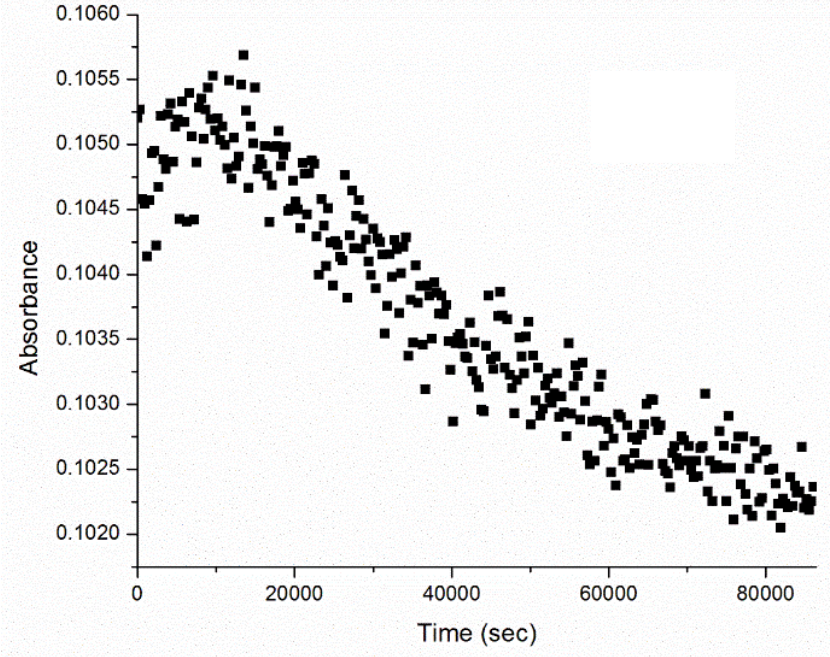

Figure 21. Absorbance vs Time plot of complex **1** in PBS (pH = 7.4). Cycle Time: 900 s, Temperature: 25 °C, [Complex] = 24 µM.

For metal complexes, DNA binding can occur via a variety of mechanisms including base pair intercalation, groove binding, and electrostatic binding.[281] In order to quantitatively determine the binding strength of complex **1** to DNA, the intrinsic binding constants (K_b) were obtained by monitoring the changes in lower energy bands of complex **1**, with increasing concentration of DNA using the equation[282]:

$$[DNA]/[\varepsilon_a-\varepsilon_f] = [DNA]/[\varepsilon_b-\varepsilon_f] + 1/K_b[\varepsilon_b-\varepsilon_f] \quad (1)$$

where: [DNA] is the concentration of DNA in base pairs, the apparent absorption coefficients ε_a, ε_f, and ε_b correspond to A_{obsd}/[Complex], the extinction coefficient for the complex

in free solution, and the extinction coefficient for the complex in the fully bound form, respectively. A plot of [DNA]/[$\varepsilon_b - \varepsilon_f$] vs [DNA] gave a slope and the intercept which are equal to 1/[$\varepsilon_a - \varepsilon_f$] and (1/$K_b$)/[$\varepsilon_b - \varepsilon_f$], respectively; K_b is the ratio of the slope to the intercept. The magnitude of K_b was calculated to be 6.69×10^4 M^{-1}. The observed K_b value revealed that complex **1** binds weakly with CT DNA. The nature of the results suggest that the complex interacts weakly with DNA via an intercalation mechanism. It is however, possible that the cationic nature of the complex could provide for electrostatic interactions.

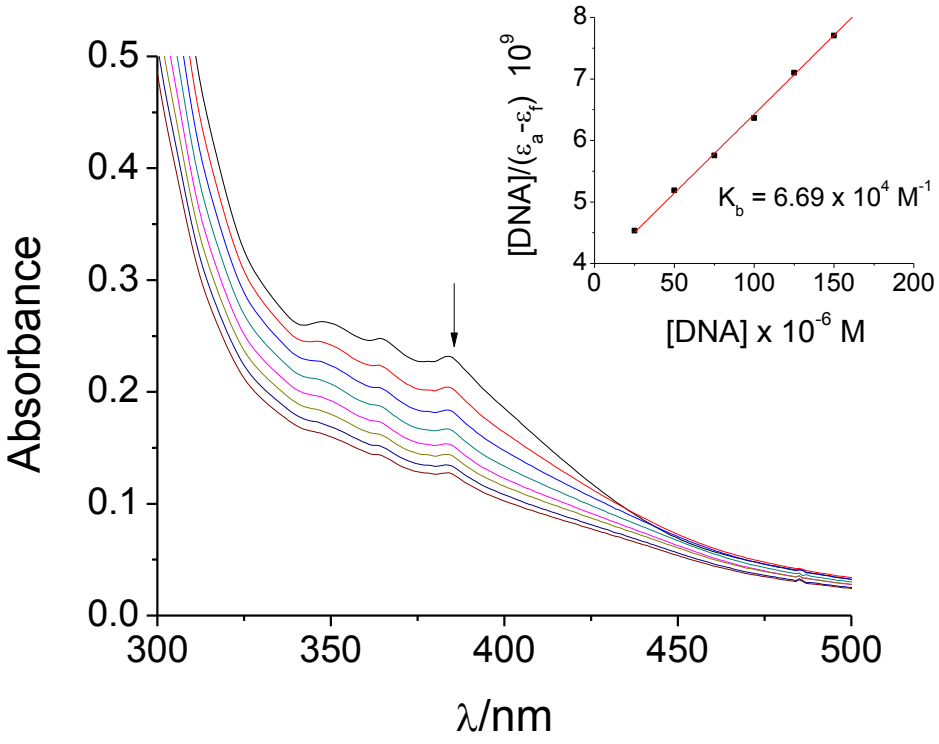

Figure 22. UV-visible spectral changes observed during titration of complex **1** with CT DNA. [Co] = 50 µM, [DNA] = 0 - 200 µM, buffer PBS (pH = 7.4). Arrow indicates the change upon increasing DNA concentration. Inset: Plot of [DNA]/($\varepsilon_a - \varepsilon_f$) vs. [DNA].

Steady-state competitive binding experiments using complex **1** as a quencher were undertaken to get further determine if complex **1** interacts with DNA via and intercalative fashion, similar to other metallointercallators. Ethidium bromide (EB) is a planar cationic dye which is widely utilized as a sensitive fluorescence probe for native DNA as it intercalates well through interactions with the minor groove.[283] EB emits an intense fluorescent signal at ≈600 nm (λ_{ex} = 525 nm) in the presence of DNA due to its strong intercalation between the adjacent DNA base pairs, however, the addition of a competitive substrate which also binds to DNA drastically reduces the observed fluorescent intensity due to displacement and subsequent quenching of the EB molecules in aqueous solution.[284, 285] As the concentration of the competitive substrate increases, the fluorescence spectra shows a significant shift (red) in wavelength with a reduction in the fluorescence intensity clearly indicating that the EB molecules are displaced from their DNA binding sites and are replaced by the substrate under investigation.[286]

The fluorescence quenching spectra of DNA-bound EB by complex **1** is shown in figure 23 (and supporting figure 1) and illustrates that the quenching of EB bound to DNA **1** is in good agreement with the linear Stern–Volmer equation[287, 288]:

$$\frac{F_0}{F} = 1 + K_{SV}[Q] \qquad (2)$$

The Stern-Volmer quenching constant (K_{sv}) obtained by taking the ratio of the slope to the intercept (obtained by plotting F_0/F vs [Q]) yielded a value of $3.46 \times 10^4\ M^{-1}$. This values suggested that the complex **1** shows high quenching efficiency. Furthermore, the apparent binding strength (K_{app}) values obtained for the complex using the equation: K_{EB} [EB] = K_{app} [complex] (where the complex concentration has the value at a 50% reduction of the fluorescence intensity

of EB and $K_{EB} = 1.2 \times 10^6\ M^{-1}$, ([EB] = 4 μM)) was $3.2 \times 10^5\ M^{-1}$, which suggest moderate binding strength. An alternative calculation of the binding constant (K_b) value obtained from a plot of log[$(F_0-F)/F$] vs log [Q] were found to be $1.68 \times 10^5\ M^{-1}$ as shown in figure 24, confirming the moderate binding ability. A typical DNA intercalator like EB has a binding constant of $3.0 \times 10^6\ M^{-1}$.[283, 289] Given that the K_{app} from the competition experiments are an order of magnitude less than a known intercalator it confirms complex **1** is in fact a weak-moderate intercalator.

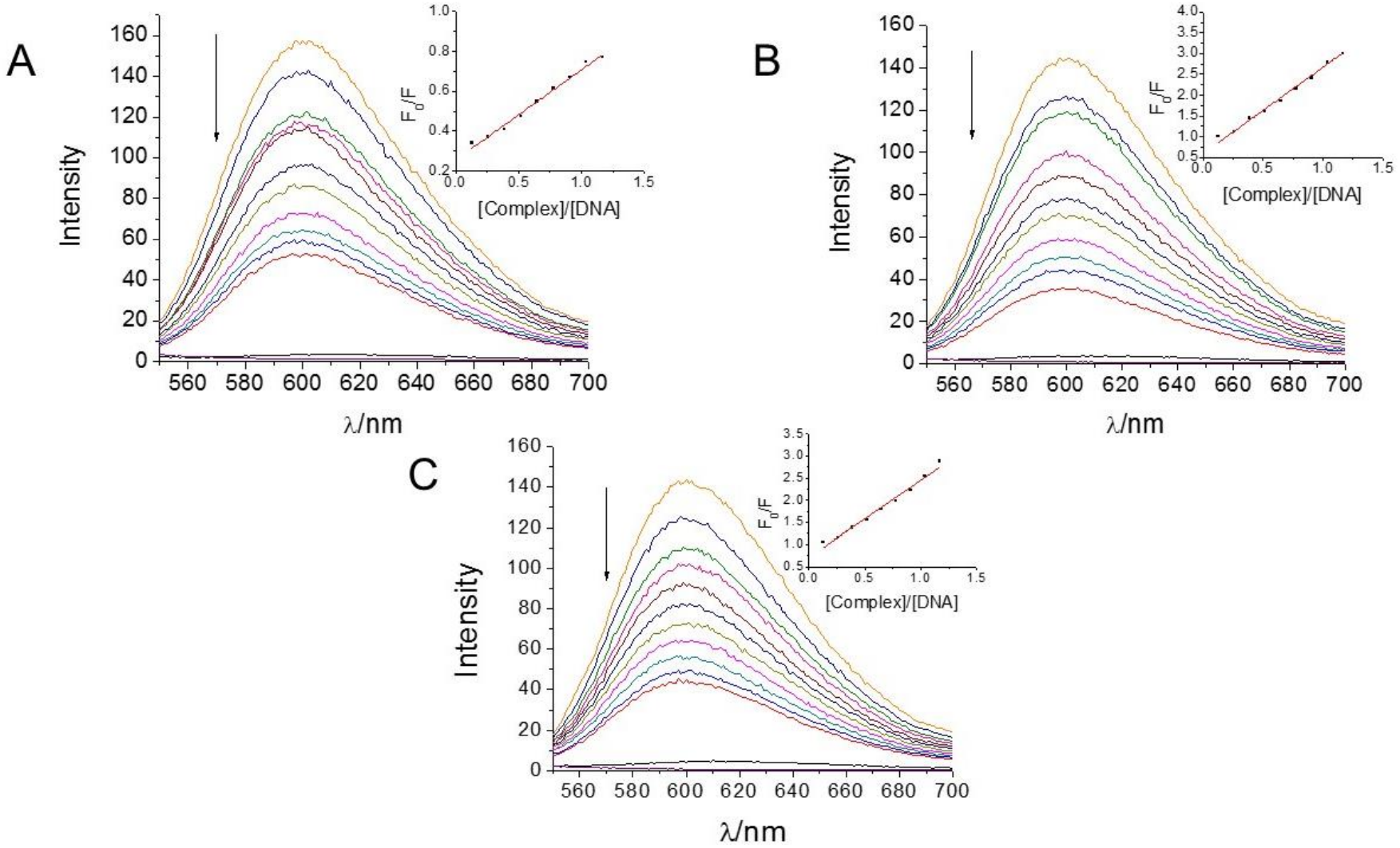

Figure 23. Fluorescence spectra of competition of EB and complex **1** binding with CT DNA. λex = 520 nm, [EB] = 0.33 µM, [DNA] = 10 µM, [M] (µM): 0 – 30 in 5 µM increments. Temperature = A) 293 K, B) 298 K, C) 304 K. Inset: Plot of Fo/F vs. [Complex].

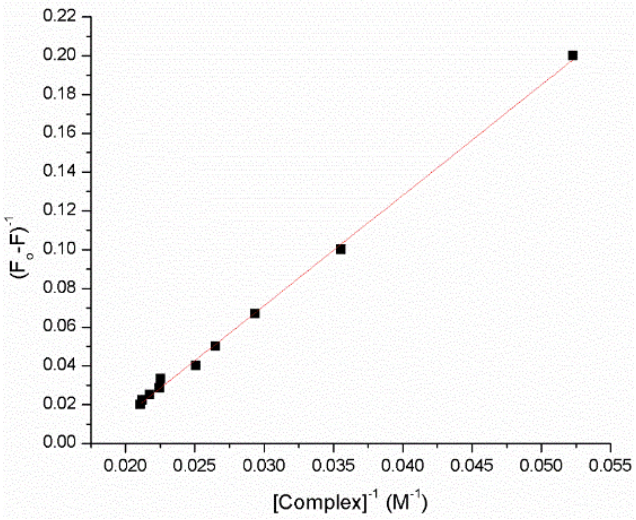

Figure 24. A plot of $(F_o\text{-}F)^{-1}$ vs. $[Complex]^{-1}$ obtained from the fluorescence titration of complex **1**.

The quenching of the fluorescence can occur via two mechanisms – dynamic and static quenching.[287] It is proposed that in the reaction here, predominantly static mechanism is operating. In this scenario a quencher-fluorphore complex is formed. This is inferred from the bimolecular quenching constant (K_q) calculated using τ_0 = 22 ns for the EB-DNA complex. K_{eq} for the reactions are on the order of 10^{12} $M^{-1}s^{-1}$ which are two orders of magnitude larger than the limiting value of 10^{10} M^{-1} s^{-1} considered the largest possible value in aqueous solution.

The typical thermodynamic parameters for a reaction can be calculated from the obtained binding constants using the following relationships:

$$ln\frac{K_2}{K_1} = \frac{\Delta H}{R}\left(\frac{1}{T_1} - \frac{1}{T_2}\right) \quad (3)$$

$$\Delta G = \Delta H - T\Delta S = -RTlnK \quad (4)$$

Table 3. Binding constants and thermodynamic parameter for interactions of complex **1** with the EB-DNA complex

T/K	K (10^{-4})/ (M^{-1})	R^2	$\Delta G°$ / kJ mol^{-1}	$\Delta H°$ / kJ mol^{-1}	$\Delta S°$ / J mol^{-1} K^{-1}
298	12	0.9899	-30.8	40	237
304	16.5	0.9942	-32.4		

The values obtained are given in table 3. There are several intermolecular forces at play when a small molecule binds to a macromolecule. Both the ΔH^o and ΔS^o are positive which suggest that the major force in the action is hydrophobic in nature. This is most likely attributed the water molecules around the DNA being displaced upon binding to the compound and the whole system acquiring a more random configuration.

The cytotoxicity of complex **1** against a model metastatic breast cancer cell line was measure by means of the MTS (colorometric) assay, which serves as an index of cell viability by detecting the reduction of a tetrazolium compound to purple formazan product in the presents of NADPH or NADH produced by dehydrogenase enzymes in metabolically active cells. As shown in figure 25, the compound exhibited a concentration-dependent decrease in cell viability after a 24 h treatment. An IC_{50} value of 34.4 ± 5.2 μM was calculated indicating moderate anti-cancer activity for complex **1**. Additionally, the precursor $[Co(phen)_2(OH_2)_2](NO_3)_3$ has previously been shown to be non-toxic in multiple cell lines therefore the observed activity by this complex **1**, must be derived from the biological activity of this specific architecture, and not simply from the chaperoning of "free" Co(III) into cells by the ligand. The inhibition of cancer cell proliferation induced by anti-cancer drugs could be a result of regulated cell death (i.e. apoptosis and necrosis)

or cell cycle arrest, or a combination of these two modes.[290, 291] Due to the many potential cellular targets (i.e. nuclear DNA, mitochondria, etc.) as well as potential background absorbance of the complex confirmation of the calculated IC_{50} values were attempted utilizing two other assays which measure different cellular function, specifically lactate dehydrogenase and ATP activity, however protocols were never fully optimized for these methods.

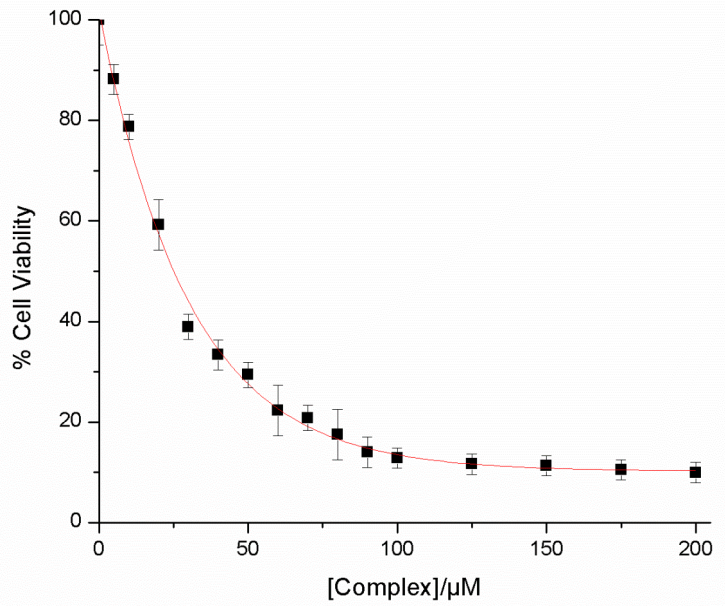

Figure 25. 4T1-luc cellular viability following exposure to complex **1**. Graphs represent minimum (n = 3) replicates of data with plates being 1 h post incubation with MTS reagent. Data was fit using an exponential function using Origin 8 software. IC50 value = 34 ± 3.5 μM

Apoptosis can be initiated by two main mechanisms, extrinsic (death receptor) and intrinsic (mitochondrial) pathways. Caspases, members of the cysteine acid proteases family, are known effectors in both the mitochondrial and receptor mediated apoptotic pathways.[292, 293] The roles of known caspases are outline in table 4. To determine the molecular events initiated by complex **1**, the activity of "executioner" capsases-3 and -7 were examined, using fluorometric assays.

Monitoring the activity of this effector proteins would discern whether cell-death induced by complexes was due to apoptosis or other biological factors. Figure 26 shows the complex **1** induces increases in caspase-3/7 cleavage in a concentration dependent manner over a five hour time period, with peak activity occurring at 4 hours. Additionally, the preincubation of a common pan caspase inhibitor z-VAD-fmk completely inhibits caspase cleavage in all concentrations. Following this observation, the effect of inhibiting the caspase cascade on cellular viability was investigated. As shown in figure 27, the presence of z-VAD-fmk, shifted the calculated IC_{50} value to the higher concentrations with the calculated IC_{50} value for the complex almost doubling to ≈ 64.6 ± 4.7 μM. This data indicated that complex **1** induces a caspase dependent, apoptotic cell death, which is the proposed major mechanism of cell death in response to this complex. However, without monitoring other upstream effector caspases (i.e. caspases-8,-9) and proteins (i.e. BAX, Bcl-2, BAD, BID, and PKB) it is impossible to determine whether the observed apoptotic event stems from either the extrinsic or intrinsic pathways. However, given the data obtained from the UV-vis and fluorescence binding assays previously discussed, which indicate DNA intercalation/interaction, it is hypothesize that the apoptotic event is initiated after DNA damage which would activate the intrinsic (mitochondrial) pathway. However, further experimentation will be needed to validate this hypothesis.

Table 4. Role of caspases

Caspase	Conventional Role	Other Roles
Caspase-1	Inflammatory Response	Unknown
Caspase-2	Apoptosis (Initiator)	DNA damage response
Caspase-3	Apoptosis (Executioner)	Cell differentiation
Caspase-4	Unknown, presumed inflammatory response	
Caspase-5	Inflammatory Response	Possible tumor suppressor
Caspase-6	Apoptosis (Initiator)	Unknown
Caspase-7	Apoptosis (Executioner)	Unknown
Caspase-8	Apoptosis (Executioner)	Embryonic development, motility, tumor metastasis, T cell proliferation, cell cycle regulation, bacterial infection response
Caspase-9	Apoptosis (Initiator)	Differentiation of cell type
Caspase-10	Apoptosis (Initiator)	Immune response to dsRNA, possible tumor suppressor
Caspase-11	Inflammatory Response	Cell migration
Caspase-12	Inflammatory Response	Unknown
Caspase-14	Keratinocyte differentiation	Unknown
Caspase-15	Apoptosis (Initiator)	Unknown
Caspase-16	Unknown, phylogenetic association with caspase-14	Unknown
Caspase-17	Unknown, phylogenetic association with caspase-3	Unknown
Caspase-18	Unknown, phylogenetic association with caspase-8	Unknown

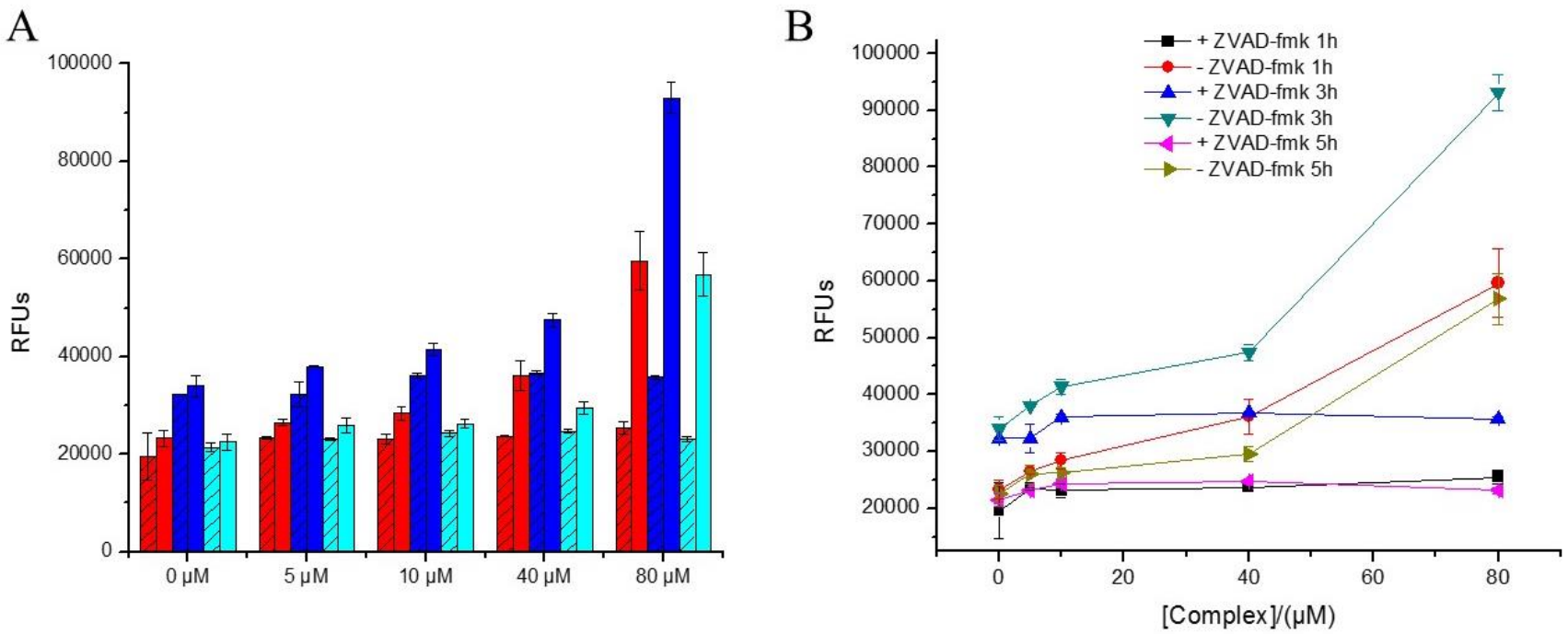

Figure 26. Complex **1** induces increase in cleavage of caspase 3/7 in 4T1-luc cells in a concentration dependent manner. 4T1-luc cells were preincubated in the presence or absence of 10 µM pan caspase inhibitor z-VAD-fmk for four hours followed by exposure to **1** for various time: 1 h (red), 3 h (blue), 5 h (cyan). ‖ indicate cells pre-incubated with zVAD-fmk for 4 hours. The activity of caspase-3/7 was measured using Caspase-Glo assay with DEVD-aminoluciferin as a substrate. Data represents the mean ± SE (n = 3).

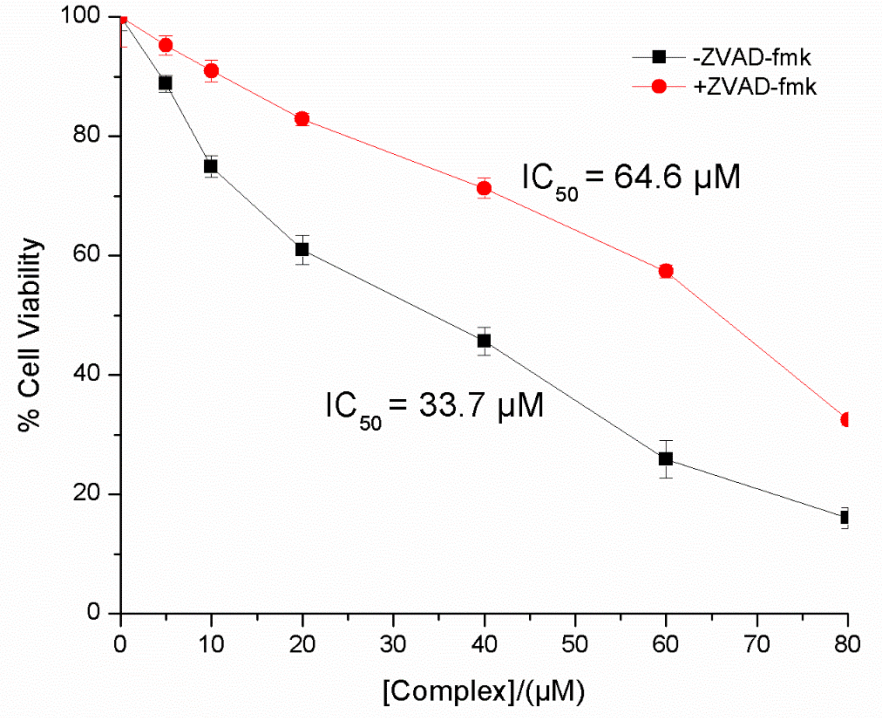

Figure 27. Determination of effect of inhibition of caspase cleavage on cell death in 4T1-luc cells following exposure to complex **1**. Absence (black line) or presence (red line) of z-VAD-fmk. Values from each point were normalized to control values. Values represent the mean ± SE (n=3).

The mitochondria is often described as an essential target for cancer chemotherapy as it plays a critical role in the regulation of cell fate by integrating the apoptotic signals which originate both from intrinsic and extrinsic pathways.[294-296] Disruptions in mitochondrial-mediated events often lead to increases in caspase-3 activity.[297] The mitochondrial pathway is activated by BH3-only subset of Bcl-2 family proteins (BID and BIM) which subsequently activated multidomain BH123 proteins (BAX and BAK), the latter of which permeabilize the mitochondrial membrane. Due to the increases in caspase-3 activity, the ability of complex **1** to modulate the mitochondrial membrane potential ($\Delta\Psi_m$) was investigated via flow cyotometric analysis using

tetramethylrhodamine methyl ester (TMRE). As observed in figure 28A there are two distinct cell populations prior to treatment with approximately 83% of cells exhibiting a higher membrane potential (upper left quadrant) and 17% with a lower membrane potential (lower left quadrant). After two hours of incubation with complex **1**, there is a concentration-dependent increase in the number of cells with a low membrane potential beginning at 40 µM and a maximum of 47% of cells exhibiting with a lower membrane potential at the highest concentration tested (Figure 28B-F). Table 4 further shows a concentration dependent modulation in the ΔΨm beginning at approximately the IC_{50} for **1** (A2 – A5). While there do not appear to be many clear trends based on the data in table 5, a few conclusion can be drawn. Low concentration of complex **1** seem incapable of inducing an effect on the $\Delta\Psi_m$ after 2 h of incubation, however at 4 h a concentration dependent increase in low membrane potential cells is observed, indicating it takes longer for low concentrations to affect the mitochondria. At the 4 h time point, effects on $\Delta\Psi_m$ at higher concentration of the complex showed that populations of cell remaining at that time had a $\Delta\Psi_m$ like cells of the original control levels. However, at 6 h the higher complex concentrations now indicated populations of cells that again exhibited lower $\Delta\Psi_m$ values, while lower complex concentrations exhibited lesser effects on the remaining populations after effects observed at 4 h. This interpretation is consistent with effects on cells at intermediate complex concentrations, where 40 µM had effects at all three time points. This indicates that the 4T1 cells have different levels of sensitivity to complex **1** with higher concentration affecting some cells rapidly (2 h) and affecting a more resistant population later (6 h). These results are, however, consistent with the increase in caspase activity observed with the fluorogenic assays, therefore further validating the proposed intrinsic apoptotic pathway as the major cell death regulator.

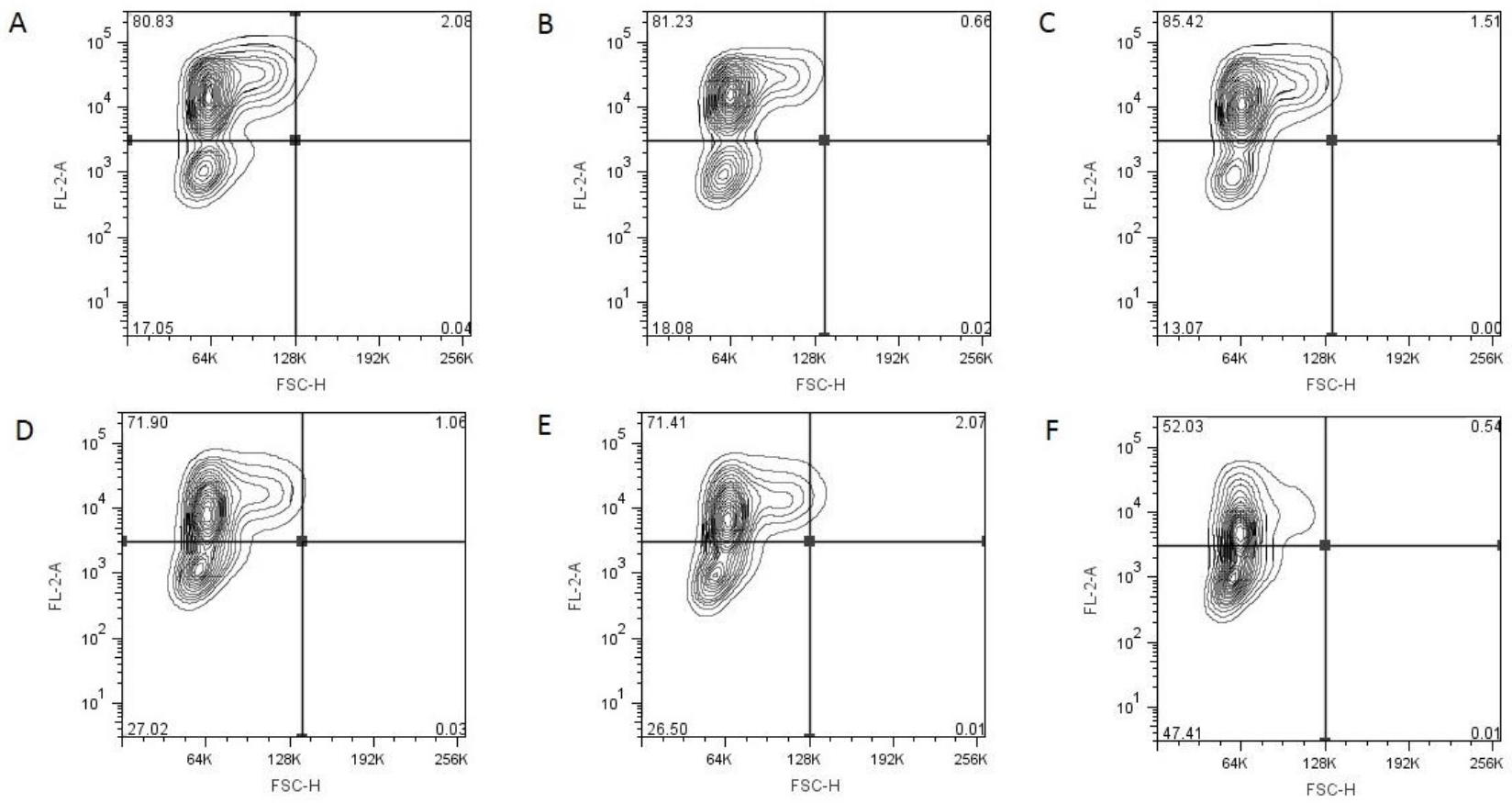

Figure 28. Representative contour plots of fluorescence resulting from $\Delta\Psi_m$ after two hours (FL2-H, Y-axis) and FSC-H (Y-axis).A) 0 µM; B) 5 µM; C) 20 µM; D) 40 µM; E) 60 µM; F) 80 µM complex **1**. Data represents 20,000 molecular events collected.

Table 5. Percentage of cell population positive and negative for TMRE

Complex (μM)	2 hours			4 hours			6 hours	
	-	+		-	+		-	+
0	17.05	80.83		24.92	73.21		16.96	78.88
5	18.08	81.23		36.63	60.72		14.16	79.37
20	13.07	85.42		48.76	49.73		31.86	61.65
40	27.02	71.90		42.35	55.63		50.11	46.01
60	26.50	71.41		39.93	58.44		52.42	45.26
80	47.41	52.03		17.33	80.58		45.21	53.42

With another potential molecular target identified in the mitochondria, further investigation into other regulated cell death (RCD) mechanisms were undertaken to discern other molecular events initiated in response to complex **1**. Autophagy is a conserved process of cellular degeneration in eukaryotic cells, in which unfolded, aggregated, or long-lived cytoplasmic proteins are delivered to the lysosome for degradation.[298] Under "normal" conditions, autophagy remains at low levels for maintenance of cellular homeostatis, however, autophagy can be readily induced in response to nutrient deprivation, metabolic stress, radiation, anticancer drugs, endoplastic reticulum (ER) stress, and reactive oxygen species.[299] The ability of the complex **1** to induce autophagy was monitored using flow cytometric methods and is shown in figure 29 to determine if the complex can induce activation of other RCD pathways. As shown in figure 29 after 24 hour treatment with complex **1**, the mean fluorescent intensity of cells treated with 5 μM (cyan) and 10 μM (yellow/orange) are significantly increased (shifted right) compared to unstained (red) and control, untreated cells (dark green). This shift in fluorescence intensity indicates the presence of

the autophagasome and other organelles associated with the induction of the autophagy process. Conversely, in high dose treatments there is a decrease in the mean fluorescence intensity (left shift) indicative of the absence of the organelles associated with autophagy, which is likely attributed to the movement of cells from the initial stages of autophagy to cell death. However, as evident in figure 30C/D high concentrations of complex **1** also induce autophagy, however, the effect is only observable at shorten time periods (1-7 hours vs 24 hours). This finding is not uncommon as it is known that autophagy can be induced as a protective mechanism depending on the extent and duration of the treatment. The induction of autophagy in a time dependent manner also could explain the observed increase in cellular viability at early time points in low doses in a time course of viability (supporting figure A5).

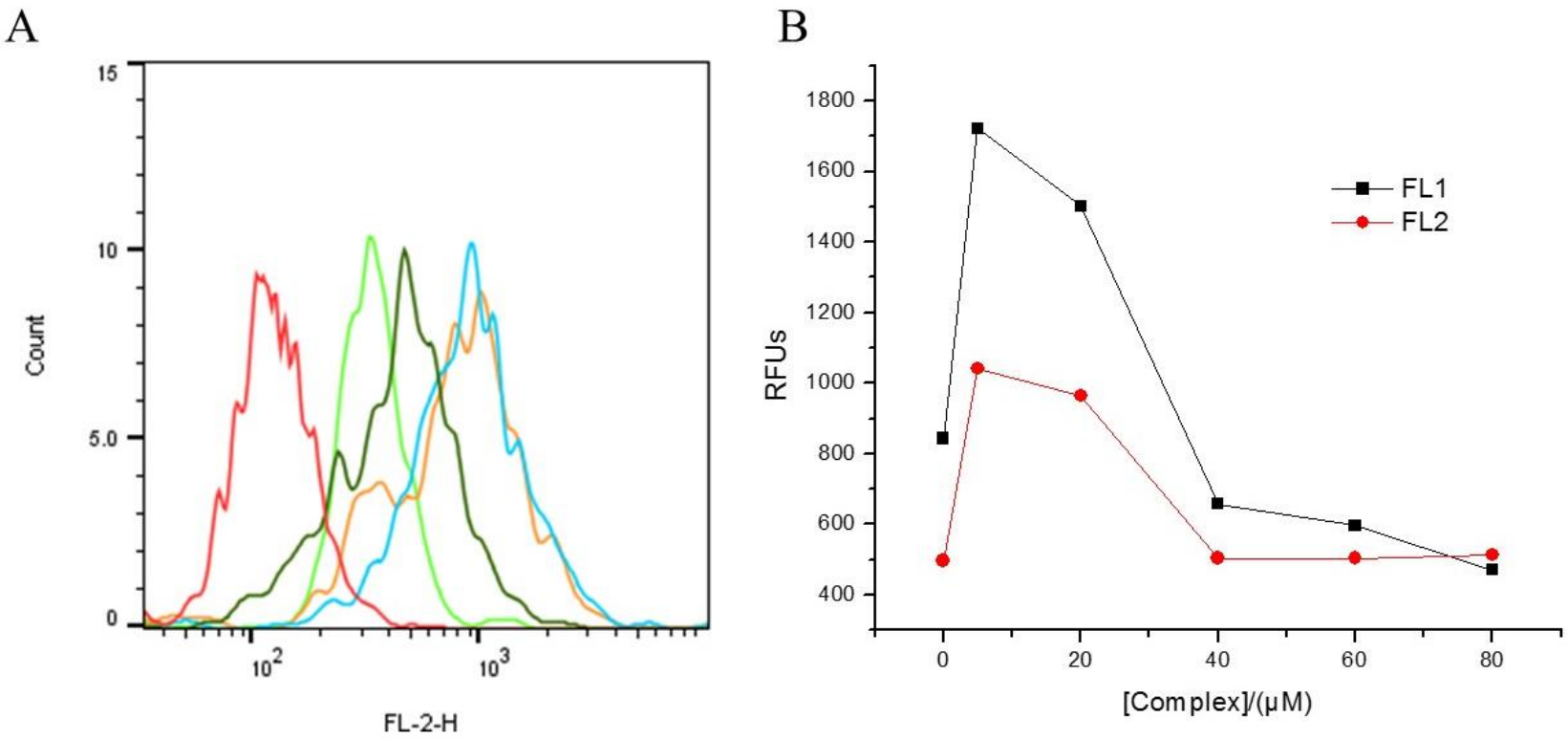

Figure 29. Complex **1** induced autophagic flux after 24 hour treatment. A) Representative histograms are shown of fluorescence resulting from autophagic flux (FL2-H, X-axis) and cell counts (Y-axis). B) Plot of the RFUs vs [Complex]. Red – unstained cells, dark green – 0 μM, cyan – 5 μM, yellow – 10 μM, lime green – 80 μM. Data represent mean of 10,000 molecular events.

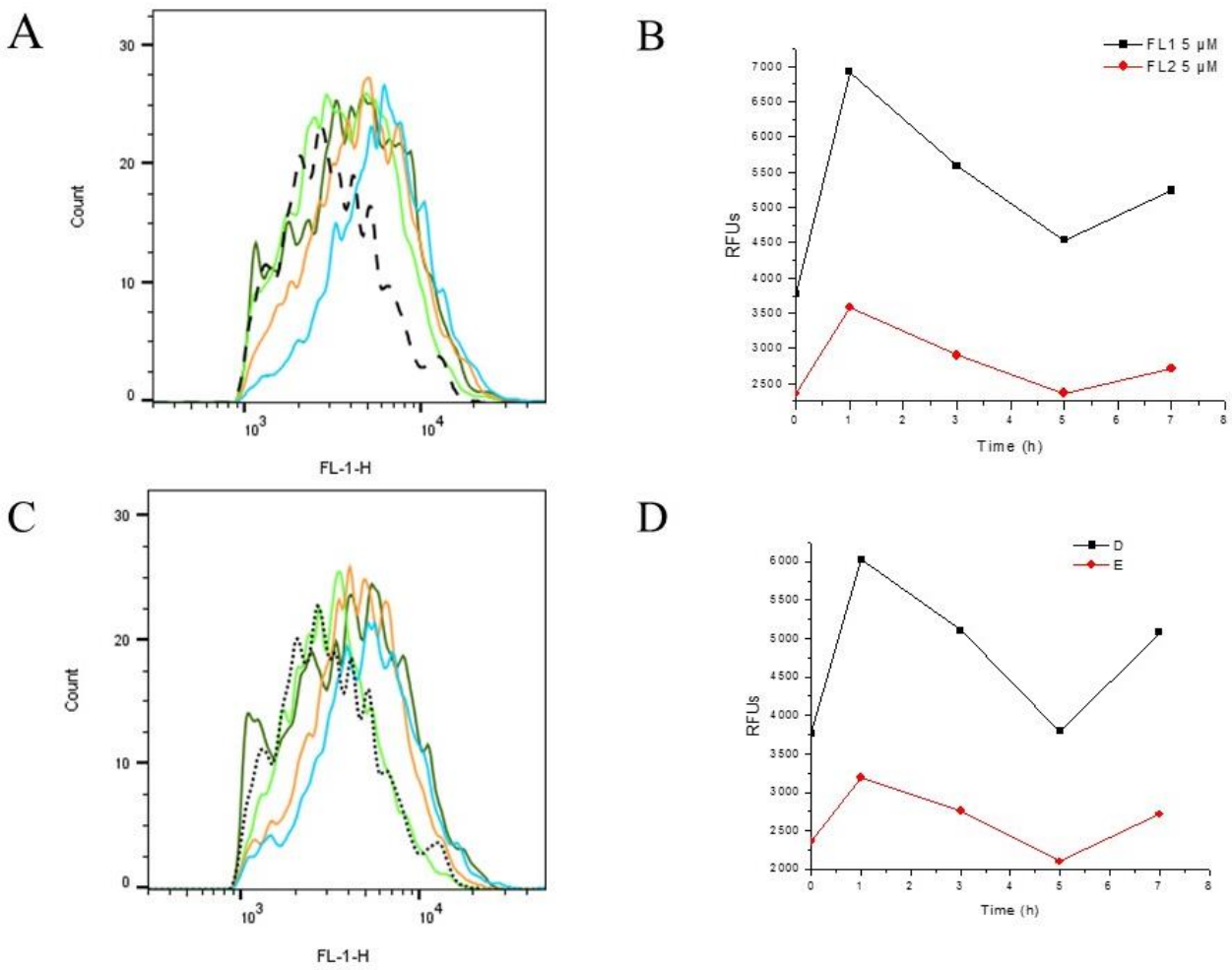

Figure 30. Time course induction of autophagic process following exposure to complex **1**, upper and lower rows indicate treatment with 5 and 80 µM complex **1**, respectively. A/C) Representative histograms are shown of fluorescence resulting from autophagic flux (FL1-H, X-axis) and cell counts (Y-axis). B/D) Plot of the RFUs vs time. Data represent mean of 20,000 molecular events.

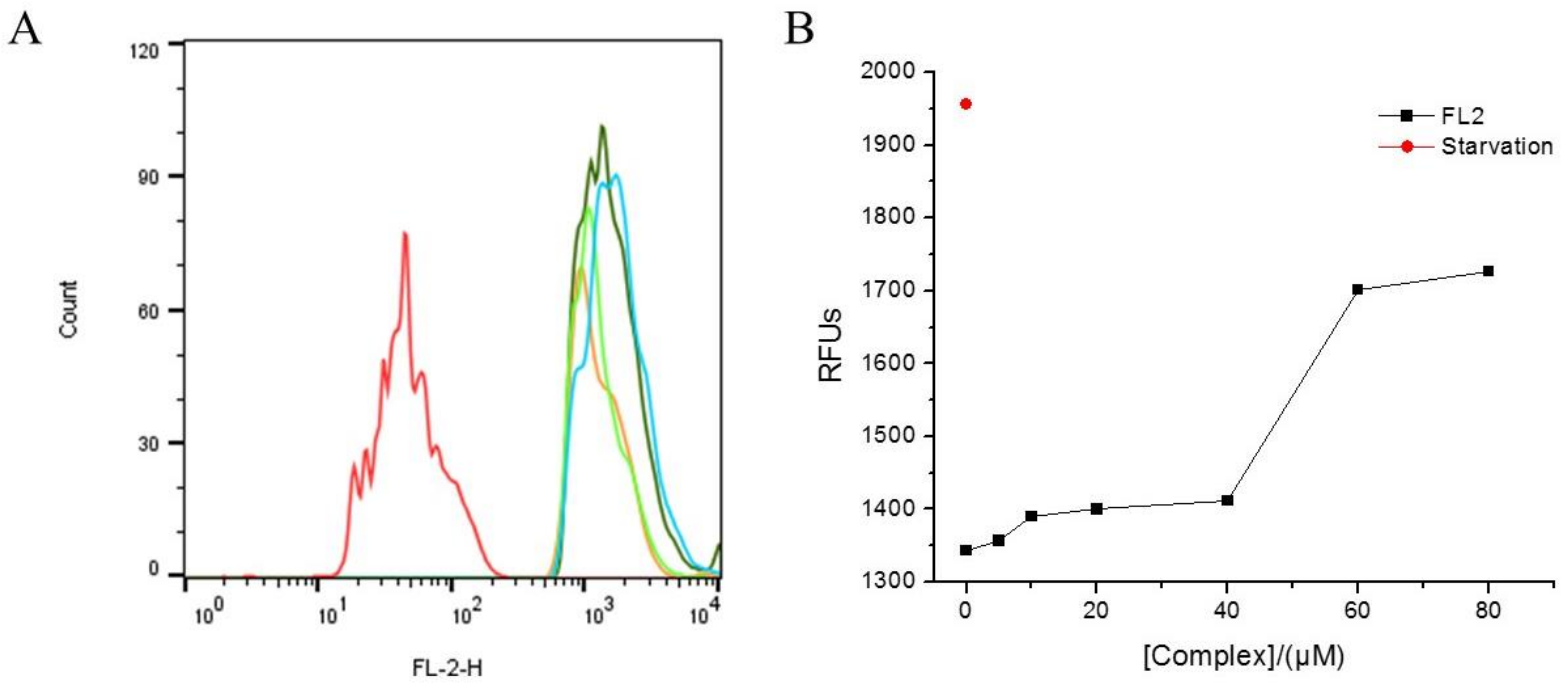

Figure 31. Necrostatin-1 inhibits autophagy induced by complex **1** in concentration dependent manner. A) Representative histograms are shown of fluorescence resulting from autophagic flux (FL2-H, X-axis) and cell counts (Y-axis). Red – unstained cells, dark green – 0 μM, cyan – 5 μM, yellow – 10 μM, lime green – 80 μM. B) Plot of the RFUs vs [Complex]. Data represent mean of 10,000 molecular events.

Although autophagy can be often viewed as a protective mechanism, it can also lead to post-autophagic death after autophagic cell protection has failed. Thus the appearance of large scale cell death in a time- and concentration-dependent manner in figures 29 and 30. The regulatory events that facilitate the switch from a "protective" event to autophagic death mechanism are poorly defined.[299-301] In order to determine the role of autophagic death in the overall regulated cell death processes following exposure to complex **1**, viability was determined in the presence and absence of necrostatin-1. Necrostatin-1 is commonly utilized as a necroptosis inhibitor, although, it has recently been shown to be an applicable inhibitor of autophagy and minimally apoptosis.[302, 303] As shown in figure 31 it is possible to inhibit the autophagy process by utilizing necrostatin-1, however, eventually the protective nature of this event is overcome at concentrations greater than the IC_{50} (>40 μM, complex **1**). A comparison of the IC_{50} values in the absence or presence of the inhibitor shows only a slight difference (figure 32), of approximately 10 μM. This shift is most likely attributed to the loss of the initial "protection" afforded to the cells by the activation of the aautophagic pathway. Unlike the effect observed with caspase inhibition this shift is minimal and only contributes minimally to the overall observed cell death.

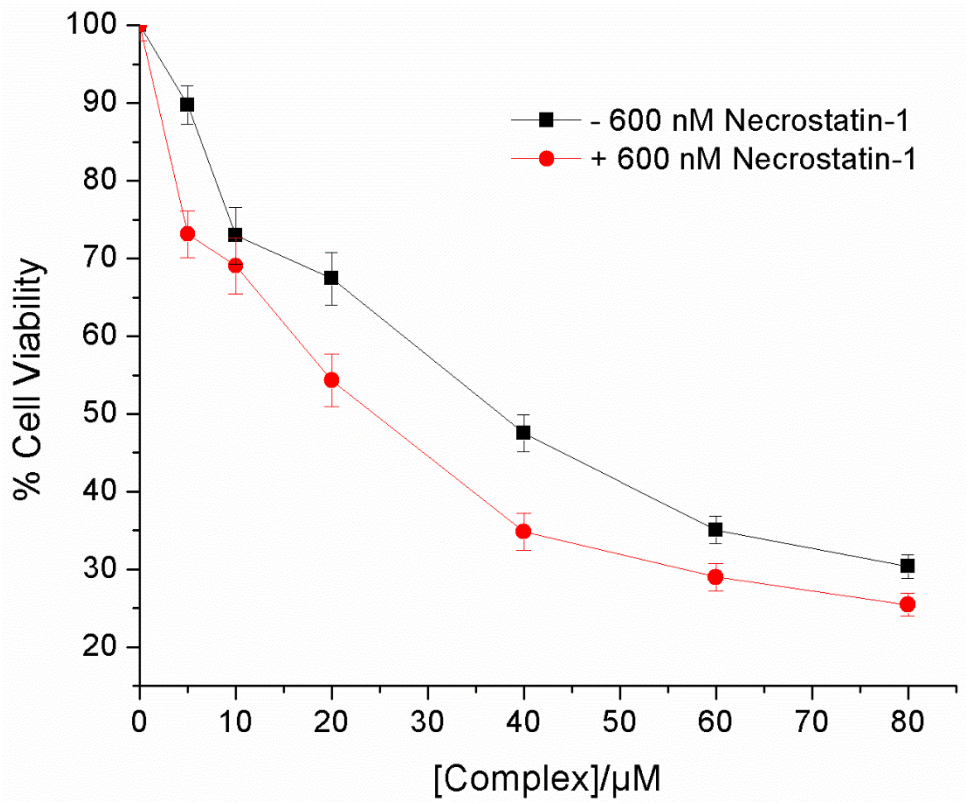

Figure 32. Cell viability graphs following treatment of 4T1-luc cells with complex **1** in the presence or absence of necrostatin-1. Cells were seeded at 2.5 x 10^4 cells per well for 24 h prior to addition to treatment. Graphs represent n = 3 replicates of data with plates being 1 h post incubation with MTS reagent. Data was fit using an exponential function using Origin 8 software.

Nanosecond pulsed electric fields (nsPEFs) are an emerging bioelectrical technology that has showed its potential in cancer therapy.[304, 305] NsPEFs can generate pulsed high voltage electric field in ultra-short nanosecond duration to produce immediate power, which could ablate targeted tumor.[306-308] NsPEFs mediates cell destruction by multiple mechanisms.[255, 256, 309] The nanosecond pulses with a high intensity electric field changes the permeability and change the electric properties of the plasma membrane and intracellular organelle membrane, which results in apoptosis or apoptosis-like cell death. Unlike RFA or PEI, nsPEFs does not rely on heat production

or chemical ablation, thus producing a lower risk of local complications, such as thermal or chemical injuries.[257, 264, 309]

Prior to determining if an inherent synergy exists between the use of transition metal complexes and nsPEF, we must first investigate the effect of applying nsPEFs to 4T1-luc cells. To complement the experimental data on complex **1** (i.e. IC_{50} values) we first set to determine the effect of modulating the pulse electric field strength and number on 4T1-luc cells to determine an EF_{50} value. The effect of nsPEF on cellular viability 24 hours post treatment is shown in figure 33 as determined by the MTS assay. It is clear that nsPEFs produced a dramatic decreased on *in vitro* cell survival with increases in pulse number and electric field strength. Surprisingly, there is little effect on viability from variable pulse numbers (1 – 10 pulses). In a manner similar to complex **1**, this information allowed for the calculation of EF_{50} following treatment which was calculated at approximately 30 kV/cm for pulses with 60 ns durations.

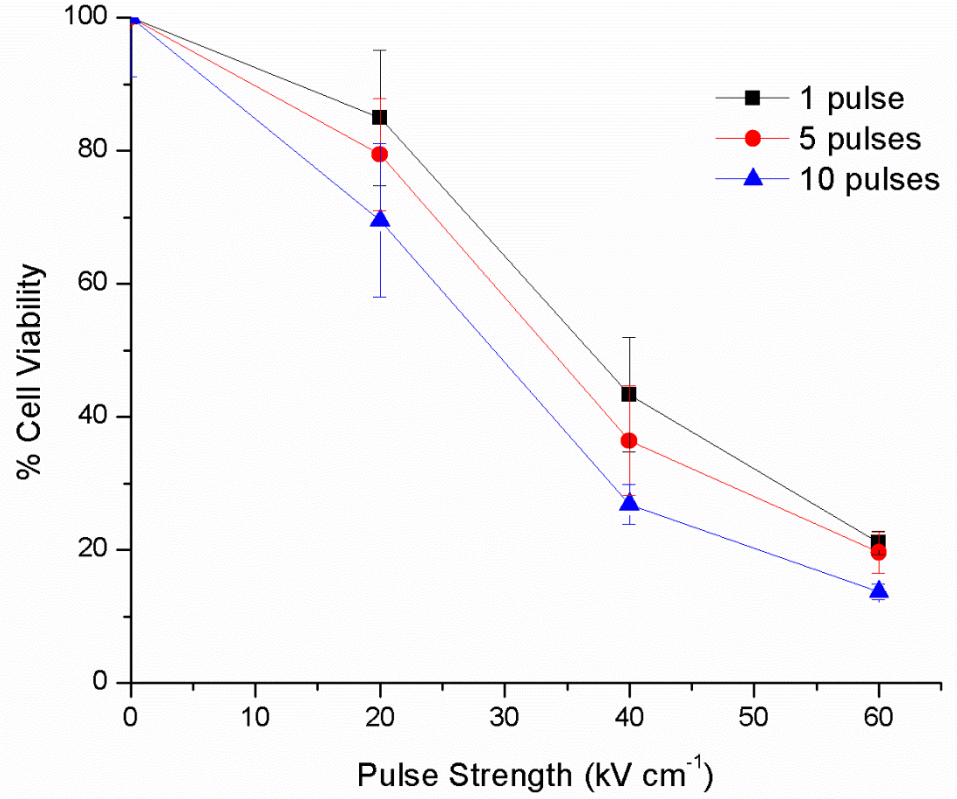

Figure 33. 4T1-luc cellular viability following exposure to nsPEFs utilizing various pulse strength at a 60 ns pulse duration. Cells were seeded at 2.5 x 10^4 cells per well for 12 hours. Graphs represent n = 3 replicates of data with plates being 1 h post incubation with MTS reagent.

It was previously observed a synergistic effect exist between a chemotherapeutic small organic molecule 4-amino-1-(2-deoxy-2,2-difluoro-β-D-erythro-pentofuranosyl)pyrimidin-2(1H)-on (gemcitabine) and low dose nsPEF technology in human oral squamous cell and breast cancer carcinoma due to increases in intracellular calcium levels following nsPEF treatment.[310] It is important to note that while nsPEFs induce formation of nanopores in plasma membranes, these pulses do not enhance delivery of drugs to cells as has been observed with ECT.[311-313] We therefore set out to determine whether a similar underlying synergistic effect exists between complex **1** and nsPEF technology. To investigate this effect 4T1-luc cells were incubated with low concentrations

of complex **1** (5 or 7.5 µM) for 24 hours and then were exposed to 60 nsPEFs of varying pulse numbers, with cellular viability being determined 24 hours post pulsing. Low dose treatments are required for both treatments in order for a synergism quotient to be calculated. Initially strictly synergism studies where carried out utilizing the IC_{15} and EF_{10} of the individual treatments (7.5 µM and 20 kV/cm, respectively), which would result in a 10 – 15 % decrease in cellular viability, individually. If a synergism were to exist a killing efficiency >25%, should be observed. However, as shown in figure 34 dual treated cells receiving either 1 or 5 20 kV/cm pulses and 7.5 µM complex **1** showed a slight increase in cellular viability as shown by the increase in the absorbance reading compared with the untreated control cells the opposite of the predicted effect.

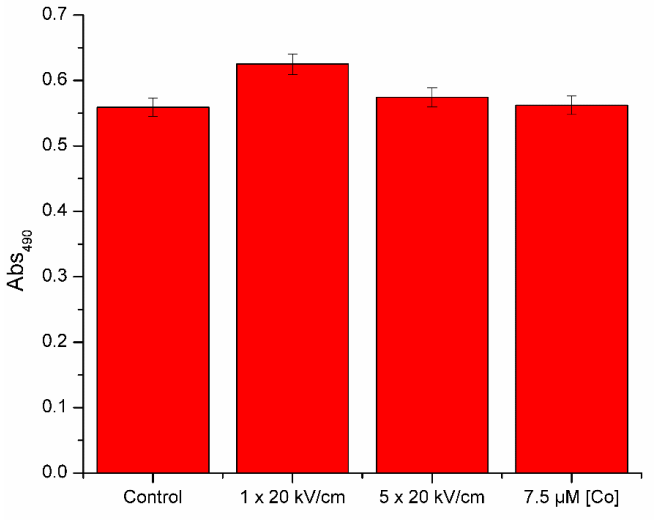

Figure 34. Viability of 4T1-luc cells following dual treatment with complex **1** and nsPEFs (60 ns pulse duration).

Following initial experiments a protocol similar to that reported by Wang *et al.*[310] was adopted, in which one concentration of drug treatment and varied electric field strengths were

employed. In these studies, electric field strengths were varied from 0 to 60 kV/cm following incubation with complex **1** at 7.5 μM. Similar to figure 33, in figure 35A/B an electric field strength dependent decrease in cellular viability in cells only exposed to nsPEF was observed, however, in pulse strengths greater than 20 kV/cm there appears to be a protective event in cells preincubated with **1** prior to exposure to nsPEFs which seemingly negates the effect of the nsPEF. In the high dose electric field, ≥40 kV/cm, the protective effect observed increases cellular viability 2-fold greater than when nsPEFs are utilized alone. As previously shown, low concentration dose treatments with complex **1** leads to the induction of autophagy which could potentially place the cells within a heighten protective state and lead to increased cell survival. As previously shown for this cell line autophagy can be inhibited by the addition of necrostatin-1 and therefore, preincubating the cells with necrostatin-1 would negate any protective event occurring from the induction of autophagy. As shown in figure 35, the addition of necrostatin-1 to inhibit the autophagic process showed minimal differences on cellular viability when compared to cells not exposed to necrostatin-1, indicating that autophagy is not the cause of the protective event observed. While both treatments were shown to be effective inhibitors of cell grown individually, a synergism was not detecting when utilized in combination.

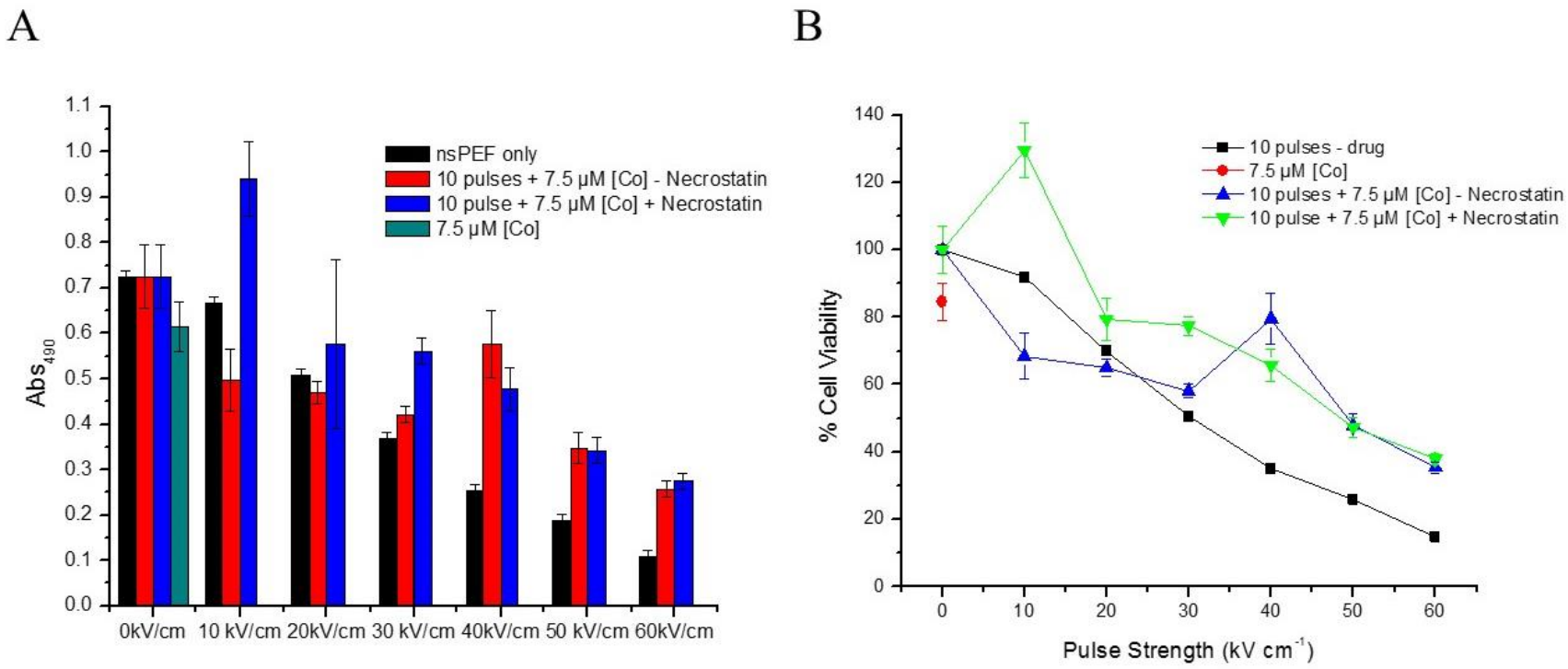

Figure 35. 4T1-luc viability following exposure to complex **1**, nsPEFs (60 ns duration), or a combination. A) Plot of absorbance vs electric field strength; B) Plot of percentage of viable cells vs pulse strength. [Necrostatin-1] = 600 nM

While there have been no previous reports of a combination therapy involving a transition metal complex and nsPEFs, previous studies by Pakhomov and coworkers,[314, 315] reported that lanthanide ions (Gd^{3+} and La^{3+}) could block plasma membrane electropermeabilization induced by nsPEFs thereby reducing cell death. Permeabilization of both the plasma membrane and mitochondrial membrane have be implicated to be important in cell death in treatment of various cancers.[255, 316-318] Furthermore, while the application of transition metal complexes is increasing in frequency for chemotherapeutic purposes, little mechanistic knowledge is reported on cobalt drugs specifically, with the exception of studies involving DNA intercalation and *in vitro* toxicity.[158, 168, 319, 320] While it is interesting to speculate on the hypothesis that a synergism must exists between **1** and nsPEFs, extensive studies are needed to further elucidate the mechanism of action of both techniques individually prior to offering an explanation on the nature of the observed protective effects.

CONCLUSION

In conclusion, preliminary mechanistic investigations of the potential mechanism of action of a cobalt(III) complexes beating a thiosemiacarboazone ligand (MeATSC) were presented. Our data indicates that complex **1**, similar to many other polypridyl transition metal complexes, binds and interacts to DNA in an intercalative manner albeit in a weak fashion. Competition assays conducted with EB calculate a K_{app} value of 3.2×10^5 M^{-1} making the complex a weak to moderate metallointercallator, an unsurprising finding given not only the heteroaromatic ligands but additionally the large anthracene moiety present which may stack between DNA base pairs. *In vitro* analysis of the complex indicates the complex **1** is moderately toxic ($IC_{50} \approx 34$ μM) to the model metastatic breast cancer cell line, with the most significant contribution to cell dearth arising from the intrinsically activated apoptotic pathway, as evident by the increase in caspase catalytic

activity and dissipation of the $\Delta\Psi_m$. Additionally, the complex was also shown to induce autophagy in both a concentration- and time-dependent manner. While the results of H2AX were inconclusive (due to lack of optimization of protocol), it can be most likely concluded from the caspase, mitochondrial, and spectroscopic studies that the complex induces apoptosis through a mitochondrial mediate (intrinsic) pathway stemming from DNA damage, however, more intensive and localized mechanistic studies will be necessary to confirm.

Additionally, a potentially novel dual mode treatment therapy for cancer was discussed involving nsPEFs and transition metal chemotherapeutics. Following exploration of the effect of nsPEFs on the model breast cancer cell line, synergistic studies were undertaken to explore the effect of "sensitizing" cells to the nsPEFs. Contradictory to the hypothesized synergistic killing effect, a protective effect was observed in cells which were treated with both complex **1** and nsPEFs. Inhibiting the "protective" autophagic process yielded little to no change on cell survival following dual treatment illustrating autophagy is not the reason for the observed protective effect. A previous study with "free" Gd^{3+} ions hypothesized that the uncoordinated metal could stabilize or revert electropermeablization of the plasma membrane thereby inhibiting the effect of the nsPEF.[314] Future studies will focus on the effect of the nanosecond pulses on the intact Co(III) complex in both cell-free and cell-based environments.

These findings provide valuable insight into the mechanism of action of Co(III)-containing metallodrugs. Mechanistic insights into the bioactivity of such materials may inform the design of drugs which are better suited and selective towards target molecules and pathways. To further elucidate the mechanism or to guide the addition of an adjuvant treatment more intensive mechanistic investigations must be conducted on both Co(III)-based therapeutics and nsPEFs treatments individually.

CHAPTER 3

SYNTHESIS, CHARACTERIZATION, AND *IN VITRO* ACTIVITY OF V(IV) AND BINUCLEAR Ru(II)–V(IV) COMPLEXES FOR USE AS PHOTODYNAMIC THERAPEUTIC AGENTS

INTRODUCTION

With the recent emergence of photoactivated chemotherapy (PACT), or more commonly photodynamic therapy (PDT), as a non-invasive therapeutic treatment of cancer, comes the important challenge of designing new anticancer agents that show both nucleolytic and anti-metastatic activity selectively in cancer cells. As previously discussed, coordination complexes containing d^6 metal centers and polypyridyl ligand architectures have been developed as structure- and site-specific DNA binding agents.[113, 114] Due to the attractive photophysical properties, much research has focused on complexes containing d^6 ruthenium metal centers. As previously discussed in chapter 1, many examples exist of ruthenium(II) complexes which have been utilized as PDT metallodrugs with low toxicity and good selectively for tumor cells.[321]

As the search for adequate photodynamic therapeutic agents continues to evolve the systems being utilized are also constantly evolving. While DNA interactions with mononuclear ruthenium complexes have flooded literature recently,[322-325] similar interaction are possible with dinuclear ruthenium-containing species,[326-332] however their applications as potential DNA-binding agents remains largely unexplored. Dinuclear complexes offer increased variation in shape and size and have the potential to show greater specificity. Mixed metal dinuclear complexes offer even further advantages over ruthenium-ruthenium dinuclear complexes as the second metal center

utilized can possess its own unique biological application making for dual-application complexes or enhanced biological function.

Vanadium is a widespread element in the environment and an ultra-trace element in biological systems.[333, 334] The current interest in the chemistry of oxovanadium complexes has grown exponentially in recent years due in part to the resurgence in research that has shown that vanadium plays a large role in several biological processes,[335, 336] such as the regulation of carbohydrate metabolism.[337, 338] As early as the 19th century the insulin-mimetic properties of vanadium substrates have been reported.[339] Unsurprisingly, there are many reports of vanadium compounds displaying interesting effects at pharmacological doses both *in vivo* and *in vitro* systems.[340, 341] As an early first row d-block metal vanadium is capable of exhibiting a wide range or oxidation states, the most relevant valences of vanadium are +3, +4, and +5. Vanadium(III) and Vanadium(V) are unstable at physiological pH and in the presence of oxygen, however, the stability of V(IV) coordination compounds is strongly impacted by the ligands coordinated to the metal center.[342, 343] For instance, an example of a particularly stable V(IV) compound is the complex formed by V(IV)O with transferrin.[344] Additionally, while vanadium(III) complexes are rare, a recent study has shown that an organovanadium(III) compound, VC-III,[345] can mitigate cisplatin-induced genotoxocity and myelosuppression in mice.[346]

While the mechanism of vanadium toxicity are poorly understood, it has been reported that vanadium compounds can behave as growth factors which regulate cell growth.[347, 348] These mimetic properties allow vanadium agents to exert action upon signal transduction pathways and promote morphological changes in cells.[349-351] In some cases this has be extended to induction of anti-metastatic behavior, decreasing cell spreading and adhesion to the extracellular matrix as well as cell migration and clonogenicity.[352, 353] Extensive research has demonstrated that vanadium

compounds induce the generation of reactive oxygen species (ROSs) to produce adverse biological effect including: modulation of signaling pathway and DNA photocleavage.[354-359] On the other hand, other studies have reported that vanadium compounds promote apoptosis and convey the cells to death through the increasing of ROS levels and disturbance of the redox status, especially by alteration of mitochondria functions in the cells.[360, 361]

More recently, mechanistic investigations have focused on gaining deeper insights into the presumptive mechanism of action of vanadium derivatives. It has been shown that organically chelated vanadium compounds facilitate more pharmacological potency when compared with simple vanadium salts.[362] This facet can be attributed to the poor absorption of some vanadium species in the gastrointestinal tract, thereby increasing the effective dose of vanadium required to produce the pharmacological effect.[363, 364] Studies with oxidovanadium(IV) complexes, specifically, have demonstrated that some compounds cause substantial single strand breaks in DNA and produce lipid peroxidation.[359, 365] In this sense, the synthesis of vanadium complexes with ligands that hold multiple donor atoms is of considerable interest in vanadium biochemistry and in relation to their potential therapeutic applications.[366]

As previously stated, d^1-V(IV) complexes have been shown to photocleave DNA via generation of ROS, albeit with limited specificity.[367] As part of a continuing project related to vanadium compounds with potential pharmacological applications, the present study deals with the effects of an oxidovanadium(IV) complexes ([VO(oda)(phen)]·1.5H_2O or [VO(sal-*L*-tryp)(phen)]·H_2O), as well as binuclear Ru(II)-V(IV) species structurally similar to those reported by Holder *et al.*[127] on a mouse breast cancer cell line (4T1-luc). It is envisioned that these compounds will serve as photodynamic therapeutic agents as they possess a Ru(II) photosensitizing moiety and a potentially bioactive V(IV) moiety. Additionally, we have

investigated the interactions of these compounds with CT DNA as a model for the interactions of these compounds with cellular DNA. Understanding how both the mononuclear and binuclear species interact with DNA is pivotal to discerning the mechanism of action of these compounds. Increased understanding into the mechanism can also inform the rational design of future photodynamic therapeutic agents.

EXPERIMENTAL

General and Instrumentation

All reagents used in the syntheses, if not specified, were obtained from either Sigma-Aldrich (St. Louis, MO, USA) or VWR International (Radnor, PA, USA) and were used without further purification. $[Ru(pbt)_2(phen_2DTT)](PF_6)_2 \cdot 1.5H_2O$ and $[VO(oda)(H_2O)_2]$ were previously prepared by Holder *et al.*[127] and were utilized without further purification. [VO(sal-*L*-tryp)(phen)]$\cdot H_2O$ was synthesized using the procedure by Sasmal *et al.*[368]

The reagents utilized for the MTS assays were purchased from Promega Corporation (Madison, WI, USA). Microanalyses (C, H, N) were performed by Intertek Pharmaceutical Services, P.O. Box 470, Salem Industrial Park Bldg. #5, Whitehouse, NJ 08888. FT IR and ATR data was obtained using a Nicolet AVATAR 370 DTGS spectrophotometer. Ultraviolet absorption spectra were obtained using an Agilent 8453 diode array system. X-ray crystallography studies were conducted by Dr. Colin McMillen Director of the Molecular Structure Center, Department of Chemistry of the Clemson University (Clemson, SC, USA). ITC studies were performed utilizing a MicroCaliTC$_{200}$.

Synthesis of phen•HCl•H_2O

1,10-phenanthroline (2.00 g, 11.10 mmol) was dissolved in concentrated HCl (50 mL, 2.04 mol) in a 100 mL beaker. The resulting solution was transferred to a porcelain evaporating dish and evaporated over a steam bath. Upon drying an off-white crystalline power was obtained. Yield = 2.60 g (100 %). FT IR (KBr) cm^{-1}: 3094 (H_2O, s), 1406 (C=N, s).

Synthesis of complexes

Synthesis of [$VO(acac)_2$]

V_2O_5 (5.00 g, 27.5 mmol) was dissolved in H_2O (12 mL) H_2SO_4 (9 mL), and EtOH (25 mL) in a 250 mL round bottom flask and was placed in a boiling water bath. The reaction was stirred continuously for 30 minutes and the color changed from orange, to dark green to dark blue. After 30 minutes H_2O (20 mL) was added and the filtrate was collected in a 600 mL beaker. 2,4-pentanedione (13 mL, 126.3 mmol) was added the solution was stirred for 10 minutes. The solution was neutralized via the dropwise addition of aqueous sodium carbonate (20 g in 120 mL H_2O). The precipitate was collected by filtration and was recrystallized from chloroform to yield a blue powder. Yield (4.24 g, 60%). FT IR (KBr) cm^{-1}: 1529.35 (C=C=C, vs), 1373.14 (C=O, s.br), 997.07 (V=O, vs).

Synthesis of [VO(oda)(phen)]•1.5 H_2O (1) as by Álvarez *et al.*[369]

[$VO(oda)(OH_2)$] (0.1803 g, 0.8 mmol) was dissolved in H_2O (20 mL) in a 50 mL round bottom flask. Then solid o-phenanthroline (0.1607 g, 0.8 mmol) was added to the flask and it was stoppered and allowed to stand at room temperature of four days. After four days the solid green crystals in the reaction flask were collected by vacuum filtration. Yield = 0.2571 g (85%). FT IR (KBr) cm^{-1}: 3401.98 (OH, s,br), 1677.86 (COO asym, vs), 1143.64 (C-O-C, m), 1000.93 (V=O, vs), 451.28 (V-O, s).

Synthesis of [VO(oda)(phen)]•1.5 H_2O

[VO(oda)(OH_2)] (0.1803 g, 0.8 mmol) was dissolved in H_2O (20 mL) in a 50 mL round bottom flask. Then solid o-phenanthroline (0.1607 g, 0.8 mmol) was added to the flask and the contents were thoroughly mixed resulting in an opaque green solution, which was allowed to stand for at room temperature of four days. After four days the solution was filtered to afford a green powder. Yield = 0.2366 g (78%). FT IR (KBr) cm^{-1}: 3401.98 (OH, s,br), 1677.86 (COO asym, vs), 1143.64 (C-O-C, m), 1000.93 (V=O, vs), 451.28 (V-O, s).

Synthesis of [VO(oda)(phen)]•1.5 H_2O as by Del Rio *et al*.[370]

[VO(oda)(OH_2)] (0.1803 g, 0.8 mmol) was dissolved in H_2O (20 mL) in a 50 mL round bottom flask. Then solid freshly prepared phen•HCl (0.185 g, 0.8 mmol) was added to the flask and it was stoppered and allowed to stand at room temperature of four days. After four days the solid green crystals in the reaction flask were collected by vacuum filtration. Yield = 0.1041 g (34%). FT IR (KBr) cm^{-1}: 3401.98 (OH, s,br), 1677.86 (COO asym, vs), 1143.64 (C-O-C, m), 1000.93 (V=O, vs), 451.28 (V-O, s).

Synthesis of [Ru(pbt)$_2$(phen$_2$DTT)VO(oda)](PF$_6$)$_2$•2.0H_2O•0.5C_2H_5OH (2). NOTE: The synthesis of this compound was carried out by Ms. Kathy Currie and Dr. Alvin Holder.

[Ru(pbt)$_2$(phen$_2$DTT)](PF$_6$)$_2$•1.5H_2O (0.100 g, 0.074 mmol) and [VO(oda)(H_2O)$_2$] (0.0174 g, 0.074 mmol), were dissolved in a 2:1 ethanol/acetonitrile mixture (78 mL) in a 100 mL round bottom flask, and the reaction mixture was refluxed for three hours with stirring under argon at 110 °C. The reaction mixture was rotary evaporated to dryness, and the product was washed with ether and collected. Yield = 0.0993 g (85%). Calc. for $C_{57}H_{49}F_{12}N_8O_{10.5}P_2RuS_4V$, C, 43.21; H, 3.12; N, 7.07. Found: C, 43.24; H, 3.04; N, 6.66. FT IR (ν/cm^{-1}): 3421 (O-H, br, s), 1643 (C=O, s), 973 (V=O, m), 842 (PF_6^-, vs).

Preparation of buffers

The phosphate buffered saline (PBS) buffer was prepared by adding NaCl (8.004 g), KCl (0.2001 g), Na_2HPO_4 (1.7520 g), and K_2PO_4 (0.2003 g) to a 1000 mL volumetric flask and diluted with water. The 50 mM Tris-HCl buffer pH 8.0 was prepared by dissolving tris (6.057 g, 0.05 mol) in H_2O (700 mL) in a 1 L volumetric flask. Then 1 N HCl (8.98 mL of HCl conc. diluted to 100 mL with H_2O) (29.2 mL) was added to the volumetric flask and the solution was diluted to the mark. The pH of the solution was checked using a pH meter (8.01). The 5 mM Tris, 25 mM NaCl buffer pH 7.0 was prepared by dissolving tris (0.6057, 5 mmol) and NaCl (1.460 g, 25 mmol) in H_2O (700 mL) in a 1000 mL beaker. The pH of the solution was then adjusted to 7 via slow dropwise addition of concentrated HCl and was monitored via a pH meter. The solution was then transferred to a 1 L volumetric flask and was diluted with water.

Preparation of CT DNA stock solutions in various buffers

Stock solutions of CT DNA were prepared in each of the three buffers prepared above (PBS, 50 mM Tris-HCl pH = 8.0, 5 mM Tris/25mM NaCl pH = 7.0) by dissolving CT DNA (9 mg) in 25 mL of buffer in a 50 mL conical tube. The solutions were places in the refrigerator at 4 °C for twenty-four hours prior to use. Prior to each use of the stock solution the [CT DNA] was checked spectrophotometrically in a 0.2 cm quartz curvette using a ε_{260} = 6600 M^{-} cm^{-}. Dilutions were made quantitatively using the appropriate buffer and [CT DNA] was recalculated based on electronic absorbance spectrum. All solutions were used within four days of preparation.

Preparation of Ethidium Bromide stock solution for Isothermal titration calorimetry.

Ethidium bromide (0.216 g, 0.548 mmol) was dissolved in various buffers (50 mL) in a 50 mL conical tube. The concentration of the stock solution was determined spectrophotometrically prior to use using ε_{460} = 5600 M^{-} cm^{-}.

Isothermal titration calorimetry

ITC experiments were performed using a Microcal iTC200 microcalorimeter (MicroCal, Massachusetts, USA). Prior to ITC experiments, instrument calibrations were conducted using water/water, Ca^{2+}/EDTA, and EB/DNA titrations. All experiments were performed at 25 °C with a 60 s pre-titration delay and 1000 rpm stirring speed. After optimization, appropriate concentration of complex was titrated into the sample cell containing DNA in a total of 20 or 40 injections. The titrant (1 µL) was delivered over 2 s with an appropriate interval between injections to ensure complete equilibration. The heat generated per injection of complex bound to DNA was recorded and displayed as differential power (µcal s^{-1}) vs time (min). The area under each injection peak was integrated and is presented as kcal mol^{-1} of injectant vs the molar ratio of [Complex]/[DNA]. Reference data was obtained by titrating the same concentration of test compound into the corresponding buffer, without DNA, and the value was then subtracted from the raw heat of reaction to obtain the effective heat of binding. The resulting data was analyzed and fit using a Levenberg-Marquardt non-linear least squares curve fitting algorithm using Origin 7 software (OriginLabs, Northhampton, MA, USA). Full experimental instrumental parameters are listed in supporting tables A1 – A3.

Cell Culture

4T1 cells were obtained from American Type Culture Collection (ATCC). 4T1 cells were transformed with pGL4.50*luc2*/CMV/H_{ygro}. 4T1-luc cells were cultured in high glucose RPMI 1640 or DMEM medium supplemented with 10% fetal bovine serum at 37 °C in a humidified atmosphere containing 5% CO_2.

Cytotoxicity studies

Cellular viability after treatment with compounds was evaluated by means of the MTS colorometric assay using the CellTiter 96® AQueous One Solution Cell Proliferation Assay kits from Promega (Madison, WI, USA). Briefly, cells were seeded at 2.5 x 10^4 per well for 24 hours prior to treatment on a 96 well plate. The following day media supplemented with drug treatment was added to each well, ranging from 0 – 70 µM. 24 hours later CellTiter 96® AQueous One Solution Reagent (100µL) was added to each well and plates were further incubated for one hour. Cellular proliferation was determined spectrophotometrically using an enzyme-linked immunosorbent assay (ELISA) plate reader at 490 nm. Percentage viability was calculated relative to the DMSO vehicle control (taken as 100% viability).

RESULTS AND DISCUSSION

Scheme 4. Synthesis of [VO(oda)(phen)]·1.5H_2O

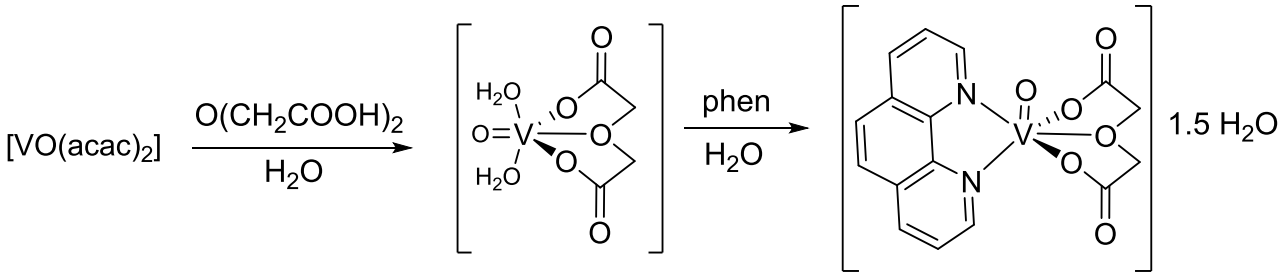

The proposed scheme for the synthesis of [VO(oda)(phen)]•1.5H_2O is presented in scheme 4 and mirrors a literature protocol by Álvarez *et al.*[369] Following this protocol, green crystal precipitated from a solution of water after a four day reaction. One noticeable difference was the lack of solubility of the compound according to literature characterization (previously reported to

be soluble in DMSO).[369] With uncertainties around the purity of the product due to lack of spectroscopic characterization of the compound, multiple attempts were made to obtained a product with chemical properties similar to literature reports. The first attempt involved utilizing freshly prepared phen•HCl•H_2O as by Del Rio *et al*.[370] in order to eliminate any undissolved phenanthroline impurity, as this starting material would be more water soluble over the four day time period of the reaction. This preparation led to a drastic decrease in the yield of the reaction (34 vs 85% yield) when compared with the yield of the reaction utilizing solid o-phenanthroline as the starting material as by Álvarez *et al*.[369] Additionally, crystals of a different morphology and size were obtained from phen·HCl as opposed to solid o-phenanthroline. In yet another preparation of the target compound, a procedure similar to that employed by Holder *et al*.[127] yielded a milky green powdery substance as opposed to the crystalline product obtained by the first two preparation of the compound. In total all efforts to increase the solubility of the compound in DMSO were futile as no obtained product showed full solubility in DMSO as reported by León *et al*.[371] All complexes were instead characterized with FT IR spectroscopy with major stretching frequencies easily identifiable in all spectra including: 451.28 (V-O, s); 1000.92 (V=O, vs) and 3401.98 (OH, s, br) cm^{-1} (Figure 36). A table of the full assignment of FT IR stretching frequencies for this compound is presented below in table 6. Interestingly, an overlay of all FT IR spectra for each preparation of the target molecules, is identical despite the obvious physical differences in the product obtained (supplemental figure A9). As shown figure 36 and table 6 the compound as synthesized matches well with literature reports.

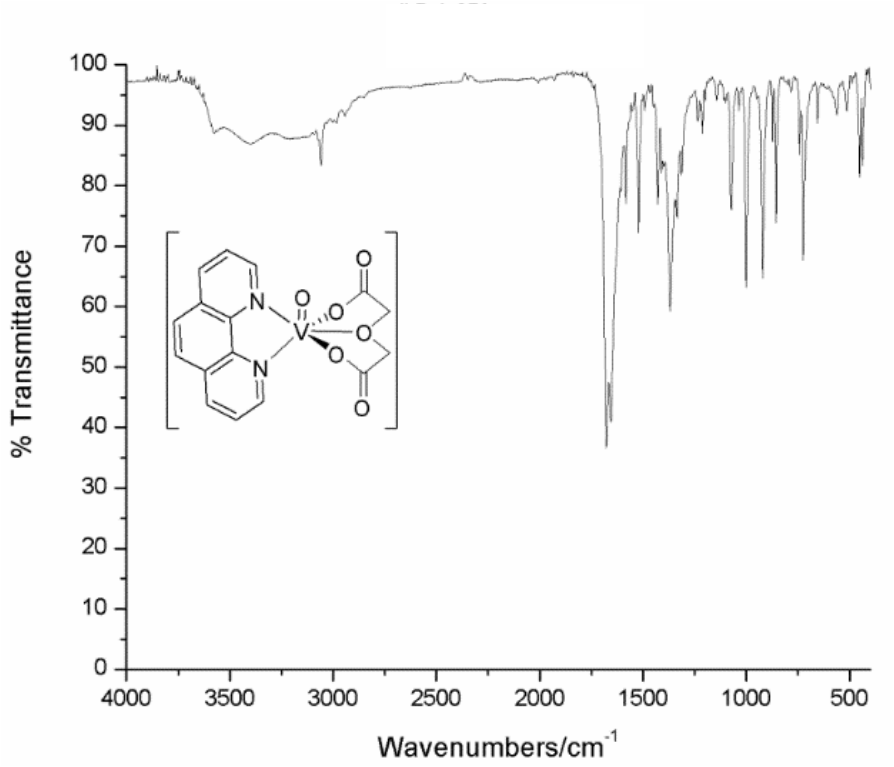

Figure 36. FT IR Spectrum of [VO(oda)(phen)]·1.5H_2O. Prepared utilizing the method as by Álvarez *et al*.[369]

Table 6. Full assignment of the vibrational spectra of [VO(oda)(phen)]·1.5H_2O.

Wavenumbers/cm^{-1}	Assignment	Literature[372]
451.28	V-O	452 s
725.14	CH out of plane (ophen)	724 vs
783	CH out of plane (ophen)	784 w
856.28	CH out of plane (ophen)	856 vs
873.64	C-O-C	875 m
921.85	C-C	922 vs
1000.92	V=O	1000 vs
1072.28	CH in plane (ophen)	1074 s
1143.64	C-O-C	1143 m
1213.07	Ring (ophen)	1212 m
1234.28	Ring (ophen)	1238 m
1313.35	CH in plane (ophen)	1312 m
1334.56	CH in plane (ophen)	1335 s
1369.28	COO-	1365 vs
1429.06	CH_2	1428 m
1521.64	CH in plane (ophen)	1521 m
1677.85	COO (asym)	1669 vs
3058.7	CH_2 (ophen)	3058 m
3401.98	OH	3403 s, br

While FT IR is a powerful tool for the identification of function groups present within a molecule further in-depth characterization was conducted to ensure the correct product was obtained. The procedure by Álvarez *et al.*[369] provided the best crystalline product and while the crystal were not readily characterized via conventional spectroscopic techniques (i.e. UV-Vis), the crystal were of sufficient quality for X-ray crystallographic studies to be obtained. An ORTEP diagram of the crystals of **1** is shown below in figure 37 and confirms the structure as proposed. The coordination geometry around the metal center is confirmed to be a distorted octahedron. The 1.5 H_2O solvate lie in channels that run parallel to the *c*-axis of the unit cell and most likely play a role in the hydrogen bonding network. The crystal structure is in agreement with previous literature

reports confirming the structure as proposed despite the aforementioned solubility issues (Table 7).[370]

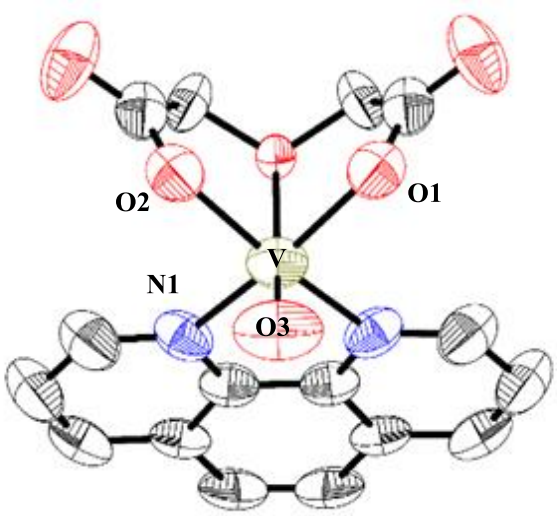

Figure 37. ORTEP diagram of [VO(oda)(phen)]·1.5H_2O. water molecules of crystallization are not shown for clarity.

Table 7. Selected bond distances (Å) and angles (°) for compound 1.

	Literature[370]	Experimental
V(1)-O(1)	1.585(3)	1.619(9)
V(1)-O(2)	1.974(2)	1.973(6)
V(1)-N(1)	2.109(2)	2.123(7)
V(1)-O(3)	2.297(2)	2.302(7)
O(1)-V(1)-O(2)	101.32(8)	100.2(3)
O(1)-V(1)-N(1)	101.91(9)	102.7(4)
O(1)-V(1)-O(3)	176.09(11)	175.8(4)
N(1)-V(1)-O(3)	81.10(7)	80.6(2)

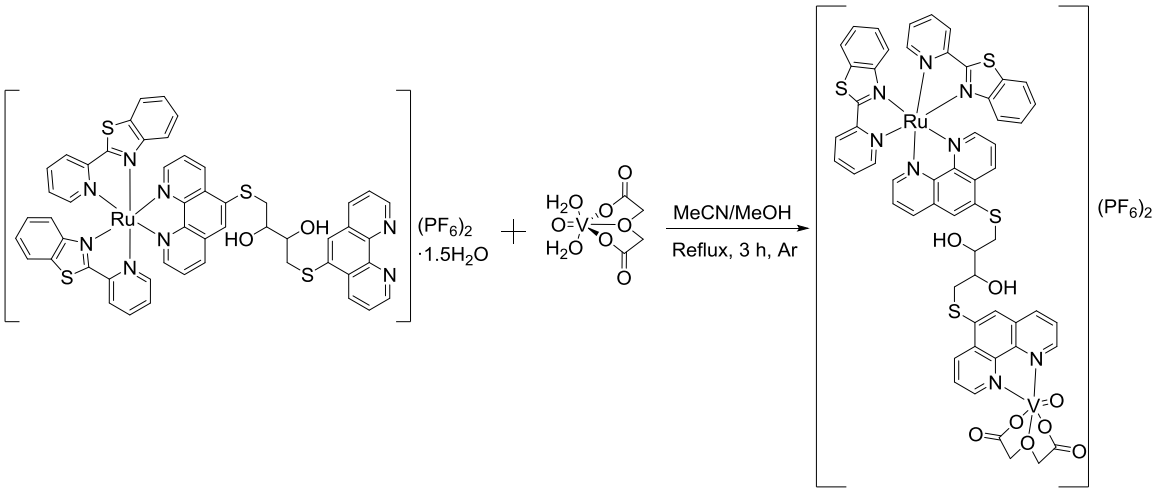

Scheme 5. Synthesis of binuclear Ru(II)-V(IV) complex

The binuclear Ru(II)-V(IV) complex $[Ru(pbt)_2(phen_2DTT)VO(oda)](PF_6)_2 \bullet 2.0H_2O \bullet 0.5C_2H_5OH$ was synthesized in a method similar to previous reports by Holder *et al.*[127] as shown in the above scheme 5. The compound was obtained in good yield and was characterized via FT IR and elemental analysis. FT IR characterization again shows major stretching frequencies: 3421 (O-H, br, s), 1643 (C=O, s), 973 (V=O, m), 842 (PF_6^-, vs). There is a significant shift to lower energy for the V=O bond in the binuclear complex when compared with the mononuclear complex, a similar effect was previously reported for similar compounds.[127] Additionally the C,H,N analysis revealed there to be two water and half a methanol molecules in the solvation shell of the molecule. Further intensive characterization and crystallographic studies are underway to further confirm the structure.

Previously, calometric approaches have been utilized to characterize Hoechest-DNA interaction, and ethidium bromide/propidium iodide–DNA associated.[284] Due to incomplete solubility in DMSO, $[VO(oda)(phen)] \cdot 1.5H_2O$ could not be probed for its activity with CT DNA via any conventional techniques, i.e. ITC, UV-Visible or fluorescence titration experiments.

Therefore, only the interactions with a related compound, [VO(sal-*L*-tryp)(phen)]•H_2O and the binuclear complex [Ru(pbt)$_2$(phen$_2$DTT)VO(oda)](PF$_6$)$_2$•2.0H_2O•0.5C_2H_5OH were conducted.

Prior to completion of isothermal titrations with metal complexes a known DNA intercalator, ethidium bromide, was utilized to optimize many of the protocols for the instrument. The resultant isotherms for the interactions of the synthesize complexes are presented in figure 38 below. It can be observed that the mononuclear [VO(sal-*L*-tryp)(phen)]•H_2O shows little interaction with DNA, (lower panel 38A) due to the minimal differences between the heat exchanges of the titrations conducted in the present (■) and absence (○) of DNA. Previously, it was reported utilizing UV-Visible titration methods, that a K_b value of 0.6 (± 0.1) X 10^5 M^{-1} exists for this complex indicating moderate interaction with DNA.[368] While the complex does possess a phenanthroline moiety with the potential to intercalate between DNA base pairs, it is likely this π-π stacking interaction would be quite weak, therefore making it difficult to detect surface binding and/or partial groove binding even with this ultra-sensitive technique. Conversely, the novel binuclear complex **2**, shows significant interaction with CT DNA and the apparent dissociation constants for three binding sites were determined using nonlinear curve fitting analysis: K_1 = 9.36 x 10^4, K_2 = 8.36 x 10^4, and K_3 = 1.08 x 10^5 M^{-1}. This complex not only possesses the heteroaromatic intercalating moieties but also possesses as net positive charge allowing for electrostatic interaction with the negatively charged phosphate backbone of DNA. Therefore, the nature of the observed interaction most likely stems from both the heteroaromatic ligands and the electrostatic interaction between the complex and DNA. Based upon obtained apparent dissociation constants the complex possess moderate affinity for DNA, albeit much lower than that of ethidium bromide.[373]

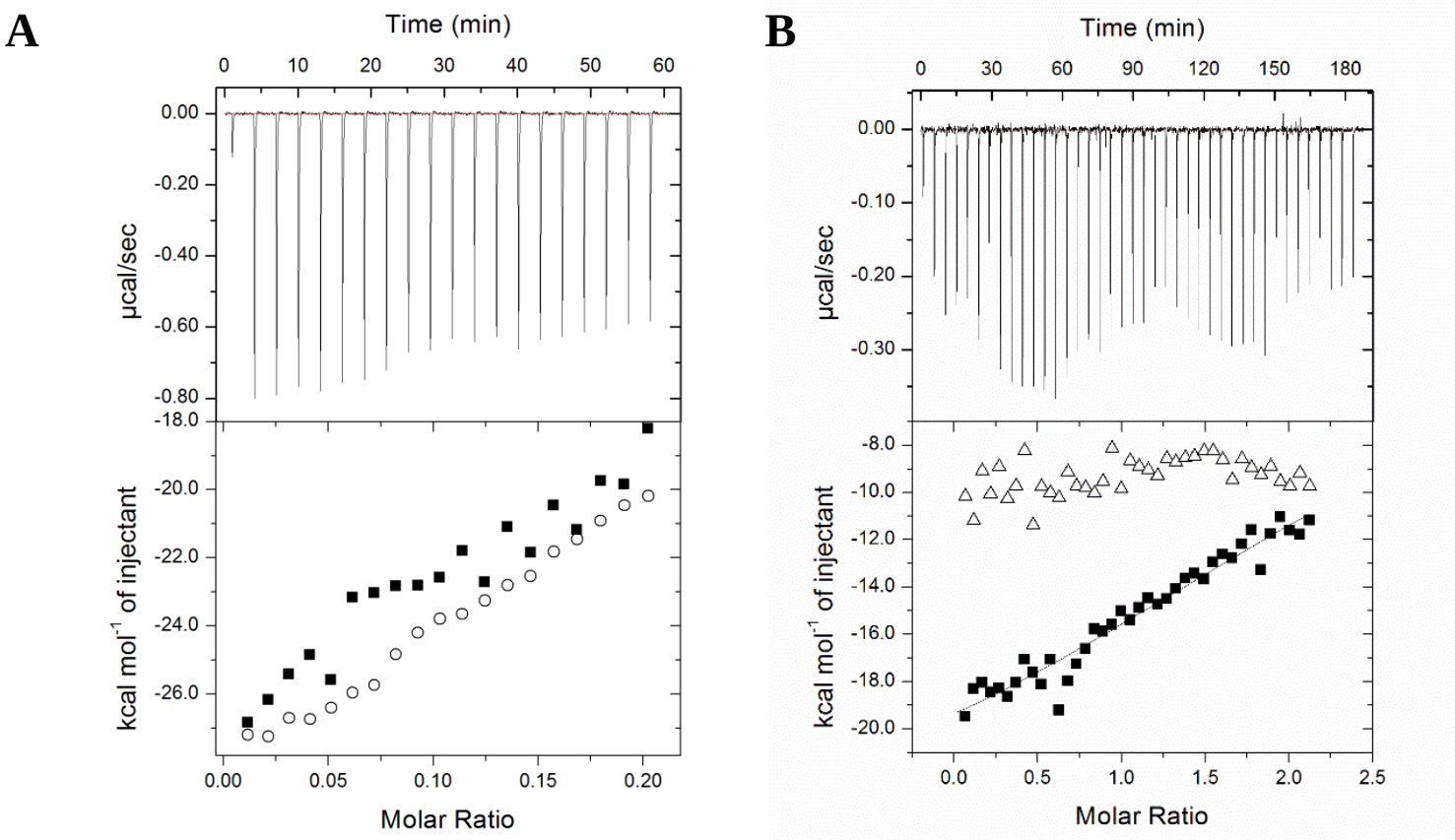

Figure 38. ITC profile for the association of [VO(sal-L-tryp)(phen)]·1.5H_2O (A) and **2** (B) with CT DNA in PBS buffer. The upper panels in the ITC profile show the heat of association for complex/CT DNA interactions. The lower panels show the heat exchanged per mole of injectant as a function of molar ratio of complex to DNA (■).The thermograms have been fitted after subtracting appropriate controls indicated by open circles or triangles (○ or Δ).

To determine the antimetastatic activity of the complexes, 4T1-luc breast cancer cells were treated with increasing concentrations of the complexes for 24 hours, and the viability was measure by means of the MTS assay. As shown in figure 39, the mononuclear [VO(sal-*L*-tryp)(phen)]•H_2O exhibits a concentration-dependent decrease in cellular viability, with an IC_{50} value of approximately 18 μM. Our finding is not staggering as previously it has been reported that this compound possess significant cytotoxicity, with IC_{50} values of 41.6 ± 5.8 and 63.1 ± 28.3 μM in A431 and HFF cell lines, respectively.[374] Interestingly while high antimeastatic activity is reported for this compound our ITC studies indicate the complex shows little to no interaction directly with DNA, indicating organelles other the nucleus are a potential target for V(IV) drugs. Due to large molar absorptivity values for the binuclear complexes within the range of the assay reading and low solubility of the [VO(oda)(phen)]·1.5H_2O the *in vivo* activity could not be assessed utilizing colorometric assays. Efforts are being made to optimize luminescent assay protocols and increase the solubility of [VO(oda)(phen)]·1.5H_2O, so that they may be screened for their antimetastatic potential.

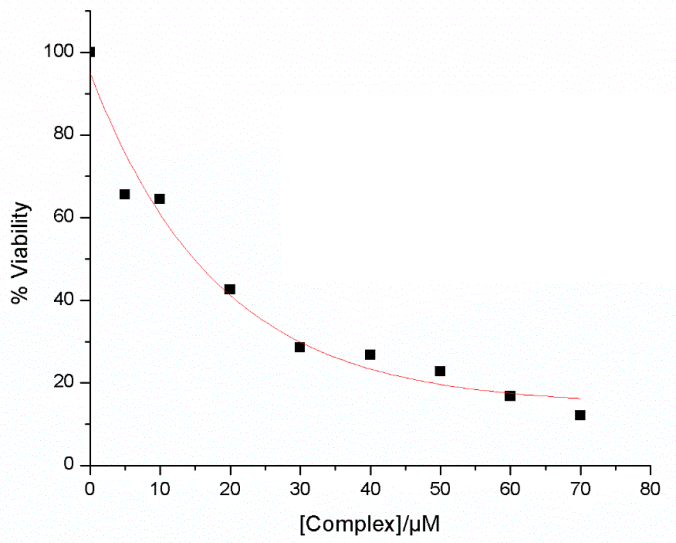

Figure 39. Cell viability graphs following treatment of 4T1-luc cells with [VO(sal-*L*-tryp)(phen)]·1.5H_2O. Graphs generated using uncompensated raw data with plate being read 1 h post incubation of MTS reagent. Data was fit using an exponential function, using Origin 8 software. IC_{50} = 18 μM.

CONCLUSION

In continuation of the work began by Holder *et al.*[127] we have synthesized a oxidovanadium(IV) complex which incorporates an OOO donor group, [VO(oda)(phen)]·1.5H_2O.[370] Upon initial characterization of the complex following literature reports, solubility issue arose forcing us the re-evaluate the purity of this product. One prep by Álvarez *et al.*[369] yield crystals suitable to X-ray analysis, which confirmed the target molecule despite the solubility issues. Additionally, a binuclear Ru(II)-V(IV) complex was synthesized to incorporate the new oxidovanadium(IV) complex into a supramolecular scaffold incorporating a Ru(II) photosensitizer as by Holder *et al.*[127] Due to solubility issue of the precursor molecule only a related mononuclear complex, [VO(sal-*L*-tryp)(phen)]·H_2O, and the binuclear Ru(II)-V(IV)

complexes were able to be tested *in vitro* for their bioactivity. The novel binuclear complex showed moderate interaction with CT DNA via isothermal titration calorimetry experiments, whereas the mononuclear vanadium complex showed minimal interaction. Despite minimal interaction with CT DNA the mononuclear [VO(sal-*L*-tryp)(phen)]·H_2O, showed significant toxicity to breast cancer cells under dark incubation conditions over a twenty-four hour period. While our efforts suggest that DNA is not the direct cellular target of oxovanadium compounds, Sasmal *et al*.[375-378] have reported photoactivated cleavage of DNA with similar compounds. It is thus most likely then that these complexes serves as a means to generate reactive oxygen species which cause DNA cleavage following irradiation. While currently employed methods have not allowed us to quantitatively probe the chemotherapeutic properties and mechanism of the binuclear complex, the addition of the intercalating photosensitizing Ru(II) metal center should allow for cancer selectivity (via uptake and transport proteins) and enhanced activity, however, future mechanistic studies will needed to further probe this idea.

CHAPTER 4

DESIGN, SYNTHESIS, AND CHARACTERIZATION OF A NEW SERIES PYRIDINE-2-THIOCARBOXAMIDE-CONTAINING Co(III) AND Ru(II) COMPLEXES AS POTENTIAL METALLODRUGS

INTRODUCTION

Thioamides are carboxylic acid derivatives that have recently become a very important functional group in organic synthesis and medicinal chemistry.[379, 380] Thioamides exhibit many interesting properties, for example, typically the thioamide-NH is a stronger hydrogen donor and the sulfur a weaker hydrogen bond acceptor than the corresponding amide.[381] In addition, when compared to amides and formamides, thioamides possess different bond-lengths and bond-rotation characteristics and these unique properties have been exploited in both medicinal chemistry (including peptidomimetics) and polymer chemistry applications.[382, 383]

The most utilized metho for the preparation of thioamides is the Willgerodt reaction with a Kindler modification, which usually employs aryl ketones as starting materials.[380, 384-388] However, it has also been shown that this reaction can also be applied when 2-methylpyridine it utilized as the starting material as opposed to aryl ketones.[386, 389] Thus, *N*-substituted 2-pyridinecarbothioamides (PCAs) have been prepared by reactions of 2-methylpyridine with primary amines,[389] nitro compounds,[380] or *N*-substituted formamides as amine sources in the presence of sulfur at elevated temperatures.[390] Harsh reaction condition and low yield utilizing common Willgerodt-Kindler conditions prompted the search for alternative methods and in 2004, Kingele and Brooker proposed a modification which included utilizing a catalytic amount of $Na_2S{\cdot}9H_2O$.[391] The proposed modification drastically increased yields (>70 %) and allowed for better tunability of the steric and electronic properties of the products. These molecules are

considered to be bioactive in particular their utility as gastric mucosal protectants was described in *in vivo* rat models in the early 1990s.[392] The inherent bioactivity of these molecules makes them an ideal candidate as ligands of potentially active metallodrugs.

Like Schiff bases, thioamides possess excellent chelating properties and have proven their useful as building blocks for the synthesis of numerous biologically relevant molecules which often possess a variety of interesting pharmacological properties.[393, 394] Specifically, PCAs are versatile and easily accessible building blocks for the synthesis of *S,N*-bidentate ligands for organometallic and coordination compounds. When utilized as ligands the molecules have the potential to coordinate to metal centers in a variety of different ways as shown in Scheme 6. Deprotonation of the ligand may occur prior to coordination and because thioamides have two tautomeric forms they may act as either a monoanionic N, N' (coordination of thioketo tautomer **1**) or S, N (coordination of the thiol form **2**) bidentate ligand. Alternatively, the neutral ligand may coordinate to the metal center via the pyridyl nitrogen and sulfur atoms, **3**. In these cases, five-membered chelates result. However, coordination via the amide nitrogen and the sulfur (either as the neutral ligand **4** or after deprotonation **5**) would give four-membered metallacycles.

Scheme 6. Possible bidentate coordination modes of *N*-substituted pyridine-2-thiocarboxamide ligands.

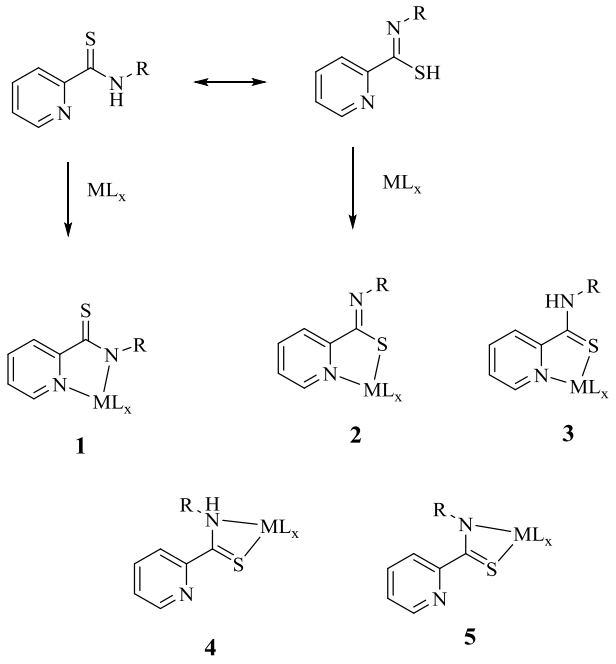

While the inherent biological activity of PCAs has been known since the early 1990s,[392] there have been sparse reports on the bioactivity of transition metal complexes bearing these ligands.[395-399] Though several cobalt(III) and ruthenium(II) complexes bearing thiosemicarbazone (a seemingly similar class of compounds see scheme 7) ligands have been reported for their anticancer applications,[102, 103, 109, 400-405] the biological application of these structurally related complexes bearing thioamides is not well explored.[396, 399, 406] Over the past decade there is a single report on the use of a ruthenium(II) thioamide complexes as a potential anticancer agent.[396] In this study a series of Ru(II) and Os(II) complexes bearing PCAs were synthesized and characterized and were shown to have high *in vitro* toxicity.[396] Additionally, the complexes were stabilized by an arene system and were stable in highly acidic condition giving the potential to be the first non-platinum based orally-activated anticancer drugs.[396]

Scheme 7. General Structure of PCAs and TSCs

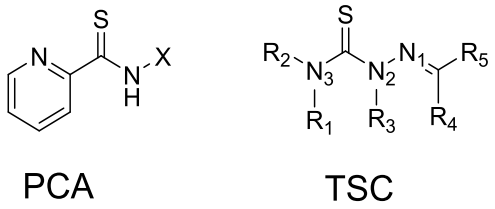

Subscribing to a similar point of view, we have decided to investigate the potential of polypyridyl Co(III) and Ru(II) complexes bearing PCAs as anticancer agents. To the best of our knowledge the complexes described herein are of novel nature and represent a new series of potentially active biomolecules. Additionally, in chapter 2 we reported on the potential antitumor mechanism of $[Co(phen)_2(MeATSC)]\cdot 2.5H_2O\cdot C_2H_5OH$, and thus we can directly compare the activity of our novel compounds to that of an established bioactive complex and gain insight into differences in the mechanism of action of the structurally related complexes. It is envisioned that the removal of the hydrolysable imine linkage and enlargement of the moiety directly adjacent to the coordinating thioketone moiety (referred to as the N3 position on thiosemicarbazone ligands see scheme 4) is expected to increase the stability and cytotoxic potential of these complexes when compared with Schiff base analogues.

EXPERIMENTAL

General and Instrumentation

All reagents used in the syntheses, if not specified, were obtained from either Sigma-Aldrich (St. Louis, MO) or VWR International (Radnor, PA) and were used without further purification. $[Co(phen)_2(OH_2)_2](NO_3)_3$ and $[Ru(phen)_2Cl_2]$ were prepared and provided by Dr.

Mark Lawrence (Post-doctoral fellow – ODU) and were used without further purification. ^{1}H, ^{13}C and ^{19}F NMR spectra were collected on a Varian *Inova 400 MHz* NMR Spectrometer. ^{1}H NMR spectroscopic samples were standardized relative to sodium 3-(trimethylsilyl)propionate ($\delta = 0.0$ ppm) or appropriate residual solvent peaks. ^{13}C NMR spectroscopic samples were all standardized to residual solvent peaks as indicated by respective compounds. ^{19}F NMR spectroscopic samples were standardized relative to the external standard trifluoroacetic acid ($\delta = -78.5$ ppm). FT IR and ATR data was obtained using a Nicolet AVATAR 370 DTGS spectrophotometer. The mass spectral data was obtained from a Bruker 12 Tesla APEX-Qe FTICR-MS with an Apollo II ion source in positive ion mode at a flow rate of 2 µL/min. Ultraviolet absorption spectra was obtained using an Agilent 8453 diode array system. Thin-layer chromatography (TLC) was performed using TLC aluminum sheets (silica gel 60 F_{254}) from Merck (Darmstadt, Germany) for determination of retention factors (R_f). Column chromatography was performed using either high purity grade silica gel or Sephadex LH-20 from Sigma-Aldrich. Microanalyses (C, H, N) were performed by Intertek Pharmaceutical Services, P.O. Box 470, Salem Industrial Park Bldg. #5, Whitehouse, NJ 08888. X-ray crystallographic studies were conducted by Dr. Colin McMillen Director of the Molecular Structure Center, Department of Chemistry of the Clemson University (Clemson, SC, USA)

Synthesis of ligands.

Generation of *N*-substituted pyridine-2-thiocarboxamide ligand library

General procedure for synthesis of *N*-substituted 2-pyridinecarbothioamide. The methods of Klingele and Brooker was adapted.[391] In brief, a mixture of *N*-substituted aniline and sulfur (1:3 mol ratio) and sodium sulfide nonhydrate (2 mol %, 0.24g, 1 mmol) was refluxed in 2-picoline (30 mL) for 48 hours at 135 °C under atmospheric conditions. The reaction mixture was cooled to

room temperature and the solvent was evaporated under high vacuum. The residue was dissolved in an appropriate solvent (as indicated), purified on a silica gel column (length = 46 cm, inner diameter = 14.5 cm) and the solvent was evaporated to yield analytically pure *N*-substituted 2-pyridinecarbothioamide. All compounds were synthesized by this procedure unless expressly stated.

_N_-[3,5-bis(trifluromethyl)phenyl]pyridine-2-thiocarboxamide (TPTA) (1)

Column solvent: $CHCl_3$/MeOH (20:1). A single crystal suitable for X-ray analysis was grown via the slow evaporation technique from chloroform. Yield = 5.90 g (77%), yellow solid. IR: 3170 (NH, m); 1380 (C=S, s); 1278 (C-F, vs) cm^{-1}. ^{1}H NMR ($CDCl_3$, 400MHz): δ_H/ppm 12.38 - 12.28 (m, 1H), 8.76 (d, *J*=7.8 Hz, 1H), 8.67 (s, 2H), 8.61 - 8.54 (m, 1H), 7.93 (dt, *J*=1.6, 7.8 Hz, 1H), 7.77 (s, 1H), 7.54 (ddd, *J*=1.2, 4.7, 7.4 Hz, 1H); ^{13}C NMR (101MHz, $CDCl_3$) δ_C/ppm 189.36, 150.69, 146.61, 140.00, 137.84, 132.43, 132.09, 126.66, 124.87, 122.19, 121.66, 119.51 ^{19}F NMR (376MHz, $CDCl_3$): δ_F/ppm -62.94 (s, 6F).

_N_-(anthracene)pyridine-2-thiocarboxamide (APTA) (2)

Column solvent: $CHCl_3$. A single crystal suitable for X-ray analysis was grown via the slow evaporation of a saturated solution of the compound in chloroform layered with methanol. Yield = 0.1353 g (33 %), orange powder. IR: 3216 (NH, m); 1384 (C=S, s) cm^{-1}. ^{1}H NMR (400 MHz, DMSO-d_6): δ_H/ppm 12.55 (s, 1H), 8.97-8.98 (m, 1H), 8.70-8.80 (m, 1H), 8.60-8.61 (m, 3H), 8.03-8.21 (m, 6H), 7.92 (dd, *J*=2.15, 9.18 Hz, 1H), 7.70 (ddd, *J*=1.17, 4.69, 7.42 Hz, 1H), 7.49-7.59 (m, 3H). ^{13}C NMR ($CDCl_3$, 101MHz): δ_C/ppm 187.1, 151.4, 146.4, 137.8, 135.5, 132.2, 131.7, 131.3, 130.0, 129.1, 128.2, 128.1, 126.7, 126.2, 126.1, 125.8, 125.5, 124.9, 122.3, 119.2.

***N*-(4-fluorphenyl)pyridine-2-thiocarboxamide (3)**

Column solvent: $CHCl_3$. Yield = 4.134 g (83%), golden yellow solid. IR: 3170 (NH, m); 1380 (C=S, s); 1278 (C-F, vs) cm^{-1}. ^1H NMR ($CDCl_3$, 400MHz): δ_H/ppm 12.14 (s, 1H), 8.71 (d, *J*=7.8 Hz, 1H), 8.55 (d, 2H), 8.06 (td, *J* = 7.7 Hz 1H), 7.78 (dt, *J*=1.6, 7.8 Hz, 1H),, 7.30 (d, *J* = 8.7 Hz, 1H), 7.01 (dd, *J* =8.73) ; ^{13}C NMR (101MHz, $CDCl_3$) δ_C/ppm 190.8, 160.5, 149.0, 136.7, 136.1, 123.4, 121.9, 118.7, 117.0 ^{19}F NMR (376MHz, $CDCl_3$): δ_F/ppm -114.9 (s, 1F).

***N*-(2,4-difluorphenyl)pyridine-2-thiocarboxamide (4)**

Colum solvent: $CHCl_3$/MeOH (20:1). Yield = 0.5803 g (81%), yellow solid. IR: 3170 (NH, m); 1380 (C=S, s); 1278 (C-F, vs) cm^{-1}. ^1H NMR ($CDCl_3$, 400MHz): δ_H/ppm 12.14 (s, 1H), 8.61 (d, *J*=7.8 Hz, 1H), 8.55 (d, 2H), 8.06 (td, *J* = 7.7 Hz 1H), 7.78 (dt, *J*=1.6, 7.8 Hz, 1H), 7.70 (m, 1H), 7.43 (td, *J*=1.2, 4.7, 7.4 Hz, 1H), 7.19 (td, *J* = 1.64, 8.73) ; ^{13}C NMR (101MHz, $CDCl_3$) δ_C/ppm 190.3, 162.3, 152.5, 152.0, 149.0, 138.7, 129.9, 129.8, 127.2, 125.3, 112.0, 105.1 ^{19}F NMR (376MHz, $CDCl_3$): δ_F/ppm -110.8 (s, 1F), -115.1 (s, 1F).

***N*-(3,4,5-trimethoxyphenyl)pyridine-2-thiocarboxamide (5)**

Column solvent: $CHCl_3$/MeOH (10:1). Yield = 2.01 g (67 %), brown/yellow solid. IR: 3170 (NH, m); 1380 (C=S, s); 1278 (C-F, vs) cm^{-1}. ^1H NMR ($CDCl_3$, 400MHz): δ_H/ppm 12.22 (s, 1H), 8.68 (d, *J*=7.8 Hz, 1H), 8.55 (d, 2H), 8.05 (td, *J* = 7.7 Hz 1H), 7.67 (dt, *J*=1.6, 7.8 Hz, 1H), 7.62 (s, 2H), 3.71 (s, 6H), 3.33 (s, 3H) ; ^{13}C NMR (101MHz, $CDCl_3$) δ_C/ppm 188.9, 153.1, 152.9, 147.7, 138.3, 135.9, 126.8, 124.9, 101.6, 60.58, 56.49.

***N*-(4-Pyridinyl)pyridine-2-thiocarboxamide (PPTA) (6) as by Kingle and Brooker.** [107]

A mixture of 4-aminopyridine (9.31 g, 0.10 mol), sulfur (9.62 g, 0.30 mol) and sodium sulfide nonahydrate (0.48 g, 2 mol %) in 2-methylpyridine (60 mL) was refluxed for 48 h. After cooling and removal of all volatiles *in vacuo*, the dark solid residue was taken up in 2 M aqueous sodium hydroxide (200 mL), and the mixture was filtered. The filtrate was diluted with water (400 mL) and acidified to pH 5 by dropwise addition of concentrated hydrochloric acid. The resulting very voluminous yellow precipitate was filtered off and washed thoroughly with water. Drying *in vacuo* gave pure *N*-(4-pyridyl)pyridine-2-thiocarboxamide as a yellow powder. Yield = 14.87 g (75 %). IR(KBr):3170 (NH, m); 1357 (C=S, s); 1519 and 1357 (ArH, s); 815 (=C-H bend, s) cm^{-1}. ^{1}H NMR ($CDCl_3$, 400MHz): δ_H/ppm 12.23 (s, 1H), 8.74 (d, *J*=8.2 Hz, 1H), 8.65-8.69 (m, 2H), 8.57 (dd, *J*=4.7, 0.8 Hz, 1H), 8.14-8.20 (m, 2H), 7.91 (td, *J*=7.8, 1.6 Hz, 1H), 7.52 (dd, *J*=7.4, 4.7 Hz, 1H). ^{13}C NMR ($CDCl_3$, 101MHz): δ_C/ppm 189.5, 150.9, 150.8, 146.5, 145.4, 137.7, 126.5, 124.7, 115.3.

***N*-[4-benyzl alcohol]pyridine-2-thiocarboxamide (7**). **The preparation of this ligand first required the reduction of the carboxylic acid moiety present in 4-aminobenzoic acid**. **Safety notes: LAH is extremely water reactive and must be handled with care!**

Lithium aluminum hydride (5.0 g, 0.132 mol) was dissolved in Et_2O (500 mL) in a 500 mL RBF. 4-aminobenzoic acid (7.54g, 55 mmol) was placed in a cellulose sohxlet thimble and was placed in a sohxlet extractor and the reaction mixture was allowed to reflux for 7 days. After 7 day the remaining lithium aluminum hydride was neutralized by the addition of H_2O (150 mL). Then 10 % NaOH solution (150 mL) was added and the ether layer was separated. The water layer was washed with excess Et_2O (2 x 50 mL) and the organic layers were combined and solvents removed

in vacuo to yield a yellow oil. Yield = 2.56 g (33 %) 4-aminobenzyl alcohol. ^{1}H NMR (400 MHz, DMSO-d_6): δ_H/ppm 6.81 (dd, *J*=0.78, 7.03 Hz, 1H), 6.45-6.50 (m, 1H), 4.27 (s, 1H), 3.99 (s, 1H).

4-aminobenzyl alcohol (0.5733 g, 4.65 mmol) (oil from above) was combined with sulfur (0.5733 g, 13.95 mol) sodium sulfide nonahydrate (0.447 g, 2 mol %) in 2-methylpyridine (15 mL) was refluxed for 48 h. After cooling and removal of all volatiles *in vacuo*, the dark brown oil residue was taken up in $CHCl_3$ and was purified using column chromatography on silica gel. Fractions containing the desired product were combined and the filtrate was evaporated under reduced pressure to yield a yellow solid. Yield = 0.7158 g (65 %). ^{1}H NMR (400 MHz, DMSO-d_6): δ_H/ppm 12.23 (br. s., 1H), 8.67 (qd, *J*=0.89, 4.73 Hz, 1H), 8.50-8.55 (m, 1H), 8.03 (dt, *J*=1.95, 7.81 Hz, 1H), 7.84 (d, *J*=8.59 Hz, 2H), 7.64 (ddd, *J*=1.17, 4.69, 7.81 Hz, 1H), 7.25 (d, *J*=8.20 Hz, 2H), 3.36 (s, 1H). ^{13}C NMR (101 MHz, DMSO-d_6): δ_C/ppm 189.3, 152.7, 147.4, 137.8, 136.7, 135.9, 129.0, 126.4, 124.7, 123.8, 20.8.

4-[(pyridine-2-ylcarbothioyl)amino]benzoic acid (8)

N-[4-benyzl alcohol]pyridine-2-thiocarboxamide (0.200 g, 1.02 mmol) was dissolved in acetone (18 mL) in a 50 mL RBF and placed under argon at 0 °C. Then to the mechanically stirred solution was added a dropwise solution of 2 mL of Jones reagent (2.67 g CrO_3, 2.3 mL of H_2SO_4 diluted to 10 mL) and acetone (10 mL) over a one hour period (color change from green to orange). After the solution persisted at the orange coloration for thirty minutes at 0 °C excess isopropyl alcohol was added to destroy excess Jones reagent. The reaction mixture was decanted and concentrated to a minimal volume. The desired product was extracted from a brine/$CHCl_3$ (1:1) mixture. The organic layer was washed with H_2O (20 mL), 20 % sodium bicarbonate (10 mL), and brine (10 mL). The yellow organic layer was dried in a dessicator. Yield = 0.148 g (56 %) ^{1}H NMR

(400 MHz, DMSO-d_6): δ_H/ppm 12.23 (br. s., 1H), 8.67 (qd, *J*=0.89, 4.73 Hz, 1H), 8.50-8.55 (m, 1H), 8.03 (dt, *J*=1.95, 7.81 Hz, 1H), 7.84 (d, *J*=8.59 Hz, 2H), 7.64 (ddd, *J*=1.17, 4.69, 7.81 Hz, 1H), 7.25 (d, *J*=8.20 Hz, 2H), 3.36 (s, 1H). ^{13}C NMR (101 MHz, DMSO-d_6): δ_C/ppm 190.7, 168.2, 152.0, 149.1, 136.7, 136.1, 130.3, 123.4, 122.0, 116.9

Synthesis of Complexes.

Attempted [Co(phen)$_2$(PPTA)](PF$_6$)$_3$ (9)

[Co(phen)$_2$(OH$_2$)$_2$](NO$_3$)$_3$ (0.16 g, 0.249 mmol) and **1** (0.080 g, 0.3735 mmol) were combined in a 250 RBF in EtOH (80 mL) and were refluxed under argon with stirring for 24 hours. After 24 hours at reflux the flask was allowed to cool to room temperature and NH_4PF_6 (0.284 g, 1.75 mmol) was added. The solvent was removed under reduced pressure and resulting solid was suspended in water (20 mL) and collected by vacuum filtration. The crude product was purified using column chromatography on Sephadex LH-20 (pre-soaked in acetonitrile) using acetonitrile as the mobile phase. Two distinct bands were collected (confirmed via simultaneous collection of UV-visible spectra) and the solvents were removed from each to yield brown solids. Yield = 0.1488 g. ^{19}F NMR (376 MHz, DMSO-d_6): δ_F/ppm -69.18 (d, 18 F)

[Ru(phen)$_2$(PPTA)](PF$_6$)$_2$·1.5H$_2$O (10)

[Ru(phen)$_2$Cl$_2$] (1.00 g, 1.90 mmol) and **1** (0.84 g, 3.90 mmol) were combined in a 1L RBF in 2:1 EtOH/H_2O (850 mL) and were refluxed with stirring for 24 hours. After 24 hours at reflux the flask was allowed to cool to room temperature and NH_4PF_6 (3.51 g, 21.5 mmol) was added. The solvent was removed under reduced pressure and resulting solid was collected by vacuum filtration from diethyl ether and allowed to air dry. The crude product was purified using column

chromatography on Sephadex LH-20 (pre-soaked overnight in acetonitrile) using acetonitrile as the mobile phase. Three distinct bands were collected (confirmed via simultaneous collection of UV-visible spectra) and the solvents were removed from each to yield brown solids. A single crystal for X-ray analysis was grown via the slow evaporation technique from MeCN/Toulene (1.5:1) supplemented with an equimolar amount of triphenylphosphine oxide (0.100 mmol). Yield = 1.23 g (67%). ESI-MS: *m/z* 676.0849 [**10**]$^{+}$, Elemental Analysis: Calculated: C 43.49; H 2.88; N 9.82, Found: C 43.57; H 2.89, N 9.91. ^{1}H NMR (400 MHz, DMSO-d_6): δ_H/ppm 9.73 (dd, *J*=1.37, 5.27 Hz, 1H), 8.83 (ddd, *J*=1.17, 8.40, 9.57 Hz, 3H), 8.72 (dd, *J*=1.17, 8.20 Hz, 2H), 8.61 (d, *J*=7.03 Hz, 2H), 8.52 (dd, *J*=0.98, 8.40 Hz, 1H), 8.32-8.44 (m, 7H), 8.24 (d, *J*=8.98 Hz, 1H), 8.16 (dd, *J*=5.47, 8.20 Hz, 2H), 8.05 (dd, *J*=5.08, 8.20 Hz, 1H), 7.94-8.00 (m, 2H), 7.77 (dd, *J*=1.17, 5.08 Hz, 1H), 7.72 (dd, *J*=5.08, 8.20 Hz, 1H), 7.57 (d, *J*=7.03 Hz, 3H), 7.49 (dd, *J*=5.47, 8.20 Hz, 1H), 7.30 (ddd, *J*=1.56, 5.86, 7.42 Hz, 1H). ^{19}F NMR (376 MHz, DMSO-d_6): δ_F/ppm -69.18 (d, 12 F)

Attempted [Co(phen)$_2$(TPTA)](PF$_6$)$_3$ (11)

[Co(phen)$_2$(OH$_2$)$_2$](NO$_3$)$_3$ (1.00 g, 1.56 mmol) and **2** (0.546 g, 1.56 mmol) were combined in a 1L RBF with EtOH (850 mL) and were refluxed with stirring for 24 hours under Ar (g). After 24 hours the contents were concentrated to 200 mL and NH_4PF_6 was added followed by H_2O (100 mL). The mixture was further concentrated to 50 mL and cooled to room temperature. The mixture was filtered through a fine glass frit and air dried. A single crystal for X-ray analysis was grown via the slow evaporation technique from MeCN/Toulene (1.5:1) supplemented with an equimolar amount of triphenylphosphine oxide (0.100 mmol). Yield = 1.25 g (66%). Elemental Analysis: Calculated: C 35.89, H 2.01, N 6.98; Found: C 41.98, H 2.53, N 7.74. ESI-MS: *m/z* 384.0465 [**11**]$^{2+}$. ^{1}H NMR (400 MHz, DMSO-d_6): δ_H/ppm 9.80 (dd, *J*=1.17, 5.47 Hz, 1H), 9.19-9.29 (m,

2H), 9.09 (dd, *J*=1.17, 8.20 Hz, 1H), 8.84 (dd, *J*=0.98, 8.40 Hz, 1H), 8.48-8.61 (m, 5H), 8.23-8.41 (m, 4H), 7.94 (dd, *J*=5.47, 8.20 Hz, 1H), 7.86-7.90 (m, 1H), 7.74 (d, *J*=0.78 Hz, 3H), 7.52-7.66 (m, 3H), 7.23-7.30 (m, 1H) ^{19}F NMR (376 MHz, DMSO-d_6): δ_F/ppm -61.31 (s, 6 F), -69.19 (d, 18 F).

Attempted [Co(phen)$_2$(APTA)](PF$_6$)$_3$ (12)

[Co(phen)$_2$(OH$_2$)$_2$](NO$_3$)$_3$ (64 mg, 0.1 mmol) and **3** (31 g, 0.1 mmol) were combined in a 100 mL RBF with EtOH (32 mL) and were refluxed with stirring for 65 hours under Ar (g). After 65 hours the contents were concentrated to 10 mL and NH_4PF_6 (0.163 g, 1 mmol) was added followed by H_2O (32 mL). The flask was placed in an ice bath then filtered through a fine glass frit and washed with H_2O (2 x 40 mL) and then air dried. Yield = 74.7 mg (64%). Elemental Analysis: Calculated: C 45.22, H 2.59, N 7.19; Found: C 55.99, H 3.45, N 8.55. ^{1}H NMR (400 MHz, DMSO-d_6): δ_H/ppm 12.55 (s, 1H), 7.51-9.01 (m, 29 H). ^{19}F NMR (376 MHz, DMSO-d_6): δ_F/ppm -69.25 (s, 18 F)

RESULTS AND DISCUSSION

Scheme 8. General synthesis of PCA ligands.[a]

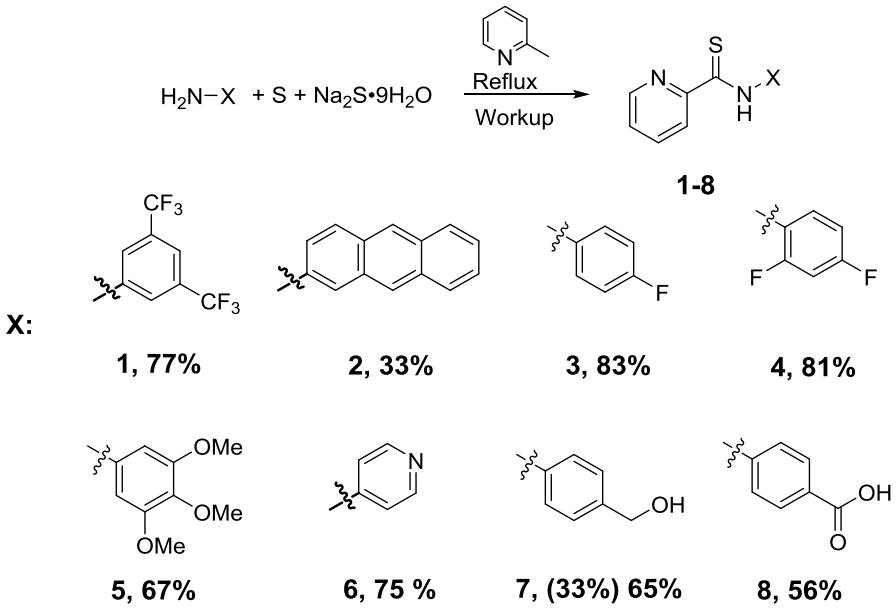

[a] (i) S, $Na_2S \cdot 9H_2O$, R-NH_2

The general synthesis of the PCA ligands (**1**-**6**) is shown in scheme 8 and was adapted from previously reported literature protocols which gives the synthesis of compound **6**.[107] PCAs were generated in a one pot synthetic scheme utilizing a modified Willgerodt-Kindler reaction where the substituted aniline and elemental sulfur were refluxed for the specified time period in 2-picoline in the presence of a catalytic amount of sodium sulfide nonhydrate. TLC analysis during the course of the reaction shows almost complete disappearance of the substituted aniline precursor with the concurrent appearance of the desired products as indicated by a decrease in the overall polarity of the compounds. After column purification the PCA ligands were generally obtained in moderate yield (75-77%), except in the case of **2** which may have been inhibited due to steric factors. The ^{1}H and ^{13}C NMR spectra of the PCAs showed some characteristic features, *i.e.* in

aprotic deutrated solvents, the thioamide proton was detected at ~12 ppm and the thiocarbonyl was detected at ~188 ppm (see Supporting figure A8-A11). These values correlate with the previous reports in literature for similar compounds.[107,120] As shown in figure 40 the ^{1}H and ^{13}C resonance for the pyridinyl moieties are well conserved among all derivatives (**1**-**8**) allowing for simplified assignment of the remaining resonances present. Additionally, the inclusion of other nuclei, such as fluorine, allows for further characterization by ^{19}F NMR. Compounds **1**, **3**, and **4**, show resonances in their ^{19}F NMR spectra further confirming the purity of these compounds (see figure 41). Furthermore, the formation of the thioketone moiety is observed by analyzing the FT IR spectra of all of the compounds and its shift value of 1380 cm^{-1} is highly conserved in all cases. Despite spectroscopic characterization confirming the purity of the synthesized compounds, no comprehendible mechanism exists for a Willgernot-Kindler reaction utilizing methylpyridine as the starting material, and therefore further characterization was conducted. In an attempt to prove the structure of these novel compounds crystallization experiments were conducted utilizing various techniques, *i.e.* vapor diffusion, slow evaporation, convection, etc. X-ray quality crystals of compound **1** were produced by slow evaporation of $CHCl_3$ and the structure was solved (Dr. Colin McMillen – Clemson University) unequivocally proving the structure and the utility of the employed reaction scheme. The ORTEP diagram of this compound is presented in figure 42.

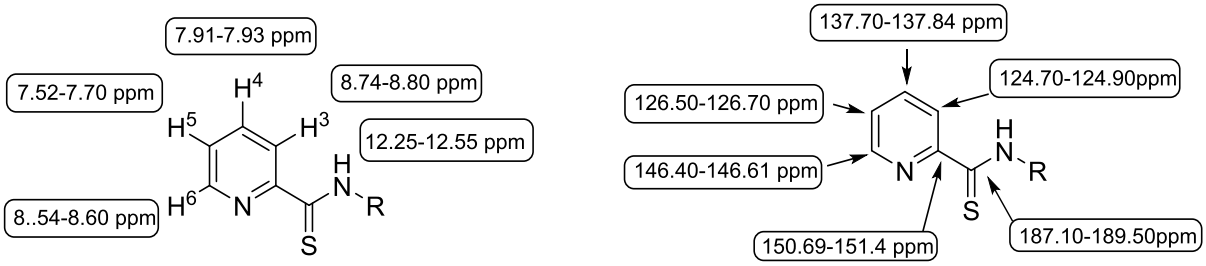

Figure 40. Conserved chemical shifts observed in the ^{1}H and ^{13}C NMR spectra of PCAs **1-8** in $CDCl_3$**.**

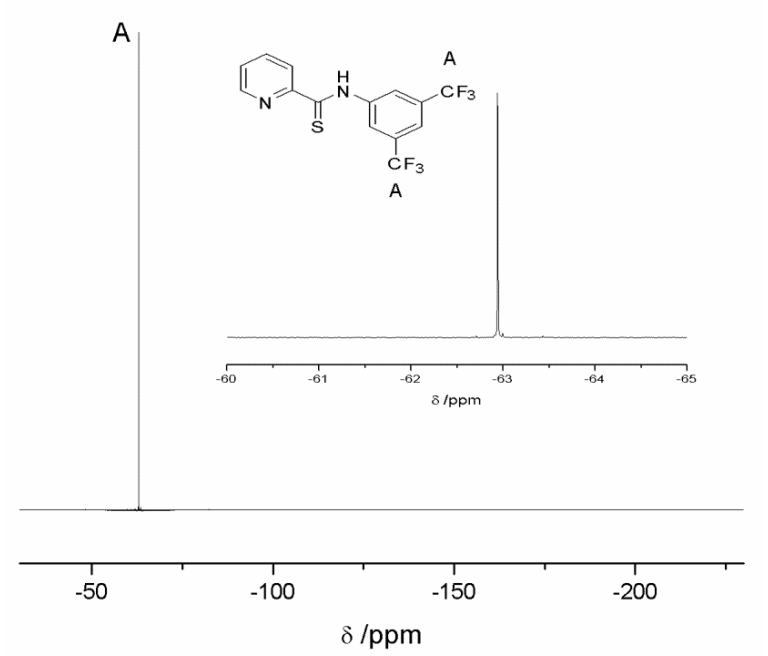

Figure 41. ^{19}F NMR spectrum of **1** in $CDCl_3$ showing the equivalence of the *bis*-trifluoromethyl moieties.

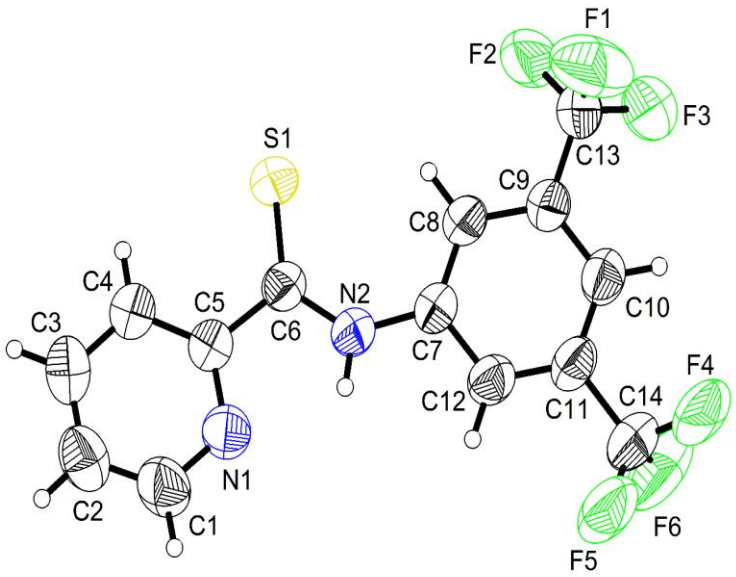

Figure 42. ORTEP diagram of **1**.

In the case of compound **7**, a modified two-step reaction scheme was utilized which first required the reduction of the carboxylic acid moiety present in 4-aminobenzoic acid to a benzyl alcohol via lithium aluminum hydride (LAH) due to both the competitive ketone moiety and the cost of pure *p*-aminobenzyl alcohol.[407] Following the reduction, the obtained 4-aminobenzyl alcohol was reacted by the same scheme as the other PCAs. Interestingly, the methylene protons and carbon of **7** do not correlate well to literature or with predicted expectations, with the methylene carbons resonance shifted upfield 40 ppm from the predicted values of ~60 ppm. However, following oxidation of **7** with Jones' reagent the desired carboxylic acid containing thiocarboxaimde (**8**) is obtained as confirmed by the appearance of the downfield resonance in the ^{13}C NMR spectrum attributed to the reformation of the carboxylic acid moiety, with remaining resonances being similar to all other synthesized PCA ligands.

Table 8. PCA-containing complexes (**9-12**) composition.

Compound	Metal Center	PCA Ligand
9	Co^{III}	**6**
10	Ru^{II}	**6**
11	Co^{III}	**1**
12	Co^{III}	**2**

Scheme 9. Synthesis of cyclometallated PCA complexes.

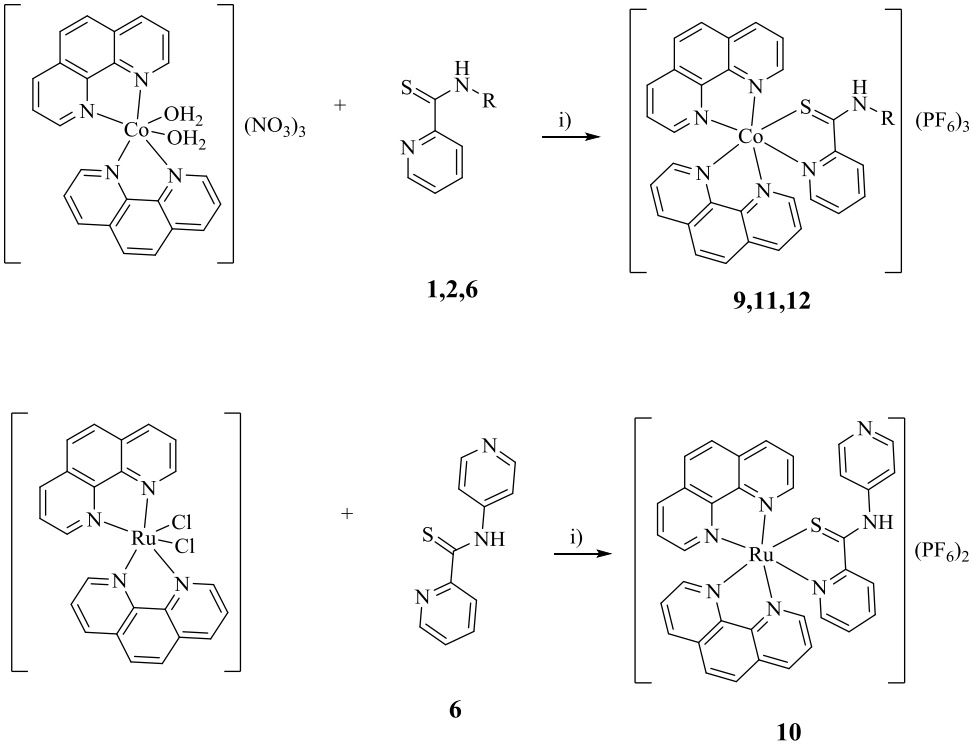

Complexes **9-12** are generated via a substitution reaction involving an appropriate amount of the purified PCAs (**1,2,** or **6**) with either a Co(III) or Ru(II) precursor as indicated by table 8 and shown in scheme 9. Compounds **9**, **11**, and **12** were generated by refluxing the respective PCAs with a previously prepared Co(III) precursor complex. The ^{1}H NMR and FT IR spectra of complexes **9** and **11** show upfield shift of the thioamide proton and thioketone, respectively, indicating coordination in an N,S- bidentate fashion. A similar phenomenon occurs with the signal

attributed to the hydrazinic proton upon N,S coordination in thiosemicarbazones.[108,109,121] The conservation of the thioketone moitey in the FT IR spectra also gives indication that ligands eixit in the thione form when coordinated to the metal center. Alternatively, in compound **12** similar shift in the FT IR spectrum are not observed potentially indicating a difference in the coordination made for this ligand. Additionally, the purity of the **11** was confirmed using ^{19}F NMR and ESI-MS (Supporting figures A11-12). The presence of a singlet, attributed to the equivalent *bis*-trifluoromethyl moieties, and a doublet for the hexaflurophosphate counter ion is observed in the ^{19}F NMR spectrum. As shown in figure 43, a peak of *m/z* 384.0465 was observed in the mass spectrum which was attributed to the [**11**]$^{2+}$ species. With the ligand coordinating in the thione form (as indicated by ^{1}H NMR and FT IR characterization), it is suggested that the complex tautomerizes to the thiol form within the mass spectrometer chamber. Elemental analysis of complexes **11** and **12** raised questions on the purity of these complexes due to drastic differences in the calculated and found C and N ratios for these complexes. With all resonances in the aromatic region of the ^{1}H NMR spectra it is difficult to confirm the purity of the complexes using conventional spectroscopic studies due to extensive overlap, however, the shift of the hydrazinic proton from 12 ppm to 10 ppm in the ^{1}H NMR spectra does give hope to coordination of the ligand in an N,S bidentate fashion. Additionally, spurious peaks were observed in aromatic region of the ^{13}C NMR indicating an impurity may be present within these samples.

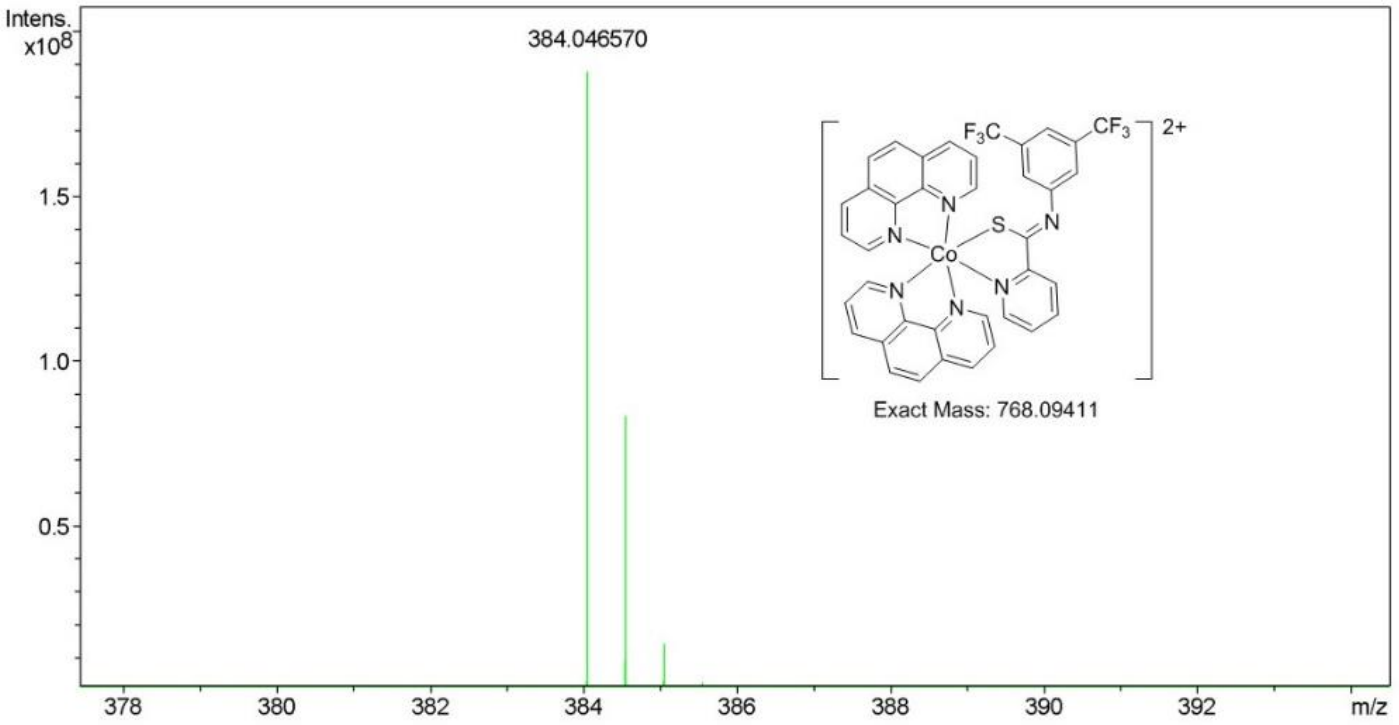

Figure 43. ESI mass spectrum of **11** in MEOH. Indicated the presence of a doubly charged species (**[11]**$^{2+}$).

Compound **10** the ruthenium analogue of **9** was generated in a similar reaction scheme. Shifts of the thioamide proton and thioketone resonance are observed similar to compounds **9** and **11** indicating an N,S- bidentate thione coordination mode for this complex. In the ESI-MS spectrum of **10**, a peak at *m/z* 676.0849 was observed and is attributed to the $[\mathbf{10}]^+$ species supporting the proposed structure (figure 44). Elemental analysis of this complex indicated the structure as proposed and also shows there are 1.75 H_2O molecules coordinated within the inner coordination sphere of the complex. During the purification step of the complex a second high molecular weight band was identified by UV-visible spectroscopy and it is hypothesized that this secondary band is due to the formation of a binuclear species following the coordination of the pendant pyridine to a second Ru(II) metal center, however, this has yet to be fully investigated (Figure 45).

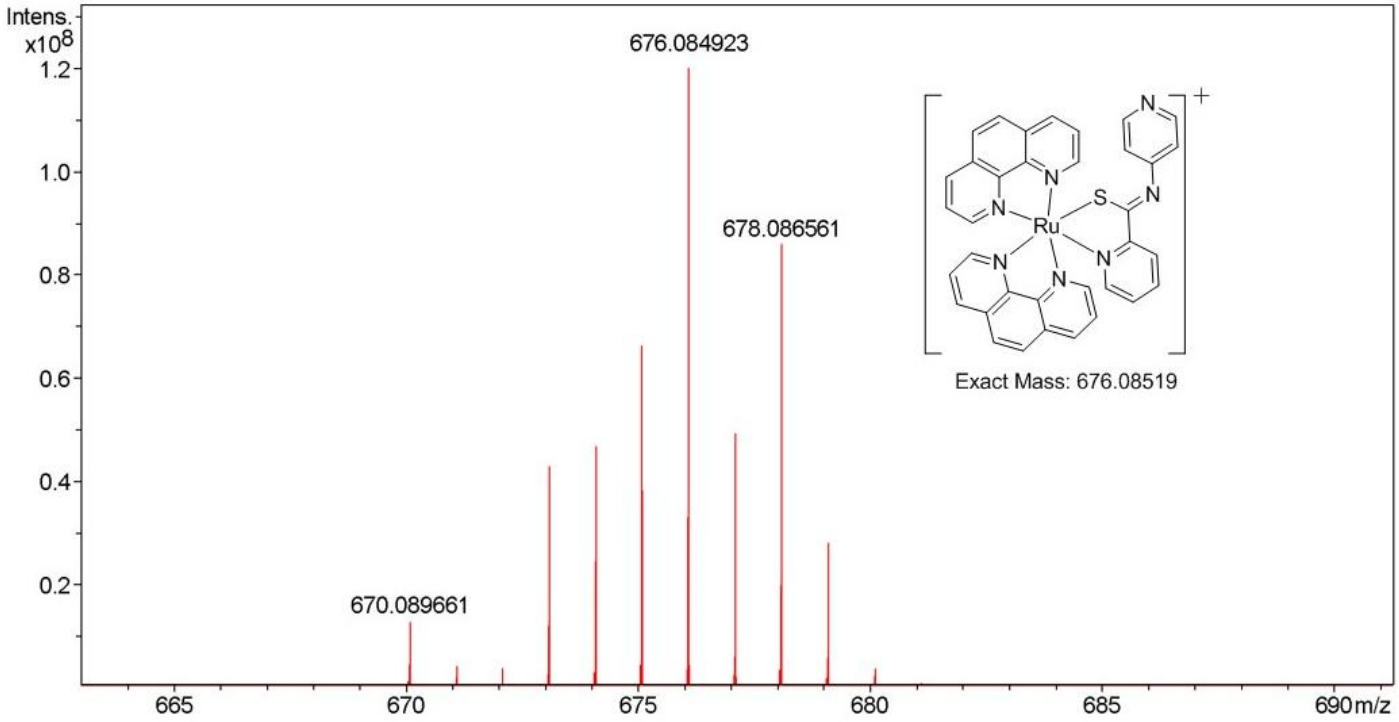

Figure 44. ESI mass spectrum of **10** in MeCN. Confirming the presence of a singly charged species ([**10**]$^{+}$).

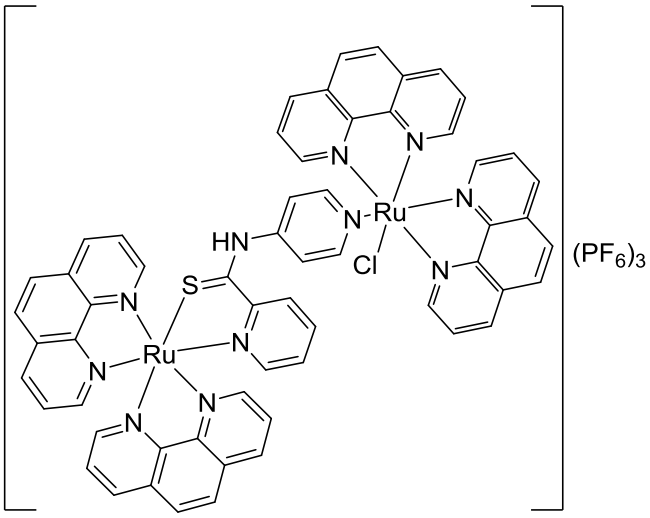

Figure 45. Potential binuclear product obtained from reaction of $[Ru(phen)_2Cl_2]$ and PPTA.

These PCA ligands can coordinate in multiple bidentate manners to the metal center, despite spectroscopic evidence of coordination in the thione N,S-fashion more detailed conformation was sought. Triclinc crystals obtained from a diffusion of Et_2O into a saturated solution of **12** in MeCN provided a structure of $[Co^{II}(phen)_3](PF_6)_2$ with 2 high disordered MeCN molecules within the crystallization sphere (Figure 46). Due to the previously discussed characterizations of these compounds it is likely the $[Co^{II}(phen)_3]^{2+}$ is a trace byproduct present in the precursor, $[Co(phen)_2(OH_2)_2](NO_3)_3$, utilized in the preparation of these compounds. This byproduct can also be observed in the ESI MS of compound **11** with an *m/z* of 299.56 attributed to the species $[Co^{II}(phen)_3]^{2+}$ (supporting figure A12). The presence of this byproduct in the all Co(III) samples has halted the ability of these complexes to be utilized in any cell free or cell based assay for their potential bioactivity.

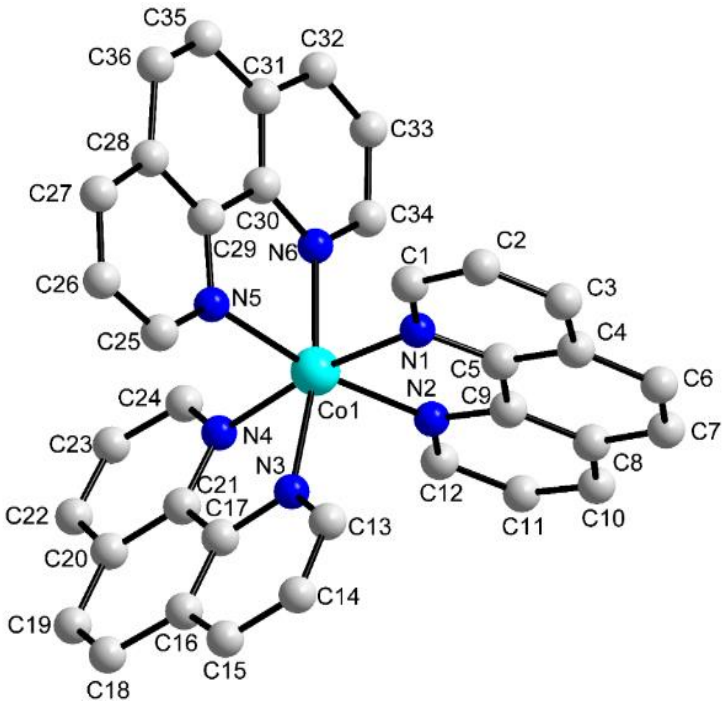

Figure 46. Trace impurity, $[Co^{II}(phen)_3]^{2+}$, present in all prepared Co(III) complexes.

CONCLUSION

The design, synthesis and characterization of a new series of PCA ligands (**1**-**8**) and PCA-containing complexes (**9**-**12**) are present. While the definitive mechanism of the employed Willgernot-Kindler reaction employed remains elusive, characterizations of the **1**-**8** indicate high yield and purity of synthesized PCAs. In one case X-ray crystallographic studies confirmed the structure as proposed thereby corroborating the employed scheme. Compound **8** in this series represent a PCA which will be future functionalized in the future for not only biological applications but for it use in bridging ligands potentially capable of facilitating election transport (See chapter 6). Characterization of the cyclometallated complexes **9**-**12** proved more difficult, however, it was confirmed by FT-IR analysis in most cases that the PCAs coordinate in an N,S bidentate fashion. While spectroscopic data for the Co(III) compounds provided some indication

the proposed complexes were synthesized, X-ray crystallographic studies show a trace impurity, $[Co(phen)_3]^{2+}$, to be present in all samples. This fact was further confirmed by EA and MS data (Supporting Figure A12). This impurity restricts the ability of in-depth characterization to be performed as well as negates the usage of these compounds in bioassays. Alternatively, the Ru(II) complex (**10**) was obtained in moderate yield with high purity confirming the utility of the employed reaction scheme. These PCAs represent a new series of compounds synthesized by a clean, versatile, process that potentially allows for rapid generation of a library of functionalize PCAs in the future. Furthermore, these PCA ligands and PCA-containing complexes represent a series of complexes which can be evaluated for their biological activity, specifically their ability to induce apoptosis in mammary breast cancer cell lines. The relative ease of preparation should allow for future SAR studies to be conducted and allow for easy comparison with thiosemicarbazone data. A solid understanding of the structure of the complexes, mechanism of action, and bioactivity with various cell markers is necessary for developing more active and efficient system for specific cell lines.

CHAPTER 5

SYNTHESIS AND CHARACTERIZATION OF A SERIES OF THIADIAZOLE- AND TRIAZOLOTHIADAIZOLE-CONTAINING COMPOUNDS FOR BIOLOGICAL APPLICATIONS

INTRODUCTION

Heterocyclic compounds have attracted much attention in the field of medicinal chemistry given their unique chemical properties and wide ranging biological activities. Despite the widespread success of these systems, a recent upheaval in research progress on these systems has begun to identify novel heterocyclic compounds with potent bioactivities.[408] Of the various heterocylces often five member systems, such as imidazole, oxaxole, thiazol, oxadiazole and thiadiazole are typically the most studies as they often possess biological activity. In particular, the thiadiazole ring has been extensively studied and has been linked to drugs which possess antiparasitic and antimicrobial properties, with some of the resultant drugs still in clinical use today.[409] More recently, research has indicated that the thiadaizole ring is an increasingly important framework, with broad spectrum bioactivity. As shown in figure 47 there are four major types of thiadiazole rings: 1,2,4-, 1,3,4-, 1,2,3- , and 1,2,5-thiadiazole, with the most investigated being the 1,2,4- and 1,3,4-thiadiazoles. It has been widely reported that compounds which bear the thiadiazole ring exhibit anticancer, anti-inflammatory, antibacterial, antifungal, antiviral, anticonvulsant and antiparasitic activities.[410-412]

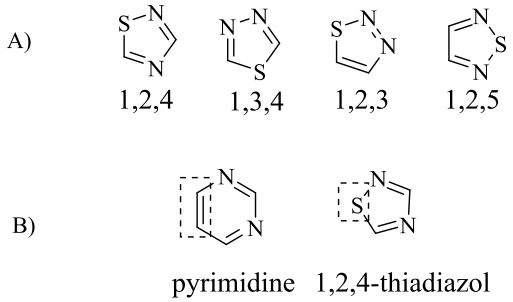

Figure 47. A) Core structures of thiadiazoles. B) A side by side comparison of the basic structures of pyrimidine and 1,2,4-thiadiazole scaffolds.

There are a variety of thiadiazole-containing drugs currently on the market with a variety of activities (figure 48). For example, methazolamide and acetazolamide are diuretics which inhibit carbonic anhydrase.[412] While the main mechanism of action of these drug is the inhibition on carbonic anhydrase closely related derivatives have found applications as anticonvulsants and cerebral vasodilators.[411, 413] Perhaps the most important thiadiazole containing drugs are: cefazolin sodium and cefazedone which are first generation cephalosporins that possess broad spectrum activity against gram-negative and gram-positive bacteria;[414] and timolol which is a β–blocker used for treatment of hypertension and migraine headaches.[413] All are listed on the World Health Organizations List of Essential Medicine needed for basic health systems. Additionally, megazol is a nitroimidazole based drug which is has been found to be more effective than the standard benznidazole therapy for treatment of Chagas disease (a protozoan infection).[415, 416]

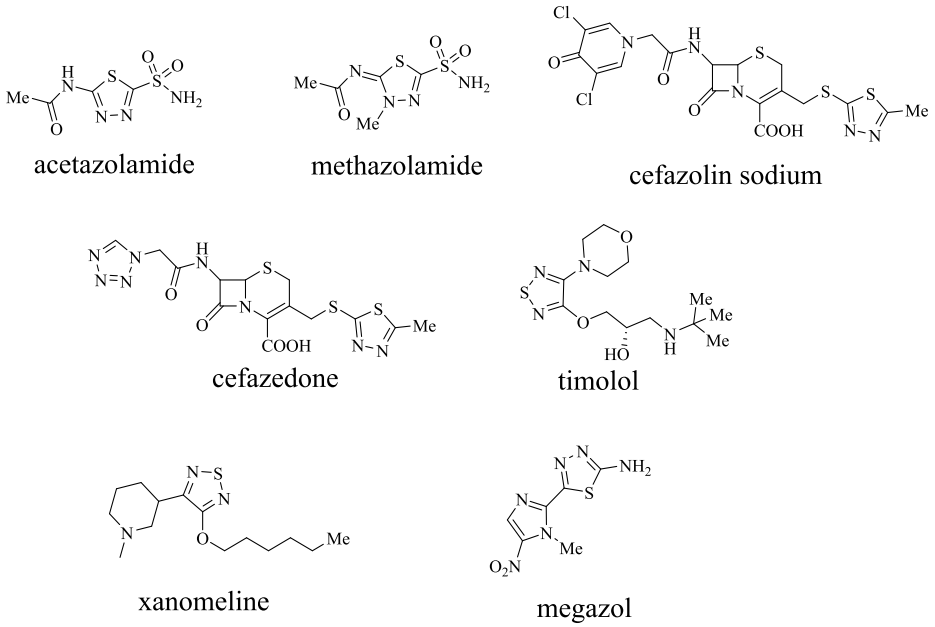

Figure 48. Some thiadiazole-containing drugs currently on the market.

The widespread activity of thiadiazole compounds is ascribed to the idea that 1,2,4-thiadizoles are bioisosteres to pyrimidines based upon the theory of ring equivalents proposed by Burger (shown in figure 48). With the pyrimidine ring playing a prominent role in nucleobases found in DNA and RNA, specifically, cytosine, uracil, and thymine it is predicted that these compounds many interfere with normal metabolism of nucleic acids.[417] Cellular uptake of compounds which incorporate the thiadiazole moiety is often aided leading to enhanced activity due to the sulfur atom imparting improved liposolubility.[418] Additionally, the 1,3,4-thiadiazoles are mesoionic - with conjugated p and π electrons and regions of positive and negative charges.[419] This unique property may give ligands incorporating these systems the ability to facilitate electron transfer reactions, a property which has been exploited in many other applications.[420-423]

While the thiadiazole moiety is independently powerful,[424-427] current trends are focused on incorporating multiple heterocylic systems into one molecule to further increase the various

utility of these molecules. Another moiety, 1,2,4-triazoles have been reported to possess similar widespread activity similar to thiadiazoles.[428, 429] Commonly, triazoles are combined with thiadiazoles or thiazdiazines to create triazolothiadiazoles and triazolothiadiazines, respectively. These multiple heterocylic compound have been reported to have broad spectrum therapeutic activity from antiviral and antitumoral activity to CNS-stimulants and phosphodiesterase-4 inhibitors.[430-437]

Our design strategy was to generate a library of these thiadiazole and triazolothiadiazole ligands to conduct SAR studies on their biological activity. Several protocols exist for the preparing of both thiadiazole- and triazolothiadiazole-containing compounds, however we have chosen to follow recent literature examples on the preparation of both systems.[438, 439] The use of 4-amino-5-(pyridine-2-yl)-1,2,4-triazol-3-thiol (**4**) in the preparations of our triazolothiadiazole systems (**5-11**) allows for the incorporation of a third heterocycle for future coordination to metal centers. The amino and mercapto groups present also serve as ready-made nucleophilic center for the synthesis of condensed heterocyclic rings.[440, 441] Herein we report the synthesis and characterization of a series of thiadiazole and triazolothiadiazole compounds, as shown in schemes 7 and 8, respectively. These compounds represent proof of concept model and are the beginning stages of a library of heterocyclic compounds which can complexed to various metal centers and assayed for their biological activities.

EXPERIMENTAL

General

All reagents used in the syntheses, if not specified, were obtained from either Sigma-Aldrich (St. Louis, MO) or VWR International (Radnor, PA) and were used without further

purification. ^{1}H, ^{13}C and ^{19}F NMR spectra were collected on a Varian *Inova 400 MHz* NMR Spectrometer. ^{1}H NMR spectroscopic samples were standardized relative to sodium 3-(trimethylsilyl)propionate (δ = 0.0 ppm) or appropriate residual solvent peaks. ^{13}C NMR spectroscopic samples were all standardized to residual solvent peaks as indicated by respective compounds. FT IR and ATR data was obtained using a Nicolet AVATAR 370 DTGS spectrophotometer. X-ray crystallography studies were conducted by Dr. Colin McMillen, Director of the Molecular Structure Center, Department of Chemistry of the Clemson University (Clemson, SC, USA).

Synthesis of *N*-phenyl-1,3,4-thiadiazole-2-amine ligands

5-(2-pyridinyl)-*N*-phneyl-1,3,4-thiadiazole-2-amine (1)

N-phenylthiosemicarbazide (1.67 g, 0.01mol) and 2-picolinc acid (1.23 g, 0.01mol) in DMF (25ml) were combined in a 100 mL RBF. A few drops of concentrated HCl were added to the reaction and the reaction flask was placed in a silicon oil bath to reflux for 72 hours at 95 °C. After 72 hours the blue/green reaction mixture was slowly poured into crushed ice forming an immediate yellow precipitate. The separated solid was filtered, washed with water, dried and purified by recrystallization from methanol. A single crystal suitable for X-ray analysis was grown via slow evaporation technique by dissolving 50 mg of the obtained yellow solid in a 2 M HCl solution and allowing the solvent to evaporate. Yield = 0.346 g (13.7 %), yellow solid. FT IR (KBr) cm^{-1} = 3230 (NH, m); 3006 (CH, m); 1600 (C=N, s); 1554 (C=C, vs), 746 (ArH, s), 694 (ArH, s). ^{1}H NMR (400 MHz, DMSO-d_6): δ_H/ppm 6.93 (t, *J*=7.22 Hz, 1 H) 7.30 (t, *J*=8.01 Hz, 3 H) 7.55 (d, *J*=7.81 Hz, 3 H) 8.71 (s, 1 H) 9.85 (s, 1 H). ^{13}C NMR (100 MHz, DMSO-d_6): δ_C/ppm 163.9, 162.9, 153.2, 149.1, 139.1, 136.7, 129.1, 124.7, 123.4, 122.0, 117.9.

5-(3,4-dimethoxyphenyl)-*N*-phenyl-1,3,4-thiadiazole-2-amine (2)

N-phenylthiosemicarbazide (1.67 g, 0.01mol) and 3,4-dimethoxybenzoic acid (1.82 g, 0.01mol) in DMF (25ml) were combined in a 100 mL RBF. A few drops of concentrated HCl were added to the reaction and the reaction flask was placed in a silicon oil bath to reflux for 72 hours at 95 °C. After 72 hours the blue/green reaction mixture was slowly poured into crushed ice forming an immediate white precipitate. The separated solid was filtered, washed with water, dried and purified by recrystallization from methanol. Yield = 0.880 g (28 %), white powder. FT IR (KBr) cm^{-1}: 3230 (NH, m); 2966 (CH, m); 1677 (C=N, s); 1598 (C=C, vs); 1483 and 1268 (ArH, vs); 746 and 630 ArH, m). ^{1}H NMR (400 MHz, DMSO-d_6): δ_H/ppm 9.88 (s, 1H), 7.57 (dd, *J*=2.15, 8.40 Hz, 2H), 7.44 (d, *J*=1.95 Hz, 1H), 7.31 (s, 1H), 7.26-7.36 (m, 1H), 7.04 (d, *J*=8.59 Hz, 1H), 6.94 (s, 1H), 6.94 (d, *J*=14.84 Hz, 1H), 3.81 (d, *J*=10.54 Hz, 6H). ^{13}C NMR (100 MHz, DMSO-d_6): δ_C/ppm 163.9, 162.9, 161.9, 139.1, 131.0, 129.1, 124.7, 117.9, 111.0, 101.3, 55.5.

2-(dithiocarboxy)hydrazide-4-pyridinecarboxylic acid (potassium salt) (3)

Isonicotinic hydrazine (5.00 g, 36.5 mmol) was treated with a solution of potassium hydroxide (2.16 g, 54.75 mmol) dissolved in ethanol (100 mL) in a 250 mL RBF. The flask was cooled to 0 °C, then CS_2 (3273 µL, 54.75 mmol) was slowly added with constant stirring resulting in a clear yellow solution. After 24 hour of stirring at room temperature, the opaque yellow solution was filtered through a fine glass frit to yield a yellow powder. The product was washed with chilled ethanol and air dried. Yield = 9.01 g (96 %). FT IR (KBr): 3311 (-NH, s); 3081 (-CH, s); 1677 (C=O, vs); 1508 and 1473 (ArH, m); C=S (1093, m); 692 (C-S, m). ^{1}H NMR (400 MHz, DMSO-d_6): δ_H/ppm 7.78 (d, *J*=5.47 Hz, 1 H) 8.72 (d, *J*=5.47 Hz, 1 H) 9.76 (s, 1 H) 10.61 (s, 1 H).

4-amino-5-(pyridine-2-yl)-4H-1,2,4-triazole-3-thiol (4).

2-(dithiocarboxy)hydrazide-4-pyridinecarboxylic acid (2.0 g, 7.95 mmol) was dissolved in H_2O (63 mL) in a 250 mL RBF with a stir bar resulting in a yellow solution. Then hydrazine hydrate (4952 µL, 159 mmol) was added dropwise to the flask and it was allowed to reflux for 24 h. During the progress of the reaction, the reaction mixture turned green with the evolution of hydrogen sulfide gas and became homogeneous. After 24 hours at reflux the flask was cooled to room temperature and evaporated to a minimum volume (~ 20 mL). Then HCl (conc.) was added dropwise to the flask resulting in the formation of a white precipitate. The solid was collected by filtration through a glass frit. The HCl addition process was repeated on the filtrate until no further product was obtained. The crude product was washed with water and air dried to yield an off white powder. Yield = 1.47 g (96 %). FT IR (KBr, cm^{-1}): 3320 (NH, m), 2598 (SH, s), 1610 (C=N, m), 1572(C–H, m). ^{1}H NMR (400 MHz, DMSO-d_6): δ_H/ppm 5.85 (s, 1 H) 7.82 (br. s., 2 H) 8.03 (br. s., 2 H) 8.81 (d, *J*=3.51 Hz, 2 H)

Generation of 6-substituted-1-2,4-triazolo-[3,4-*b*]-1,3,4-thiadiazole library

General procedure for synthesis of 6-substituted-1-2,4-triazolo-[3,4-*b*]-1,3,4-thiadiazoles was adapted from the methods of Gilani *et al.*[438] In brief, an equimolar mixture 4-amino-5-(pyridine-2-yl)-4H-1,2,4-triazole-3-thiol (**4**) and aromatic acids in phosphorus oxychloride (20 mL) were refluxed for five hours. The reaction mixture was cooled to room temperature and then gradually poured on to crushed ice with stirring. The mixture was allowed to stand overnight and the solid separated out, was filtered, treated with dilute sodium hydroxide solution and washed thoroughly with cold water, yield: 45 – 76%.

6-phenyl-3-(4-pyridyl)-1,2,4-triazolo-[3,4-*b*][1,3,4-]thiadiazole (5)

Yield = 0.5312 g (73 %). ^{1}H NMR (400 MHz, $CDCl_3$): δ_H/ppm 8.84-8.89 (m, 2H), 8.31-8.34 (m, 2H), 7.96-8.03 (m, 2H), 7.56-7.71 (m, 3H). ^{13}C NMR (100 MHz, DMSO-d_6): δ_C/ppm 175.7, 158.1, 149.9, 149.7, 132.8, 130.4, 129.2, 128.9, 125.9, 121.5.

6-(3,4-dimethoxyphenyl)-3-(4-pyridyl)-1,2,4-triazolo-[3,4-*b*][1,3,4-]thiadiazole (6)

Yield = 0.3787 g (72 %). ^{1}H NMR (400 MHz, $CDCl_3$): δ_H/ppm 8.85 (d, *J*=5.08 Hz, 2H), 8.30 (d, *J*=5.47 Hz, 2H), 7.50-7.55 (m, 1H), 7.46 (d, *J*=1.56 Hz, 1H), 7.02 (d, *J*=8.20 Hz, 1H), 4.04 (s, 3H), 4.00 (s, 3H). ^{13}C NMR (100 MHz, DMSO-d_6): δ_C/ppm 175.7, 158.1, 149.8, 149.7, 148.3, 132.8, 130.4, 129.2, 128.9, 125.9, 121.5.

5-hydroxyl-2-[3-(4-pyridinyl)-1,2,4-triazolo-[3,4-*b*][1,3,4]-thiadiazole-6-yl]-phenol (7)

Yield = 1.18 g (74 %). ^{1}H NMR (400 MHz, $CDCl_3$): δ_H/ppm 8.81 (s, 1H), 8.63 (m, 2H), 7.74 (m, 2H), 7.23 (d, *J*=8.44 Hz, 1H), 6.48 (s,1H), 6.32 (d,, *J*=8.44, 3H), 3.96 (s, 2H).

2-[3-(4-pyridinyl)-1,2,4-triazolo-[3,4-*b*][1,3,4]-thiadiazole-6-yl]-benzamine (8)

Yield = 27 mg (45 %). ^{1}H NMR (400 MHz, $CDCl_3$): δ_H/ppm 8.67-8.75 (m, 2H), 8.04-8.09 (m, 2H), 7.95 (dd, *J*=1.71, 7.81 Hz, 1H), 7.57 (dt, *J*=1.71, 7.94 Hz, 1H), 7.42 (dt, *J*=0.98, 7.81 Hz, 1H), 6.68 (dd, *J*=1.22, 8.06 Hz, 1H)

6-(anthracen-1-yl)-3-(pyridin-4-yl)[1,2,4]triazolo[3,4-*b*][1,3,4]thiadiazole (9)

Yield = 52 mg (52 %). ^{1}H NMR (400 MHz, $CDCl_3$): δ_H/ppm 9.15 (m, 1H), 8.84 (dd, 2H), 8.73 (m, 1H), 8.47 (m, 1H), 8.34 (m, 2H), 8.20 (dd, 2H), 7.87 (dt, 1H), 7.69 (m, 1H), 7.55 (m, 1H);

^{13}C NMR (100 MHz, DMSO-d_6): δ_C/ppm 158.1, 156.2, 150.4 149.6, 136.7, 132.8, 131.9, 131.3, 130.7, 130.6, 128.2,127.8, 126.5, 121.5, 120.4.

4-[3-(pyridin-4-yl)[1,2,4]triazolo[3,4-*b*][1,3,4]thiadiazole-6-yl]benzene-1,2-diamine (10).

Yield = 30 mg (55 %). ^{1}H NMR (400 MHz, $CDCl_3$): δ_H/ppm 8.64 (dd, 2H), 8.13 (d, 1H), 8.04 (dd, 2H), 7.02 (t, 1 H), 6.66 (dd, 1H). ^{13}C NMR (100 MHz, DMSO-d_6): δ_C/ppm 158.1, 156.7, 150.1, 149.6, 141.0, 137.9, 132.6, 130.1, 127.4, 121.5, 115.2.

4-[3-(pyridin-4-yl)[1,2,4]triazolo[3,4-*b*][1,3,4]thiadiazole-6-yl]phenol (11)

Yield = 27 mg (45 %). ^{1}H NMR (400 MHz, $CDCl_3$): δ_H/ppm 8.67-8.75 (m, 2H), 8.04-8.09 (m, 2H), 7.95 (dd, *J*=1.71, 7.81 Hz, 1H), 7.57 (dt, *J*=1.71, 7.94 Hz, 1H), 7.42 (dt, *J*=0.98, 7.81 Hz, 1H), 6.68 (dd, *J*=1.22, 8.06 Hz, 1H)

RESULTS AND DISCUSSION

Scheme 10. Synthetic route for preparation of thiadiazole-containing compounds.[439, 442]

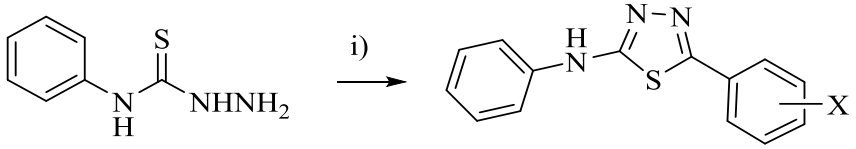

[a] (i) RCOOH, DMF, HCl

The synthesis of compounds **1** and **2** are shown in Scheme 10. The preparation involves the cyclization of 4-phenylthiosemicarbazide to a 1,3,4-thiadiazole in the presence of various aromatic carboxylic acids. Typically, reactions of this type are carried out under microwave conditions in order to reduce the reaction time and to afford a cleaner product,[439, 442] however, using a method adapted from Sahoo *et al*.[439] conventional synthetic methods have been employed.

The ^{1}H NMR spectrum of **1** indicates high conversion and it consistent with reported literature values for the compound as shown in figure 49.[442] The ^{13}C NMR spectrum shows the losses of the resonances at ≈180 and ≈160 ppm attributed to thiourea and carboxylic acid moieties in the starting materials, respectively. In addition, a similar pattern is observed in compound **2,** a 3,4-dimethoxy derivative. Despite the confirmation of **1** by NMR spectroscopic studies, a crystal of **1** was shown to have a unit cell dimension matching *N*,*N*-diphenyl-[1,3,4]thiadiazole-2,5-diamine, a symmetrical 1,3,4-thiadiazole compound with 2 equivalent phenyl rings.[443] Interestingly, the ^{1}H NMR resonances are similar for the two structures,[443] however, the ^{13}C resonances show significant differences. This formation of *N*,*N*-diphenyl-[1,3,4]thiadiazole-2,5-diamine was further confirmed with ESI-MS where the molecular ion peak can be observed at an m/z of 269.08 (supporting figure A21). Interestingly, no such symmetrical compound was obtained when utilizing the same reaction scheme and a substituted (3,4-dimethoxy) carboxylic acid as the starting material. An alternative route for the preparation of the target molecule has been proposed starting from 2-picoline utilizing an isothiocyante intermediate.

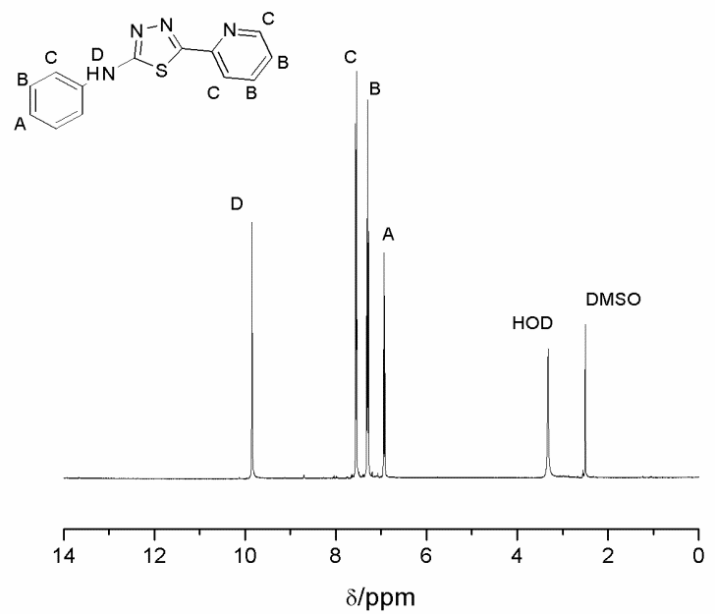

Figure 49. ^{1}H NMR spectrum of 5-(2-pyridinyl)-*N*-phneyl-1,3,4-thiadiazole-2-amine (**1**) in DMSO-d_6.

Scheme 11. Route for preparation of triazolothiadiazole-containing compounds.[438]

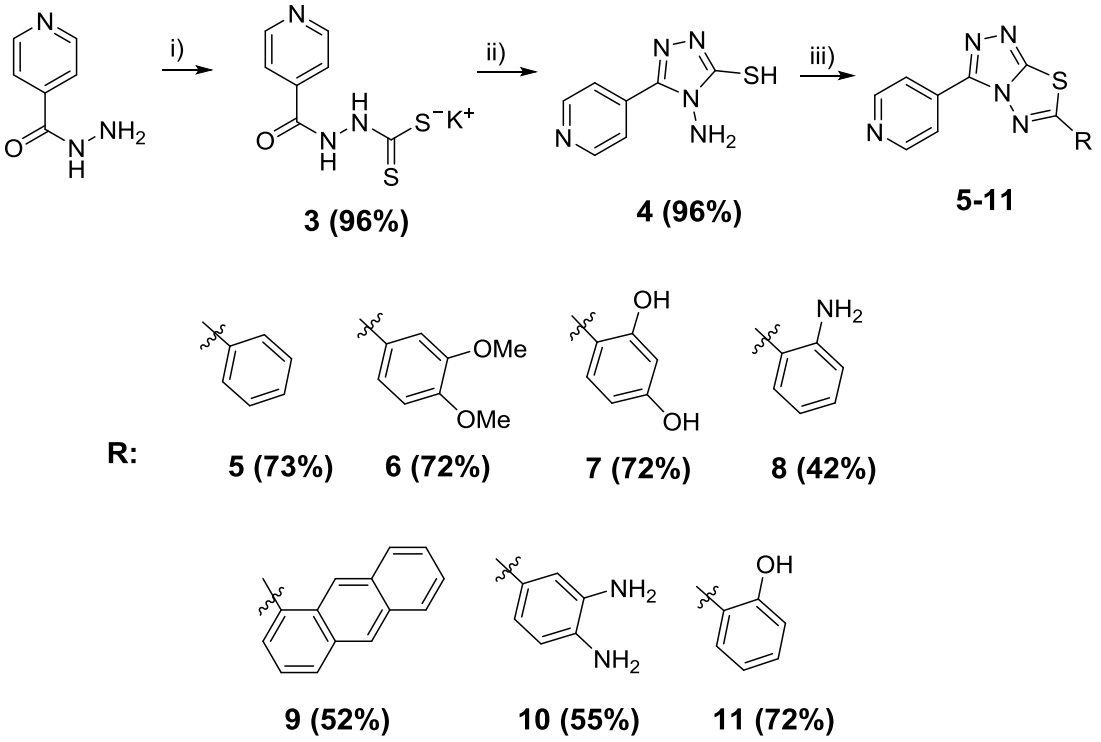

[a] (i) KOH, EtOH, CS_2; (ii) $NH_2NH_2 \cdot H_2O$, H_2O, HCl; (iii) RCOOH, $POCl_3$

Compounds **3** and **4** serve as the synthetic precursors to forming 6-substituted-1,2,4-triazolo[3,4-*b*]-1,3,4-thiadiazoles **5-11** and the synthesis is shown in scheme 11. The key step in the synthesis of these systems is the acid catalyzed condensation, where, for example, benzoic acid is reacted with **4** in the presence of $POCl_3$ to generate **5** in high yields. The required dithiocarbazinate **3** was synthesized by reacting isonicotinic acid hydrazide with carbon disulfide and potassium hydroxide in ethanol. This salt underwent ring closure with an excess of 99% hydrazine hydrate to afford **4**, in high yields. Full caution (closed hood, lab coats and gloves) must be taken when working with hydrazine hydrate as it is extremely flammable and during the work up of this reaction as hydrogen sulfide gas is evolved. The ^{1}H NMR spectrum of the desired product

(**4**) matches well with literature characterization for the compound (Figure 50);[438] and ring closure can be confirmed by the appearance of the stretching frequency at 2598 cm^{-1} in the FT IR spectrum, indicative of the formed thiol moiety.

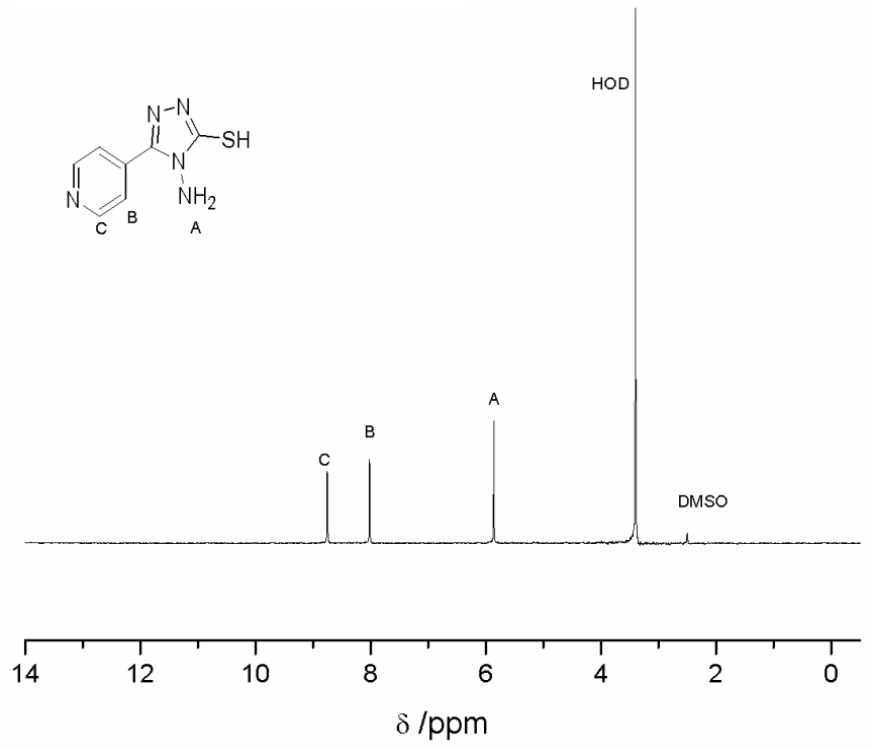

Figure 50. ^{1}H NMR spectrum of 4-amino-5-(pyridine-2-yl)-4H-1,2,4-triazole-3-thiol (**4**) in DMSO-d_6**.**

The triazole containing precursor (**4**) was converted to the desired 6-substituted-1,2,4-triazolo[3,4-*b*]-1,3,4-thiadiazoles **5-9** in a one-pot reaction by condensation with various aromatic acids in the presence of $POCl_3$ utilizing the protocol by Gilani *et al.*[438] For example, **5** was prepared in high yield and high purity as indicated by ^{1}H NMR data (Figure 51), which is consistent with previous reports for this compound.[410, 444] In an attempt to introduce a fourth heterocycle into the system a

reaction was completed using **4** and 2-picolinic acid. Unfortunately, FT IR characterization indicated no conversion to the desired product due the conservation of the broad stretching frequency at 3200 cm^{-1} attributed to the carboxylic acid.

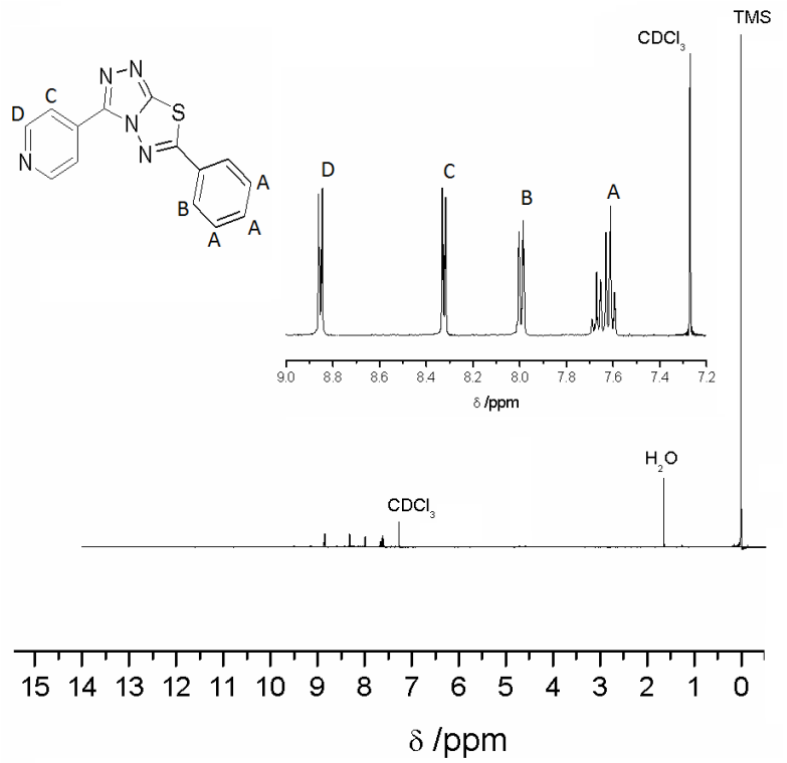

Figure 51. ^{1}H NMR spectrum of **5** in $CDCl_3$. Inset shows blow up of peaks present in the aromatic region.

In order to further determine the utility of this reaction scheme and rapidly generate a library of compounds, various substituted aromatic acids were condensed in $POCl_3$ in the presence **4**. As shown in scheme 10, we have synthesized a variety of compounds which include common functional groups such as amines, alcohols, methoxy, and aryl. Spectroscopic characterization of all analogues is similar to **5**. Of the employed functional groups employed only the addition of a

heterocylic compound failed to produce a compound for characterization. This small library of compounds shows the widespread utility of the employed reaction scheme which can further be utilized to quickly and efficiently generate a large library of compounds for SAR studies.

CONCLUSION

The synthesis and characterization data of various thiadiazole or triazole-thiadiazole containing compounds is discussed in this chapter. First, using conventional methods similar to those employed by Sahoo *et al*.[439] we have prepared or attempted to prepare two thiadiazole containing compounds **1** and **2**. Similar to reports by Efirmova *et al*.[442] conventional methods proved unsuccessful at preparing **1**; instead X-ray crystallographic data suggests *N*,*N*-diphenyl[1,3,4]thiadiazole-2,5-diamine was prepared. A scheme starting from 2-picolinc acid has been proposed as a possible alternative route to preparing the compound without employing microwave conditions. Additionally, a series of triazole-thiadiazole containing compound were created **5-9** via a condensation reaction of the precursor **4** with various aromatic acids. We have utilized mono- and di-substituted aromatic acids with some success and a small of compounds has been prepared. Future studies will focus on coordination of these compound to various metal centers (notably Ru(II) and Co(III)) as well as studying the *in vitro* bioactivities, most notably anti-microbial and anti-cancer. As both triazole and thiadiazole rings are often found in drug molecules both series of prepared compounds are predicted to have high biological activity and therefore have merit in their continued exploration.

CHAPTER 6

CONCLUSIONS AND FUTURE WORKS

The primary focuses of the studies outlined in this thesis were to design, synthesize and characterize novel ligands and transition metal complexes for biomedical applications and to provide enhanced knowledge on the mechanism of action of transition metal complexes and nsPEF technology in breast cancer cell lines. Transition metal complexes remain to be one of the largest and most studies class of compounds as they relate to medicinal chemistry owing to the success of cisplatin.[97] Despite significant research progress on a variety of these metal complex systems, there are ongoing efforts to discover novel compounds with potent bioactivities and elucidate their mechanism of action.

Mechanistic investigations

To investigate the mechanism of action of a new drug molecule is to fully describe the functional or anatomical changes of a living organism elicited by the introduction of the substance at the molecular level. In chapter 2, we investigated the mechanism of action of $[Co(phen)_2(MeATSC)](NO_3)_3 \cdot 2.5H_2O \cdot C_2H_5OH$,[273] via various cell-free and cell based assays. It was revealed through fluorescence and UV-visible titration experiments that the complex interacts with DNA in an intercalative manner, most likely stemming from the inclusion of polypyridyl heteroaromatic phenanthroline ligands. The complex demonstrated moderate toxicity in the model aggressive metastatic breast cancer cell line with an IC_{50} = 34 μM. Additionally, it was established that the complex induced autophagy, apoptosis, and dissipation of the $\Delta\Psi_m$ in breast cancer cells in both concentration- and time-dependent manners. It was concluded that the apoptotic cascade

was activated in a caspase-dependent manner and was this signaling pathway was most involved in cell death. Given other observations of the molecular target of the complex, it is most likely that the caspase cascade is activated via the intrinsic pathway following initial DNA damage. Initial studies conducted involving a novel dual treatment strategy involving nsPEF technology and Co(III) chemotherapeutic agents were also described. It was observed that dual treatment resulted in an increase in cellular viability, the opposite of the hypothesized synergistic killing effect. The nature of the "protective" event occurring was further investigated by the inhibition of the autophagic pathway, however, inhibition of this signaling pathway yield no significant change in observed effect.

While the assays conducted here have provided interesting preliminary information on the punitive mechanism of action of $[Co(phen)_2(MeATSC)](NO_3)_3 \cdot 2.5H_2O \cdot C_2H_5OH$, there is much room for improvement on current studies and future work. One of the biggest unanswered questions for our studies is: what is the effect of typsin-EDTA on our cells? Trypsin is a prolytic enzyme utilized to remove adherent cells from culture flasks prior to many assays. We have some preliminary results which suggest that this harsh method of removing cells could cloud some of the results but have yet to determine its overall effect. Other protocols could be optimized to further validate our hypotheses moving forward for instance, in the Enzo autophagy assay only a small shift in the fluorescence signal via flow cytometric analysis is observed. To further confirm the activation of this pathway staining and imagining using confocal microscopy could greatly aid in the visualization of the formed autophagosomes. Viability assays conducted were heavily reliant on the MTS assay which monitors NADPH production (which occurs in the mitochondria) to detect viable cells, however, our studies have shown that the complex affect the mitochondria in addition to DNA. This observation indicates that other viability assays should be considered to

confirm the activity of the complex perhaps monitoring ATP levels or luminescence signals from viable cells following exposure to luciferase, as the cells contain a plasmid for luciferin.

The studies conducted within this thesis can be considered preliminary in nature and in order to fully discern the mechanism of action of $[Co(phen)_2(MeATSC)](NO_3)_3 \cdot 2.5H_2O \cdot C_2H_5OH$ much more intensive mechanistic studies will be required. Initial efforts will focus on studying the uptake and trafficking of the compound using ICP-AES, confocal fluorescence microscopy, and flow cytometry coupled with tracking dyes such as Lyso-tracker DND-99 (Sigma-Aldrich), Mito-tracker Red CMXRos (Sigma Aldrich), and DAPI. Additionally, monitoring the activity of various endocytosis pathways such as: clathrin-mediated, lipid-raft, dynamin-mediated lipid raft, and transferrin-mediated will be important to determine an uptake mechanism and various inhibitors such as: sodium azide/2-deoxy-D-glucose, sucrose, nystatin, and dynasore will be utilized to study these pathways in detail.

From our studies we have proposed the activation of the intrinsic apoptotic pathway is necessary to facilitate cell death based upon caspase 3 activation, dissipation of the $\Delta\Psi_m$ and spectroscopic evidence, however, this hypothesis should be investigated in greater detail. While caspase 3 was investigated in these studies, an increase in its' activity is implicated in both the intrinsic and extrinsic apoptotic pathways. Mitochondrial signaling leading to $\Delta\Psi_m$ collapse, results in cytoplasmic release of effectors (cytochrome c, pro-caspase 9, etc.) constituting the apoptosome, which promotes caspase-9 and then caspase-3 activation, and the intracellular levels of these effectors should be monitored to validate the hypothsized caspase-dependent cell death mechanism proposed. Studies should also be conducted monitoring the activation of the extrinsic death receptor pathway by monitoring caspase 8, apoptosis inducing factor (AIF), Fas ligand and TNF. Additional experiments involving various protein markers will be utilized to delineate the

role of apoptosis related the caspase cascade including APAF-1, Bax, Bid, Bcl-2. Perhaps the most important information will come from monitoring the trafficking and cellular distribution of p53, which is stabilized by post-translational modifications following stress. Phosphorylation of Ser15 and Thr18 and upregulation leading to either nuclear or mitochondrial accumulation of this protein could be telling of the transcriptional events activated.

All current studies have only been conducted in one TNBC cell line (due in part to time and available resources), however, it would be in the best interest of future researchers to conducted all studies in other cancerous cell lines such as: HeLa (adenocarcinoma), HEK-293 (kidney), A2780cis (cisplatin resistant ovarian), and MDA-MD-435 (melanoma) as well as "normal" control cell lines such as: MCF-10A (mammary) and HFF-1 (fibroblasts) to determine the specificity of this particular compound for certain cell types and cancerous vs noncancerous cells. Additionally, it is also required that an appropriate control drug such cisplatin or doxorubicin be utilized in order for comparison to known anticancer chemotherapeutics. The inclusion of multiple cell line while a daunting task in terms of labor will provide essential information on the complexes activity. For instance, NAMI-A has very low cytotoxic potential but has shown remarkable antimetastatic potential.

The activation of the autophagic signaling pathway provided an interesting phenomenon upon addition of the test compound and it would be of interest to further study the activation of this signaling pathway, by monitoring cellular ATP levels. While the molecular event which provoke autophagic cell death or post-autophagic cell death are highly and intensively debated, drastic oxidative stress has been shown to lead to autophagic or necrotic cell death, thus modulation of intracellular ROS levels should be investigated. There are also many key proteins which are

involved in both the autophagic and apoptotic pathways and therefore it would be of interest to further investigate and probe for potential crosstalk between these two RCD pathways.

Finally, the nature of the "protective" event observed in the synergistic dual treatment studies must be further investigated. First it is imperative that the stability of the complex following exposure to nsPEF be established utilizing a combination of HRMS, ^{1}H, ^{13}C and ^{59}Co NMR spectroscopic studies be conducted. Transients formed during the nsPEF exposure process may be ultimately detected using a modified pulse radiolytic technique to provide information on whether reduction and therefore potential "activation" of the Co^{III} metal center is occurring. Alternatively, if localized and selective uptake of the compound is observed and a reduction can be achieved following nsPEF exposure, an interesting, localized treatment therapy may be developed.

ITC studies

In chapter 3, we utilized isothermal titration calorimetry to probe the interaction of mononuclear V(IV) and binuclear Ru(II)-V(IV) complexes with CT DNA. Following the work conducted by Holder *et al.*[127] we have synthesized a new oxidovanadium(IV) complex which incorporates an OOO donor group. This complex, $[VO(oda)(phen)]\cdot 1.5H_2O$ was characterized via conventional spectroscopic techniques and X-ray crystallography. Despite a crystal structure confirming the target molecule, solubility issues, not previously reported in literature, inhibited our ability to conduct bio-physical and bio-chemical studies on the complex.[370, 445] The complex was however, successfully incorporated into a supramolecular scaffold to generate a binuclear Ru(II)-V(IV) complex. Isothermal titration calorimetry experiments revealed that this novel binuclear Ru(II)-V(IV) complex showed significant binding interactions with DNA with three observable binding constants. Future efforts will be focused on conducting similar binding studies

with the mononuclear Ru(II) precursor molecule as well as complementing this studies using alternative techniques such as UV-Vis or fluorescence spectroscopy. We were unable to assess the chemotherapeutic activity of this binuclear complex due to complications with background absorbance, however, optimization of protocols utilizing different assays (i.e. luminescence or flow cytometric) methods are underway to circumvent this problem. Future studies will also focus on further characterization of the interactions of these supramolecular complexes with DNA and their chemotherapeutic activity in the absence/presence of light irradiation. Following initial studies on these complexes studies similar to those described in Chapter 2 will be conducted to fully describe their mechanism of action.

Synthesis of Ligands and Complexes

Despite significant research progress on heterocyclic ring systems, there are ongoing efforts to discover novel compounds with potent bioactivities. The goal of this research was to design a series of sulfur containing molecules as they are bioisosteres of common functionalities found within many drug molecules and often have enhanced liposolubility owing to the sulfur component.[418] The approaches utilized throughout this thesis open the door for the synthesis of entire libraries of compounds with clean, versatile, and relatively simple reactions.

In chapter 4 our efforts focused on generating a series of *N*-substituted pyridine-2-carbothioamides due to their structural similarity to thiosemicarbazones.[102, 103, 399, 446, 447] Due to minimal reports on the application of metal complexes incorporating *N*-substituted PCAs,[392, 395, 397, 399, 448] the work described in this thesis seeks to developed a series of these PCAs and PCA-containing complexes which may possess anticancer bioactivity. Several PCA ligands were synthesized in a one-pot synthetic scheme and characterized via conventional spectroscopic

techniques as well as X-ray crystallography, where appropriate. One derivative required an alternative path due to a competitive ketone moiety, however, following a simple reduction with LAH the desired PCA was obtained in high yield similar to others prepared. Successful complexation a transition metal precursor, $[Ru(phen)_2Cl_2]$, was achieved, however, impurities in the $[Co(phen)_2(OH_2)_2](NO_3)_3$ precursor limited success of these analogues. While ESI MS, FT IR, and ^{19}F NMR spectroscopic studies exhibit peaks and shifts from the proposed complexes crystallographic studies indicate the presence of a byproduct, $[Co(phen)_3]^{2+}$. Future studies will focus on purifying the synthesized Co(III) complexes and generating a larger library of PCAs for complexation. Despite only sparse reports on the application of this class of ligands we envision these complexes to exhibit enhanced anticancer activity and stability when compared with Schiff base containing thiosemicarbzaone complexes. Following initial screening of the bioactivity of the complexes structure-activity relationship studies will be conducted to allow for rational design of future ligands. Furthermore, mechanistic studies will be carried out these complexes and compared with current and any future data on the mechanism of complexes similar to those in Chapter 2 for direct comparison of the mechanisms of these related structures.

Finally in chapter 5, a series of thiadiazol and triazolothiadiazol compounds were synthesized via simple reactions involving either *N*-phenylthiosemicarbazide or isonicotinc hydrazine hydrate. Similar to previous reports on the synthesis of thiadiazol compound we were unsuccessful at preparing the proposed compounds via conventional methods, however a modified scheme has been proposed for their synthesis in an attempt to continue to avoid the adjuvant of a microwave reactor. Additionally, a series of triazolothiadiazol compound were synthesized via a condensation reaction of the prepared precursor 4-amino-5-(pyridine-2-yl)-1,2,4-triazol-3-thiol with various aromatic acids. We have utilized a variety of substituted aromatic acids to prove the

utilized of the employed reaction scheme in rapidly generating a library of related compounds. As both triazole and thiadiazole rings are often found in drug molecules of many drug classes both series of prepared compounds are predicted to have high biological activity and therefore have merit in their continued exploration. Future studies will seek to study the bioactivities of the free ligands as well as of transition metal complexes which incorporate them.

Additionally, in a cross over between the major projects of our lab a novel bridging ligand has been conceptualized from the two major reaction schemes in this thesis (schemes found in chapters 4 and 5). The proposed ligand and complex shown below incorporate both a bidentate PCA moiety and a pendent pyridine allowing for complexation with multiple metal centers. It is hypothesized that the electron withdrawing nature of the centralized electron deficient thiadiazol ring present may facilitate electron transfer processes from the Ru(II) photosensitizing unit to the coboloxime moiety which is an important event in artificial photosynthetic process of H_2 generation.

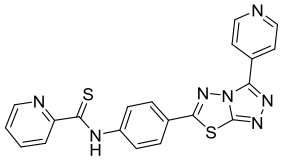

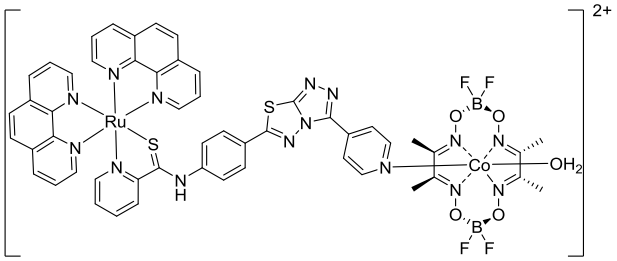

In summary, designing, synthesizing and fully discerning the mechanism of action of even a single compound is an extremely complex, arduous, and time consuming endeavor. Cisplatin, arguably the most famous transition metal anticancer drug, was first described in 1845, but it wasn't until 1965 that by happenstance the cell growth inhibitory properties were discovered. Even

now, almost 40 years after its FDA approval questions are still swirling around its utilization as a chemotherapeutic agent given the rise of cisplatin-resistant cancers. Given the challenges faced with this famous and widely prescribed drug, it seems the real question remaining is: will we ever fully understand exactly what pathways in the interconnected signaling web are the most important to effect to obtain only our desired result? Looking forward from an evolutionary perspective, what can we as scientists learn from the evolution of cisplatin resistance and how can we apply that knowledge to non-platinum based chemotherapeutics? With near infinite design possibilities of transition metal complexes and rapidly advancing scientific methods we may never fully understand the complete mechanisms of many of the drugs but that should not stop one from investigating in detail. As targeted therapies involving small interfering technology move towards clinical application, infinite opportunities to target specific genes may offer some complementary way forward on a patient-by patient basis for these drugs. Considering the emergence of these new targeted treatment options, it would appear that the days of serendipitous discoveries are behind us, but like all hypothesis-driven science, in some cases requires a bit of serendipity, is always much appreciated.

REFERENCES

1. P. B. Tchounwou, C. G. Yedjou, A. K. Patlolla and D. J. Sutton, in *Molecular, Clinical, and Environmental Toxicology*, Springer, 2012, vol. 101, pp. 133-164.
2. J. J. R. F. d. Silva and R. J. P. Williams, *The Biological Chemistry of the Elements: The Inorganic Chemistry of Life*, Oxford University Press, Oxford, 2nd edn., 2001.
3. W. Kaim, B. Schwederski and A. Klein, *Bioinorganic Chemistry -- Inorganic Elements in the Chemistry of Life: An Introduction and Guide, 2nd Edition*, John Wiley & Sons Ltd, 2013.
4. N. J. Farrer and P. J. Sadler, in *Bioinorganic Medicinal Chemistry*, Wiley-VCH Verlag GmbH & Co. KGaA, 2011, pp. 1-47.
5. L. N. Magner, *A History of Medicine*, 2005.
6. C. Orvig and M. J. Abrams, *Chem. Rev.*, 1999, **99**, 2201-2204.
7. K. H. Thompson, C. Orvig, H. B. Kraatz and N. Metzler-Nolte, *Concepts and Models in Bioinorganic Chemistry*, 2006.
8. G. Borkow and J. Gabbay, *Curr. Chem. Biol.*, 2009, **3**, 272-278.
9. L. Thunus and R. Lejeune, *Coord. Chem. Rev.*, 1999, **184**, 125-155.
10. P. Ehrlich and A. Bertheim, *Berichte der deutschen chemischen Gesellschaft*, 1912, **45**, 756-766.
11. N. C. Lloyd, H. W. Morgan, B. K. Nicholson and R. S. Ronimus, *Angew. Chem. Int. Ed.*, 2005, **44**, 941-944.
12. D. Hanahan and R. A. Weinberg, *Cell*, 2000, **100**.
13. D. Hanahan and Robert A. Weinberg, *Cell*, 2011, **144**, 646-674.
14. P. Mehlen and A. Puisieux, *Nat Rev Cancer*, 2006, **6**, 449-458.
15. B. Weigelt, J. L. Peterse and L. J. van't Veer, *Nat Rev Cancer*, 2005, **5**, 591-602.
16. M. R. Ray and D. M. Jablons, in *Lung cancer metastasis*, Springer, 2009, pp. 29-46.
17. M. A. Swartz, N. Iida, E. W. Roberts, S. Sangaletti, M. H. Wong, F. E. Yull, L. M. Coussens and Y. A. DeClerck, *Cancer Res.*, 2012, **72**, 2473-2480.
18. S. C. P. Williams, *Proc. Natl. Acad. Sci. U. S. A.*, 2015, **112**, 4509-4511.
19. E. Koutsogiannouli, A. G. Papavassiliou and N. A. Papanikolaou, *Cancer Med.*, 2013, **2**, 164-177.
20. A. Persidis, *Nat. Biotechnol.*, 1999, **17**, 94-95.
21. J. M. Rosen and C. T. Jordan, *Science*, 2009, **324**, 1670-1673.
22. E. Sugihara and H. Saya, *Int. J. Cancer*, 2013, **132**, 1249-1259.
23. J. Ferlay, H.-R. Shin, F. Bray, D. Forman, C. Mathers and D. M. Parkin, *Int. J. Cancer*, 2010, **127**, 2893-2917.
24. A. Jemal, F. Bray, M. M. Center, J. Ferlay, E. Ward and D. Forman, *CA Cancer J. Clin.*, 2011, **61**, 69-90.
25. A. Jemal, M. M. Center, C. DeSantis and E. M. Ward, *Cancer Epidemiol. Biomarkers & Prev.*, 2010, **19**, 1893-1907.
26. R. Lozano, M. Naghavi, K. Foreman, S. Lim, K. Shibuya, V. Aboyans, J. Abraham, T. Adair, R. Aggarwal, S. Y. Ahn, M. A. AlMazroa, M. Alvarado, H. R. Anderson, L. M. Anderson, K. G. Andrews, C. Atkinson, L. M. Baddour, S. Barker-Collo, D. H. Bartels, M. L. Bell, E. J. Benjamin, D. Bennett, K. Bhalla, B. Bikbov, A. B. Abdulhak, G. Birbeck, F. Blyth, I. Bolliger, S. Boufous, C. Bucello, M. Burch, P. Burney, J. Carapetis,

H. Chen, D. Chou, S. S. Chugh, L. E. Coffeng, S. D. Colan, S. Colquhoun, K. E. Colson, J. Condon, M. D. Connor, L. T. Cooper, M. Corriere, M. Cortinovis, K. C. de Vaccaro, W. Couser, B. C. Cowie, M. H. Criqui, M. Cross, K. C. Dabhadkar, N. Dahodwala, D. De Leo, L. Degenhardt, A. Delossantos, J. Denenberg, D. C. Des Jarlais, S. D. Dharmaratne, E. R. Dorsey, T. Driscoll, H. Duber, B. Ebel, P. J. Erwin, P. Espindola, M. Ezzati, V. Feigin, A. D. Flaxman, M. H. Forouzanfar, F. G. R. Fowkes, R. Franklin, M. Fransen, M. K. Freeman, S. E. Gabriel, E. Gakidou, F. Gaspari, R. F. Gillum, D. Gonzalez-Medina, Y. A. Halasa, D. Haring, J. E. Harrison, R. Havmoeller, R. J. Hay, B. Hoen, P. J. Hotez, D. Hoy, K. H. Jacobsen, S. L. James, R. Jasrasaria, S. Jayaraman, N. Johns, G. Karthikeyan, N. Kassebaum, A. Keren, J.-P. Khoo, L. M. Knowlton, O. Kobusingye, A. Koranteng, R. Krishnamurthi, M. Lipnick, S. E. Lipshultz, S. L. Ohno, J. Mabweijano, M. F. MacIntyre, L. Mallinger, L. March, G. B. Marks, R. Marks, A. Matsumori, R. Matzopoulos, B. M. Mayosi, J. H. McAnulty, M. M. McDermott, J. McGrath, Z. A. Memish, G. A. Mensah, T. R. Merriman, C. Michaud, M. Miller, T. R. Miller, C. Mock, A. O. Mocumbi, A. A. Mokdad, A. Moran, K. Mulholland, M. N. Nair, L. Naldi, K. M. V. Narayan, K. Nasseri, P. Norman, M. O'Donnell, S. B. Omer, K. Ortblad, R. Osborne, D. Ozgediz, B. Pahari, J. D. Pandian, A. P. Rivero, R. P. Padilla, F. Perez-Ruiz, N. Perico, D. Phillips, K. Pierce, C. A. Pope, E. Porrini, F. Pourmalek, M. Raju, D. Ranganathan, J. T. Rehm, D. B. Rein, G. Remuzzi, F. P. Rivara, T. Roberts, F. R. De León, L. C. Rosenfeld, L. Rushton, R. L. Sacco, J. A. Salomon, U. Sampson, E. Sanman, D. C. Schwebel, M. Segui-Gomez, D. S. Shepard, D. Singh, J. Singleton, K. Sliwa, E. Smith, A. Steer, J. A. Taylor, B. Thomas, I. M. Tleyjeh, J. A. Towbin, T. Truelsen, E. A. Undurraga, N. Venketasubramanian, L. Vijayakumar, T. Vos, G. R. Wagner, M. Wang, W. Wang, K. Watt, M. A. Weinstock, R. Weintraub, J. D. Wilkinson, A. D. Woolf, S. Wulf, P.-H. Yeh, P. Yip, A. Zabetian, Z.-J. Zheng, A. D. Lopez and C. J. L. Murray, *The Lancet*, 2012, **380**, 2095-2128.

27. R. Horton, *The Lancet*, 2012, **380**, 2053-2054.
28. C. Mathers, D. M. Fat and J. Boerma, *The global burden of disease: 2004 update*, World Health Organization, 2008.
29. C. J. L. Murray and A. D. Lopez, *N. Engl. J. Med.*, 2013, **369**, 448-457.
30. J.-F. Bosset, M. Gignoux, J.-P. Triboulet, E. Tiret, G. Mantion, D. Elias, P. Lozach, J.-C. Ollier, J.-J. Pavy, M. Mercier, T. Sahmoud, P. Ségol, J.-B. Flamant, J.-P. Arnaud, J.-P. Plachot, A.-M. Mandard and G. Chaillard, *New Engl. J. Med.*, 1997, **337**, 161-167.
31. A. Recht, S. E. Come, I. C. Henderson, R. S. Gelman, B. Silver, D. F. Hayes, L. N. Shulman and J. R. Harris, *New Engl. J. Med.*, 1996, **334**, 1356-1361.
32. W. A. Denny, *Eur. J. Med. Chem.*, 2001, **36**, 577-595.
33. C. Holohan, S. Van Schaeybroeck, D. B. Longley and P. G. Johnston, *Nat Rev Cancer*, 2013, **13**, 714-726.
34. B. Lippert, *Cisplatin - Chemistry and Biochemistry of a Leading Anticancer Drug*, 1999.
35. T. Nakamura and T. Miki, *Int. J. Urol.*, 2010, **17**, 148-157.
36. D. Wang and S. J. Lippard, *Nat. Rev. Drug. Discov.*, 2005, **4**, 307-320.
37. S. M. Cohen and S. J. Lippard, *Prog. Nucleic Acid. Res. Mol. Biol.*, 2001, **67**, 93-130.
38. Z. H. Siddik, *Oncogene*, 2003, **22**, 7265-7279.
39. J. Reedijk, *Chem. Rev.*, 1999, **99**, 2499-2510.

40. Z. Q. Wang, F. Porreca, S. Cuzzocrea, K. Galen, R. Lightfood, E. Masini, C. Muscoli, V. Mollace, M. Ndengele, H. Ischiropoulos and D. Salvemini, *J. Pharmacol. Exp. Ther.*, 2004, **309**, 869-878.
41. N. Pabla and Z. Dong, *Kidney Int.*, 2008, **73**, 994-1007.
42. M. J. Sullivan, *Cancer*, 2009, **115**, 5623-5626.
43. K. Kasahara, Y. Fujiwara, K. Nishio, T. Ohmori, Y. Sugimoto, K. Komiya, T. Matsuda and N. Saijo, *Cancer Res.*, 1991, **51**, 3237-3242.
44. M. J. Siegsmund, C. Marx, O. Seemann, B. Schummer, A. Steidler, L. Toktomambetova, K. U. Kohrmann, J. Rassweiler and P. Alken, *Urol. Res.*, 1999, **27**, 157-163.
45. E. Meggers, *Chem. Commun.*, 2009, 1001.
46. T. Storr, K. H. Thompson and C. Orvig, *Chem. Soc. Rev.*, 2006, **35**, 534.
47. K. H. Antman, *Oncologist*, 2001, **6**, 1-2s.
48. Y. L. Kwong and D. Todd, *Blood*, 1997, **89**, 3487-3497.
49. W. Collier and F. Krauss, *Z. Krebsforsch.*, 1931, **34**, 526-530.
50. B. Rosenberg, L. Vancamp, J. E. Trosko and V. H. Mansour, *Nature*, 1969, **222**, 385-386.
51. B. Rosenberg, L. Van Camp and T. Krigas, *Nature*, 1965, **205**, 698-699.
52. P. C. A. Bruijnincx and P. J. Sadler, *Curr. Opin. Chem. Biol.*, 2008, **12**, 197-206.
53. T. W. Hambley, *Dalton Trans.*, 2007, 4929-4937.
54. Simon P. Wisnovsky, Justin J. Wilson, Robert J. Radford, Mark P. Pereira, Maria R. Chan, Rebecca R. Laposa, Stephen J. Lippard and Shana O. Kelley, *Chemistry & Biology*, 2013, **20**, 1323-1328.
55. L. J. Gershell and J. H. Atkins, *Nat Rev Drug Discov*, 2003, **2**, 321-327.
56. B. K. Keppler, M. R. Berger, T. H. Klenner and M. E. Heim, in *Adv. Drug Res.*, ed. T. Bernard, Academic Press, 1990, vol. Volume 19, pp. 243-310.
57. V. N. Pitchkov, *Platinum Metals Rev.*, 1996, **40**, 181.
58. E. Antonarakis and A. Emadi, *Cancer Chemother Pharmacol*, 2010, **66**, 1-9.
59. C. S. Allardyce and P. J. Dyson, *Platinum Metals Rev.*, 2001, **45**, 62-69.
60. M. R. Gill, H. Derrat, C. G. W. Smythe, G. Battaglia and J. A. Thomas, *ChemBioChem*, 2011, **12**, 877-880.
61. C. Tan, S. Wu, S. Lai, M. Wang, Y. Chen, L. Zhou, Y. Zhu, W. Lian, W. Peng, L. Ji and A. Xu, *Dalton Trans.*, 2011, **40**, 8611-8621.
62. C. Tan, S. Lai, S. Wu, S. Hu, L. Zhou, Y. Chen, M. Wang, Y. Zhu, W. Lian, W. Peng, L. Ji and A. Xu, *J. Med. Chem.*, 2010, **53**, 7613-7624.
63. J.-F. Kou, C. Qian, J.-Q. Wang, X. Chen, L.-L. Wang, H. Chao and L.-N. Ji, *J Biol Inorg Chem*, 2012, **17**, 81-96.
64. E.-S. A. K. Yacoub, A.-G. El-Kourashy and M. A. Al-Hajjaji, *Arabian J. Chem.*, 2013, **6**, 111-114.
65. M. J. Clarke, B. Jansen, K. A. Marx and R. Kruger, *Inorg. Chim. Acta*, 1986, **124**, 13-28.
66. M. J. Clarke, B. Jansen, K. A. Marx and R. Kruger, *Inorg. Chim. Acta*, 1986, **124**, 13-28.
67. V. M. Rodriguez-Bailey, K. J. LaChance-Galang, P. E. Doan and M. J. Clarke, *Inorg. Chem.*, 1997, **36**, 1873-1883.
68. M. J. Clarke, M. Buchbinder and A. D. Kelman, *Inorg. Chim. Acta*, 1978, **27**, L87-L88.
69. D. R. Frasca, J. Ciampa, J. Emerson, R. S. Umans and M. J. Clarke, *Met.-Based Drugs*, 1996, **3**, 197-209.
70. M. J. Clarke, F. Zhu and D. R. Frasca, *Chem. Rev.*, 1999, **99**, 2511-2534.

71. E. d. Silveira-Lacerda, C. Vilanova-Costa, F. d. Pereira, A. Hamaguchi, L. Pavanin, L. Goulart, M. Homsi-Brandenburgo, A. Soares, W. Santos and A. Nomizo, *Biol. Trace Elem. Res.*, 2010, **133**, 270-283.
72. M. J. Clarke, S. Bitler, D. Rennert, M. Buchbinder and A. D. Kelman, *J. Inorg. Biochem.*, 1980, **12**, 79-87.
73. E. Alessio, G. Mestroni, G. Nardin, W. M. Attia, M. Calligaris, G. Sava and S. Zorzet, *Inorg. Chem.*, 1988, **27**, 4099-4106.
74. M. Coluccia, G. Sava, F. Loseto, A. Nassi, A. Boccarelli, D. Giordano, E. Alessio and G. Mestroni, *Eur. J. Cancer*, 1993, **29A**, 1873-1879.
75. G. Sava, G. Salerno, A. Bergamo, M. Cocchietto, R. Gagliardi, E. Alessio and G. Mestroni, *Met.-Based Drugs*, 1996, **3**, 67-73.
76. E. Gallori, C. Vettori, E. Alessio, F. G. Vilchez, R. Vilaplana, P. Orioli, A. Casini and L. Messori, *Arch. Biochem. Biophys.*, 2000, **376**, 156-162.
77. A. Barca, B. Pani, M. Tamaro and E. Russo, *Mutat. Res.*, 1999, **423**, 171-181.
78. M. R. Berger, F. T. Garzon, B. K. Keppler and D. Schmal, *Anticancer Res.*, 1989, **9**, 761-765.
79. F. Kratz, M. Hartmann, B. Keppler and L. Messori, *J. Biol. Chem.*, 1994, **269**, 2581-2588.
80. M. Pongratz, P. Schluga, M. A. Jakupec, V. B. Arion, C. G. Hartinger, G. Allmaier and B. K. Keppler, *J. Anal. At. Spectrom.*, 2004, **19**, 46-51.
81. F. P. Dwyer, E. C. Gyarfas, W. P. Rogers and J. D. Koch, *Nature*, 1952, **170**, 190-191.
82. F. P. Dwyer, E. C. Gyarfas and M. F. O'Dwyer, *Nature*, 1950, **167**, 1036.
83. F. P. Dwyer and E. C. Gyarfas, *J. Proc. Roy. Soc. N.S.W*, 1949, **83**, 170.
84. O. Novakova, J. Kasparkova, O. Vrana, P. M. van Vliet, J. Reedijk and V. Brabec, *Biochemistry (Mosc).* 1995, **34**, 12369-12378.
85. A. H. Velders, H. Kooijman, A. L. Spek, J. G. Haasnoot, D. de Vos and J. Reedijk, *Inorg. Chem.*, 2000, **39**, 2966-2967.
86. A. C. G. Hotze, A. H. Velders, F. Ugozzoli, M. Biagini-Cingi, A. M. Manotti-Lanfredi, J. G. Haasnoot and J. Reedijk, *Inorg. Chem.*, 2000, **39**, 3838-3844.
87. P. M. van Vliet, S. M. S. Toekimin, J. G. Haasnoot, J. Reedijk, O. Nováková, O. Vrána and V. Brabec, *Inorg. Chim. Acta*, 1995, **231**, 57-64.
88. J. A. van Rijn, P. Marques-Gallego, J. Reedijk, M. Lutz, A. L. Spek and E. Bouwman, *Dalton Trans.*, 2009, 10727-10730.
89. C. Tan, S. Wu, S. Lai, M. Wang, Y. Chen, L. Zhou, Y. Zhu, W. Lian, W. Peng, L. Ji and A. Xu, *Dalton Trans.*, 2011, **40**, 8611-8621.
90. I. Lakomska, M. Fandzloch, T. Muziol, T. Lis and J. Jezierska, *Dalton Trans.*, 2013, **42**, 6219-6226.
91. Y. K. Yan, M. Melchart, A. Habtemariam and P. J. Sadler, *Chem. Commun.*, 2005, 4764-4776.
92. A. Habtemariam, M. Melchart, R. Fernández, S. Parsons, I. D. H. Oswald, A. Parkin, F. P. A. Fabbiani, J. E. Davidson, A. Dawson, R. E. Aird, D. I. Jodrell and P. J. Sadler, *J. Med. Chem.*, 2006, **49**, 6858-6868.
93. C. M. Clavel, E. Păunescu, P. Nowak-Sliwinska, A. W. Griffioen, R. Scopelliti and P. J. Dyson, *J. Med. Chem.*, 2014, **57**, 3546-3558.
94. C.-H. Wu, D.-H. Wu, X. Liu, G. Guoyiqibayi, D.-D. Guo, G. Lv, X.-M. Wang, H. Yan, H. Jiang and Z.-H. Lu, *Inorg. Chem.*, 2009, **48**, 2352-2354.

95. R. Pettinari, C. Pettinari, F. Marchetti, B. W. Skelton, A. H. White, L. Bonfili, M. Cuccioloni, M. Mozzicafreddo, V. Cecarini, M. Angeletti, M. Nabissi and A. M. Eleuteri, *J. Med. Chem.*, 2014.
96. C. S. Allardyce, P. J. Dyson, D. J. Ellis and S. L. Heath, *Chem. Commun.*, 2001, 1396-1397.
97. F. Schmitt, P. Govindaswamy, G. Suess-Fink, W. H. Ang, P. J. Dyson, L. Juillerat-Jeanneret and B. Therrien, *J. Med. Chem.*, 2008, **51**, 1811-1816.
98. C. Scolaro, A. Bergamo, L. Brescacin, R. Delfino, M. Cocchietto, G. Laurenczy, T. J. Geldbach, G. Sava and P. J. Dyson, *J. Med. Chem.*, 2005, **48**, 4161-4171.
99. A. Castonguay, C. Doucet, M. Juhas and D. Maysinger, *J. Med. Chem.*, 2012, **55**, 8799-8806.
100. R. E. Morris, R. E. Aird, P. del Socorro Murdoch, H. Chen, J. Cummings, N. D. Hughes, S. Parsons, A. Parkin, G. Boyd, D. I. Jodrell and P. J. Sadler, *J. Med. Chem.*, 2001, **44**, 3616-3621.
101. R. E. Aird, J. Cummings, A. A. Ritchie, M. Muir, R. E. Morris, H. Chen, P. J. Sadler and D. I. Jodrell, *Br. J. Cancer*, 2002, **86**, 1652.
102. F. A. Beckford, G. Leblanc, J. Thessing, M. Shaloski Jr, B. J. Frost, L. Li and N. P. Seeram, *Inorg. Chem. Commun.*, 2009, **12**, 1094-1098.
103. F. Beckford, D. Dourth, M. Shaloski Jr, J. Didion, J. Thessing, J. Woods, V. Crowell, N. Gerasimchuk, A. Gonzalez-Sarrías and N. P. Seeram, *J. Inorg. Biochem.*, 2011, **105**, 1019-1029.
104. M. Auzias, B. Therrien, G. Süss-Fink, P. Štěpnička, W. H. Ang and P. J. Dyson, *Inorg. Chem.*, 2007, **47**, 578-583.
105. F. d. r. Pelletier, V. Comte, A. Massard, M. Wenzel, S. p. Toulot, P. Richard, M. Picquet, P. Le Gendre, O. Zava, F. Edafe, A. Casini and P. J. Dyson, *J. Med. Chem.*, 2010, **53**, 6923-6933.
106. M. G. Mendoza-Ferri, C. G. Hartinger, A. A. Nazarov, W. Kandioller, K. Severin and B. K. Keppler, *Appl. Organomet. Chem.*, 2008, **22**, 326-332.
107. M.-G. Mendoza-Ferri, C. G. Hartinger, R. E. Eichinger, N. Stolyarova, K. Severin, M. A. Jakupec, A. A. Nazarov and B. K. Keppler, *Organometallics*, 2008, **27**, 2405-2407.
108. M. Gras, B. Therrien, G. Suss-Fink, O. Zava and P. J. Dyson, *Dalton Trans.*, 2010, **39**, 10305-10313.
109. T. Stringer, B. Therrien, D. T. Hendricks, H. Guzgay and G. S. Smith, *Inorg. Chem. Commun.*, 2011, **14**, 956-960.
110. W. H. Ang, Z. Grote, R. Scopelliti, L. Juillerat-Jeanneret, K. Severin and P. J. Dyson, *J. Organomet. Chem.*, 2009, **694**, 968-972.
111. J. Mattsson, P. Govindaswamy, A. K. Renfrew, P. J. Dyson, P. Štěpnička, G. Süss-Fink and B. Therrien, *Organometallics*, 2009, **28**, 4350-4357.
112. N. P. E. Barry, N. H. Abd Karim, R. Vilar and B. Therrien, *Dalton Trans.*, 2009, 10717-10719.
113. M. J. Clarke, *Coord. Chem. Rev.*, 2002, **232**, 69-93.
114. M. J. Clarke, *Coord. Chem. Rev.*, 2003, **236**, 209-233.
115. S. C. Srivastava, P. Richards, P. Som, G. Meinken, H. L. Atkins, A. Sewatkar and T. H. Ku, in *Frontiers in Nuclear Medicine*, eds. W. Horst, H. Wagner, Jr. and J. Buchanan, Springer Berlin Heidelberg, 1980, ch. 11, pp. 123-133.
116. B. Armitage, *Chem. Rev.*, 1998, **98**, 1171-1200.

117. C. V. Kumar, J. K. Barton and N. J. Turro, *J. Am. Chem. Soc.*, 1985, **107**, 5518-5523.
118. C. Tanielian, C. Wolff and M. Esch, *J. Phys. Chem.*, 1996, **100**, 6555-6560.
119. V. Pierroz, T. Joshi, A. Leonidova, C. Mari, J. Schur, I. Ott, L. Spiccia, S. Ferrari and G. Gasser, *J. Am. Chem. Soc.*, 2012, **134**, 20376-20387.
120. T. Joshi, V. Pierroz, C. Mari, L. Gemperle, S. Ferrari and G. Gasser, *Angew. Chem.*, 2014, **126**, 3004-3007.
121. P. Lincoln and B. Norden, *Chem. Commun.*, 1996, 2145-2146.
122. X.-H. Zou, B.-H. Ye, H. Li, J.-G. Liu, Y. Xiong and L.-N. Ji, *J. Chem. Soc., Dalton Trans.*, 1999, 1423-1428.
123. F. M. O'Reill and J. M. Kelly, *J. Phys. Chem. B*, 2000, **104**, 7206-7213.
124. B. Önfelt, P. Lincoln and B. Nordén, *J. Am. Chem. Soc.*, 2001, **123**, 3630-3637.
125. K. Sakai, H. Ozawa, H. Yamada, T. Tsubomura, M. Hara, A. Higuchi and M.-a. Haga, *Dalton Trans.*, 2006, 3300-3305.
126. X. Liang, X. Zou, L. Tan and W. Zhu, *J. Inorg. Biochem.*, 2010, **104**, 1259-1266.
127. A. A. Holder, P. Taylor, A. R. Magnusen, E. T. Moffett, K. Meyer, Y. Hong, S. E. Ramsdale, M. Gordon, J. Stubbs, L. A. Seymour, D. Acharya, R. T. Weber, P. F. Smith, G. C. Dismukes, P. Ji, L. Menocal, F. Bai, J. L. Williams, D. M. Cropek and W. L. Jarrett, *Dalton Trans.*, 2013, **42**, 11881-11899.
128. R. Miao, M. T. Mongelli, D. F. Zigler, B. S. J. Winkel and K. J. Brewer, *Inorg. Chem.*, 2006, **45**, 10413-10415.
129. W. M. Sharman, C. M. Allen and J. E. van Lier, *Drug Discov. Today*, 1999, **4**, 507-517.
130. M. Capella and L. Capella, *J. Biomed. Sci.*, 2003, **10**, 361-366.
131. J. Onuki, A. V. Ribas, M. H. G. Medeiros, K. Araki, H. E. Toma, L. H. Catalani and P. Di Mascio, *Photochem. Photobiol.*, 1996, **63**, 272-277.
132. T. Gianferrara, I. Bratsos, E. Iengo, B. Milani, A. Ostric, C. Spagnul, E. Zangrando and E. Alessio, *Dalton Trans.*, 2009, 10742-10756.
133. T. Gianferrara, A. Bergamo, I. Bratsos, B. Milani, C. Spagnul, G. Sava and E. Alessio, *J. Med. Chem.*, 2010, **53**, 4678-4690.
134. S. Rani-Beeram, K. Meyer, A. McCrate, Y. Hong, M. Nielsen and S. Swavey, *Inorg. Chem.*, 2008, **47**, 11278-11283.
135. M. Narra, P. Elliott and S. Swavey, *Inorg. Chim. Acta*, 2006, **359**, 2256-2262.
136. Z. Xu and S. Swavey, *Dalton Trans.*, 2011, **40**, 7319-7326.
137. F. Schmitt, P. Govindaswamy, G. Süss-Fink, W. H. Ang, P. J. Dyson, L. Juillerat-Jeanneret and B. Therrien, *J. Med. Chem.*, 2008, **51**, 1811-1816.
138. K. Yamada, in *Interrelations between Essential Metal Ions and Human Diseases*, eds. A. Sigel, H. Sigel and K. O. R. Sigel, Springer Netherlands, Dordrecht, 2013, pp. 295-320.
139. L. Randaccio, S. Geremia, G. Nardin and J. Wuerges, *Coord. Chem. Rev.*, 2006, **250**, 1332-1350.
140. S. Mounicou, J. Szpunar and R. Lobinski, *Chem. Soc. Rev.*, 2009, **38**, 1119-1138.
141. J. A. Schwartz, E. K. Lium and S. J. Silverstein, *J. Virol.*, 2001, **75**, 4117-4128.
142. H. Greenfield, H. W. Sternberg, R. A. Friedel, J. H. Wotiz, R. Markby and I. Wender, *J. Am. Chem. Soc.*, 1956, **78**, 120-124.
143. D. C. Ware, W. R. Wilson, W. A. Denny and C. E. F. Rickard, *J. Chem. Soc., Chem. Commun.*, 1991, 1171-1173.
144. D. C. Ware, H. R. Palmer, P. J. Brothers, C. E. F. Rickard, W. R. Wilson and W. A. Denny, *J. Inorg. Biochem.*, 1997, **68**, 215-224.

145. P. A. Ajibade and G. A. Kolawole, *Synth. React. Inorg. M.*, 2010, **40**, 273-278.
146. S. Adewuyi, K. T. Kareem, A. O. Atayese, S. A. Amolegbe and C. A. Akinremi, *Int. J. Biol. Macromol.*, 2011, **48**, 301-303.
147. F. P. Dwyer, E. C. Gyarfas, W. P. Roger and J. H. Koch, *Nature*, 1952, **170**, 190.
148. M. Patel, M. Chhasatia and B. Bhatt, *Med. Chem. Res.*, 2011, **20**, 220-230.
149. A. M. Mitchell, A. Bayomi, E. Natarajan, L. R. Barrows, F. G. West and C. B. Grissom, *Enzym. Mech.* , 1999, **27**, 150-154.
150. P. Ruiz-Sánchez, C. König, S. Ferrari and R. Alberto, *J Biol Inorg Chem*, 2010, **16**, 33-44.
151. S. Mundwiler, B. Spingler, P. Kurz, S. Kunze and R. Alberto, *Chemistry – A European Journal*, 2005, **11**, 4089-4095.
152. J. A. Bauer, B. H. Morrison, R. W. Grane, B. S. Jacobs, S. Dabney, A. M. Gamero, K. A. Carnevale, D. J. Smith, J. Drazba, B. Seetharam and D. J. Lindner, *J. Natl. Cancer Inst.*, 2002, **94**, 1010-1019.
153. J. A. Bauer, G. Frye, A. Bahr, J. Gieg and P. Brofman, *Invest. New Drugs*, 2009, **28**, 694-702.
154. K. Schmidt, M. Jung, R. Keilitz, B. Schnurr and R. Gust, *Inorg. Chim. Acta*, 2000, **306**, 6-16.
155. A. Vessières, S. Top, C. Vaillant, D. Osella, J.-P. Mornon and G. Jaouen, *Angewandte Chemie International Edition in English*, 1992, **31**, 753-755.
156. M. Jung, D. E. Kerr and P. D. Senter, *Arch. Pharm.*, 1997, **330**, 173-176.
157. I. Ott, B. Kircher and R. Gust, *J. Inorg. Biochem.*, 2004, **98**, 485-489.
158. I. Ott, K. Schmidt, B. Kircher, P. Schumacher, T. Wiglenda and R. Gust, *J. Med. Chem.*, 2005, **48**, 622-629.
159. I. Ott, T. Koch, H. Shorafa, Z. Bai, D. Poeckel, D. Steinhilber and R. Gust, *Organic & Biomolecular Chemistry*, 2005, **3**, 2282-2286.
160. C. D. Sergeant, I. Ott, A. Sniady, S. Meneni, R. Gust, A. L. Rheingold and R. Dembinski, *Organic & Biomolecular Chemistry*, 2008, **6**, 73-80.
161. M. A. Neukamm, A. Pinto and N. Metzler-Nolte, *Chem. Commun.*, 2008, 232-234.
162. F. Dimiza, A. N. Papadopoulos, V. Tangoulis, V. Psycharis, C. P. Raptopoulou, D. P. Kessissoglou and G. Psomas, *J. Inorg. Biochem.*, 2012, **107**, 54-64.
163. S. Tsiliou, L.-A. Kefala, F. Perdih, I. Turel, D. P. Kessissoglou and G. Psomas, *Eur. J. Med. Chem.*, 2012, **48**, 132-142.
164. M. D. Hall, T. W. Failes, N. Yamamoto and T. W. Hambley, *Dalton Trans.*, 2007, 3983-3990.
165. T. W. Failes, C. Cullinane, C. I. Diakos, N. Yamamoto, J. G. Lyons and T. W. Hambley, *Chem. Eur. J.*, 2007, **13**, 2974-2982.
166. J. Y.-C. Chang, R. J. Stevenson, G.-L. Lu, P. J. Brothers, G. R. Clark, W. A. Denny and D. C. Ware, *Dalton Trans.*, 2010, **39**, 11535-11550.
167. D. C. Ware, B. D. Palmer, W. R. Wilson and W. A. Denny, *J. Med. Chem.*, 1993, **36**, 1839-1846.
168. X. Fan, J. Dong, R. Min, Y. Chen, X. Yi, J. Zhou and S. Zhang, *J. Coord. Chem.*, 2013, **66**, 4268-4279.
169. F. Dimiza, A. N. Papadopoulos, V. Tangoulis, V. Psycharis, C. P. Raptopoulou, D. P. Kessissoglou and G. Psomas, *Dalton Trans.*, 2010, **39**, 4517-4528.

170. V. A. Kawade, A. A. Kumbhar, A. S. Kumbhar, C. Naether, A. Erxleben, U. B. Sonawane and R. R. Joshi, *Dalton Trans.*, 2011, **40**, 639-650.
171. A. Banerjee, A. Guha, J. Adhikary, A. Khan, K. Manna, S. Dey, E. Zangrando and D. Das, *Polyhedron*, 2013, **60**, 102-109.
172. R. Gust, I. Ott, D. Posselt and K. Sommer, *J. Med. Chem.*, 2004, **47**, 5837-5846.
173. H. Sun and Z. F. Chai, *Annu. Rep. Prog. Chem., Sect. A: Inorg. Chem.*, 2010, **106**, 20.
174. N. P. E. Barry and P. J. Sadler, *Chem. Commun.*, 2013, **49**, 5106-5131.
175. N. P. E. Barry and P. J. Sadler, *ACS Nano*, 2013, **7**, 5654-5659.
176. C. Harford and B. Sarkar, *Acc. Chem. Res.*, 1997, **30**, 123-130.
177. R. Sankararamakrishnan, S. Verma and S. Kumar, *Proteins*, 2005, **58**, 211.
178. Y. Valasatava, C. Andreini and A. Rosato, *Sci. Rep.*, 2015, **5**.
179. M. Groessl and P. J. Dyson, *Curr. Top. Med. Chem.*, 2011, **11**, 2632-2646.
180. L. J. Parker, D. B. Ascher, C. Gao, L. A. Miles, H. H. Harris and M. W. Parker, *J. Inorg. Biochem.*, 2012, **115**, 138-147.
181. M. Petković and T. Kamčeva, *Metallomics*, 2011, **3**, 550.
182. B. Meermann and M. Sperling, *Anal. Bioanal. Chem.*, 2012, **403**, 1501-1522.
183. A. K. Bytzek and C. G. Hartinger, *Electrophoresis*, 2012, **33**, 622.
184. C. Rodríguez-Rodríguez, M. Telpoukhovskaia and C. Orvig, *Coord. Chem. Rev.*, 2012, **256**, 2308-2332.
185. R. Huang, A. Wallqvist and D. G. Covell, *Biochem. Pharmacol.*, 2005, **69**, 1009-1039.
186. A. Sigel, H. Sigel and R. K. Sigel, *Metal Ions in Biological Systems & Metal Ions in Life Sciences*.
187. E. Meggers, G. E. Atilla-Gokcumen, K. Grundler, C. Frias and A. Prokop, *Dalton Trans.*, 2009, 10882-10888.
188. A. N. Bullock, S. Russo, A. Amos, N. Pagano, H. Bregman, J. É. Debreczeni, W. H. Lee, F. von Delft, E. Meggers and S. Knapp, *Plos One*, 2009, **4**, e7112.
189. A. Casini, *J. Inorg. Biochem.*, 2012, **109**, 97-106.
190. A. Casini and J. Reedijk, *Chem. Sci.*, 2012, **3**, 3135-3144.
191. W. R. Harris, C. J. Carrano, S. R. Cooper, S. R. Sofen, A. E. Avdeef, J. V. McArdle and K. N. Raymond, *J. Am. Chem. Soc.*, 1979, **101**, 6097-6104.
192. R. F. Campbell and N. D. Chasteen, *J. Biol. Chem.*, 1977, **252**, 5996.
193. O. Zak and P. Aisen, *Biochemistry (Mosc).* 1988, **27**, 1075-1080.
194. V. Sharma and D. Piwnica-Worms, *Chem. Rev.*, 1999, **99**, 2545-2560.
195. P. F. Salas, C. Herrmann and C. Orvig, *Chem. Rev.*, 2013, **113**, 3450-3492.
196. G. Gasser, I. Ott and N. Metzler-Nolte, *J. Med. Chem.*, 2011, **54**, 3-25.
197. F. Cardoso, N. Harbeck, L. Fallowfield, S. Kyriakides and E. Senkus, *Ann. Oncol.*, 2012, **23**, 19.
198. R. Weide, S. Feiten, V. Friesenhahn, J. Heymanns, K. Kleboth, J. Thomalla, C. van Roye and H. Koppler, *SpringerPlus*, 2014, **3**, 535.
199. M. Stockler, N. R. C. Wilcken, D. Ghersi and R. J. Simes, *Cancer Treat. Rev.*, 2000, **26**, 151-168.
200. J. Giuliani and A. Bonetti, *Tumori*, 2015, **101**, 347-352.
201. L. G. Eng, S. Dawood and R. Dent, *Curr, Opin. Palliat. Care*, 2015, **9**, 301-307.
202. S. Lewis, J. Yee, S. Kilbreath and K. Willis, *The Breast*, 2015, **24**, 242-247.
203. P. Wheatley–Price, M. Ali, K. Balchin, J. Spencer, E. Fitzgibbon and C. Cripps, *Curr. Oncol.*, 2014, **21**, 187-192.

204. S. Roychowdhury and A. M. Chinnaiyan, *Annu. Rev. Genom. Hum. Genet.*, 2014, **15**, 395-415.
205. R. B. Silverman and M. W. Holladay, in *The Organic Chemistry of Drug Design and Drug Action (Third Edition)*, eds. R. B. Silverman and M. W. Holladay, Academic Press, Boston, 2014.
206. H. Kaur, S. Mao, S. Shah, D. H. Gorski, S. A. Krawetz, B. F. Sloane and R. R. Mattingly, *Expert Rev. Mol. Diagn.*, 2013, **13**, 151-165.
207. K. K. Payne, A. A. Toor, X.-Y. Wang and M. H. Manjili, *Clin. Dev. Immunol.*, 2012, **2012**, 8.
208. J. Woodcock, J. P. Griffin and R. E. Behrman, *New Engl. J. Med.*, 2011, **364**, 985-987.
209. D.-L. Ma, H.-Z. He, K.-H. Leung, D. S.-H. Chan and C.-H. Leung, *Angew. Chem. Int. Ed.*, 2013, **52**, 7666-7682.
210. A. K. Renfrew, *Metallomics*, 2014, **6**, 1324-1335.
211. J. K. Barton, A. Danishefsky and J. Goldberg, *J. Am. Chem. Soc.*, 1984, **106**, 2172-2176.
212. B. Norden, P. Lincoln, B. Akerman and E. Tuite, *Metal Ions in Biological Systems*, Marcel Decker, New York, 1996.
213. M. T. Carter, M. Rodriguez and A. J. Bard, *J. Am. Chem. Soc.*, 1989, **111**, 8901-8911.
214. J. K. Barton, *Science*, 1986, **233**, 727-734.
215. L.-F. Tan, H. Chao, Y.-J. Liu, H. Li, B. Sun and L.-N. Ji, *Inorg. Chim. Acta*, 2005, **358**, 2191-2198.
216. V. Aranyos, A. Hagfeldt, H. Grennberg and E. Figgemeier, *Polyhedron*, 2004, **23**, 589-598.
217. M. Ganesan, V. K. Sivasubramanian, T. Rajendran, K. Swarnalatha, S. Rajagopal and R. Ramaraj, *Tetrahedron*, 2005, **61**, 4863-4871.
218. E. L. Chang, C. Simmers and D. A. Knight, *Pharmaceuticals*, 2010, **3**, 1711.
219. D. S. Kalinowski, P. Quach and D. R. Richardson, *Future Med. Chem.*, 2009, **1**, 1143-1151.
220. Z. Kovacevic, D. S. Kalinowski, D. B. Lovejoy, Y. Yu, Y. S. Rahmanto, P. C. Sharpe, P. V. Bernhardt and D. R. Richardson, *Curr. Top. Med. Chem.* , 2011, **11**, 483-499.
221. C. P. Meher and S. P. Sethy, *Int. Res. J. Pharm.*, 2012, **3**, 6-11.
222. B. M. Paterson and P. S. Donnelly, *Chem. Soc. Rev.*, 2011, **40**, 3005-3018.
223. Y. Yu, D. S. Kalinowski, Z. Kovacevic, A. R. Siafakas, P. J. Jansson, C. Stefani, D. B. Lovejoy, P. C. Sharpe, P. V. Bernhardt and D. R. Richardson, *J. Med. Chem.*, 2009, **52**, 5271-5294.
224. R. Sreekala and Y. K. K. Mohammed, *Synth. React. Inorg. Met.-Org. Chem.*, 1994, **24**, 1773-1788.
225. M.-X. Li, J. Zhou, Z.-L. Wang and J.-P. Wang, *Chin. J. Struct. Chem.*, 2008, **27**, 281-286.
226. E. Ramachandran, S. P. Thomas, P. Poornima, P. Kalaivani, R. Prabhakaran, V. V. Padma and K. Natarajan, *Eur. J. Med. Chem.*, 2012, **50**, 405-415.
227. R. Manikandan, P. Viswanathamurthi, K. Velmurugan, R. Nandhakumar, T. Hashimoto and A. Endo, *J. Photochem. Photobiol. B*, 2013, **130C**, 205-216.
228. M. Belicchi-Ferrari, F. Bisceglie, C. Casoli, S. Durot, I. Morgenstern-Badarau, G. Pelosi, E. Pilotti, S. Pinelli and P. Tarasconi, *J. Med. Chem.*, 2005, **48**, 1671-1675.
229. D. Zhang, Q. Li, M.-X. Li, D.-Y. Chen and J.-Y. Niu, *J. Coord. Chem.*, 2010, **63**, 1063-1070.

230. S. Jagadeesan, V. Balasubramanian, P. Baumann, M. Neuburger, D. Häussinger and C. G. Palivan, *Inorg. Chem.*, 2013, **52**, 12535-12544.
231. M. N. M. Milunovic, É. A. Enyedy, N. V. Nagy, T. Kiss, R. Trondl, M. A. Jakupec, B. K. Keppler, R. Krachler, G. Novitchi and V. B. Arion, *Inorg. Chem.*, 2012, **51**, 9309-9321.
232. J. Brechbiel, K. Miller-Moslin and A. A. Adjei, *Cancer Treat. Rev.*, 2014, **40**, 750-759.
233. K. Imai and A. Takaoka, *Nat Rev Cancer*, 2006, **6**, 714-727.
234. M. Goldstein and M. B. Kastan, *Annu. Rev. Med.*, 2015, **66**, 129-143.
235. G. Sersa, M. Cemazar and M. Snoj, *Curr. Oncol.*, 2009, **16**, 34-35.
236. M. Cemazar, D. Miklavcic, L. M. Mir, J. Belehradek Jr, M. Bonnay, D. Fourcault and G. Sersa, *Eur. J. Cancer*, 2001, **37**, 1166-1172.
237. R. Cadossi, M. Ronchetti and M. Cadossi, *Future Oncology*, 2014, **10**, 877-890.
238. D. Miklavcic, B. Mali, B. Kos, R. Heller and G. Sersa, *Biomed. Eng. Online*, 2014, **13**, 29.
239. P. Philips, Y. Li, S. Li, C. R. St Hill and R. C. G. Martin, *Molecular Therapy — Methods & Clinical Development*, 2015, **2**, 15001.
240. N. Jourabchi, K. Beroukhim, B. A. Tafti, S. T. Kee and E. W. Lee, *Gastrointes. Interv.*, 2014, **3**, 8-18.
241. D. Miklavčič, G. Serša, E. Brecelj, J. Gehl, D. Soden, G. Bianchi, P. Ruggieri, C. R. Rossi, L. G. Campana and T. Jarm, *Med Biol Eng Comput*, 2012, **50**, 1213-1225.
242. R. Nuccitelli, U. Pliquett, X. Chen, W. Ford, S. R. James, S. J. Beebe, J. F. Kolb and K. H. Schoenbach, *Biochem. Biophys. Res. Commun.*, 2006, **343**, 351-360.
243. S. J. Beebe, *J. Nanomed. Nantotech.*, 2013, **4**, 1-8.
244. K. H. Schoenbach, S. Katsuki, R. H. Stark, E. S. Buescher and S. J. Beebe, *Plasma Science, IEEE Transactions on*, 2002, **30**, 293-300.
245. R. Kötz and M. Carlen, *Electrochim. Acta*, 2000, **45**, 2483-2498.
246. E. H. Hall, K. H. Schoenbach and S. J. Beebe, *Apoptosis*, 2007, **12**, 1721-1731.
247. S. J. Beebe, P. M. Fox, L. J. Rec, E. L. K. Willis and K. H. Schoenbach, *FASEB J.*, 2003, **17**, 1493-1495.
248. S. J. Beebe, P. M. Fox, L. J. Rec, K. Somers, R. H. Stark and K. H. Schoenbach, *IEEE Trans. Plasma Sci.*, 2002, **30**, 286-292.
249. W. Ren and S. J. Beebe, *Apoptosis*, 2011, **16**, 382-393.
250. P. T. Vernier, Y. Sun, L. Marcu, S. Salemi, C. M. Craft and M. A. Gundersen, *Biochem. Biophys. Res. Commun.*, 2003, **310**, 286-295.
251. S. S. Scarlett, J. A. White, P. F. Blackmore, K. H. Schoenbach and J. F. Kolb, *Biochimica et Biophysica Acta (BBA) - Biomembranes*, 2009, **1788**, 1168-1175.
252. P. T. Vernier, M. J. Ziegler, Y. Sun, W. V. Chang, M. A. Gundersen and D. P. Tieleman, *J. Am. Chem. Soc.*, 2006, **128**, 6288-6289.
253. D. A. Stewart, T. R. Gowrishankar and J. C. Weaver, *Plasma Science, IEEE Transactions on*, 2004, **32**, 1696-1708.
254. T. R. Gowrishankar, A. T. Esser, Z. Vasilkoski, K. C. Smith and J. C. Weaver, *Biochem. Biophys. Res. Commun.*, 2006, **341**, 1266-1276.
255. S. J. Beebe, N. M. Sain and W. Ren, *Cells*, 2013, **2**, 136-162.
256. W. Ren, N. M. Sain and S. J. Beebe, *Biochem. Biophys. Res. Commun.*, 2012, **421**, 808-812.
257. X.-H. Chen, S. J. Beebe and S.-S. Zheng, *Hepatobiliary Pancreat. Dis. Int.*, 2012, **11**, 122-124.

258. J. T. Camp, Y. Jing, J. Zhuang, J. F. Kolb, S. J. Beebe, J. Song, R. P. Joshi, S. Xiao and K. H. Schoenbach, *IEEE Trans. Plasma Sci.*, 2012, **40**, 2334-2347.
259. S. J. Beebe, X. Chen, J. A. Liu and K. H. Schoenbach, *Conf Proc IEEE Eng Med Biol Soc*, 2011, **2011**, 6861-6865.
260. K. Zhang, J. Guo, Z. Ge and J. Zhang, *Scientific Reports*, 2014, **4**, 5836.
261. I. Semenov, S. Xiao and A. G. Pakhomov, *Biochim. Biophys. Acta*, 2013, **1828**, 981-989.
262. H. Hirai, M. Miyake, A. Nagano, K. Teranishi, N. Shimomura and S. Oyadomari, 2014.
263. S. J. Beebe, Y.-J. Chen, N. M. Sain, K. H. Schoenbach and S. Xiao, *Plos One*, 2012, **7**, e51349.
264. S. J. Beebe, *Int. J. Nanomedicine*, 2012, **8**, 3401-3404.
265. X. Chen, Z. Ren, C. Li, F. Guo, D. Zhou, J. Jiang, X. Chen, J. Sun, C. Yao and S. Zheng, *Sci Rep*, 2015, **5**, 9851.
266. S. Yin, X. Chen, C. Hu, X. Zhang, Z. Hu, J. Yu, X. Feng, K. Jiang, S. Ye, K. Shen, H. Xie, L. Zhou, R. James Swanson and S. Zheng, *Cancer Lett.*, 2014, **346**, 285-291.
267. X. Miao, S. Yin, Z. Shao, Y. Zhang and X. Chen, *Journal of Orthopaedic Surgery and Research*, 2015, **10**, 1-7.
268. A. C. Sabuncu, J. A. Liu, S. J. Beebe and A. Beskok, *Biomicrofluidics*, 2010, **4**, No pp. given.
269. R. Nuccitelli, X. Chen, A. G. Pakhomov, W. H. Baldwin, S. Sheikh, J. L. Pomicter, W. Ren, C. Osgood, R. J. Swanson, J. F. Kolb, S. J. Beebe and K. H. Schoenbach, *Int. J. Cancer*, 2009, **125**, 438-445.
270. X. Chen, J. F. Kolb, R. J. Swanson, K. H. Schoenbach and S. J. Beebe, *Pigm. Cell. Melanoma Res.*, 2010, **23**, 554-563.
271. R. Nuccitelli, K. Tran, B. Athos, M. Kreis, P. Nuccitelli, K. S. Chang, E. H. Epstein and J. Y. Tang, *Biochem. Biophys. Res. Commun.*, 2012, **424**, 446-450.
272. R. Nuccitelli, K. Tran, S. Sheikh, B. Athos, M. Kreis and P. Nuccitelli, *Int. J. Cancer*, 2010, **127**, 1727-1736.
273. J. F. Arca, BS Honors Thesis, University of Southern Mississippi, 2012.
274. K. Tao, M. Fang, J. Alroy and G. G. Sahagian, *BMC Cancer*, 2008, **8**, 228.
275. L. C. Bailey-Downs, J. E. Thorpe, B. C. Disch, A. Bastian, P. J. Hauser, T. Farasyn, W. L. Berry, R. E. Hurst and M. A. Ihnat, *PLoS ONE*, 2014, **9**, e98624.
276. G. H Heppner, F. R Miller and P. Malathy Shekhar, *Breast Cancer Res*, 2000, **2**, 331 - 334.
277. S. Wu, Y. Wang, J. Guo, Q. Chen, J. Zhang and J. Fang, *Cancer Lett.*, 2014, **343**, 268-274.
278. D. Jingdong, R. H. Stark and K. H. Schoenbach, 2000.
279. J. Mankowski and M. Kristiansen, *Plasma Science, IEEE Transactions on*, 2000, **28**, 102-108.
280. P. Krishnamoorthy, P. Sathyadevi, A. H. Cowley, R. R. Butorac and N. Dharmaraj, *Eur. J. Med. Chem.*, 2011, **46**, 3376-3387.
281. H. J. Schneider, *Angew. Chem. Int. Ed.*, 2009, **48**, 3924-3977.
282. J. D. McGhee and P. H. von Hippel, *J. Mol. Biol.*, 1974, **86**, 469-489.
283. P. V. Scaria and R. H. Shafer, *J. Biol. Chem.*, 1991, **266**, 5417-5423.
284. A. Banerjee, P. Majumder, S. Sanyal, J. Singh, K. Jana, C. Das and D. Dasgupta, *FEBS Open Bio*, 2014, **4**, 251-259.
285. W. C. Tse and D. L. Boger, *Acc. Chem. Res.*, 2004, **37**, 61-69.

286. N. W. Luedtke, J. S. Hwang, E. Nava, D. Gut, M. Kol and Y. Tor, *Nucleic Acids Res.*, 2003, **31**, 5732-5740.
287. L. K. Fraiji, D. M. Hayes and T. Werner, *J. Chem. Educ.*, 1992, **69**, 424.
288. J. R. Lakowicz, *Principles of fluorescence spectroscopy*, Springer Science & Business Media, 2013.
289. J. B. Lepecq and C. Paoletti, *J. Mol. Biol.*, 1967, **27**, 87-106.
290. R. S. Wong, *J. Exp. Clin. Cancer Res.*, 2011, **30**, 1-14.
291. G. I. Shapiro and J. W. Harper, *J. Clin. Invest.*, 1999, **104**, 1645-1653.
292. S. J. Riedl and Y. Shi, *Nat Rev Mol Cell Biol*, 2004, **5**, 897-907.
293. R. Singh, S. Pervin and G. Chaudhuri, *J Biol Chem.* , 2002, **277**, 37630-37636.
294. C. Trejo-Solís, G. Palencia, S. Zuñiga, A. Rodríguez-Ropon, L. Osorio-Rico, S. Torres Luvia, I. Gracia-Mora, L. Marquez-Rosado, A. Sánchez, M. E. Moreno-García, A. Cruz, M. E. Bravo-Gómez, L. Ruiz-Ramírez, S. Rodríquez-Enriquez and J. Sotelo, *Neoplasia*, 2005, **7**, 563-574.
295. L. Galluzzi, N. Larochette, N. Zamzami and G. Kroemer, *Oncogene*, 2010, **25**, 4812-4830.
296. V. Gogvadze, B. Zhivotovsky and S. Orrenius, *Mol. Aspects Med.*, 2010, **31**, 60-74.
297. F. Qi, A. Li, Y. Inagaki, H. Xu, D. Wang, X. Cui, L. Zhang, N. Kokudo, G. Du and W. Tang, *Food Chem. Toxicol.*, 2012, **50**, 295-302.
298. K. H. Kim and M.-S. Lee, *Nat Rev Endocrinol*, 2014, **10**, 322-337.
299. J. D. Rabinowitz and E. White, *Science*, 2010, **330**, 1344-1348.
300. N. Mizushima, *Genes Dev.*, 2007, **21**, 2861-2873.
301. K. Kirkegaard, M. P. Taylor and W. T. Jackson, *Nat Rev Micro*, 2004, **2**, 301-314.
302. Y.-Q. Wang, L. Wang, M.-Y. Zhang, T. Wang, H.-J. Bao, W.-L. Liu, D.-K. Dai, L. Zhang, P. Chang, W.-W. Dong, X.-P. Chen and L.-Y. Tao, *Neurochem. Res.*, 2012, **37**, 1849-1858.
303. P. Chang, W. Dong, M. Zhang, Z. Wang, Y. Wang, T. Wang, Y. Gao, H. Meng, B. Luo, C. Luo, X. Chen and L. Tao, *J. Mol. Neurosci.*, 2014, **52**, 242-249.
304. M. Breton and L. M. Mir, *Bioelectromagnetics*, 2012, **33**, 106-123.
305. R. P. Joshi and K. H. Schoenbach, *Crit. Rev. Biomed. Eng.*, 2010, **38**, 255-304.
306. S. J. Beebe, J. White, P. F. Blackmore, Y. Deng, K. Somers and K. H. Schoenbach, *DNA Cell Biol.*, 2003, **22**, 785-796.
307. M. Stacey, J. Stickley, P. Fox, V. Statler, K. Schoenbach, S. J. Beebe and S. Buescher, *Mutat. Res.-Genet. Toxicol. Environ. Mutag.*, 2003, **542**, 65-75.
308. K. H. Schoenbach, S. J. Beebe and E. S. Buescher, *Bioelectromagnetics*, 2001, **22**, 440-448.
309. G. Long, P. K. Shires, D. Plescia, S. J. Beebe, J. F. Kolb and K. H. Schoenbach, *IEEE Trans. Biomed. Eng.*, 2011, **58**.
310. J. Wang, J. Guo, S. Wu, H. Feng, S. Sun, J. Pan, J. Zhang and S. J. Beebe, *Plos One*, 2012, **7**, e43213.
311. G. Serša, B. Štabuc, M. Čemažar, D. Miklavčič and Z. Rudolf, *Clin. Cancer. Res.*, 2000, **6**, 863-867.
312. M. J. Jaroszeski, R. Gilbert and R. Heller, *Adv. Drug Del. Rev.*, 1997, **26**, 185-197.
313. L. M. Mir, S. Orlowski, J. Belehradek Jr, J. Teissié, M. P. Rols, G. Serša, D. Miklavčič, R. Gilbert and R. Heller, *Bioelectrochem. Bioenerg.*, 1995, **38**, 203-207.

314. F. M. André, M. A. Rassokhin, A. M. Bowman and A. G. Pakhomov, *Bioelectrochemistry*, 2010, **79**, 95-100.
315. E. C. Gianulis and A. G. Pakhomov, *Arch. Biochem. Biophys.*, 2015, **570**, 1-7.
316. N. Chen, A. L. Garner, G. Chen, Y. Jing, Y. Deng, R. J. Swanson, J. F. Kolb, S. J. Beebe, R. P. Joshi and K. H. Schoenbach, *Biochem. Biophys. Res. Commun.*, 2007, **364**, 220-225.
317. B. L. Ibey, D. G. Mixon, J. A. Payne, A. Bowman, K. Sickendick, G. J. Wilmink, W. P. Roach and A. G. Pakhomov, *Bioelectrochemistry*, 2010, **79**, 114-121.
318. A. G. Pakhomov, J. F. Kolb, J. A. White, R. P. Joshi, S. Xiao and K. H. Schoenbach, *Bioelectromagnetics*, 2007, **28**, 655-663.
319. T. F. S. Silva, L. M. D. R. S. Martins, M. F. C. Guedes da Silva, A. R. Fernandes, A. Silva, P. M. Borralho, S. Santos, C. M. P. Rodrigues and A. J. L. Pombeiro, *Dalton Trans.*, 2012, **41**, 12888-12897.
320. M.-X. Li, J. Zhou, Z.-L. Wang and J.-P. Wang, *Chin. J. Struct. Chem.*, 2008, **27**, 281-286.
321. O. Silva Dde, *Anti-cancer agents Med. Chem.*, 2010, **10**, 312-323.
322. F. Gao, H. Chao and L.-N. Ji, *Chem. Biodiversity*, 2008, **5**, 1962-1979.
323. S. Neidle, *Nat. Chem.*, 2012, **4**, 594-595.
324. A. M. Pizarro and P. J. Sadler, *Biochimie*, 2009, **91**, 1198-1211.
325. J. A. Smith, J. G. Collins and F. R. Keene, 2009.
326. P. Lincoln and B. Norden, *Chem. Commun.*, 1996, 2145-2146.
327. X.-H. Zou, B.-H. Ye, H. Li, J.-G. Liu, Y. Xiong and L.-N. Ji, *J. Chem. Soc., Dalton Trans.*, 1999, 1423-1428.
328. F. M. O'Reill and J. M. Kelly, *J. Phys. Chem. B*, 2000, **104**, 7206-7213.
329. B. Önfelt, P. Lincoln and B. Nordén, *J. Am. Chem. Soc.*, 2001, **123**, 3630-3637.
330. A. Brodkorb, A. Kirsch-De Mesmaeker, Todd J. Rutherford and F. R. Keene, *Eur. J. Inorg. Chem.*, 2001, **2001**, 2151-2160.
331. J. A. Smith, J. G. Collins, B. T. Patterson and F. R. Keene, *Dalton Trans.*, 2004, 1277-1283.
332. J. Aldrich-Wright, C. Brodie, E. C. Glazer, N. W. Luedtke, L. Elson-Schwab and Y. Tor, *Chem. Commun.*, 2004, 1018-1019.
333. J. O. Nriagu, ed., *Vanadium in the Environment, Part 2; Health Effects*, Wiley, 1998.
334. K. H. Thompson, Y. Tsukada, Z. Xu, M. Battell, J. H. McNeill and C. Orvig, *Biol. Trace Elem. Res.*, 2002, **86**, 31-44.
335. D. C. Crans, *Comments Inorg. Chem.*, 1994, **16**, 1-33.
336. D. C. Crans, J. J. Smee, E. Gaidamauskas and L. Yang, *Chem. Rev.*, 2004, **104**, 849-902.
337. K. Kimura, *Nihon Rinsho*, 1996, **54**, 79-84.
338. D. C. Crans, A. D. Keramidas, H. Hoover-Litty, O. P. Anderson, M. M. Miller, L. M. Lemoine, S. Pleasic-Williams, M. Vandenberg, A. J. Rossomando and L. J. Sweet, *J. Am. Chem. Soc.*, 1997, **119**, 5447-5448.
339. B. M. Lyonnet and E. Martin, *La Presse Medicale*, 1899, **1**, 191-192.
340. K. H. Thompson and C. Orvig, *J. Inorg. Biochem.*, 2006, **100**, 1925-1935.
341. K. H. Thompson, J. Lichter, C. LeBel, M. C. Scaife, J. H. McNeill and C. Orvig, *J. Inorg. Biochem.*, 2009, **103**, 554-558.
342. D. Rehder, in *Bioinorganic Vanadium Chemistry*, John Wiley & Sons, Ltd, 2008, pp. 87-155.

343. D. Rehder, *Inorg. Chem. Commun.*, 2003, **6**, 604-617.
344. S. Mehtab, G. Gonçalves, S. Roy, A. I. Tomaz, T. Santos-Silva, M. F. A. Santos, M. J. Romão, T. Jakusch, T. Kiss and J. C. Pessoa, *J. Inorg. Biochem.*, 2013, **121**, 187-195.
345. A. Papaioannou, M. Manos, S. Karkabounas, R. Liasko, A. M. Evangelou, I. Correia, V. Kalfakakou, J. C. Pessoa and T. Kabanos, *J. Inorg. Biochem.*, 2004, **98**, 959-968.
346. A. Basu, P. Ghosh, A. Bhattacharjee, A. R. Patra and S. Bhattacharya, *Mutagenesis*, 2015.
347. A. Cortizo and S. Etcheverry, *Mol. Cell. Biochem.*, 1995, **145**, 97-102.
348. D. A. Barrio, M. D. Braziunas, S. B. Etcheverry and A. M. Cortizo, *J. Trace Elem. Med Biol.*, 1997, **11**, 110-115.
349. M. D. Hall, C. T. Dillon, M. Zhang, P. Beale, Z. Cai, B. Lai, A. P. Stampfl and T. W. Hambley, *J Biol Inorg Chem*, 2003, **8**, 726-732.
350. S. K. Pandey, J. L. Chiasson and A. K. Srivastava, *Mol. Cell. Biochem.*, 1995, **153**, 69-78.
351. A. M. Cortizo and S. B. Etcheverry, *Mol. Cell. Biochem.*, 1995, **145**, 97-102.
352. T. Cruz, A. Morgan and W. Min, *Mol. Cell. Biochem.*, 1995, **153**, 161-166.
353. M. Molinuevo, D. Barrio, A. Cortizo and S. Etcheverry, *Cancer Chemother. Pharmacol.*, 2004, **53**, 163-172.
354. Z. Zhang, S. S. Leonard, C. Huang, V. Vallyathan, V. Castranova and X. Shi, *Free Radical Biol. Med.*, 2003, **34**, 1333-1342.
355. Z. Zhang, C. Huang, J. Li, S. S. Leonard, R. Lanciotti, L. Butterworth and X. Shi, *Arch. Biochem. Biophys.*, 2001, **392**, 311-320.
356. Q. Wang, T.-T. Liu, Y. Fu, K. Wang and X.-G. Yang, *J Biol Inorg Chem*, 2010, **15**, 1087-1097.
357. S. Matsugo, K. Kanamori, H. Sugiyama, H. Misu and T. Takamura, *J. Inorg. Biochem.*, 2015, **147**, 93-98.
358. B. Balaji, B. Balakrishnan, S. Perumalla, A. A. Karande and A. R. Chakravarty, *Eur. J. Med. Chem.*, 2015, **92**, 332-341.
359. S. Banerjee, A. Dixit, A. A. Karande and A. R. Chakravarty, *Eur. J. Inorg. Chem.*, 2015, **2015**, 447-457.
360. J. Rivadeneira, A. L. Di Virgilio, D. A. Barrio, C. I. Muglia, L. Bruzzone and S. B. Etcheverry, *Medicinal chemistry (Shariqah (United Arab Emirates))*, 2010, **6**, 9-23.
361. C. Huang, Z. Zhang, M. Ding, J. Li, J. Ye, S. S. Leonard, H.-M. Shen, L. Butterworth, Y. Lu, M. Costa, Y. Rojanasakul, V. Castranova, V. Vallyathan and X. Shi, *J. Biol. Chem.*, 2000, **275**, 32516-32522.
362. M. N. Islam, A. A. Kumbhar, A. S. Kumbhar, M. Zeller, R. J. Butcher, M. B. Dusane and B. N. Joshi, *Inorg. Chem.*, 2010, **49**, 8237-8246.
363. J. H. McNeill, V. G. Yuen, H. R. Hoveyda and C. Orvig, *J. Med. Chem.*, 1992, **35**, 1489-1491.
364. Y. Shechter, A. Shisheva, R. Lazar, J. Libman and A. Shanzer, *Biochemistry (Mosc).* 1992, **31**, 2063-2068.
365. A. Sreedhara, N. Susa, A. Patwardhan and C. P. Rao, *Biochem. Biophys. Res. Commun.*, 1996, **224**, 115-120.
366. D. A. Barrio and S. B. Etcheverry, *Curr. Med. Chem.*, 2010, **17**, 3632-3642.
367. P. K. Sasmal, S. Saha, R. Majumdar, R. R. Dighe and A. R. Chakravarty, *Chem. Commun.*, 2009, 1703-1705.

368. P. K. Sasmal, Patra, A. K., Nethaji, M., and A. R. Chakravarty, *Inorganic Chemistry*, 2007, **46**, 11112-11121.
369. L. Álvarez, Grirrane, A., Moyanoa, R., Álvarez, E., Pastor, A., and A. Galindo, *Polyhedron*, 2010, **29**, 3028-3035.
370. D. del Rio, A. Galindo, R. Vicente, C. Mealli, A. Ienco and D. Masi, *Dalton Trans.*, 2003, 1813-1820.
371. I. León, S. Etcheverry, B. Parajón-Costa and E. Baran, *Biol. Trace Elem. Res.*, 2012, **147**, 403-407.
372. I. E. León, S. B. Etcheverry, B. S. Parajón-Costa and E. J. Baran, *J. Mex. Chem. Soc.*, 2013, **57**, 175-179.
373. R. E. McKinght, in *Applications of Calorimetry in a Wide Context - Differential Scanning Calorimetry, Isothermal Titration Calorimetry and Microcalorimetry*, ed. A. A. Elkordy, InTech, 2013, vol. 1.
374. A. A. Holder, Taylor, P., Magnusen, A.R., Moffett, E.T., Meyer, K., Hong, Y., Ramsdale, S.E., Gordon, M., Stubbs, J., Seymour, L.A., Acharya, D., Weber, R.T., Smith, P.F., Dismukes, G.C., Ji, P., Menocal, L., Bai, F., Williams, J.L., Cropekg D.M., and W. L. Jarrett, *Dalton Transactions*, 2013, **42**, 11881-11899.
375. B. Balaji, K. Somyajit, B. Banik, G. Nagaraju and A. R. Chakravarty, *Inorg. Chim. Acta*, 2013, **400**, 142-150.
376. P. K. Sasmal, S. Saha, R. Majumdar, R. R. Dighe and A. R. Chakravarty, *Inorg. Chem.*, 2010, **49**, 849-859.
377. P. K. Sasmal, S. Saha, R. Majumdar, S. De, R. R. Dighe and A. R. Chakravarty, *Dalton Trans.*, 2010, **39**, 2147-2158.
378. P. K. Sasmal, A. K. Patra, M. Nethaji and A. R. Chakravarty, *Inorg. Chem.*, 2007, **46**, 11112-11121.
379. T. S. Jagodziński, *Chem. Rev.*, 2002, **103**, 197-228.
380. R. N. Hurd and G. DeLaMater, *Chem. Rev.*, 1961, **61**, 45-86.
381. H.-J. Lee, Y.-S. Choi, K.-B. Lee, J. Park and C.-J. Yoon, *J. Phys. Chem. A*, 2002, **106**, 7010-7017.
382. S. Mukherjee, H. Verma and J. Chatterjee, *Org. Lett.*, 2015, **17**, 3150-3153.
383. E. J. Petersson, J. M. Goldberg and R. F. Wissner, *PCCP*, 2014, **16**, 6827-6837.
384. E. V. Brown, *Synthesis*, 1975, **1975**, 358-375.
385. D. L. Turner, *J. Am. Chem. Soc.*, 1948, **70**, 3961-3962.
386. H. D. Porter, *J. Am. Chem. Soc.*, 1954, **76**, 127-128.
387. M. Carmack, *J. Heterocycl. Chem.*, 1989, **26**, 1319-1323.
388. M. Carmack, M. Behforouz, G. A. Berchtold, S. M. Berkowitz, D. Wiesler and R. Barone, *J. Heterocycl. Chem.*, 1989, **26**, 1305-1318.
389. B. Emmert and M. Groll, *Chem. Ber.*, 1953, **86**, 208-213.
390. R. Wegler, E. Kühle and W. Schäfer, *Angew. Chem.*, 1958, **70**, 351-367.
391. Marco H. Klingele and S. Brooker, *Eur. J. Org. Chem.*, 2004, 3422-3434.
392. W. A. Kinney, N. E. Lee, R. M. Blank, C. A. Demerson, C. S. Sarnella, N. T. Scherer, G. N. Mir, L. E. Borella, J. F. DiJoseph and C. Wells, *J. Med. Chem.*, 1990, **33**, 327-336.
393. P.-H. Leung, Y. Qin, G. He, K. F. Mok and J. J. Vittal, *J. Chem. Soc., Dalton Trans.*, 2001, 309-314.
394. I. Papazoglou, P. J. Cox, A. G. Papadopoulos, M. P. Sigalas and P. Aslanidis, *Dalton Trans.*, 2013, **42**, 2755-2764.

395. K. J. Kilpin, W. Henderson and B. K. Nicholson, *Inorg. Chim. Acta*, 2010, **363**, 41-48.
396. S. M. Meier, M. Hanif, Z. Adhireksan, V. Pichler, M. Novak, E. Jirkovsky, M. A. Jakupec, V. B. Arion, C. A. Davey, B. K. Keppler and C. G. Hartinger, *Chem. Sci.*, 2013, **4**, 1837-1846.
397. R. Raj Kumar, M. K. Mohamed Subarkhan and R. Ramesh, *RSC Advances*, 2015, **5**, 46760-46773.
398. V. Chauhan and S. K. Dikshit, *Transition Met. Chem.*, 1986, **11**, 403-405.
399. E. Sindhuja, R. Ramesh, N. Dharmaraj and Y. Liu, *Inorg. Chim. Acta*, 2014, **416**, 1-12.
400. F. A. Beckford, M. Shaloski, Jr., G. Leblanc, J. Thessing, L. C. Lewis-Alleyne, A. A. Holder, L. Li and N. P. Seeram, *Dalton Trans.*, 2009, 10757-10764.
401. G. Prakash, R. Manikandan, P. Viswanathamurthi, K. Velmurugan and R. Nandhakumar, *J. Photochem. Photobiol. B: Biol.*, 2014, **138**, 63-74.
402. S. Huang, F. Zhu, Q. Qian, Q. Xiao and W. Su, *Biol. Trace Elem. Res.*, 2015, **164**, 150-161.
403. H. Beraldo and D. Gambinob, *Mini Reviews in Medicinal Chemistry*, 2004, **4**, 31-39.
404. R. Manikandan, P. Viswanathamurthi, K. Velmurugan, R. Nandhakumar, T. Hashimoto and A. Endo, *J. Photochem. Photobiol. B: Biol.*, 2014, **130**, 205-216.
405. R. Manikandan, P. Vijayan, P. Anitha, G. Prakash, P. Viswanathamurthi, R. J. Butcher, K. Velmurugan and R. Nandhakumar, *Inorg. Chim. Acta*, 2014, **421**, 80-90.
406. B. Singh, P. Srivastava and A. K. Srivastav, *Synth. React. Inorg. Met.-Org. Chem.*, 1992, **22**, 299-310.
407. R. F. Nystrom and W. G. Brown, *J. Am. Chem. Soc.*, 1947, **69**, 2548-2549.
408. I. Khan, A. Ibrar and N. Abbas, *Eur. J. Med. Chem.*, 2013, **63**, 854-868.
409. D. Kumar, N. Maruthi Kumar, K.-H. Chang and K. Shah, *Eur. J. Med. Chem.*, 2010, **45**, 4664-4668.
410. M. M. Kamel and N. Y. Megally Abdo, *Eur. J. Med. Chem.*, 2014, **86**, 75-80.
411. Y. Li, J. Geng, Y. Liu, S. Yu and G. Zhao, *ChemMedChem*, 2013, **8**, 27-41.
412. B. Masereel, S. Rolin, F. Abbate, A. Scozzafava and C. T. Supuran, *J. Med. Chem.*, 2001, **45**, 312-320.
413. C. B. Mishra, S. Kumari and M. Tiwari, *Eur. J. Med. Chem.*, 2015, **92**, 1-34.
414. S. Haider, M. S. Alam and H. Hamid, *Eur. J. Med. Chem.*, 2015, **92**, 156-177.
415. P. Poli, M. Aline de Mello, A. Buschini, R. A. Mortara, C. Northfleet de Albuquerque, S. da Silva, C. Rossi and T. M. A. D. Zucchi, *Biochem. Pharmacol.*, 2002, **64**, 1617-1627.
416. K. Salomão, E. M. de Souza, S. A. Carvalho, E. F. da Silva, C. A. M. Fraga, H. S. Barbosa and S. L. de Castro, *Antimicrob. Agents Chemother.*, 2010, **54**, 2023-2031.
417. M. T. Rabkin, E. W. Frederick, M. Lotz and L. H. Smith, Jr., *J. Clin. Invest.*, 1962, **41**, 871-883.
418. R. Tripathy, A. Ghose, J. Singh, E. R. Bacon, T. S. Angeles, S. X. Yang, M. S. Albom, L. D. Aimone, J. L. Herman and J. P. Mallamo, *Bioorg. Med. Chem. Lett.*, 2007, **17**, 1793-1798.
419. N. Grynberg, A. C. Santos and A. Echevarria, *Anti-Cancer Drugs*, 1997, **8**, 88-91.
420. B. Hemmateenejad, R. Miri, U. Niroomand, A. Foroumadi and A. Shafiee, *Chem. Biol. Drug Des.*, 2007, **69**, 435-443.
421. P. Rajakumar, A. Thirunarayanan, S. Raja, S. Ganesan and P. Maruthamuthu, *Tetrahedron Lett.*, 2012, **53**, 1139-1143.

422. G. Aydoğdu, G. Günendi, D. K. Zeybek, B. Zeybek and Ş. Pekyardımcı, *Sensors Actuators B: Chem.*, 2014, **197**, 211-219.
423. Y. Hu, C.-Y. Li, X.-M. Wang, Y.-H. Yang and H.-L. Zhu, *Chem. Rev.*, 2014, **114**, 5572-5610.
424. M. Kritsanida, A. Mouroutsou, P. Marakos, N. Pouli, S. Papakonstantinou-Garoufalias, C. Pannecouque, M. Witvrouw and E. De Clercq, *Il Farmaco*, 2002, **57**, 253-257.
425. G. L. Almajan, S.-F. Barbuceanu, G. Bancescu, I. Saramet, G. Saramet and C. Draghici, *Eur. J. Med. Chem.*, 2010, **45**, 6139-6146.
426. S. G. Alegaon, K. R. Alagawadi, P. V. Sonkusare, S. M. Chaudhary, D. H. Dadwe and A. S. Shah, *Bioorg. Med. Chem. Lett.*, 2012, **22**, 1917-1921.
427. S. S. Karki, K. Panjamurthy, S. Kumar, M. Nambiar, S. A. Ramareddy, K. K. Chiruvella and S. C. Raghavan, *Eur. J. Med. Chem.*, 2011, **46**, 2109-2116.
428. B. Shivarama Holla, K. Narayana Poojary, B. Sooryanarayana Rao and M. K. Shivananda, *Eur. J. Med. Chem.*, 2002, **37**, 511-517.
429. B. S. Holla, P. M. Akberali and M. K. Shivananda, *Il Farmaco*, 2001, **56**, 919-927.
430. D. H. Purohit, B. L. Dodiya, R. M. Ghetiya, P. B. Vekariya and H. S. Joshi, *Acta Chimica Slov*, 2011, **58**, 53-59.
431. A. Varvaresou, T. Siatra-Papastaikoudi, A. Tsotinis, A. Tsantili-Kakoulidou and A. Vamvakides, *Il Farmaco*, 1998, **53**, 320-326.
432. Z. A. Kaplancıklı, G. Turan-Zitouni, A. Özdemir and G. Revial, *Eur. J. Med. Chem.*, 2008, **43**, 155-159.
433. H. Chen, Z. Li and Y. Han, *J. Agric. Food. Chem.*, 2000, **48**, 5312-5315.
434. Y. A. Ammar, M. M. Ghorab, A. M. S. El-Sharief and S. I. Mohamed, *Heteroat. Chem*, 2002, **13**, 199-206.
435. N. D. Heindel and J. R. Reid, *J. Heterocycl. Chem.*, 1980, **17**, 1087-1088.
436. A. Kamal, M. N. A. Khan, Y. V. V. Srikanth, K. Srinivasa Reddy, A. Juvekar, S. Sen, N. Kurian and S. Zingde, *Biorg. Med. Chem.*, 2008, **16**, 7804-7810.
437. A. P. Skoumbourdis, C. A. LeClair, E. Stefan, A. G. Turjanski, W. Maguire, S. A. Titus, R. Huang, D. S. Auld, J. Inglese, C. P. Austin, S. W. Michnick, M. Xia and C. J. Thomas, *Bioorg. Med. Chem. Lett.*, 2009, **19**, 3686-3692.
438. S. J. Gilani, S. A. Khan and N. Siddiqui, *Bioorg. Med. Chem. Lett.*, 2010, **20**, 4762-4765.
439. B. M. Sahoo, S. C. Dinda and B. V. V. Ravi Kumar, *Int. J. Pharm. Pharm. Sci.*, 2012, **4**, 747-751.
440. K. D. Robarge, S. A. Brunton, G. M. Castanedo, Y. Cui, M. S. Dina, R. Goldsmith, S. E. Gould, O. Guichert, J. L. Gunzner, J. Halladay, W. Jia, C. Khojasteh, M. F. T. Koehler, K. Kotkow, H. La, R. L. LaLonde, K. Lau, L. Lee, D. Marshall, J. C. Marsters Jr, L. J. Murray, C. Qian, L. L. Rubin, L. Salphati, M. S. Stanley, J. H. A. Stibbard, D. P. Sutherlin, S. Ubhayaker, S. Wang, S. Wong and M. Xie, *Bioorg. Med. Chem. Lett.*, 2009, **19**, 5576-5581.
441. S. M. El-Khawass and N. S. Habib, *J. Heterocycl. Chem.*, 1989, **26**, 177-181.
442. Y. A. Efimova, G. G. Karabanovich, T. V. Artamonova and G. I. Koldobskii, *Russ. J. Org. Chem.*, 2009, **45**, 631-632.
443. A. R. Cowley, J. R. Dilworth, P. S. Donnelly, A. D. Gee and J. M. Heslop, *Dalton Trans.*, 2004, 2404-2412.
444. A. Cansız, A. Cetin, C. Orek, M. Karatepe, K. Sarac, A. Kus and P. Koparir, *Spectrochim. Acta. Mol. Biomol. Spectros.*, 2012, **97**, 606-615.

445. I. E. León, N. Butenko, A. L. Di Virgilio, C. I. Muglia, E. J. Baran, I. Cavaco and S. B. Etcheverry, *J. Inorg. Biochem.*, 2014, **134**, 106-117.
446. W. Antholine, J. Knight, H. Whelan and D. H. Petering, *Mol. Pharmacol.*, 1977, **13**, 89-98.
447. T. K. Venkatachalam, G. K. Pierens and D. C. Reutens, *Magn. Reson. Chem.*, 2014, **52**, 98-105.
448. M. U. Raja and R. Ramesh, *J. Organomet. Chem.*, 2012, **699**, 5-11.

APPENDIX A

SUPPORTING FIGURES

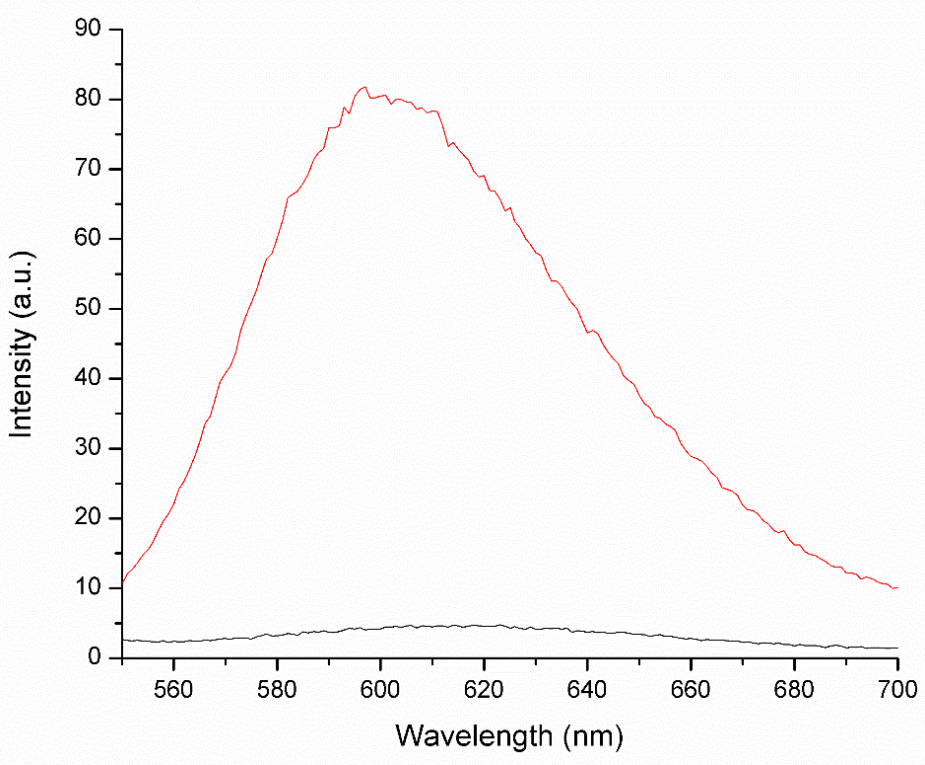

Figure A 1. Fluorescence spectra of Ethidium bromide in the absence (black) and presence (red) of DNA in PBS buffer (pH = 7.4), λ_{ex} = 520 nm.

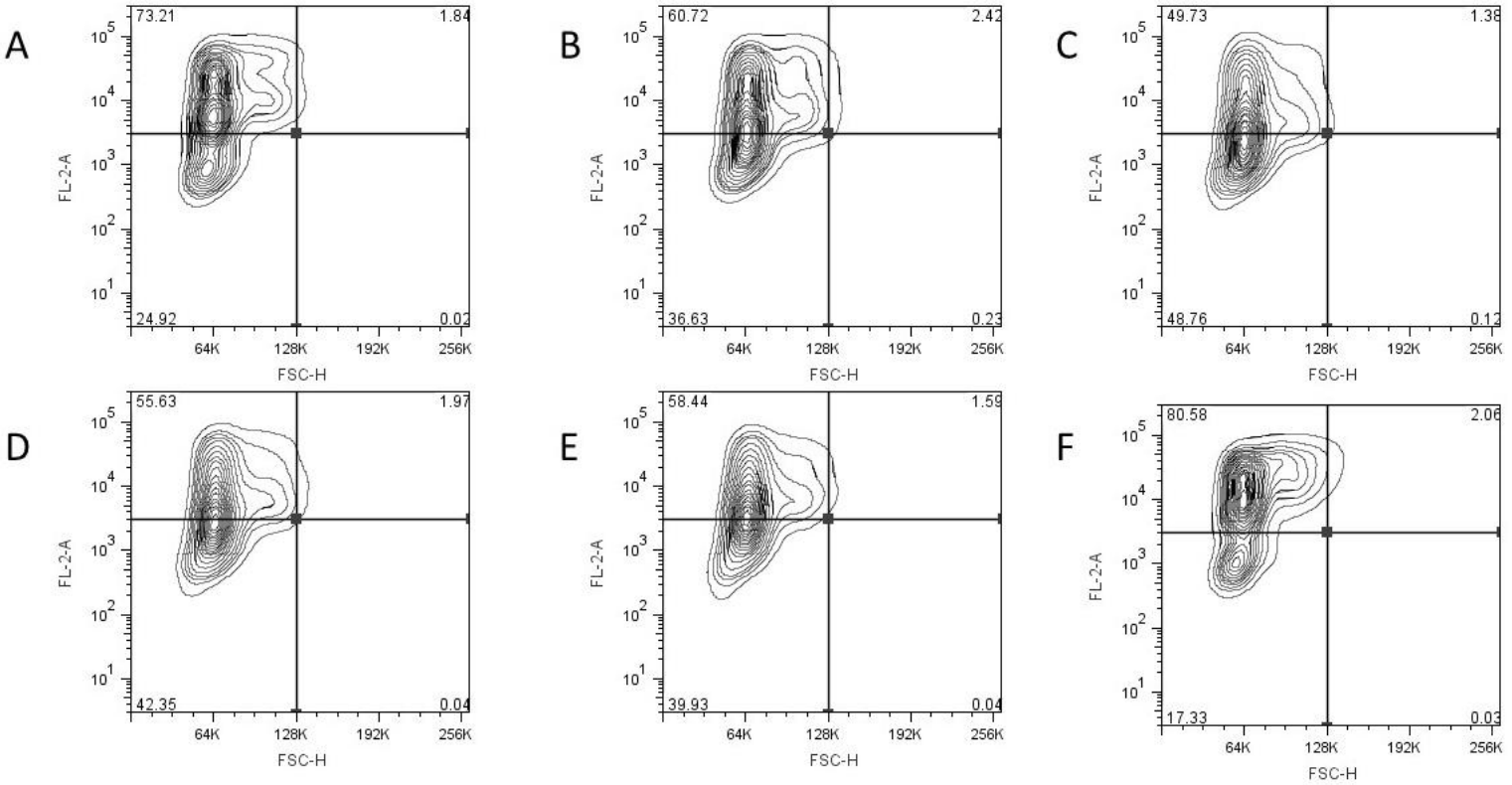

Figure A 2. Contour plots of fluorescence resulting from $\Delta\Psi_m$ after four hours (FL2-H, Y-axis) and FSC-H (Y-axis). A) 0 µM; B) 5 µM; C) 20 µM; D) 40 µM; E) 60 µM; F) 80 µM $[Co(phen)_2(MeATSC)](NO_3)_3 \cdot 2.5H_2O \cdot C_2H_5OH$. Data represents 20,000 molecular events collected.

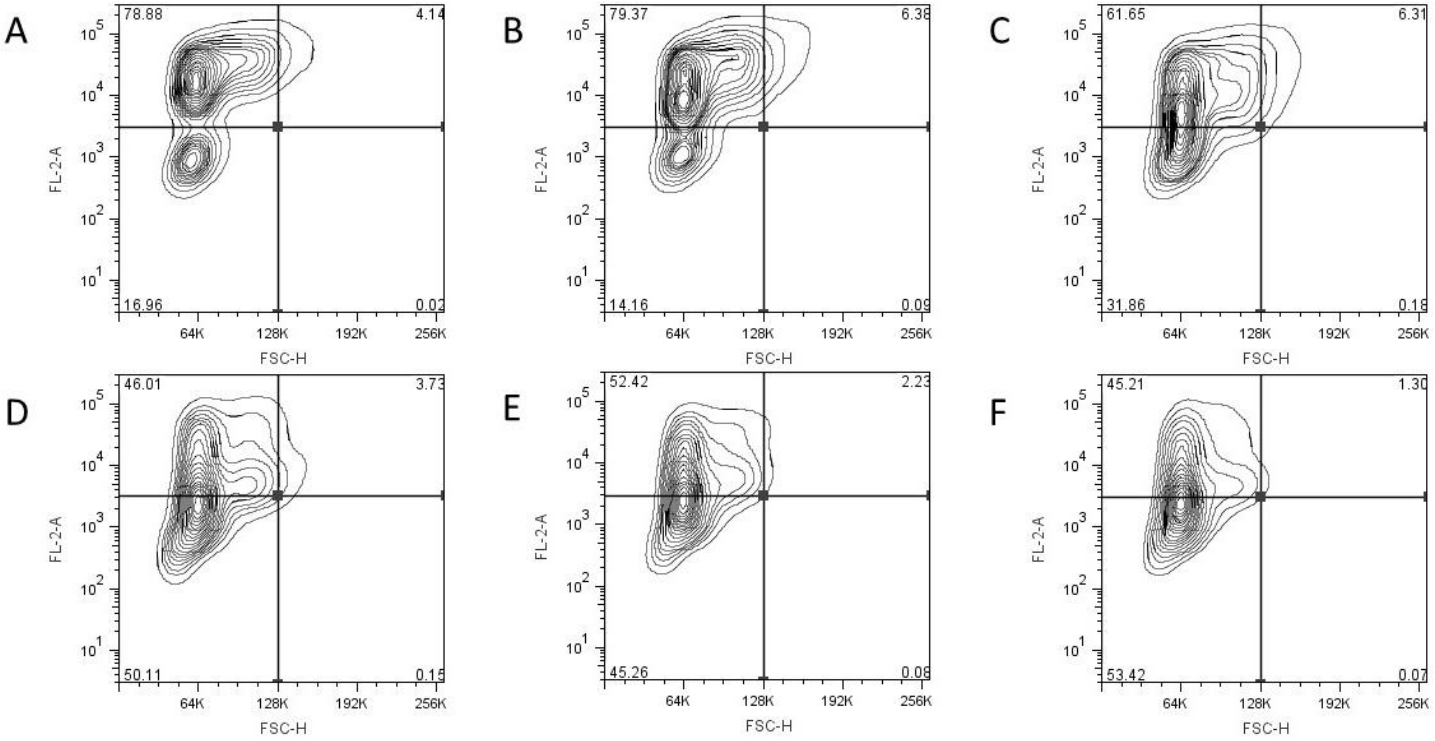

Figure A 3. Contour plots are shown of fluorescence resulting from $\Delta\Psi_m$ after six hours (FL2-H, Y-axis) and FSC-H (Y-axis). A) 0 µM; B) 5 µM; C) 20 µM; D) 40 µM; E) 60 µM; F) 80 µM $[Co(phen)_2(MeATSC)](NO_3)_3 \cdot 2.5H_2O \cdot C_2H_5OH$. Data represents 20,000 molecular events collected.

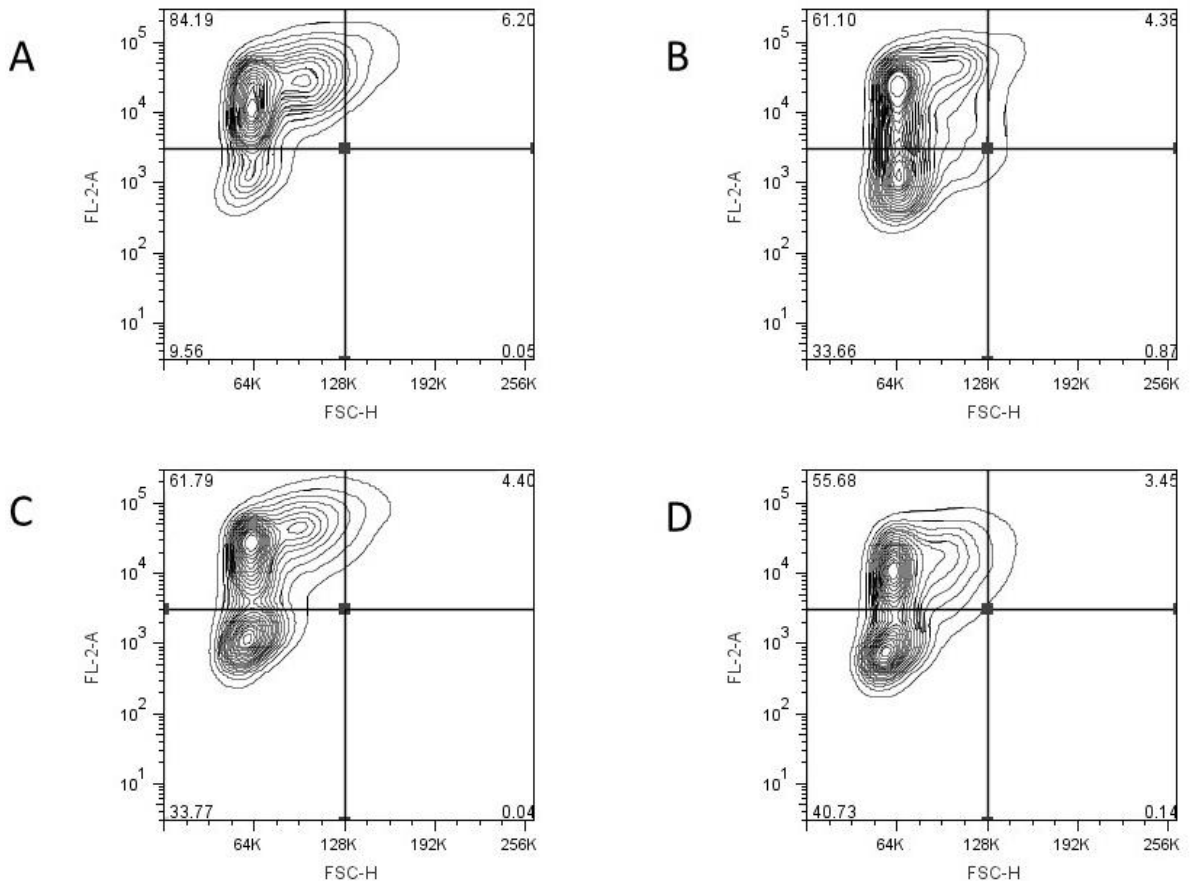

Figure A 4. Contour plots of fluorescence resulting from $\Delta\Psi_m$ after delayed TMRE stain addition (FL2-H, Y-axis) and FSC-H (Y-axis) after 24 h exposure to 5 µM $[Co(phen)_2(MeATSC)](NO_3)_3 \cdot 2.5H_2O \cdot C_2H_5OH$. A) 0 min; B) 15 min; C) 30 min; D) 1 hour delay. Data represents 20,000 molecular events collected.

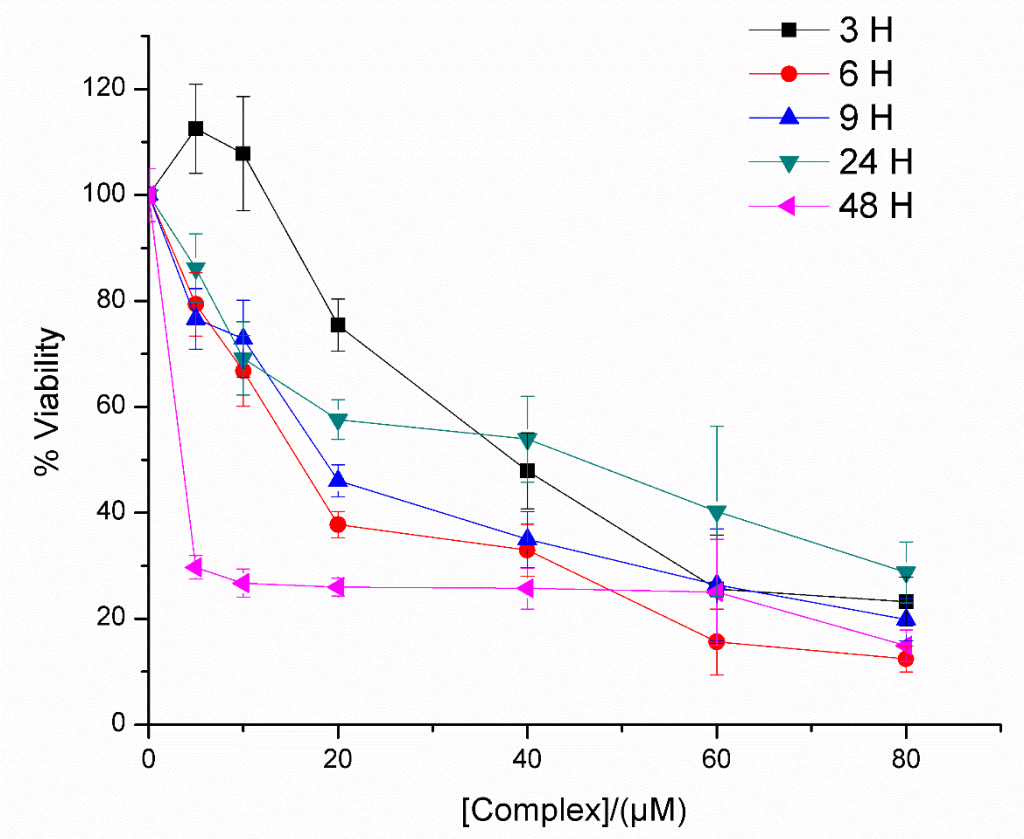

Figure A 5. Cell viability graphs following treatment of 4T1-luc cells with $[Co(phen)_2(MeATSC)](NO_3)_3 \cdot 2.5H_2O \cdot C_2H_5OH$ for various time periods. Cells were seeded at 2.5 X 10^4 cells per well for 24 h prior to addition to treatment. Graphs represent n = 3 replicates of data with plates being 1 h post incubation with MTS reagent.

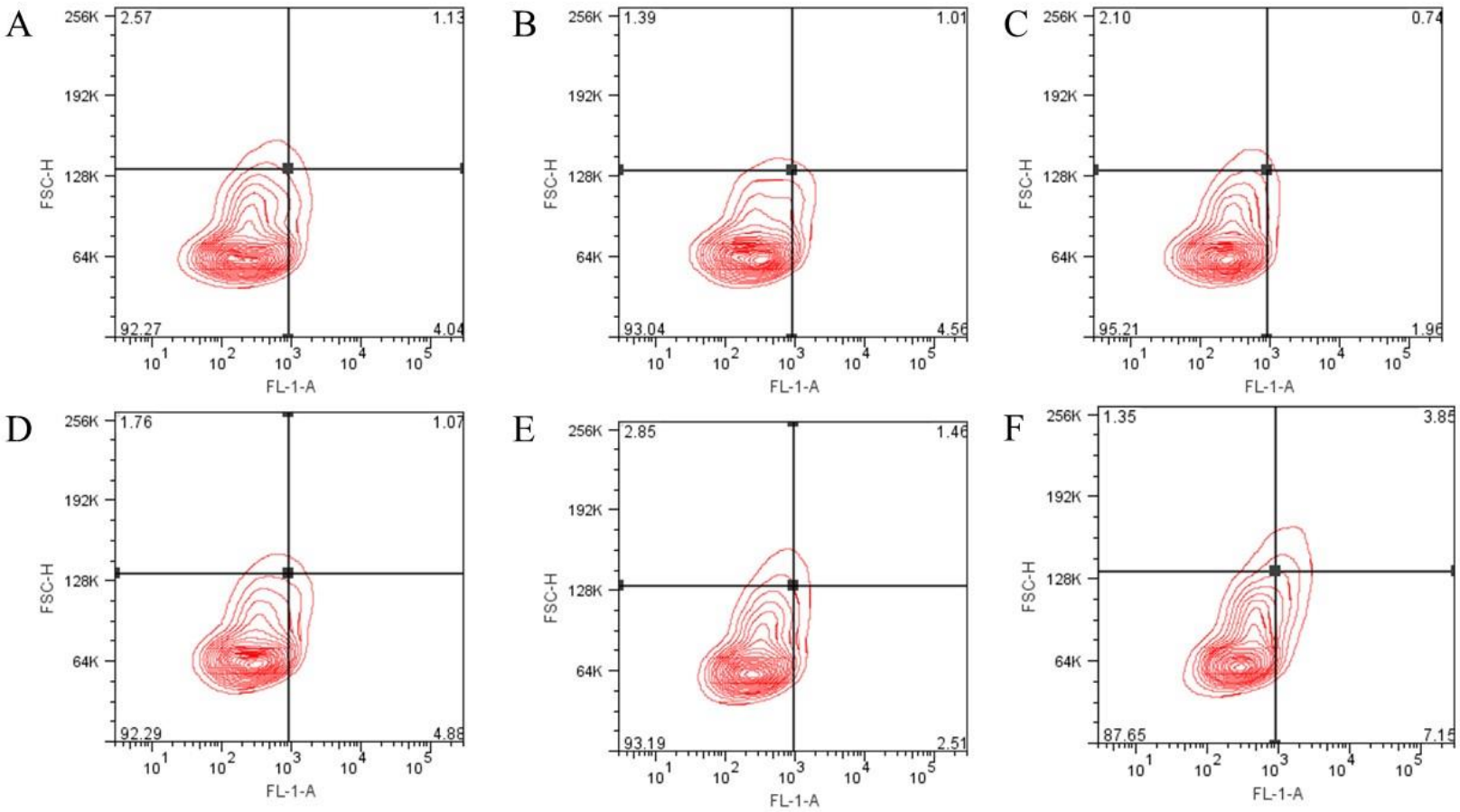

Figure A 6. Contour plots of fluorescence resulting from propidium iodide staining (FSC-H, Y-axis) and (FL1-A X-axis) after 3 h exposure to $[Co(phen)_2(MeATSC)](NO_3)_3 \cdot 2.5H_2O \cdot C_2H_5OH$. A) 0 µM; B) 5 µM; C) 20 µM; D) 40 µM; E) 60 µM; F) 80 µM $[Co(phen)_2(MeATSC)](NO_3)_3 \cdot 2.5H_2O \cdot C_2H_5OH$. Data represents 10,000 molecular events collected.

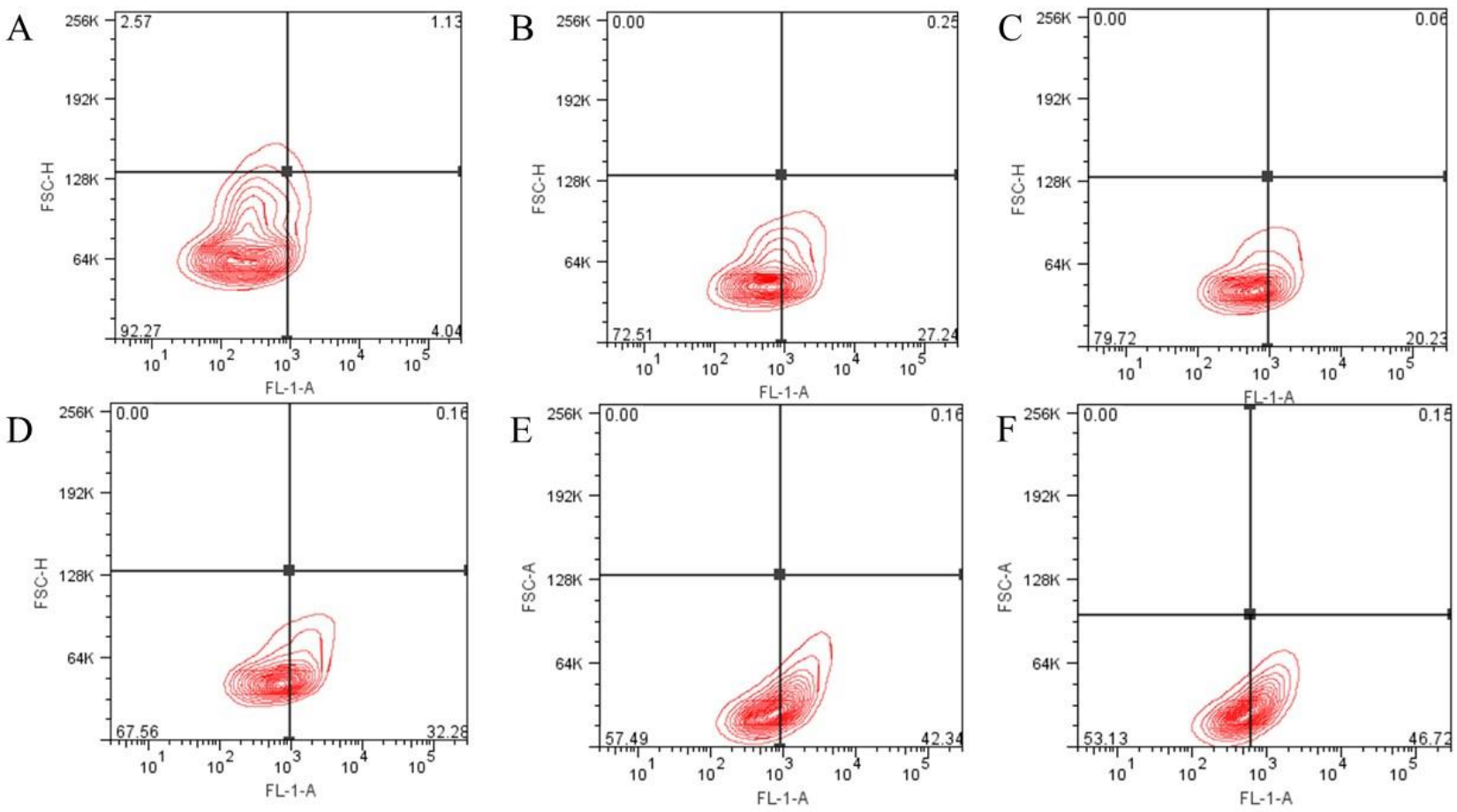

Figure A 7. Contour plots of fluorescence resulting from propidium iodide staining (FSC-H, Y-axis) and (FL1-A X-axis) after 3 h exposure to $[Co(phen)_2(MeATSC)](NO_3)_3 \cdot 2.5H_2O \cdot C_2H_5OH$. A) 0 µM; B) 5 µM; C) 20 µM; D) 40 µM; E) 60 µM; F) 80 µM $[Co(phen)_2(MeATSC)](NO_3)_3 \cdot 2.5H_2O \cdot C_2H_5OH$. Data represents 10,000 molecular events collected.

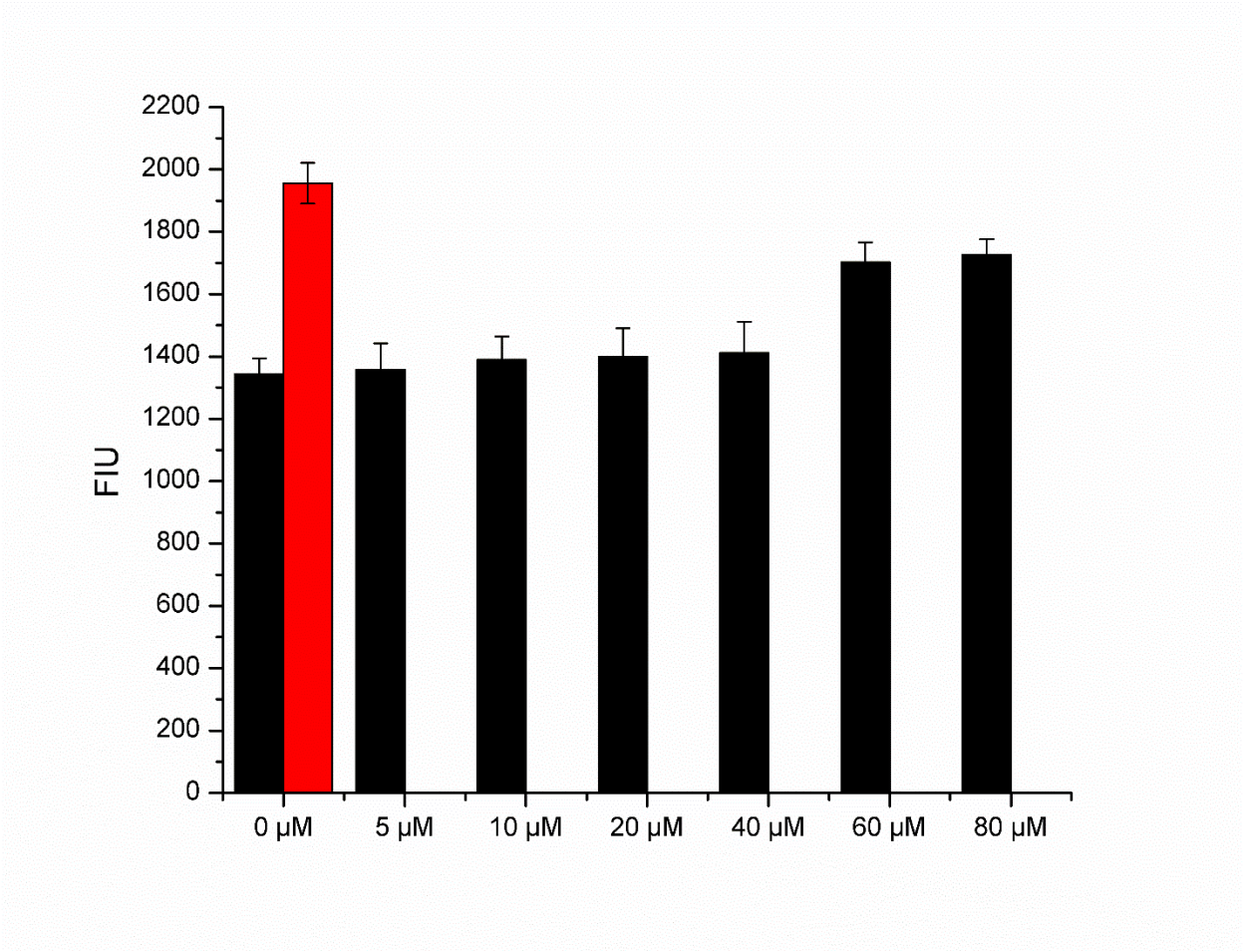

Figure A 8. Determination of inhibition of autophagy after exposure to $[Co(phen)_2(MeATSC)](NO_3)_3 \cdot 2.5H_2O \cdot C_2H_5OH$ and necrostatin-1 (600 µM). Plot of the mean fluorescent intensity vs [Complex]. Black drug treated cells, red positive control (starvation). Data represents 20,000 molecular events collected.

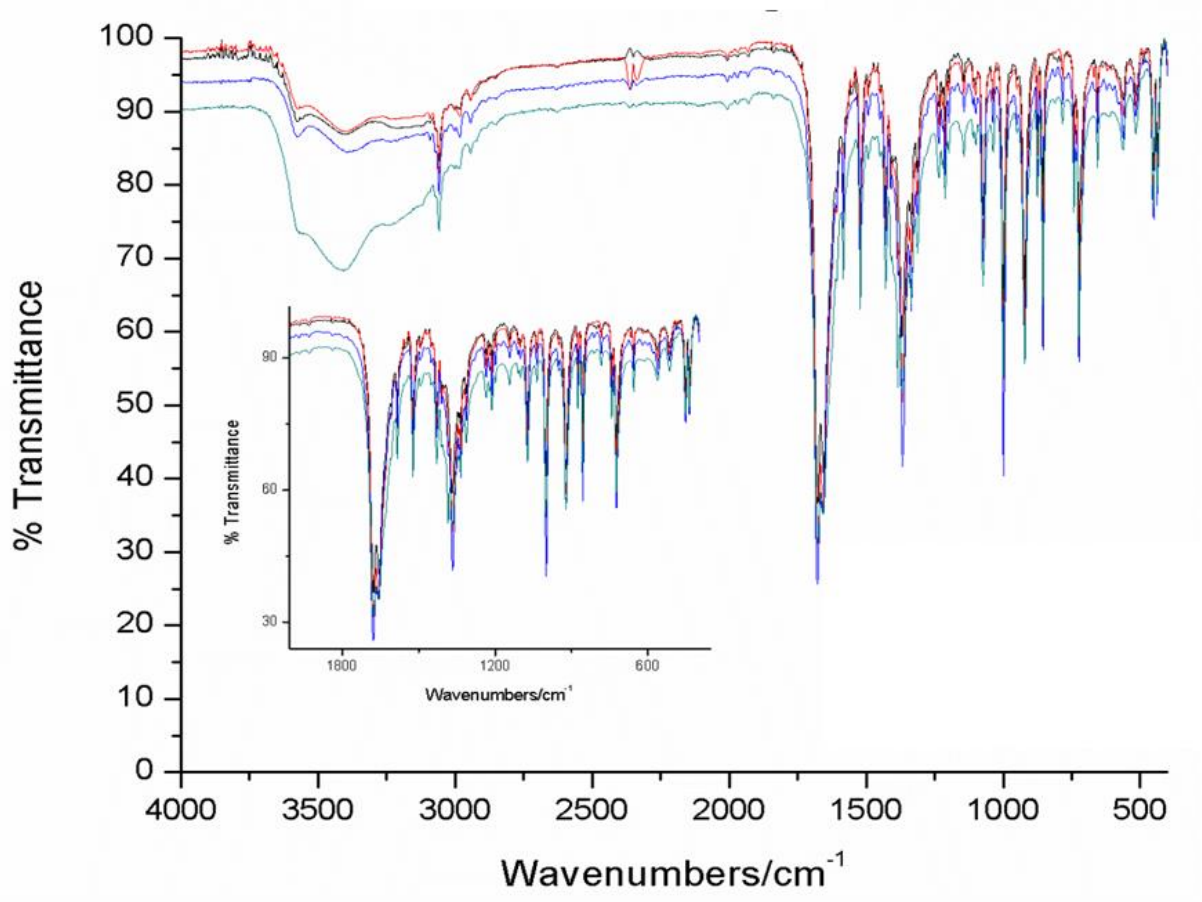

Figure A 9. Overlay of FTIR spectra obtained from various preparations of [VO(oda)(phen)]·1.5H_2O.

Table A 1. Injections parameter for Microcal ITC_{200} for Ethidium Bromide with CT DNA in PBS (pH = 7.0) for protocol optimization and instrument calibration.

Experimental Parameters			Edit Mode				
Total injections	40		Injection	Volume	Duration	Spacing	Filter
Cell Temp. (°C)	25		1	0.4	0.8	280	2
Reference Power (µcal/sec)	10		2	1	2	280	2
Initial Delay (s)	60		3	1	2	280	2
[Syringe] (mM)	1.1		…	…	…	…	2
[Cell] (mM)	0.102		39	1	2	280	2
Stirring speed	1000		40	1	2	280	2

Table A 2. Injections parameter for Microcal ITC_{200} for $[VO(phen)(sal\text{-}L\text{-}tryp)]\cdot H_2O$ with CT DNA in PBS (pH = 7.2).

Experimental Parameters			Edit Mode				
Total injections	30		Injection	Volume	Duration	Spacing	Filter
Cell Temp. (°C)	25		1	0.4	0.8	180	2
Reference Power (µcal/sec)	10		2	1	2	180	2
Initial Delay (s)	60		3	1	2	180	2
[Syringe] (mM)	0.1		…	…	…	…	…
[Cell] (mM)	0.042		19	1	2	180	2
Stirring speed	1000		20	1	2	180	2

Table A 3. Injections parameter for Microcal ITC_{200} for

$[Ru(pbt)_2(phen_2DTT)VO(oda)](PF_6)_2 \bullet 2.0H_2O \bullet 0.5C_2H_5OH$ with CT DNA in PBS (pH = 7.2).

Experimental Parameters		Edit Mode				
Total injections	40	Injection	Volume	Duration	Spacing	Filter
Cell Temp. (°C)	25	1	0.4	0.8	280	2
Reference Power (µcal/sec)	10	2	1	2	280	2
Initial Delay (s)	60	3	1	2	280	2
[Syringe] (mM)	0.1	…	…	…	…	…
[Cell] (mM)	0.01	39	1	2	280	2
Stirring speed	1000	40	1	2	280	2

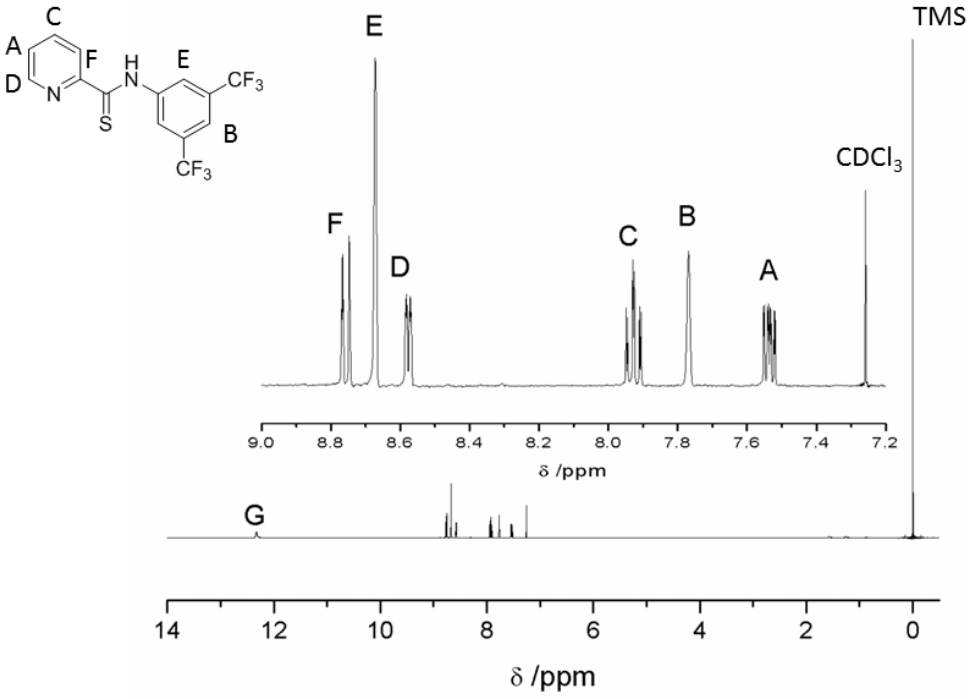

Figure A 10. ^{1}H NMR spectrum of *N*-[3,5-bis(trifluromethyl)phenyl]pyridine-2-thiocarboxamide in $CDCl_3$

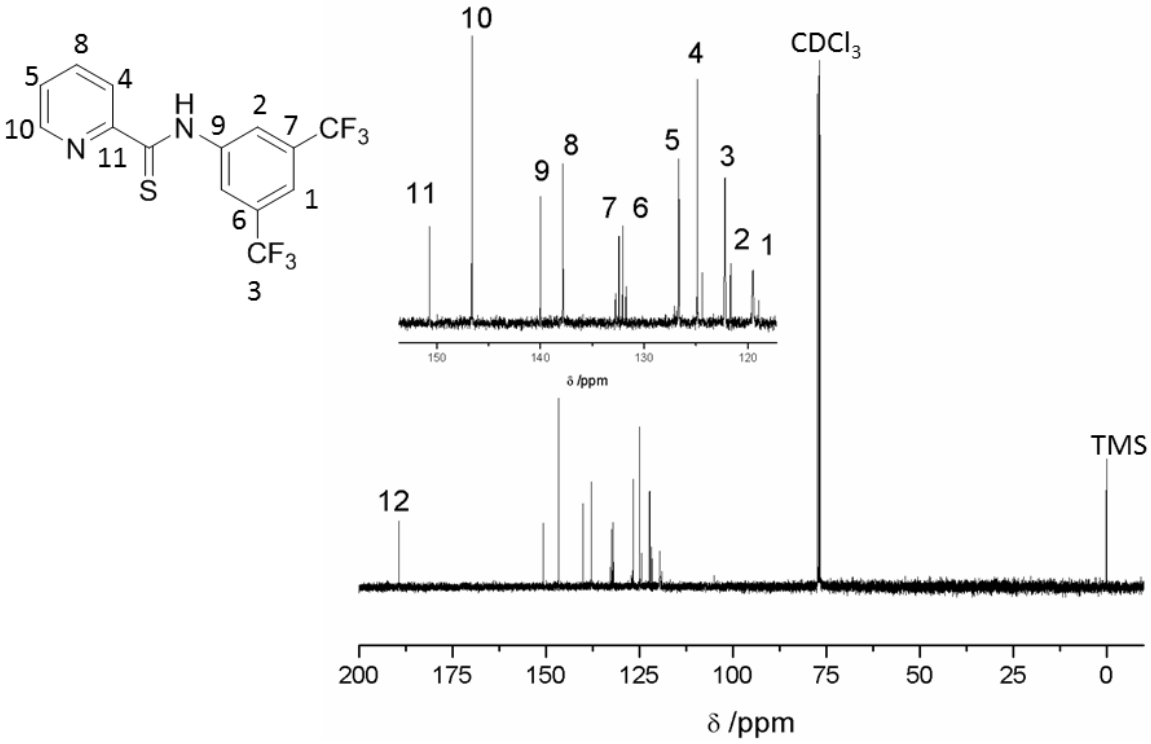

Figure A 11. ^{13}C NMR spectrum of *N*-[3,5-bis(trifluromethyl)phenyl]pyridine-2-thiocarboxamide in $CDCl_3$.

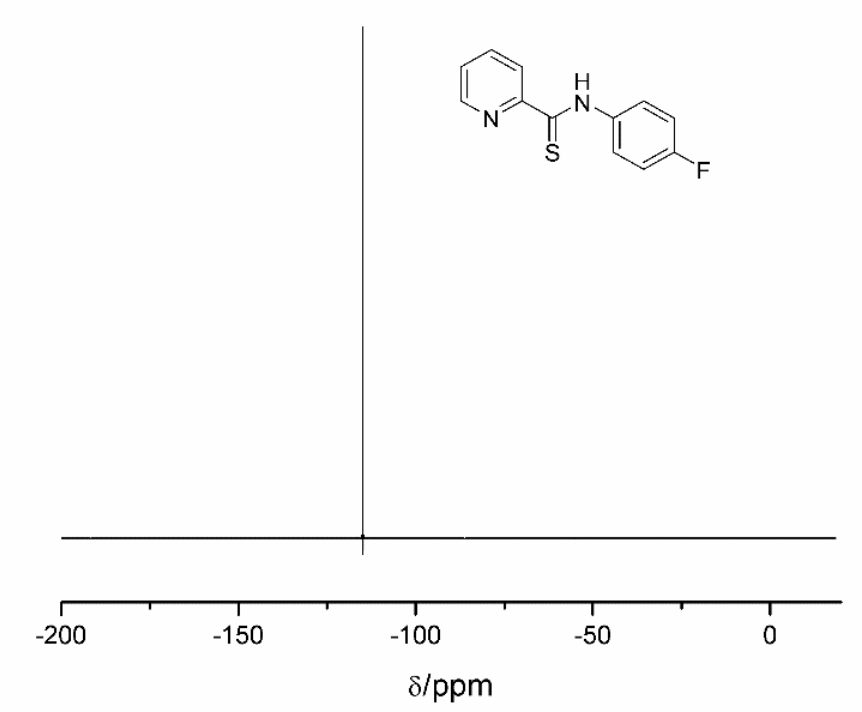

Figure A 12. ^{19}F NMR spectrum of *N*-(4-fluorphenyl)pyridine-2-thiocarboxamide in $CDCl_3$.

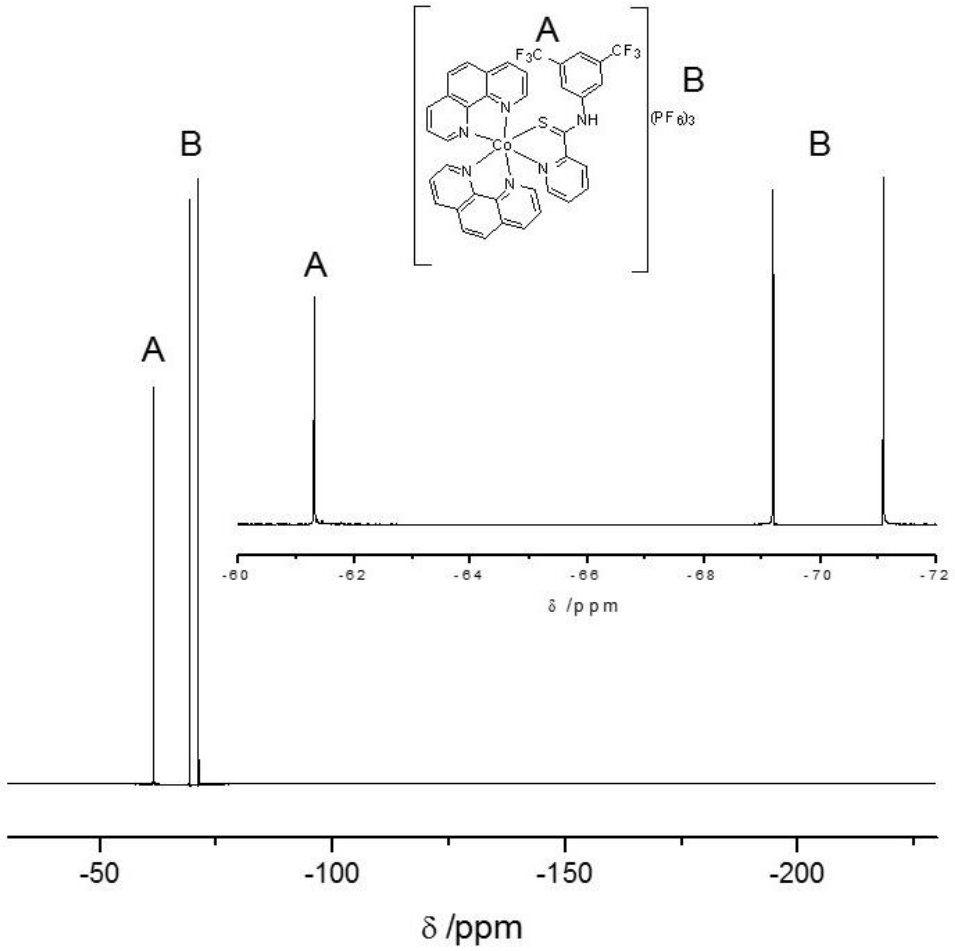

Figure A 13. ^{19}F NMR of $[Co(phen)_2(TPTA)](PF_6)_3$ in DMSO-d_6.

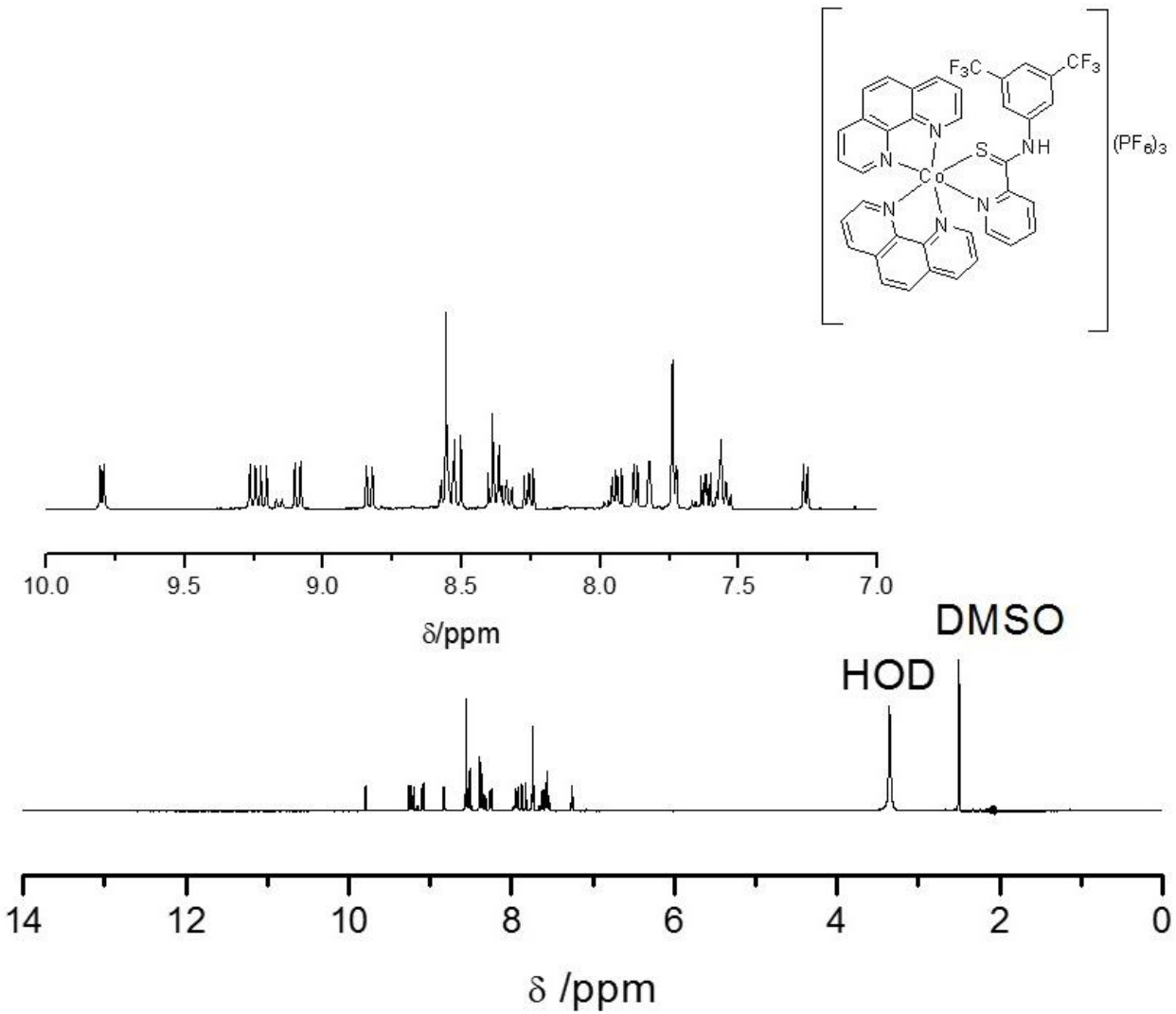

Figure A 14. ^{1}H NMR of $[Co(phen)_2(TPTA)](PF_6)_3$ in DMSO-d_6.

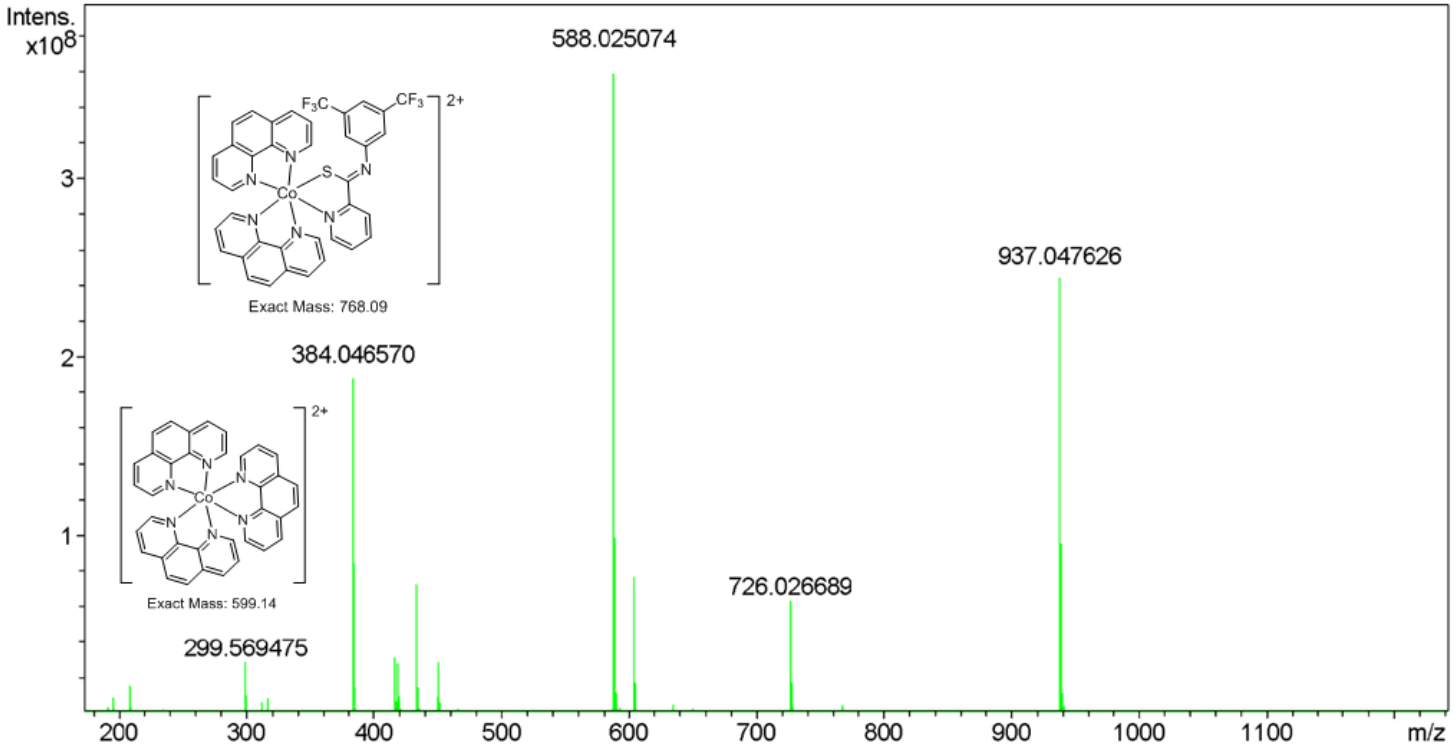

Figure A 15. Wide view of HRMS spectrum of $[Co(phen)_2(TPTA)](PF_6)_3$ in MeOH.

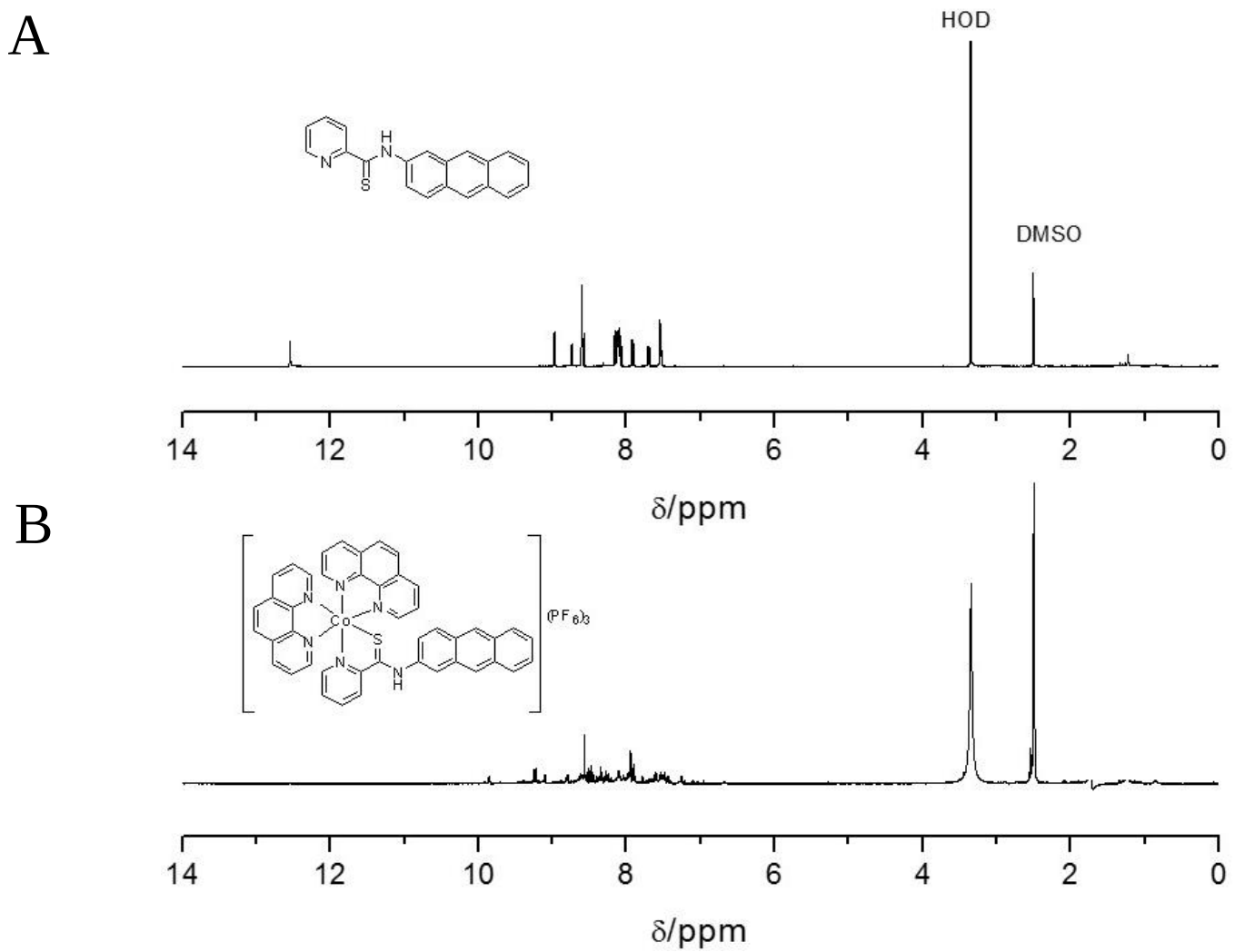

Figure A 16. Separation process of $[Co(phen)_2(APTA)](PF_6)_3$ as monitored by ^1H NMR in DMSO-d_6. A) Ligand fraction and B) Complex fraction.

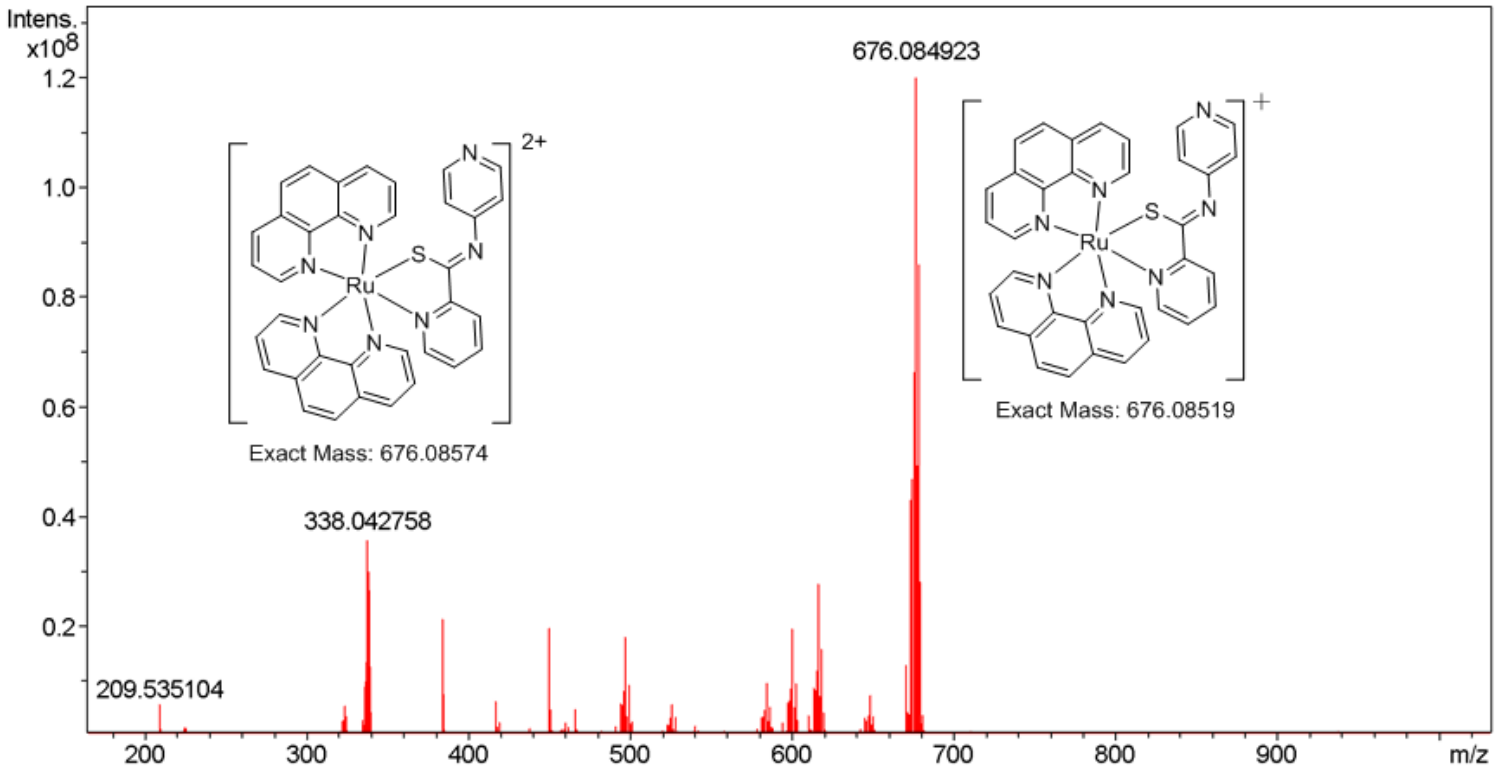

Figure A 17. Wide view of HRMS spectrum of $[Ru(phen)_2(PPTA)](PF_6)_2$ in MeCN.

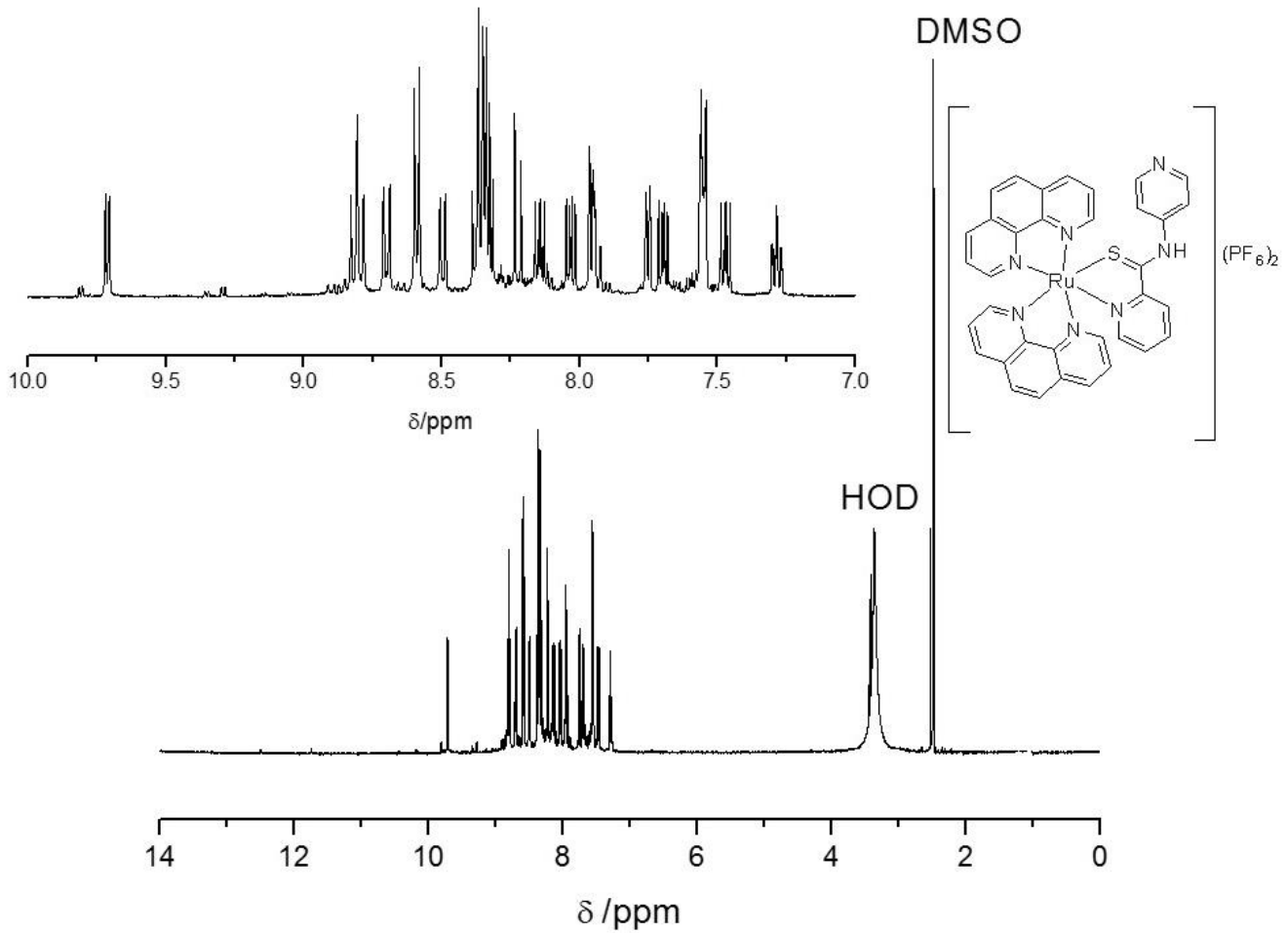

Figure A 18. ^{1}H NMR spectrum of $[Ru(phen)_2(PPTA)](PF_6)_2$ in DMSO-d_6.

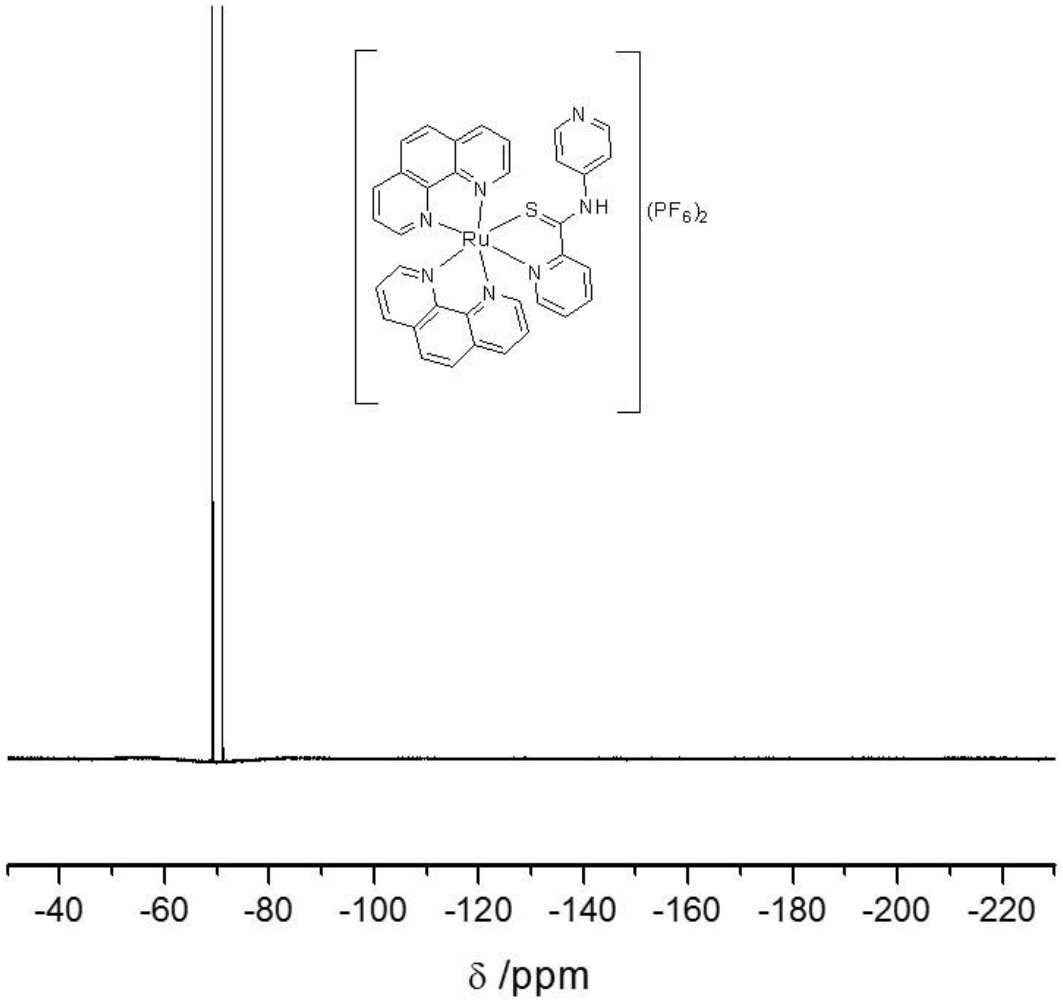

Figure A 19. ^{19}F NMR spectrum of $[Ru(phen)_2(PPTA)](PF_6)_2$ in DMSO-d_6.

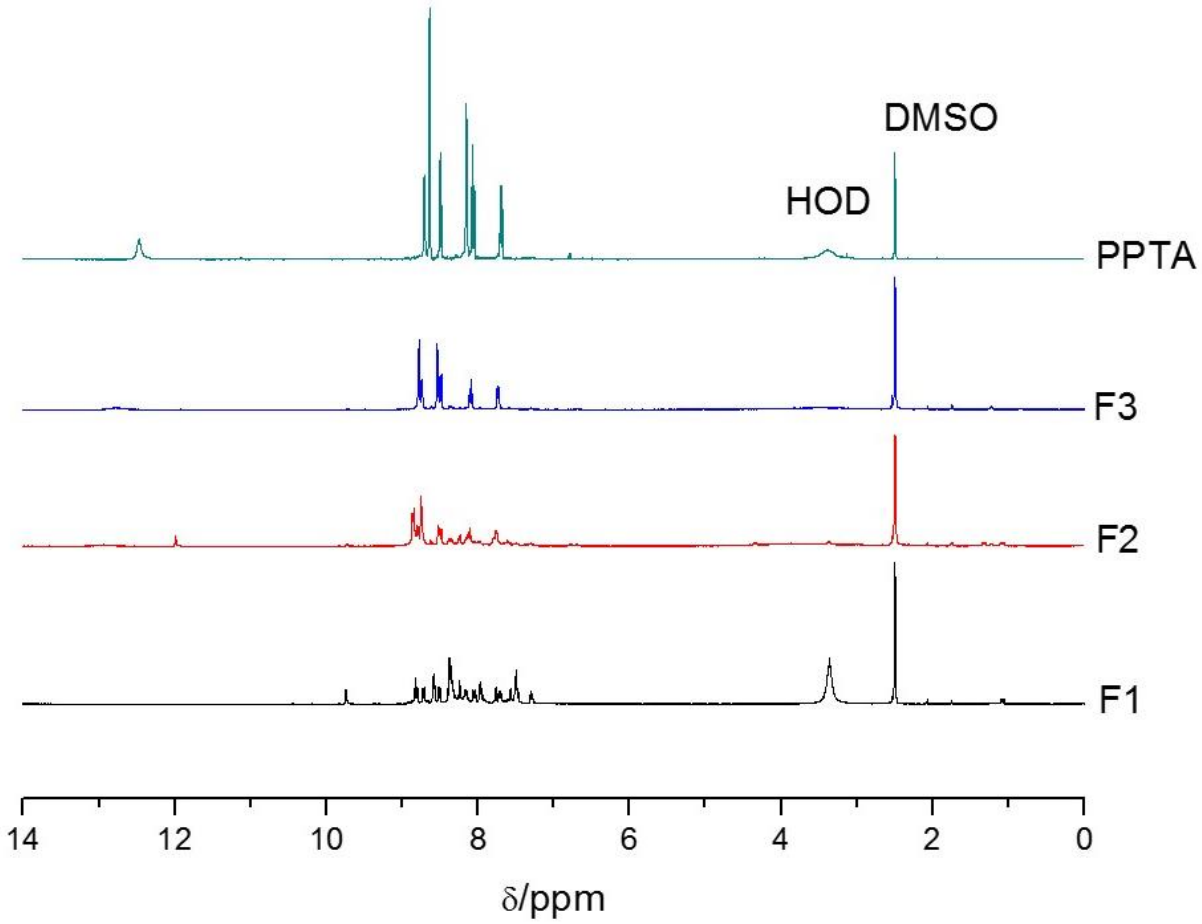

Figure A 20. ^{1}H NMR spectra of the species obtained during the separation process of $[Ru(phen)_2(PPTA)](PF_6)_2$ all in DMSO-d_6. F1 represents the complex fraction and contains the desired $[Ru(phen)_2(PPTA)](PF_6)_2$. F2 is a mixture of the metal complex $[Ru(phen)_2(PPTA)](PF_6)_2$ and free ligand PPTA. F3 represents the third band collected and is labelled as the ligand fraction and contains free uncoordinated PPTA. A ^{1}H NMR spectrum of the free PPTA ligand is shown for comparison purposes and is labelled as PPTA.

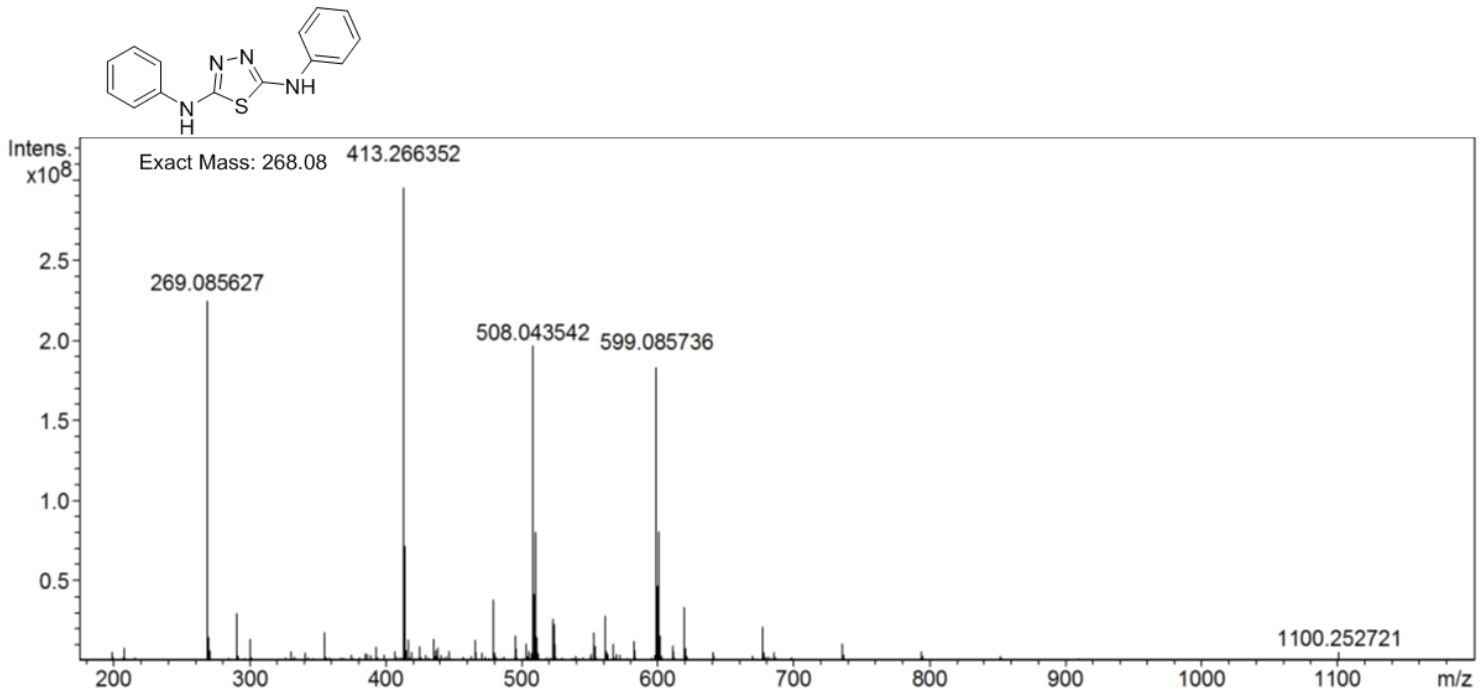

Figure A 21. ESI-MS confirming the presence of N,N-diphenyl-1,3,4-thiadiazol-2,5-amine

APPENDIX B

CRYSTALLOGRAPHIC STRUCTURAL DATA FOR *N*-[3,5-BIS(TRIFLUROMETHYL)PHENYL]PYRIDINE-2-THIOCARBOXAMIDE

Table A 4. Crystal data and structural refinement

Empirical formula	C14 H8 F6 N2 S
Formula weight	350.28
Temperature	293(2) K
Wavelength	0.71073 A
Crystal system space group	Monoclinic, C2/c
Unit cell dimensions	a = 14.326(3) A b = 8.5708(17) A c = 24.713(5) A beta = 103.10(3) deg.
Volume	2955.4(10) A^3
Z, Calculated density	8 , 1.575 Mg/m^3
Absorption coefficient	0.283 mm^-1
F(000)	1408
Crystal size	0.50 x 0.33 x 0.26 mm
Theta range for data collection	2.79 to 25.14 deg.
Limiting indices	-17<=h<=17, -9<=k<=10, -29<=l<=29
Reflections collected / unique	11020 / 2619 [R(int) = 0.0276]
Completeness to theta = 25.14	99.4 %
Absorption correction	Semi-empirical from equivalents
Max. and min. transmission	1.0000 and 0.8638
Refinement method	Full-matrix least-squares on F^2
Data / restraints / parameters	2619 / 0 / 236
Goodness-of-fit on F^2	1.043
Final R indices [I>2sigma(I)]	R1 = 0.0576, wR2 = 0.1401
R indices (all data)	R1 = 0.0656, wR2 = 0.1478
Extinction coefficient	0.0049(10)
Largest diff. peak and hole	0.284 and -0.260 e.A^-3

Table A 5. Atomic coordinates (x 10^4) and equivalent isotropic displacement parameters (A^2 x 10^3) for c2c. U(eq) is defined as one third of the trace of the orthogonalized Uij tensor.

	x	y	z	U(eq)
S(1)	3382(1)	6467(1)	-246(1)	76(1)
F(1)	4054(2)	9681(3)	1789(1)	146(1)
F(2)	4512(2)	10194(2)	1068(1)	122(1)
F(3)	5495(2)	10261(3)	1838(1)	145(1)
F(4)	6509(9)	5318(16)	2810(3)	136(5)
F(5)	6437(15)	3249(10)	2354(8)	187(8)
N(1)	3879(2)	1977(3)	-69(1)	70(1)
N(2)	4285(2)	4442(3)	523(1)	61(1)
C(1)	3664(3)	635(4)	-339(1)	85(1)
C(2)	3044(3)	532(4)	-850(2)	84(1)
C(3)	2636(2)	1857(4)	-1096(1)	85(1)
C(4)	2853(2)	3279(4)	-824(1)	70(1)
C(5)	3478(2)	3279(3)	-311(1)	56(1)
C(6)	3740(2)	4758(3)	17(1)	55(1)
C(7)	4709(2)	5392(3)	976(1)	56(1)
C(8)	4518(2)	6961(3)	1024(1)	62(1)
C(9)	4988(2)	7784(3)	1491(1)	62(1)
C(10)	5644(2)	7057(4)	1913(1)	67(1)
C(11)	5816(2)	5490(4)	1865(1)	66(1)
C(12)	5361(2)	4657(3)	1405(1)	63(1)
C(13)	4773(3)	9466(4)	1543(1)	81(1)
C(14)	6520(3)	4682(5)	2323(2)	95(1)
F(6)	7408(5)	5000(20)	2279(5)	149(4)
F(5A)	7083(11)	3740(20)	2130(4)	163(4)
F(6A)	7043(16)	5473(11)	2676(9)	212(9)
F(4A)	6075(8)	3665(19)	2580(5)	158(7)

Table A 6. Bond lengths [A] and angles [deg] for c2c.

S(1)-C(6)	1.637(3)
F(1)-C(13)	1.321(4)
F(2)-C(13)	1.308(4)
F(3)-C(13)	1.313(4)
F(4)-F(6A)	0.91(2)
F(4)-C(14)	1.326(9)
F(4)-F(4A)	1.599(16)
F(5)-F(4A)	0.92(2)
F(5)-C(14)	1.238(9)
F(5)-F(5A)	1.253(17)
N(1)-C(1)	1.330(4)
N(1)-C(5)	1.333(3)
N(2)-C(6)	1.344(3)
N(2)-C(7)	1.406(3)
N(2)-H(2A)	0.8600
C(1)-C(2)	1.373(5)
C(1)-H(1B)	0.9300
C(2)-C(3)	1.357(5)
C(2)-H(2B)	0.9300
C(3)-C(4)	1.392(4)
C(3)-H(3A)	0.9300
C(4)-C(5)	1.378(4)
C(4)-H(4A)	0.9300
C(5)-C(6)	1.505(4)
C(7)-C(8)	1.382(4)
C(7)-C(12)	1.396(3)
C(8)-C(9)	1.389(4)
C(8)-H(8A)	0.9300
C(9)-C(10)	1.383(4)
C(9)-C(13)	1.486(4)
C(10)-C(11)	1.375(4)
C(10)-H(10A)	0.9300
C(11)-C(12)	1.375(4)
C(11)-C(14)	1.502(4)
C(12)-H(12A)	0.9300
C(14)-F(6A)	1.220(9)
C(14)-F(5A)	1.308(11)
C(14)-F(4A)	1.325(11)
C(14)-F(6)	1.329(10)
F(6)-F(5A)	1.200(13)
F(6)-F(6A)	1.28(2)
F(6A)-F(4)-C(14)	62.9(10)
F(6A)-F(4)-F(4A)	106.9(13)

C(14)-F(4)-F(4A)	52.9(5)
F(4A)-F(5)-C(14)	74.2(11)
F(4A)-F(5)-F(5A)	135.8(15)
C(14)-F(5)-F(5A)	63.3(7)
C(1)-N(1)-C(5)	118.2(3)
C(6)-N(2)-C(7)	132.7(2)
C(6)-N(2)-H(2A)	113.6
C(7)-N(2)-H(2A)	113.6
N(1)-C(1)-C(2)	123.0(3)
N(1)-C(1)-H(1B)	118.5
C(2)-C(1)-H(1B)	118.5
C(3)-C(2)-C(1)	118.8(3)
C(3)-C(2)-H(2B)	120.6
C(1)-C(2)-H(2B)	120.6
C(2)-C(3)-C(4)	119.4(3)
C(2)-C(3)-H(3A)	120.3
C(4)-C(3)-H(3A)	120.3
C(5)-C(4)-C(3)	118.1(3)
C(5)-C(4)-H(4A)	120.9
C(3)-C(4)-H(4A)	120.9
N(1)-C(5)-C(4)	122.4(3)
N(1)-C(5)-C(6)	115.8(2)
C(4)-C(5)-C(6)	121.8(2)
N(2)-C(6)-C(5)	110.6(2)
N(2)-C(6)-S(1)	127.9(2)
C(5)-C(6)-S(1)	121.52(18)
C(8)-C(7)-C(12)	119.0(2)
C(8)-C(7)-N(2)	125.1(2)
C(12)-C(7)-N(2)	115.9(2)
C(7)-C(8)-C(9)	119.9(2)
C(7)-C(8)-H(8A)	120.1
C(9)-C(8)-H(8A)	120.1
C(10)-C(9)-C(8)	121.0(3)
C(10)-C(9)-C(13)	119.4(3)
C(8)-C(9)-C(13)	119.6(2)
C(11)-C(10)-C(9)	118.7(3)
C(11)-C(10)-H(10A)	120.7
C(9)-C(10)-H(10A)	120.7
C(12)-C(11)-C(10)	121.1(2)
C(12)-C(11)-C(14)	119.6(3)
C(10)-C(11)-C(14)	119.2(3)
C(11)-C(12)-C(7)	120.3(3)
C(11)-C(12)-H(12A)	119.9
C(7)-C(12)-H(12A)	119.9
F(2)-C(13)-F(3)	106.2(3)
F(2)-C(13)-F(1)	104.6(3)

F(3)-C(13)-F(1)	105.8(3)
F(2)-C(13)-C(9)	114.0(3)
F(3)-C(13)-C(9)	113.5(3)
F(1)-C(13)-C(9)	112.0(3)
F(6A)-C(14)-F(5)	123.9(7)
F(6A)-C(14)-F(5A)	106.0(10)
F(5)-C(14)-F(5A)	58.9(8)
F(6A)-C(14)-F(4A)	107.8(11)
F(5)-C(14)-F(4A)	41.7(10)
F(5A)-C(14)-F(4A)	99.8(8)
F(6A)-C(14)-F(4)	41.6(12)
F(5)-C(14)-F(4)	109.3(10)
F(5A)-C(14)-F(4)	136.2(6)
F(4A)-C(14)-F(4)	74.2(8)
F(6A)-C(14)-F(6)	60.1(10)
F(5)-C(14)-F(6)	108.2(10)
F(5A)-C(14)-F(6)	54.2(6)
F(4A)-C(14)-F(6)	138.2(7)
F(4)-C(14)-F(6)	101.5(7)
F(6A)-C(14)-C(11)	118.8(6)
F(5)-C(14)-C(11)	116.5(5)
F(5A)-C(14)-C(11)	112.1(5)
F(4A)-C(14)-C(11)	110.5(6)
F(4)-C(14)-C(11)	110.5(5)
F(6)-C(14)-C(11)	109.8(5)
F(5A)-F(6)-F(6A)	109.0(13)
F(5A)-F(6)-C(14)	62.0(7)
F(6A)-F(6)-C(14)	55.7(7)
F(6)-F(5A)-F(5)	116.0(14)
F(6)-F(5A)-C(14)	63.8(8)
F(5)-F(5A)-C(14)	57.8(7)
F(4)-F(6A)-C(14)	75.4(10)
F(4)-F(6A)-F(6)	139.1(13)
C(14)-F(6A)-F(6)	64.1(8)
F(5)-F(4A)-C(14)	64.1(10)
F(5)-F(4A)-F(4)	109.5(15)
C(14)-F(4A)-F(4)	52.9(6)

Symmetry transformations used to generate equivalent atoms:

Table A 7. Anisotropic displacement parameters (A^2 x 10^3) for c2c. The anisotropic displacement factor exponent takes the form: -2 pi^2 [h^2 a*^2 U11 + ... + 2 h k a* b* U12]

	U11	U22	U33	U23	U13	U12
S(1)	96(1)	61(1)	64(1)	3(1)	-1(1)	17(1)
F(1)	188(3)	117(2)	158(2)	3(2)	92(2)	57(2)
F(2)	209(3)	70(1)	76(1)	6(1)	8(1)	35(1)
F(3)	155(2)	81(2)	159(2)	-34(2)	-47(2)	9(1)
F(4)	180(9)	162(11)	49(2)	18(3)	-9(4)	74(9)
F(5)	220(16)	67(3)	193(14)	21(7)	-123(11)	0(8)
N(1)	84(2)	54(1)	68(1)	6(1)	9(1)	-5(1)
N(2)	69(1)	54(1)	56(1)	4(1)	2(1)	4(1)
C(1)	110(2)	57(2)	85(2)	2(2)	16(2)	-12(2)
C(2)	100(2)	72(2)	82(2)	-13(2)	23(2)	-19(2)
C(3)	89(2)	94(2)	66(2)	-15(2)	6(2)	-14(2)
C(4)	71(2)	74(2)	61(2)	-2(1)	5(1)	3(1)
C(5)	54(1)	60(2)	54(1)	3(1)	12(1)	-2(1)
C(6)	52(1)	60(2)	54(1)	2(1)	11(1)	2(1)
C(7)	54(1)	63(2)	50(1)	4(1)	7(1)	2(1)
C(8)	62(1)	65(2)	53(1)	3(1)	5(1)	9(1)
C(9)	67(2)	65(2)	52(1)	1(1)	9(1)	5(1)
C(10)	70(2)	75(2)	52(1)	2(1)	4(1)	1(1)
C(11)	66(2)	72(2)	55(2)	13(1)	1(1)	2(1)
C(12)	67(2)	59(2)	60(2)	10(1)	7(1)	4(1)
C(13)	99(2)	76(2)	59(2)	-9(1)	2(2)	14(2)
C(14)	97(3)	91(3)	79(2)	12(2)	-16(2)	16(2)
F(6)	75(3)	224(12)	127(6)	27(7)	-17(4)	34(5)
F(5A)	137(8)	190(11)	140(6)	36(8)	-17(6)	80(8)
F(6A)	226(15)	97(5)	213(15)	5(9)	-159(12)	-12(9)
F(4A)	154(6)	175(15)	132(8)	106(10)	7(5)	14(7)

Table A 8. Hydrogen coordinates (x 10^4) and isotropic displacement parameters (A^2 x 10^3) for c2c.

	x	y	z	U(eq)
H(2A)	4397	3463	582	74
H(1B)	3947	-276	-174	101
H(2B)	2905	-429	-1025	101
H(3A)	2215	1816	-1443	102
H(4A)	2584	4203	-985	84
H(8A)	4076	7464	745	74
H(10A)	5963	7617	2222	81
H(12A)	5489	3599	1380	76

Table A 9. Torsion angles [deg] for c2c.

C(5)-N(1)-C(1)-C(2)	-0.6(5)
N(1)-C(1)-C(2)-C(3)	0.7(5)
C(1)-C(2)-C(3)-C(4)	-0.2(5)
C(2)-C(3)-C(4)-C(5)	-0.2(5)
C(1)-N(1)-C(5)-C(4)	0.1(4)
C(1)-N(1)-C(5)-C(6)	179.4(3)
C(3)-C(4)-C(5)-N(1)	0.3(4)
C(3)-C(4)-C(5)-C(6)	-179.0(3)
C(7)-N(2)-C(6)-C(5)	179.8(2)
C(7)-N(2)-C(6)-S(1)	0.2(4)
N(1)-C(5)-C(6)-N(2)	-5.2(3)
C(4)-C(5)-C(6)-N(2)	174.2(2)
N(1)-C(5)-C(6)-S(1)	174.48(19)
C(4)-C(5)-C(6)-S(1)	-6.2(3)
C(6)-N(2)-C(7)-C(8)	10.9(4)
C(6)-N(2)-C(7)-C(12)	-169.8(3)
C(12)-C(7)-C(8)-C(9)	1.3(4)
N(2)-C(7)-C(8)-C(9)	-179.5(2)
C(7)-C(8)-C(9)-C(10)	-0.4(4)
C(7)-C(8)-C(9)-C(13)	-179.4(3)
C(8)-C(9)-C(10)-C(11)	-0.8(4)
C(13)-C(9)-C(10)-C(11)	178.2(3)
C(9)-C(10)-C(11)-C(12)	1.1(4)
C(9)-C(10)-C(11)-C(14)	-179.5(3)
C(10)-C(11)-C(12)-C(7)	-0.3(4)
C(14)-C(11)-C(12)-C(7)	-179.7(3)
C(8)-C(7)-C(12)-C(11)	-0.9(4)
N(2)-C(7)-C(12)-C(11)	179.8(2)
C(10)-C(9)-C(13)-F(2)	151.4(3)
C(8)-C(9)-C(13)-F(2)	-29.5(5)
C(10)-C(9)-C(13)-F(3)	29.6(4)
C(8)-C(9)-C(13)-F(3)	-151.3(3)
C(10)-C(9)-C(13)-F(1)	-90.0(4)
C(8)-C(9)-C(13)-F(1)	89.0(3)
F(4A)-F(5)-C(14)-F(6A)	78.4(18)
F(5A)-F(5)-C(14)-F(6A)	-89.0(14)
F(4A)-F(5)-C(14)-F(5A)	167.4(13)
F(5A)-F(5)-C(14)-F(4A)	-167.4(13)
F(4A)-F(5)-C(14)-F(4)	34.4(13)
F(5A)-F(5)-C(14)-F(4)	-133.0(9)
F(4A)-F(5)-C(14)-F(6)	144.1(11)
F(5A)-F(5)-C(14)-F(6)	-23.3(9)
F(4A)-F(5)-C(14)-C(11)	-91.6(12)
F(5A)-F(5)-C(14)-C(11)	100.9(7)
F(4A)-F(4)-C(14)-F(6A)	-142.8(13)

F(6A)-F(4)-C(14)-F(5)	119.8(13)
F(4A)-F(4)-C(14)-F(5)	-23.0(10)
F(6A)-F(4)-C(14)-F(5A)	55.1(18)
F(4A)-F(4)-C(14)-F(5A)	-87.7(13)
F(6A)-F(4)-C(14)-F(4A)	142.8(13)
F(6A)-F(4)-C(14)-F(6)	5.7(12)
F(4A)-F(4)-C(14)-F(6)	-137.2(7)
F(6A)-F(4)-C(14)-C(11)	-110.7(10)
F(4A)-F(4)-C(14)-C(11)	106.5(6)
C(12)-C(11)-C(14)-F(6A)	166.8(18)
C(10)-C(11)-C(14)-F(6A)	-12.6(19)
C(12)-C(11)-C(14)-F(5)	-22.6(18)
C(10)-C(11)-C(14)-F(5)	158.0(17)
C(12)-C(11)-C(14)-F(5A)	42.5(13)
C(10)-C(11)-C(14)-F(5A)	-136.9(12)
C(12)-C(11)-C(14)-F(4A)	-67.9(10)
C(10)-C(11)-C(14)-F(4A)	112.7(9)
C(12)-C(11)-C(14)-F(4)	-148.0(8)
C(10)-C(11)-C(14)-F(4)	32.6(9)
C(12)-C(11)-C(14)-F(6)	100.8(10)
C(10)-C(11)-C(14)-F(6)	-78.6(11)
F(6A)-C(14)-F(6)-F(5A)	143.9(10)
F(5)-C(14)-F(6)-F(5A)	24.7(10)
F(4A)-C(14)-F(6)-F(5A)	60.5(14)
F(4)-C(14)-F(6)-F(5A)	139.6(8)
C(11)-C(14)-F(6)-F(5A)	-103.5(7)
F(5)-C(14)-F(6)-F(6A)	-119.3(9)
F(5A)-C(14)-F(6)-F(6A)	-143.9(10)
F(4A)-C(14)-F(6)-F(6A)	-83.4(14)
F(4)-C(14)-F(6)-F(6A)	-4.3(9)
C(11)-C(14)-F(6)-F(6A)	112.6(7)
F(6A)-F(6)-F(5A)-F(5)	5.1(11)
C(14)-F(6)-F(5A)-F(5)	-25.8(7)
F(6A)-F(6)-F(5A)-C(14)	31.0(6)
F(4A)-F(5)-F(5A)-F(6)	10(2)
C(14)-F(5)-F(5A)-F(6)	27.5(7)
F(4A)-F(5)-F(5A)-C(14)	-17.5(17)
F(6A)-C(14)-F(5A)-F(6)	-32.1(10)
F(5)-C(14)-F(5A)-F(6)	-152.4(10)
F(4A)-C(14)-F(5A)-F(6)	-144.0(8)
F(4)-C(14)-F(5A)-F(6)	-66.6(14)
C(11)-C(14)-F(5A)-F(6)	99.0(7)
F(6A)-C(14)-F(5A)-F(5)	120.3(9)
F(4A)-C(14)-F(5A)-F(5)	8.5(9)
F(4)-C(14)-F(5A)-F(5)	85.8(15)
F(6)-C(14)-F(5A)-F(5)	152.4(10)

C(11)-C(14)-F(5A)-F(5)	-108.5(6)
F(4A)-F(4)-F(6A)-C(14)	30.3(8)
C(14)-F(4)-F(6A)-F(6)	-8.8(18)
F(4A)-F(4)-F(6A)-F(6)	21(2)
F(5)-C(14)-F(6A)-F(4)	-80.9(17)
F(5A)-C(14)-F(6A)-F(4)	-143.8(11)
F(4A)-C(14)-F(6A)-F(4)	-37.6(13)
F(6)-C(14)-F(6A)-F(4)	-173.6(13)
C(11)-C(14)-F(6A)-F(4)	89.0(13)
F(5)-C(14)-F(6A)-F(6)	92.7(14)
F(5A)-C(14)-F(6A)-F(6)	29.8(8)
F(4A)-C(14)-F(6A)-F(6)	136.0(9)
F(4)-C(14)-F(6A)-F(6)	173.6(13)
C(11)-C(14)-F(6A)-F(6)	-97.4(8)
F(5A)-F(6)-F(6A)-F(4)	-24(2)
C(14)-F(6)-F(6A)-F(4)	9.5(19)
F(5A)-F(6)-F(6A)-C(14)	-33.4(7)
F(5A)-F(5)-F(4A)-C(14)	16.2(16)
C(14)-F(5)-F(4A)-F(4)	-28.0(8)
F(5A)-F(5)-F(4A)-F(4)	-12(2)
F(6A)-C(14)-F(4A)-F(5)	-121.4(13)
F(5A)-C(14)-F(4A)-F(5)	-10.9(12)
F(4)-C(14)-F(4A)-F(5)	-146.3(12)
F(6)-C(14)-F(4A)-F(5)	-56.6(17)
C(11)-C(14)-F(4A)-F(5)	107.3(10)
F(6A)-C(14)-F(4A)-F(4)	24.9(10)
F(5)-C(14)-F(4A)-F(4)	146.3(12)
F(5A)-C(14)-F(4A)-F(4)	135.4(7)
F(6)-C(14)-F(4A)-F(4)	89.7(12)
C(11)-C(14)-F(4A)-F(4)	-106.4(6)
F(6A)-F(4)-F(4A)-F(5)	-2.3(18)
C(14)-F(4)-F(4A)-F(5)	31.9(11)
F(6A)-F(4)-F(4A)-C(14)	-34.2(11)

Symmetry transformations used to generate equivalent atoms:

APPENDIX C

CRYSTALLOGRAPHIC STRUCTURAL DATA FOR [VO(ODA)(PHEN)]·1.5H_2O

Table A 10. Crystal data and structural refinement for [VO(oda)(phen)]·1.5H_2O

Identification code	c2
Empirical formula	C16 H15 N2 O7.50 V
Formula weight	406.24
Temperature	293(2) K
Wavelength	0.71073 A
Crystal system space group	Monoclinic, C2/m
Unit cell dimensions	a = 18.214(4) A b = 12.857(3) A c = 7.1924(14) A beta = 90.10(3) deg.
Volume	1684.3(6) A^3
Z Calculated density	4, 1.602 Mg/m^3
Absorption coefficient	0.636 mm^-1
F(000)	832
Crystal size	0.31 x 0.04 x 0.04 mm
Theta range for data collection	3.17 to 25.02 deg.
Limiting indices	-21<=h<=21, -15<=k<=15, -8<=l<=7
Reflections collected / unique	7112 / 1572 [R(int) = 0.0595]
Completeness to theta = 25.02	99.7 %
Max. and min. transmission	0.9750 and 0.8273
Refinement method	Full-matrix least-squares on F^2
Data / restraints / parameters	1572 / 0 / 129
Goodness-of-fit on F^2	1.036
Final R indices [I>2sigma(I)]	R1 = 0.0787, wR2 = 0.1588
R indices (all data)	R1 = 0.1055, wR2 = 0.1882
Extinction coefficient	0.0039(9)
Largest diff. peak and hole	0.456 and -0.751 e.A^-3

Table A 11. Atomic coordinates (x 10^4) and equivalent isotropic displacement parameters (A^2 x 10^3) for c2. U(eq) is defined as one third of the trace of the orthogonalized Uij tensor

	x	y	z	U(eq)
V(1)	2275(1)	0	4058(3)	59(1)
O(3)	2319(4)	0	860(10)	47(2)
O(2)	2993(3)	-1105(5)	3502(10)	66(2)
O(1)	2309(6)	0	6307(12)	95(3)
O(4)	3461(4)	-2236(5)	1424(12)	93(3)
N(1)	1399(3)	1043(6)	3492(10)	58(2)
C(1)	1401(5)	2072(8)	3601(15)	75(3)
C(2)	785(5)	2682(8)	3149(16)	79(3)
C(3)	141(4)	2194(7)	2685(14)	73(3)
C(4)	115(4)	1099(6)	2586(12)	53(2)
C(5)	755(4)	553(7)	2992(11)	53(2)
C(6)	-539(4)	529(7)	2094(14)	69(3)
C(7)	3080(4)	-1461(7)	1798(14)	59(2)
C(8)	2664(5)	-946(6)	233(13)	63(2)
O(7W)	422(6)	5000	6580(20)	120(5)
O(8W)	450(40)	5000	9980(140)	380(40)

Table A 12. Bond lengths [A] and angles [deg] for c2.

V(1)-O(1)	1.619(9)
V(1)-O(2)#1	1.973(6)
V(1)-O(2)	1.973(6)
V(1)-N(1)#1	2.123(7)
V(1)-N(1)	2.123(7)
V(1)-O(3)	2.302(7)
O(3)-C(8)#1	1.442(8)
O(3)-C(8)	1.442(8)
O(2)-C(7)	1.319(11)
O(4)-C(7)	1.243(10)
N(1)-C(1)	1.325(11)
N(1)-C(5)	1.378(9)
C(1)-C(2)	1.407(12)
C(1)-H(1)	0.9300
C(2)-C(3)	1.370(11)
C(2)-H(2)	0.9300
C(3)-C(4)	1.410(12)
C(3)-H(3)	0.9300
C(4)-C(5)	1.392(10)
C(4)-C(6)	1.442(11)
C(5)-C(5)#1	1.422(17)
C(6)-C(6)#1	1.360(19)
C(6)-H(6)	0.9300
C(7)-C(8)	1.508(11)
C(8)-H(8A)	0.9700
C(8)-H(8B)	0.9700
O(1)-V(1)-O(2)#1	100.2(3)
O(1)-V(1)-O(2)	100.2(3)
O(2)#1-V(1)-O(2)	92.1(4)
O(1)-V(1)-N(1)#1	102.7(4)
O(2)#1-V(1)-N(1)#1	156.1(3)
O(2)-V(1)-N(1)#1	90.3(2)
O(1)-V(1)-N(1)	102.7(4)
O(2)#1-V(1)-N(1)	90.3(2)
O(2)-V(1)-N(1)	156.1(3)
N(1)#1-V(1)-N(1)	78.4(4)
O(1)-V(1)-O(3)	175.8(4)
O(2)#1-V(1)-O(3)	76.9(2)
O(2)-V(1)-O(3)	76.9(2)
N(1)#1-V(1)-O(3)	80.6(2)
N(1)-V(1)-O(3)	80.6(2)
C(8)#1-O(3)-C(8)	115.1(9)
C(8)#1-O(3)-V(1)	109.2(5)
C(8)-O(3)-V(1)	109.2(5)

C(7)-O(2)-V(1)	121.3(5)
C(1)-N(1)-C(5)	118.3(7)
C(1)-N(1)-V(1)	128.1(6)
C(5)-N(1)-V(1)	113.6(6)
N(1)-C(1)-C(2)	122.7(9)
N(1)-C(1)-H(1)	118.6
C(2)-C(1)-H(1)	118.6
C(3)-C(2)-C(1)	118.9(9)
C(3)-C(2)-H(2)	120.6
C(1)-C(2)-H(2)	120.6
C(2)-C(3)-C(4)	119.9(8)
C(2)-C(3)-H(3)	120.1
C(4)-C(3)-H(3)	120.1
C(5)-C(4)-C(3)	117.7(7)
C(5)-C(4)-C(6)	119.1(7)
C(3)-C(4)-C(6)	123.2(7)
N(1)-C(5)-C(4)	122.4(8)
N(1)-C(5)-C(5)#1	117.2(5)
C(4)-C(5)-C(5)#1	120.3(5)
C(6)#1-C(6)-C(4)	120.6(5)
C(6)#1-C(6)-H(6)	119.7
C(4)-C(6)-H(6)	119.7
O(4)-C(7)-O(2)	123.2(9)
O(4)-C(7)-C(8)	118.1(9)
O(2)-C(7)-C(8)	118.7(7)
O(3)-C(8)-C(7)	110.9(7)
O(3)-C(8)-H(8A)	109.5
C(7)-C(8)-H(8A)	109.5
O(3)-C(8)-H(8B)	109.5
C(7)-C(8)-H(8B)	109.5
H(8A)-C(8)-H(8B)	108.1

Symmetry transformations used to generate equivalent atoms: #1 x,-y,z #2 -x,-y+1,-z+2

Table A 13. Anisotropic displacement parameters (A^2 x 10^3) for c2. The anisotropic displacement factor exponent takes the form: -2 pi^2 [h^2 a*^2 U11 + ... + 2 h k a* b* U12]

	U11	U22	U33	U23	U13	U12
V(1)	37(1)	80(1)	61(1)	0	-7(1)	0
O(3)	44(4)	32(3)	63(4)	0	11(5)	0
O(2)	41(3)	70(4)	87(5)	20(4)	-9(3)	7(3)
O(1)	71(6)	170(11)	44(5)	0	-13(5)	0
O(4)	77(4)	73(4)	128(7)	-23(4)	-31(5)	36(4)
N(1)	40(3)	71(5)	63(5)	-17(4)	-4(3)	7(3)
C(1)	53(5)	76(6)	95(8)	-31(6)	-6(5)	0(5)
C(2)	68(6)	67(6)	101(8)	-28(6)	-5(5)	17(5)
C(3)	53(5)	85(6)	80(6)	-12(6)	12(5)	26(5)
C(4)	32(3)	78(5)	49(4)	-4(5)	6(4)	7(3)
C(5)	34(3)	75(5)	51(5)	-2(4)	1(3)	3(4)
C(6)	33(3)	101(7)	72(6)	3(5)	13(4)	11(4)
C(7)	42(4)	56(5)	78(6)	-1(4)	-13(4)	-3(4)
C(8)	66(5)	45(4)	77(6)	-11(4)	1(5)	17(4)
O(7W)	67(6)	169(13)	124(11)	0	-5(7)	0

Table A 14. Hydrogen coordinates (x 10^4) and isotropic displacement parameters (A^2 x 10^3) for c2.

	x	y	z	U(eq)
H(1)	1828	2405	3991	90
H(2)	813	3404	3165	94
H(3)	-278	2584	2436	87
H(6)	-964	887	1775	83
H(8A)	3000	-789	-775	75
H(8B)	2293	-1419	-236	75
H(7W)	38	4435	6225	215
H(8W)	292	4374	9995	200

Table A 15. Torsion angles [deg] for c2.

O(1)-V(1)-O(3)-C(8)#1	-63.3(5)
O(2)#1-V(1)-O(3)-C(8)#1	-15.6(5)
O(2)-V(1)-O(3)-C(8)#1	-110.9(5)
N(1)#1-V(1)-O(3)-C(8)#1	156.5(5)
N(1)-V(1)-O(3)-C(8)#1	76.9(5)
O(1)-V(1)-O(3)-C(8)	63.3(5)
O(2)#1-V(1)-O(3)-C(8)	110.9(5)
O(2)-V(1)-O(3)-C(8)	15.6(5)
N(1)#1-V(1)-O(3)-C(8)	-76.9(5)
N(1)-V(1)-O(3)-C(8)	-156.5(5)
O(1)-V(1)-O(2)-C(7)	171.7(7)
O(2)#1-V(1)-O(2)-C(7)	-87.5(7)
N(1)#1-V(1)-O(2)-C(7)	68.8(7)
N(1)-V(1)-O(2)-C(7)	8.0(11)
O(3)-V(1)-O(2)-C(7)	-11.5(6)
O(1)-V(1)-N(1)-C(1)	75.3(9)
O(2)#1-V(1)-N(1)-C(1)	-25.2(9)
O(2)-V(1)-N(1)-C(1)	-121.1(10)
N(1)#1-V(1)-N(1)-C(1)	175.9(8)
O(3)-V(1)-N(1)-C(1)	-101.9(9)
O(1)-V(1)-N(1)-C(5)	-103.2(6)
O(2)#1-V(1)-N(1)-C(5)	156.2(6)
O(2)-V(1)-N(1)-C(5)	60.4(10)
N(1)#1-V(1)-N(1)-C(5)	-2.7(7)
O(3)-V(1)-N(1)-C(5)	79.6(6)
C(5)-N(1)-C(1)-C(2)	-2.8(16)
V(1)-N(1)-C(1)-C(2)	178.7(8)
N(1)-C(1)-C(2)-C(3)	4.0(17)
C(1)-C(2)-C(3)-C(4)	-2.8(16)
C(2)-C(3)-C(4)-C(5)	0.7(14)
C(2)-C(3)-C(4)-C(6)	-179.5(9)
C(1)-N(1)-C(5)-C(4)	0.6(13)
V(1)-N(1)-C(5)-C(4)	179.3(6)
C(1)-N(1)-C(5)-C(5)#1	-176.4(7)
V(1)-N(1)-C(5)-C(5)#1	2.3(6)
C(3)-C(4)-C(5)-N(1)	0.5(13)
C(6)-C(4)-C(5)-N(1)	-179.3(8)
C(3)-C(4)-C(5)-C(5)#1	177.4(6)
C(6)-C(4)-C(5)-C(5)#1	-2.4(10)
C(5)-C(4)-C(6)-C(6)#1	2.4(10)
C(3)-C(4)-C(6)-C(6)#1	-177.3(7)
V(1)-O(2)-C(7)-O(4)	-171.2(6)
V(1)-O(2)-C(7)-C(8)	5.1(11)
C(8)#1-O(3)-C(8)-C(7)	106.1(9)

V(1)-O(3)-C(8)-C(7)	-17.1(8)
O(4)-C(7)-C(8)-O(3)	-173.6(8)
O(2)-C(7)-C(8)-O(3)	9.8(11)

Symmetry transformations used to generate equivalent atoms: #1 x,-y,z #2 -x,-y+1,-z+2

APPENDIX D

CRYSTALLOGRAPHIC STRUCTURAL DATA FOR $[Co(PHEN)_3]^{2+}$ OBTAINED FROM ATTEMPTED CRYSTALLIZATION OF $[Co(PHEN)_2(APTA)](PF_6)_3$

Table A 16. Crystal data and structural refinement for $[Co(phen)_3]^{2+}$

Empirical formula	C40 H30 Co F12 N8 P2
Formula weight	971.59
Temperature	293(2) K
Wavelength	0.71073 A
Crystal system space group	Triclinic P-1
Unit cell dimensions	a = 13.019(3) A b = 13.276(3) A c = 14.573(3) A alpha = 69.16(3) deg. beta = 70.78(3) deg. gamma = 68.86(3) deg.
Volume	2136.3(7) A^3
Z, Calculated density	2, 1.510 Mg/m^3
Absorption coefficient	0.570 mm^-1
F(000)	982
Crystal size	0.43 x 0.32 x 0.24 mm
Theta range for data collection	1.72 to 25.15 deg.
Limiting indices	-15<=h<=15, -15<=k<=14, -17<=l<=15
Reflections collected / unique	18249 / 7578 [R(int) = 0.0374]
Completeness to theta = 25.15	99.0 %
Max. and min. transmission	0.8754 and 0.7918
Refinement method	Full-matrix least-squares on F^2
Data / restraints / parameters	7578 / 0 / 515
Goodness-of-fit on F^2	1.174
Final R indices [I>2sigma(I)]	R1 = 0.1072, wR2 = 0.2604
R indices (all data)	R1 = 0.1291, wR2 = 0.2782
Extinction coefficient	0.0034(15)
Largest diff. peak and hole	1.192 and -0.717 e.A^-3

2 highly disordered MeCN molecules per formula unit modeled by SQUEEZE, corresponding to 88 electrons per unit cell. PLATON identified 87 electrons located in solvent accessible voids in the unit cell of this structure.

Table A 17. Atomic coordinates (x 10^4) and equivalent isotropic displacement parameters (A^2 x 10^3) for p-1_sqd. U(eq) is defined as one third of the trace of the orthogonalized Uij tensor.

	x	y	z	U(eq)
Co(1)	3099(1)	3081(1)	3020(1)	57(1)
N(1)	4236(4)	4062(4)	2099(4)	59(1)
N(2)	4109(4)	2145(4)	1968(4)	59(1)
N(3)	4125(4)	2159(4)	4091(4)	59(1)
N(4)	2195(4)	1911(4)	4015(4)	56(1)
N(5)	2110(4)	4272(4)	3874(4)	67(1)
N(6)	1862(4)	4102(4)	2172(4)	63(1)
C(1)	4276(6)	5028(5)	2153(5)	71(2)
C(2)	5120(6)	5541(6)	1555(6)	76(2)
C(3)	5974(7)	5024(7)	890(6)	84(2)
C(4)	5972(5)	4010(6)	784(5)	69(2)
C(5)	5075(5)	3573(5)	1410(4)	58(1)
C(6)	6809(6)	3435(7)	91(6)	84(2)
C(7)	6746(6)	2472(7)	31(6)	81(2)
C(8)	5841(6)	1992(6)	635(5)	69(2)
C(9)	5010(5)	2535(5)	1333(5)	59(1)
C(10)	5713(6)	1021(6)	566(6)	78(2)
C(11)	4813(7)	641(6)	1174(6)	81(2)
C(12)	4032(6)	1206(5)	1882(5)	65(2)
C(13)	5085(5)	2270(6)	4132(6)	70(2)
C(14)	5594(6)	1737(6)	4946(6)	77(2)
C(15)	5067(6)	1057(6)	5769(6)	79(2)
C(16)	4052(6)	897(5)	5778(5)	68(2)
C(17)	3620(5)	1459(5)	4915(4)	57(1)
C(18)	3447(7)	185(6)	6619(5)	82(2)
C(19)	2482(7)	46(6)	6561(5)	79(2)
C(20)	2039(6)	609(5)	5687(5)	65(2)
C(21)	2584(5)	1317(5)	4866(4)	54(1)
C(22)	1024(6)	520(6)	5601(6)	72(2)
C(23)	655(6)	1096(6)	4757(6)	72(2)
C(24)	1249(5)	1796(5)	3968(5)	64(2)
C(25)	2214(7)	4358(7)	4718(6)	85(2)
C(26)	1605(9)	5240(9)	5140(8)	111(3)
C(27)	865(10)	6091(9)	4655(10)	125(4)
C(28)	684(7)	6071(6)	3771(9)	100(3)
C(29)	1331(5)	5121(5)	3404(6)	74(2)
C(30)	1202(5)	5040(5)	2488(6)	75(2)
C(31)	440(6)	5892(7)	1952(9)	99(3)

C(32)	370(8)	5759(9)	1069(9)	119(4)
C(33)	995(8)	4838(9)	769(7)	103(3)
C(34)	1751(6)	3996(7)	1326(6)	81(2)
P(1)	2660(2)	8449(2)	2830(2)	84(1)
F(1)	2558(13)	7667(11)	3898(8)	271(7)
F(2)	2744(9)	9275(9)	1789(6)	220(5)
F(3)	2786(11)	7476(10)	2506(10)	272(6)
F(4)	3880(8)	8290(11)	2705(12)	286(7)
F(5)	2556(14)	9415(10)	3206(9)	293(8)
F(6)	1430(6)	8658(9)	3069(10)	253(6)
P(2)	8402(2)	3233(2)	2606(2)	83(1)
F(7)	9104(8)	3677(7)	2950(7)	180(3)
F(8)	7680(16)	3162(17)	3532(13)	427(14)
F(10)	9084(12)	2062(7)	2906(10)	260(6)
F(12)	9067(16)	3410(13)	1590(8)	341(10)
F(9)	7676(12)	2753(10)	2345(11)	286(7)
C(35)	-204(9)	6843(9)	2352(12)	126(5)
C(36)	-91(9)	6939(8)	3137(13)	132(5)
F(11)	7851(15)	4429(9)	2196(17)	359(11)

Table A 18. Bond lengths [A] and angles [deg] for p-1_sqd.

Co(1)-N(2)	2.114(5)
Co(1)-N(4)	2.119(5)
Co(1)-N(6)	2.121(5)
Co(1)-N(1)	2.129(5)
Co(1)-N(3)	2.135(5)
Co(1)-N(5)	2.141(5)
N(1)-C(1)	1.332(8)
N(1)-C(5)	1.361(8)
N(2)-C(12)	1.338(8)
N(2)-C(9)	1.372(8)
N(3)-C(13)	1.332(8)
N(3)-C(17)	1.365(8)
N(4)-C(24)	1.320(7)
N(4)-C(21)	1.359(7)
N(5)-C(25)	1.328(9)
N(5)-C(29)	1.360(9)
N(6)-C(34)	1.347(9)
N(6)-C(30)	1.371(9)
C(1)-C(2)	1.385(9)
C(1)-H(1A)	0.9300
C(2)-C(3)	1.364(11)
C(2)-H(2A)	0.9300
C(3)-C(4)	1.409(10)
C(3)-H(3A)	0.9300
C(4)-C(5)	1.395(8)
C(4)-C(6)	1.419(10)
C(5)-C(9)	1.456(8)
C(6)-C(7)	1.345(11)
C(6)-H(6A)	0.9300
C(7)-C(8)	1.425(10)
C(7)-H(7A)	0.9300
C(8)-C(10)	1.398(10)
C(8)-C(9)	1.400(9)
C(10)-C(11)	1.355(10)
C(10)-H(10A)	0.9300
C(11)-C(12)	1.403(9)
C(11)-H(11A)	0.9300
C(12)-H(12A)	0.9300
C(13)-C(14)	1.390(9)
C(13)-H(13A)	0.9300
C(14)-C(15)	1.363(10)
C(14)-H(14A)	0.9300
C(15)-C(16)	1.407(10)
C(15)-H(15A)	0.9300
C(16)-C(17)	1.396(8)

C(16)-C(18)	1.446(10)
C(17)-C(21)	1.455(8)
C(18)-C(19)	1.367(11)
C(18)-H(18A)	0.9300
C(19)-C(20)	1.417(10)
C(19)-H(19A)	0.9300
C(20)-C(21)	1.393(8)
C(20)-C(22)	1.417(9)
C(22)-C(23)	1.337(10)
C(22)-H(22A)	0.9300
C(23)-C(24)	1.398(9)
C(23)-H(23A)	0.9300
C(24)-H(24A)	0.9300
C(25)-C(26)	1.378(11)
C(25)-H(25A)	0.9300
C(26)-C(27)	1.341(16)
C(26)-H(26A)	0.9300
C(27)-C(28)	1.396(15)
C(27)-H(27A)	0.9300
C(28)-C(29)	1.414(11)
C(28)-C(36)	1.489(17)
C(29)-C(30)	1.444(11)
C(30)-C(31)	1.394(10)
C(31)-C(32)	1.395(15)
C(31)-C(35)	1.441(16)
C(32)-C(33)	1.333(15)
C(32)-H(32A)	0.9300
C(33)-C(34)	1.402(11)
C(33)-H(33A)	0.9300
C(34)-H(34A)	0.9300
P(1)-F(6)	1.463(7)
P(1)-F(3)	1.466(8)
P(1)-F(4)	1.482(9)
P(1)-F(5)	1.513(8)
P(1)-F(2)	1.520(7)
P(1)-F(1)	1.527(8)
P(2)-F(8)	1.361(10)
P(2)-F(12)	1.432(8)
P(2)-F(10)	1.474(8)
P(2)-F(11)	1.476(9)
P(2)-F(9)	1.512(7)
P(2)-F(7)	1.529(7)
C(35)-C(36)	1.254(17)
C(35)-H(35)	0.9300
C(36)-H(36A)	0.9300

N(2)-Co(1)-N(4)	98.03(18)
N(2)-Co(1)-N(6)	95.9(2)
N(4)-Co(1)-N(6)	97.48(19)
N(2)-Co(1)-N(1)	78.54(19)
N(4)-Co(1)-N(1)	170.87(18)
N(6)-Co(1)-N(1)	91.31(19)
N(2)-Co(1)-N(3)	94.03(19)
N(4)-Co(1)-N(3)	78.50(19)
N(6)-Co(1)-N(3)	169.8(2)
N(1)-Co(1)-N(3)	93.23(19)
N(2)-Co(1)-N(5)	170.3(2)
N(4)-Co(1)-N(5)	90.67(19)
N(6)-Co(1)-N(5)	78.6(2)
N(1)-Co(1)-N(5)	93.5(2)
N(3)-Co(1)-N(5)	92.0(2)
C(1)-N(1)-C(5)	117.1(5)
C(1)-N(1)-Co(1)	129.2(5)
C(5)-N(1)-Co(1)	113.5(4)
C(12)-N(2)-C(9)	116.6(5)
C(12)-N(2)-Co(1)	129.4(4)
C(9)-N(2)-Co(1)	113.9(4)
C(13)-N(3)-C(17)	116.7(5)
C(13)-N(3)-Co(1)	129.9(4)
C(17)-N(3)-Co(1)	112.7(4)
C(24)-N(4)-C(21)	117.5(5)
C(24)-N(4)-Co(1)	128.4(4)
C(21)-N(4)-Co(1)	113.5(4)
C(25)-N(5)-C(29)	116.7(7)
C(25)-N(5)-Co(1)	130.3(5)
C(29)-N(5)-Co(1)	112.7(5)
C(34)-N(6)-C(30)	118.5(6)
C(34)-N(6)-Co(1)	127.9(5)
C(30)-N(6)-Co(1)	113.1(5)
N(1)-C(1)-C(2)	123.5(7)
N(1)-C(1)-H(1A)	118.2
C(2)-C(1)-H(1A)	118.2
C(3)-C(2)-C(1)	118.7(7)
C(3)-C(2)-H(2A)	120.6
C(1)-C(2)-H(2A)	120.6
C(2)-C(3)-C(4)	120.6(6)
C(2)-C(3)-H(3A)	119.7
C(4)-C(3)-H(3A)	119.7
C(5)-C(4)-C(3)	116.1(7)
C(5)-C(4)-C(6)	119.7(6)
C(3)-C(4)-C(6)	124.2(7)
N(1)-C(5)-C(4)	123.9(6)

N(1)-C(5)-C(9)	117.0(5)
C(4)-C(5)-C(9)	119.1(6)
C(7)-C(6)-C(4)	120.7(6)
C(7)-C(6)-H(6A)	119.7
C(4)-C(6)-H(6A)	119.7
C(6)-C(7)-C(8)	122.4(7)
C(6)-C(7)-H(7A)	118.8
C(8)-C(7)-H(7A)	118.8
C(10)-C(8)-C(9)	117.5(6)
C(10)-C(8)-C(7)	124.4(7)
C(9)-C(8)-C(7)	118.1(6)
N(2)-C(9)-C(8)	123.6(6)
N(2)-C(9)-C(5)	116.5(5)
C(8)-C(9)-C(5)	119.9(6)
C(11)-C(10)-C(8)	119.5(7)
C(11)-C(10)-H(10A)	120.2
C(8)-C(10)-H(10A)	120.2
C(10)-C(11)-C(12)	120.0(7)
C(10)-C(11)-H(11A)	120.0
C(12)-C(11)-H(11A)	120.0
N(2)-C(12)-C(11)	122.7(6)
N(2)-C(12)-H(12A)	118.6
C(11)-C(12)-H(12A)	118.6
N(3)-C(13)-C(14)	124.9(7)
N(3)-C(13)-H(13A)	117.6
C(14)-C(13)-H(13A)	117.6
C(15)-C(14)-C(13)	117.6(7)
C(15)-C(14)-H(14A)	121.2
C(13)-C(14)-H(14A)	121.2
C(14)-C(15)-C(16)	120.7(6)
C(14)-C(15)-H(15A)	119.7
C(16)-C(15)-H(15A)	119.7
C(17)-C(16)-C(15)	117.2(6)
C(17)-C(16)-C(18)	118.9(6)
C(15)-C(16)-C(18)	123.9(6)
N(3)-C(17)-C(16)	123.0(6)
N(3)-C(17)-C(21)	116.9(5)
C(16)-C(17)-C(21)	120.1(6)
C(19)-C(18)-C(16)	120.5(6)
C(19)-C(18)-H(18A)	119.7
C(16)-C(18)-H(18A)	119.7
C(18)-C(19)-C(20)	121.0(7)
C(18)-C(19)-H(19A)	119.5
C(20)-C(19)-H(19A)	119.5
C(21)-C(20)-C(22)	116.4(6)
C(21)-C(20)-C(19)	120.4(6)

C(22)-C(20)-C(19)	123.2(6)
N(4)-C(21)-C(20)	123.9(5)
N(4)-C(21)-C(17)	117.1(5)
C(20)-C(21)-C(17)	119.1(5)
C(23)-C(22)-C(20)	119.3(6)
C(23)-C(22)-H(22A)	120.3
C(20)-C(22)-H(22A)	120.3
C(22)-C(23)-C(24)	120.7(6)
C(22)-C(23)-H(23A)	119.7
C(24)-C(23)-H(23A)	119.7
N(4)-C(24)-C(23)	122.2(6)
N(4)-C(24)-H(24A)	118.9
C(23)-C(24)-H(24A)	118.9
N(5)-C(25)-C(26)	125.0(9)
N(5)-C(25)-H(25A)	117.5
C(26)-C(25)-H(25A)	117.5
C(27)-C(26)-C(25)	117.9(10)
C(27)-C(26)-H(26A)	121.0
C(25)-C(26)-H(26A)	121.0
C(26)-C(27)-C(28)	121.3(8)
C(26)-C(27)-H(27A)	119.4
C(28)-C(27)-H(27A)	119.4
C(27)-C(28)-C(29)	116.8(9)
C(27)-C(28)-C(36)	128.3(10)
C(29)-C(28)-C(36)	114.9(11)
N(5)-C(29)-C(28)	122.2(8)
N(5)-C(29)-C(30)	117.5(6)
C(28)-C(29)-C(30)	120.2(8)
N(6)-C(30)-C(31)	122.1(9)
N(6)-C(30)-C(29)	117.2(6)
C(31)-C(30)-C(29)	120.8(8)
C(30)-C(31)-C(32)	117.5(9)
C(30)-C(31)-C(35)	117.2(11)
C(32)-C(31)-C(35)	125.3(9)
C(33)-C(32)-C(31)	120.6(8)
C(33)-C(32)-H(32A)	119.7
C(31)-C(32)-H(32A)	119.7
C(32)-C(33)-C(34)	120.5(10)
C(32)-C(33)-H(33A)	119.8
C(34)-C(33)-H(33A)	119.8
N(6)-C(34)-C(33)	120.8(9)
N(6)-C(34)-H(34A)	119.6
C(33)-C(34)-H(34A)	119.6
F(6)-P(1)-F(3)	89.0(7)
F(6)-P(1)-F(4)	172.4(10)
F(3)-P(1)-F(4)	97.2(9)

F(6)-P(1)-F(5)	92.1(8)
F(3)-P(1)-F(5)	177.2(10)
F(4)-P(1)-F(5)	81.5(8)
F(6)-P(1)-F(2)	95.8(7)
F(3)-P(1)-F(2)	96.6(7)
F(4)-P(1)-F(2)	87.9(6)
F(5)-P(1)-F(2)	85.8(7)
F(6)-P(1)-F(1)	83.8(7)
F(3)-P(1)-F(1)	86.2(7)
F(4)-P(1)-F(1)	92.2(8)
F(5)-P(1)-F(1)	91.4(7)
F(2)-P(1)-F(1)	177.2(7)
F(8)-P(2)-F(12)	173.8(14)
F(8)-P(2)-F(10)	93.0(12)
F(12)-P(2)-F(10)	92.9(10)
F(8)-P(2)-F(11)	94.2(12)
F(12)-P(2)-F(11)	80.0(10)
F(10)-P(2)-F(11)	172.3(11)
F(8)-P(2)-F(9)	87.6(9)
F(12)-P(2)-F(9)	90.8(9)
F(10)-P(2)-F(9)	85.5(7)
F(11)-P(2)-F(9)	97.4(7)
F(8)-P(2)-F(7)	88.7(9)
F(12)-P(2)-F(7)	93.1(7)
F(10)-P(2)-F(7)	93.0(6)
F(11)-P(2)-F(7)	84.6(6)
F(9)-P(2)-F(7)	175.9(7)
C(36)-C(35)-C(31)	123.0(11)
C(36)-C(35)-H(35)	118.5
C(31)-C(35)-H(35)	118.5
C(35)-C(36)-C(28)	123.8(11)
C(35)-C(36)-H(36A)	118.1
C(28)-C(36)-H(36A)	118.1

Symmetry transformations used to generate equivalent atoms:

Table A 19. Anisotropic displacement parameters (A^2 x 10^3) for p-1_sqd. The anisotropic displacement factor exponent takes the form: -2 pi^2 [h^2 a*^2 U11 + ... + 2 h k a* b* U12]

	U11	U22	U33	U23	U13	U12
Co(1)	52(1)	55(1)	60(1)	-13(1)	-12(1)	-15(1)
N(1)	61(3)	55(3)	62(3)	-12(2)	-14(2)	-20(2)
N(2)	53(3)	61(3)	61(3)	-12(2)	-13(2)	-18(2)
N(3)	54(3)	59(3)	66(3)	-16(2)	-15(2)	-16(2)
N(4)	52(3)	55(3)	61(3)	-18(2)	-11(2)	-16(2)
N(5)	60(3)	67(3)	69(3)	-24(3)	-4(2)	-17(2)
N(6)	56(3)	63(3)	69(3)	-2(2)	-20(2)	-24(2)
C(1)	70(4)	60(4)	81(4)	-17(3)	-15(3)	-22(3)
C(2)	81(5)	67(4)	85(5)	-3(4)	-23(4)	-39(4)
C(3)	74(5)	88(5)	97(5)	-7(4)	-20(4)	-47(4)
C(4)	57(4)	76(4)	70(4)	-9(3)	-15(3)	-23(3)
C(5)	49(3)	63(3)	60(3)	-7(3)	-19(3)	-18(3)
C(6)	58(4)	111(6)	77(5)	-19(4)	1(3)	-38(4)
C(7)	62(4)	104(6)	76(5)	-34(4)	0(3)	-26(4)
C(8)	62(4)	74(4)	65(4)	-20(3)	-10(3)	-14(3)
C(9)	52(3)	64(3)	59(3)	-14(3)	-16(3)	-12(3)
C(10)	74(4)	84(5)	77(5)	-39(4)	-12(4)	-11(4)
C(11)	94(5)	74(4)	77(5)	-30(4)	-9(4)	-25(4)
C(12)	72(4)	63(4)	66(4)	-21(3)	-18(3)	-21(3)
C(13)	56(3)	72(4)	87(5)	-21(3)	-20(3)	-20(3)
C(14)	64(4)	92(5)	81(5)	-23(4)	-28(3)	-17(4)
C(15)	75(4)	83(5)	84(5)	-24(4)	-38(4)	-9(4)
C(16)	76(4)	60(3)	67(4)	-18(3)	-27(3)	-8(3)
C(17)	54(3)	56(3)	59(3)	-20(3)	-13(3)	-7(3)
C(18)	97(5)	76(4)	64(4)	-10(3)	-28(4)	-14(4)
C(19)	89(5)	76(4)	63(4)	-7(3)	-16(4)	-28(4)
C(20)	72(4)	53(3)	63(4)	-18(3)	-5(3)	-16(3)
C(21)	50(3)	51(3)	58(3)	-20(3)	-8(2)	-10(2)
C(22)	71(4)	66(4)	79(4)	-19(3)	-4(3)	-31(3)
C(23)	64(4)	76(4)	89(5)	-26(4)	-12(3)	-34(3)
C(24)	58(3)	65(4)	72(4)	-18(3)	-18(3)	-21(3)
C(25)	96(5)	86(5)	79(5)	-33(4)	-4(4)	-36(4)
C(26)	120(8)	94(6)	123(8)	-66(6)	22(6)	-43(6)
C(27)	117(8)	100(7)	170(11)	-94(8)	42(8)	-53(6)
C(28)	67(5)	54(4)	153(9)	-31(5)	9(5)	-14(3)
C(29)	56(4)	58(4)	97(5)	-21(3)	2(3)	-22(3)
C(30)	51(3)	56(4)	99(5)	2(3)	-11(3)	-20(3)
C(31)	61(4)	69(5)	140(8)	18(5)	-35(5)	-21(4)
C(32)	79(6)	107(7)	136(9)	47(7)	-55(6)	-39(5)
C(33)	84(6)	118(7)	99(6)	25(5)	-49(5)	-47(5)

C(34)	74(4)	91(5)	76(5)	7(4)	-26(4)	-42(4)
P(1)	82(1)	93(1)	87(1)	-30(1)	-5(1)	-41(1)
F(1)	397(17)	282(12)	173(9)	87(9)	-125(10)	-232(13)
F(2)	255(10)	288(11)	115(6)	53(7)	-59(6)	-162(9)
F(3)	320(14)	238(10)	325(14)	-210(11)	58(11)	-140(10)
F(4)	136(7)	281(13)	412(18)	21(13)	-110(10)	-95(8)
F(5)	423(19)	248(11)	279(13)	-171(10)	93(12)	-232(13)
F(6)	76(4)	224(9)	374(15)	-29(10)	4(6)	-45(5)
P(2)	80(1)	84(1)	87(1)	-8(1)	-30(1)	-31(1)
F(7)	205(8)	196(7)	213(8)	-75(6)	-101(7)	-70(6)
F(8)	470(20)	500(30)	370(18)	-302(19)	324(18)	-390(20)
F(10)	355(15)	111(5)	345(15)	-42(7)	-243(13)	29(7)
F(12)	550(20)	319(16)	157(8)	-114(9)	169(12)	-299(18)
F(9)	348(15)	279(12)	366(15)	13(11)	-240(14)	-195(12)
C(35)	85(7)	77(6)	195(14)	-6(7)	-51(8)	-11(5)
C(36)	73(6)	60(5)	221(15)	-36(8)	6(8)	-11(4)
F(11)	410(20)	136(8)	590(30)	-61(13)	-380(20)	58(11)

Table A 20. Hydrogen coordinates (x 10^4) and isotropic displacement parameters (A^2 x 10^3) for p-1_sqd.

	x	y	z	U(eq)
H(1A)	3707	5376	2616	85
H(2A)	5105	6225	1606	92
H(3A)	6564	5343	503	101
H(6A)	7407	3727	-327	101
H(7A)	7315	2106	-421	97
H(10A)	6241	639	107	93
H(11A)	4713	6	1122	97
H(12A)	3437	915	2309	77
H(13A)	5441	2740	3573	84
H(14A)	6269	1840	4931	92
H(15A)	5381	695	6329	95
H(18A)	3717	-181	7203	99
H(19A)	2110	-425	7103	94
H(22A)	619	64	6128	86
H(23A)	-5	1031	4692	87
H(24A)	969	2193	3392	76
H(25A)	2738	3778	5049	102
H(26A)	1704	5244	5741	133
H(27A)	465	6707	4914	150
H(32A)	-118	6319	686	142
H(33A)	928	4753	187	124
H(34A)	2182	3357	1109	97
H(35)	-727	7413	2013	152
H(36A)	-517	7591	3335	158

Table A 21. Torsion angles [deg] for p-1_sqd.

N(2)-Co(1)-N(1)-C(1)	178.0(6)
N(4)-Co(1)-N(1)-C(1)	-113.2(12)
N(6)-Co(1)-N(1)-C(1)	82.3(6)
N(3)-Co(1)-N(1)-C(1)	-88.5(6)
N(5)-Co(1)-N(1)-C(1)	3.7(6)
N(2)-Co(1)-N(1)-C(5)	-6.7(4)
N(4)-Co(1)-N(1)-C(5)	62.0(13)
N(6)-Co(1)-N(1)-C(5)	-102.5(4)
N(3)-Co(1)-N(1)-C(5)	86.7(4)
N(5)-Co(1)-N(1)-C(5)	178.9(4)
N(4)-Co(1)-N(2)-C(12)	10.5(5)
N(6)-Co(1)-N(2)-C(12)	-87.9(5)
N(1)-Co(1)-N(2)-C(12)	-178.1(5)
N(3)-Co(1)-N(2)-C(12)	89.4(5)
N(5)-Co(1)-N(2)-C(12)	-142.6(11)
N(4)-Co(1)-N(2)-C(9)	-164.9(4)
N(6)-Co(1)-N(2)-C(9)	96.7(4)
N(1)-Co(1)-N(2)-C(9)	6.6(4)
N(3)-Co(1)-N(2)-C(9)	-85.9(4)
N(5)-Co(1)-N(2)-C(9)	42.1(13)
N(2)-Co(1)-N(3)-C(13)	82.1(6)
N(4)-Co(1)-N(3)-C(13)	179.5(6)
N(6)-Co(1)-N(3)-C(13)	-112.8(11)
N(1)-Co(1)-N(3)-C(13)	3.4(6)
N(5)-Co(1)-N(3)-C(13)	-90.2(6)
N(2)-Co(1)-N(3)-C(17)	-107.3(4)
N(4)-Co(1)-N(3)-C(17)	-9.9(4)
N(6)-Co(1)-N(3)-C(17)	57.8(12)
N(1)-Co(1)-N(3)-C(17)	174.0(4)
N(5)-Co(1)-N(3)-C(17)	80.4(4)
N(2)-Co(1)-N(4)-C(24)	-87.3(5)
N(6)-Co(1)-N(4)-C(24)	9.8(5)
N(1)-Co(1)-N(4)-C(24)	-154.5(11)
N(3)-Co(1)-N(4)-C(24)	-179.8(5)
N(5)-Co(1)-N(4)-C(24)	88.3(5)
N(2)-Co(1)-N(4)-C(21)	101.8(4)
N(6)-Co(1)-N(4)-C(21)	-161.2(4)
N(1)-Co(1)-N(4)-C(21)	34.5(14)
N(3)-Co(1)-N(4)-C(21)	9.3(4)
N(5)-Co(1)-N(4)-C(21)	-82.6(4)
N(2)-Co(1)-N(5)-C(25)	-125.0(11)
N(4)-Co(1)-N(5)-C(25)	81.6(6)
N(6)-Co(1)-N(5)-C(25)	179.1(6)
N(1)-Co(1)-N(5)-C(25)	-90.2(6)

N(3)-Co(1)-N(5)-C(25)	3.1(6)
N(2)-Co(1)-N(5)-C(29)	47.9(13)
N(4)-Co(1)-N(5)-C(29)	-105.4(4)
N(6)-Co(1)-N(5)-C(29)	-7.9(4)
N(1)-Co(1)-N(5)-C(29)	82.7(4)
N(3)-Co(1)-N(5)-C(29)	176.1(4)
N(2)-Co(1)-N(6)-C(34)	8.5(5)
N(4)-Co(1)-N(6)-C(34)	-90.4(5)
N(1)-Co(1)-N(6)-C(34)	87.1(5)
N(3)-Co(1)-N(6)-C(34)	-156.5(9)
N(5)-Co(1)-N(6)-C(34)	-179.6(5)
N(2)-Co(1)-N(6)-C(30)	-163.4(4)
N(4)-Co(1)-N(6)-C(30)	97.7(4)
N(1)-Co(1)-N(6)-C(30)	-84.8(4)
N(3)-Co(1)-N(6)-C(30)	31.6(12)
N(5)-Co(1)-N(6)-C(30)	8.5(4)
C(5)-N(1)-C(1)-C(2)	-0.4(10)
Co(1)-N(1)-C(1)-C(2)	174.6(5)
N(1)-C(1)-C(2)-C(3)	-1.6(11)
C(1)-C(2)-C(3)-C(4)	2.6(11)
C(2)-C(3)-C(4)-C(5)	-1.7(10)
C(2)-C(3)-C(4)-C(6)	178.1(7)
C(1)-N(1)-C(5)-C(4)	1.5(9)
Co(1)-N(1)-C(5)-C(4)	-174.4(5)
C(1)-N(1)-C(5)-C(9)	-178.2(5)
Co(1)-N(1)-C(5)-C(9)	6.0(6)
C(3)-C(4)-C(5)-N(1)	-0.4(9)
C(6)-C(4)-C(5)-N(1)	179.8(6)
C(3)-C(4)-C(5)-C(9)	179.2(6)
C(6)-C(4)-C(5)-C(9)	-0.6(9)
C(5)-C(4)-C(6)-C(7)	0.0(11)
C(3)-C(4)-C(6)-C(7)	-179.7(7)
C(4)-C(6)-C(7)-C(8)	1.2(12)
C(6)-C(7)-C(8)-C(10)	177.0(7)
C(6)-C(7)-C(8)-C(9)	-1.9(11)
C(12)-N(2)-C(9)-C(8)	-1.4(9)
Co(1)-N(2)-C(9)-C(8)	174.6(5)
C(12)-N(2)-C(9)-C(5)	178.5(5)
Co(1)-N(2)-C(9)-C(5)	-5.5(6)
C(10)-C(8)-C(9)-N(2)	2.2(10)
C(7)-C(8)-C(9)-N(2)	-178.8(6)
C(10)-C(8)-C(9)-C(5)	-177.7(6)
C(7)-C(8)-C(9)-C(5)	1.3(9)
N(1)-C(5)-C(9)-N(2)	-0.3(8)
C(4)-C(5)-C(9)-N(2)	180.0(5)
N(1)-C(5)-C(9)-C(8)	179.6(5)

C(4)-C(5)-C(9)-C(8)	-0.1(9)
C(9)-C(8)-C(10)-C(11)	-0.7(11)
C(7)-C(8)-C(10)-C(11)	-179.6(7)
C(8)-C(10)-C(11)-C(12)	-1.5(12)
C(9)-N(2)-C(12)-C(11)	-0.9(9)
Co(1)-N(2)-C(12)-C(11)	-176.2(5)
C(10)-C(11)-C(12)-N(2)	2.4(11)
C(17)-N(3)-C(13)-C(14)	-0.6(10)
Co(1)-N(3)-C(13)-C(14)	169.8(5)
N(3)-C(13)-C(14)-C(15)	-0.6(11)
C(13)-C(14)-C(15)-C(16)	0.8(11)
C(14)-C(15)-C(16)-C(17)	0.1(10)
C(14)-C(15)-C(16)-C(18)	179.7(7)
C(13)-N(3)-C(17)-C(16)	1.6(9)
Co(1)-N(3)-C(17)-C(16)	-170.4(5)
C(13)-N(3)-C(17)-C(21)	-178.8(5)
Co(1)-N(3)-C(17)-C(21)	9.2(6)
C(15)-C(16)-C(17)-N(3)	-1.4(9)
C(18)-C(16)-C(17)-N(3)	179.0(6)
C(15)-C(16)-C(17)-C(21)	179.0(6)
C(18)-C(16)-C(17)-C(21)	-0.5(9)
C(17)-C(16)-C(18)-C(19)	1.4(10)
C(15)-C(16)-C(18)-C(19)	-178.1(7)
C(16)-C(18)-C(19)-C(20)	-1.2(11)
C(18)-C(19)-C(20)-C(21)	0.1(11)
C(18)-C(19)-C(20)-C(22)	-178.1(7)
C(24)-N(4)-C(21)-C(20)	-0.7(8)
Co(1)-N(4)-C(21)-C(20)	171.3(4)
C(24)-N(4)-C(21)-C(17)	-179.4(5)
Co(1)-N(4)-C(21)-C(17)	-7.4(6)
C(22)-C(20)-C(21)-N(4)	0.3(9)
C(19)-C(20)-C(21)-N(4)	-178.0(6)
C(22)-C(20)-C(21)-C(17)	179.0(5)
C(19)-C(20)-C(21)-C(17)	0.8(9)
N(3)-C(17)-C(21)-N(4)	-1.3(8)
C(16)-C(17)-C(21)-N(4)	178.3(5)
N(3)-C(17)-C(21)-C(20)	179.9(5)
C(16)-C(17)-C(21)-C(20)	-0.5(8)
C(21)-C(20)-C(22)-C(23)	0.5(9)
C(19)-C(20)-C(22)-C(23)	178.8(7)
C(20)-C(22)-C(23)-C(24)	-1.0(10)
C(21)-N(4)-C(24)-C(23)	0.2(9)
Co(1)-N(4)-C(24)-C(23)	-170.4(5)
C(22)-C(23)-C(24)-N(4)	0.6(10)
C(29)-N(5)-C(25)-C(26)	-0.7(11)
Co(1)-N(5)-C(25)-C(26)	172.0(6)

N(5)-C(25)-C(26)-C(27)	-1.4(14)
C(25)-C(26)-C(27)-C(28)	2.3(14)
C(26)-C(27)-C(28)-C(29)	-1.1(13)
C(26)-C(27)-C(28)-C(36)	-179.5(9)
C(25)-N(5)-C(29)-C(28)	1.9(10)
Co(1)-N(5)-C(29)-C(28)	-172.0(5)
C(25)-N(5)-C(29)-C(30)	-179.7(6)
Co(1)-N(5)-C(29)-C(30)	6.3(7)
C(27)-C(28)-C(29)-N(5)	-1.1(11)
C(36)-C(28)-C(29)-N(5)	177.5(7)
C(27)-C(28)-C(29)-C(30)	-179.4(7)
C(36)-C(28)-C(29)-C(30)	-0.8(10)
C(34)-N(6)-C(30)-C(31)	-1.2(9)
Co(1)-N(6)-C(30)-C(31)	171.6(5)
C(34)-N(6)-C(30)-C(29)	179.2(6)
Co(1)-N(6)-C(30)-C(29)	-8.0(7)
N(5)-C(29)-C(30)-N(6)	1.1(9)
C(28)-C(29)-C(30)-N(6)	179.5(6)
N(5)-C(29)-C(30)-C(31)	-178.5(6)
C(28)-C(29)-C(30)-C(31)	-0.1(10)
N(6)-C(30)-C(31)-C(32)	-0.1(10)
C(29)-C(30)-C(31)-C(32)	179.4(7)
N(6)-C(30)-C(31)-C(35)	-179.6(7)
C(29)-C(30)-C(31)-C(35)	0.0(11)
C(30)-C(31)-C(32)-C(33)	1.4(12)
C(35)-C(31)-C(32)-C(33)	-179.2(9)
C(31)-C(32)-C(33)-C(34)	-1.3(13)
C(30)-N(6)-C(34)-C(33)	1.3(9)
Co(1)-N(6)-C(34)-C(33)	-170.2(5)
C(32)-C(33)-C(34)-N(6)	0.0(12)
C(30)-C(31)-C(35)-C(36)	1.2(17)
C(32)-C(31)-C(35)-C(36)	-178.1(11)
C(31)-C(35)-C(36)-C(28)	-2(2)
C(27)-C(28)-C(36)-C(35)	-179.5(12)
C(29)-C(28)-C(36)-C(35)	2.1(16)

Symmetry transformations used to generate equivalent atoms:

APPENDIX E

COPYRIGHT PERMISSIONS

Copyright permission for the use of table 2 from Chapter 1.

This Agreement between Jimmie L Bullock ("You") and Royal Society of Chemistry ("Royal Society of Chemistry") consists of your license details and the terms and conditions provided by Royal Society of Chemistry and Copyright Clearance Center.

License Number	3843940557462
License date	Apr 07, 2016
Licensed Content Publisher	Royal Society of Chemistry
Licensed Content Publication	Dalton Transactions
Licensed Content Title	Preliminary anti-cancer photodynamic therapeutic in vitro studies with mixed-metal binuclear ruthenium(ii)–vanadium(iv) complexes
Licensed Content Author	Alvin A. Holder,Patrick Taylor,Anthony R. Magnusen,Erick T. Moffett,Kyle Meyer,Yiling Hong,Stuart E. Ramsdale,Michelle Gordon,Javelyn Stubbs,Luke A. Seymour,Dhiraj Acharya,Ralph T. Weber,Paul F. Smith,G. Charles Dismukes,Ping Ji,Laura Menocal,Fengwei Bai,Jennie L. Williams,Donald M. Cropek,William L. Jarrett
Licensed Content Date	Jun 3, 2013
Licensed Content Volume Number	42
Licensed Content Issue Number	33
Type of Use	Thesis/Dissertation
Requestor type	non-commercial (non-profit)
Portion	figures/tables/images
Number of figures/tables/images	1
Format	print and electronic
Distribution quantity	20
Will you be translating?	no
Order reference number	None
Title of the thesis/dissertation	SYNTHESIS AND MECHANISTIC INVESTIGATIONS OF LIGANDS AND TRANSITION METAL COMPLEXES FOR CHEMOTHERAPEUTIC APPLICATIONS
Expected completion date	Apr 2016
Estimated size	232

VITA

Jimmie Lee Bullock Jr.

Department of Chemistry and Biochemistry jlbulloc09@gmail.com
Old Dominion University
Norfolk, VA 23529

Education

May 2016 …….…….....MS Chemistry, Old Dominion University
Norfolk, VA
May 2013 ……..BS Chemistry, BS Biology, Longwood University
Farmville, VA

Selected Publications

Bullock, **J**.**L**.; Holder, A.A. Photodynamic therapy in Medicine with Mixed Metal/Supramolecular Complexes. In *Ruthenium Complexes: Photochemical and Biomedical Applications;* Holder, A.A., **Bullock**, **J**.**L**.; Lawrence, M.A.W.; Browne, W.R.; Lilge, Lothar, Eds.; John Wiley & Sons: 2016 (Under Editor Review). ISBN: 978-3-527-33957-0

Bullock, J. L.; Celestine, M. J.; Holder, A. Solving Some of the World's Problems with Ruthenium Complexes: Their Role in Imaging and Biomedical Applications. In *Ruthenium: Synthesis, Physiochemical Properties and Applications*; Pages 1 – 60, Keller, G. P., Ed.; Nova Publisher: 2015. ISBN: 978-1-63321-657-0

Bullock, **J.L.**; Sandhaus,; S; Arca, J.F.; Tse-Dinh, Y.-C; Holder, A.A.; Beebe, S.J. Potential antitumor mechanism of a novel Co(III)-thiosemicarbazone complex: synthesis, DNA binding, topoisomerase and apoptosis induction activity (In preparation for *J. Inorg. Biochem.*)

Bullock, J.L.; Currie, K.C.; Jain, A.; Celestine, M.J.; Gurung, R.K.; Beebe, S.J.; Holder, A.A. Synthesis, characterization, photocleavage of DNA and cytotoxicity of a mixed-metal ruthenium(II)-vanadium(IV) PDT Agent. (In preparation for *Inorg. Chim. Acta.*)

Boodram, S.; **Bullock**, **J**.**L**.; Rambaran, V.H.; Holder, A.A. Recent Patents Based on the use of Inorganic Compounds in Photodynamic Therapy. (Recent Patents in Nanotechnology, Accepted)

Bullock, **J**.**L**.; Iglesias, B.C.; LeBlanc; M.A.; Baxter, C.E.; Arca, J.F.; Washington, D.M.; Celestine, M.J.; Pervin, S.; Beckford, F.A.; VanDerveer, D.; Fronczek, F.R.; Jarrett, W.L.; Beebe, S.J. Holder, A.A. Synthesis, characterization and mechanistic *in vitro* studies of cobalt(III) and ruthenium(II)-containing complexes. (ChemMedChem, Submitted).

Celestine, M.J.; **Bullock, J.L**.; Boodram, S.; Holder, A.A.; Rambaran, V.H. Interesting properties of p-,d- and f-block elements when coordinated with dipicolinic acid and its derivatives as ligands: their use as inorganic pharmaceuticals. *Reviews in Inorganic Chemistry*, **2015**, 35 (2), 57-67

Awards

University Fellowship ($18,000), Old Dominion University, Aug 2014 – May 2015

Carl Strom Minority Scholarship ($2,800), GRC Electrochemistry, Jan 2014